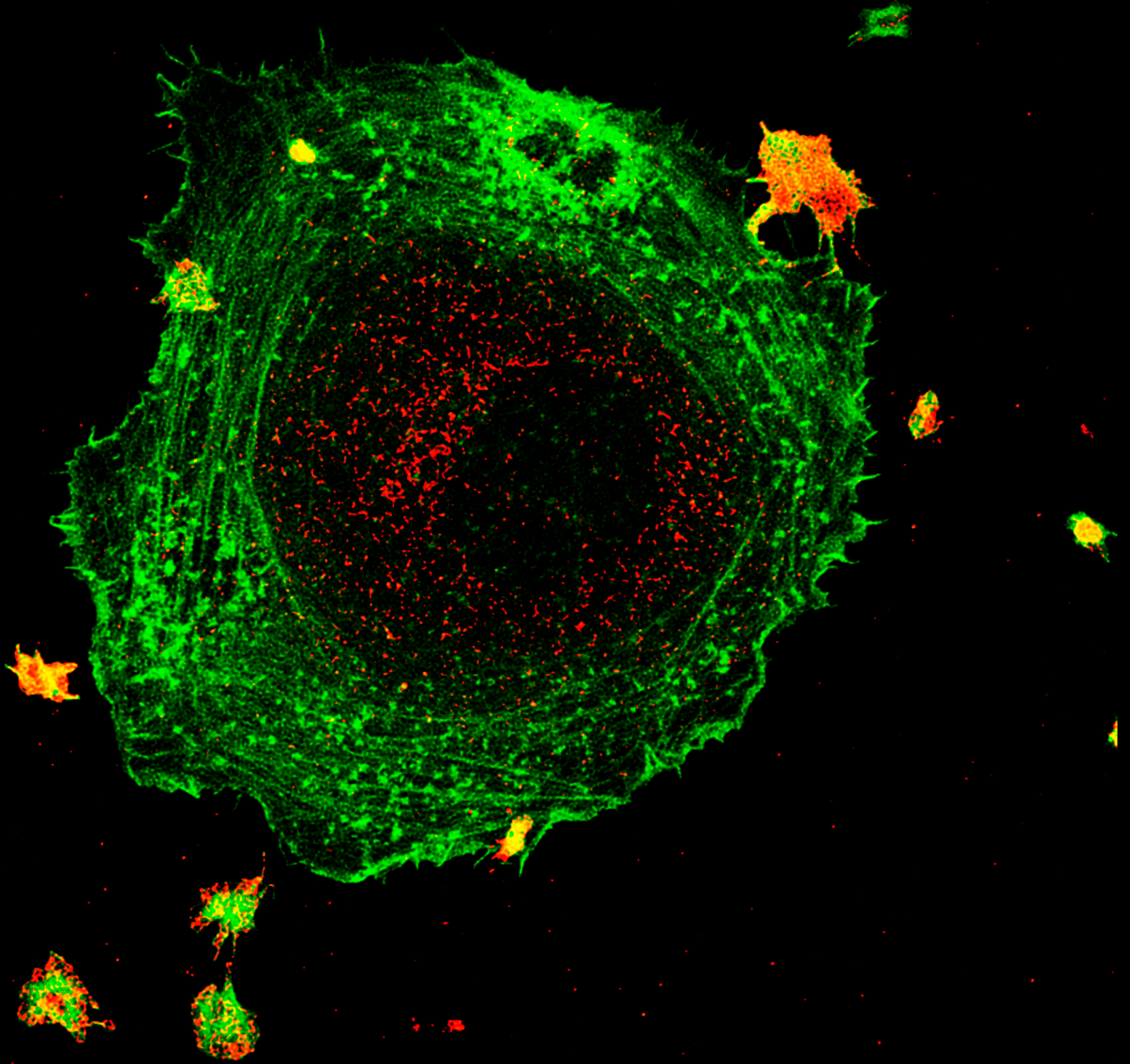




VNiVERSiDAD
D SALAMANCA

CAMPUS OF INTERNATIONAL EXCELLENCE

Universidad de Salamanca
Centro de Investigación del Cáncer



**New functions of platelet C3G:
Involvement in TPO-regulation, ischemia-induced
angiogenesis and tumor metastasis**

Luis Hernández Cano
Salamanca, 2022

UNIVERSIDAD DE SALAMANCA

**CENTRO DE INVESTIGACIÓN DEL CÁNCER
INSTITUTO DE BIOLOGÍA MOLECULAR Y CELULAR DEL CÁNCER
(CSIC-USAL)**

**New functions of platelet C3G: Involvement in TPO-
regulation, ischemia-induced angiogenesis and tumor
metastasis**

MEMORIA PARA OPTAR AL GRADO DE DOCTOR PRESENTADO POR

Luis Hernández Cano

Bajo la dirección de los Doctores

Carmen Guerrero Arroyo

Manuel Sánchez Martín



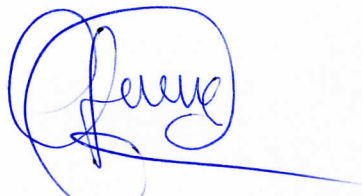
Salamanca, 2022

Dra. Carmen Guerrero Arroyo, Profesora Titular del Departamento de Medicina, Instituto de Biología Molecular y Celular del Cáncer (IBMCC, CSIC-Universidad de Salamanca); y **Dr. Manuel Sánchez Martín**, Profesor Titular del Departamento de Medicina, Universidad de Salamanca.

CERTIFICAN:

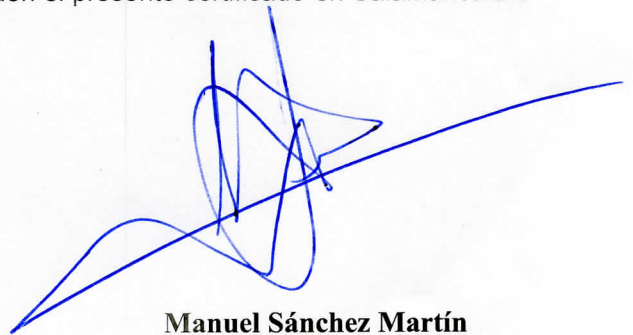
Que **D. Luis Hernández Cano**, graduado en Bioquímica por la Universidad de Murcia, ha realizado bajo su dirección el trabajo de Tesis Doctoral que lleva por título “**New functions of platelet C3G: Involvement in TPO-regulation, ischemia-induced angiogenesis and tumor metastasis**”, y consideran que éste reúne originalidad y contenidos suficientes para que sean presentados ante el Tribunal correspondiente y optar al Grado de Doctor por la Universidad de Salamanca con Mención de Doctorado Internacional.

Y para que conste, y a los efectos oportunos, expiden el presente certificado en Salamanca a 3 de marzo de 2022.



Dra. Carmen Guerrero Arroyo

Directora



Manuel Sánchez Martín

Co-director

Luis Hernández Cano ha realizado esta tesis doctoral siendo beneficiario de una ayuda destinada a la contratación predoctoral de personal investigador de la Junta de Castilla y León (Orden Edu del 10 de noviembre de 2016) cofinanciadas por el Fondo Social Europeo, durante el periodo de junio de 2017 a diciembre de 2021.

Este trabajo se ha enmarcado dentro de los proyectos del Plan nacional I+D+i: *“Función de C3G en el desarrollo tumoral y la patofisiología del hígado. Implicación de C3G en la angiogénesis y en enfermedades hepáticas y cardiovasculares”* (SAF2016-76588-C2-2-R) y *“Nuevas Funciones de C3G en la progresión tumoral, la fisiología hepática y la biología de megacariocitos y plaquetas. Contribución de C3G plaquetario a la neoangiogénesis patológica y al daño hepático”* (PID2019-104143RB-C21) financiados por el Ministerio de Economía y Competitividad y el Fondo Europeo de Desarrollo Regional (FEDER), *“Una forma de hacer Europa”* y de los proyectos del Programa de apoyo a proyectos de investigación de la Consejería de Educación de la Junta de Castilla y León *“Papel de C3G en la regulación de la función plaquetaria: Implicaciones en angiogénesis y aplicación al diagnóstico y tratamiento de la enfermedad trombótica”* (SA017U16) y *“Papel de C3G en tumores hematopoyéticos y en angiogénesis mediada por plaquetas. Evaluación de su uso como diana terapéutica”* (SA078P20), cofinanciados por el Fondo Europeo de Desarrollo Regional (FEDER), *“Una forma de hacer Europa”*. El Centro de Investigación del Cáncer (IBMCC-CIC), dónde se ha realizado este trabajo, recibe financiación del Programa de Apoyo a Planes Estratégicos de Investigación de Estructuras de Investigación de Excelencia co-financiado por la Junta de Castilla y León y FEDER (CLC-2017-01).

Luis Hernández Cano realizó parte del trabajo de esta tesis en una estancia de tres meses de duración en el laboratorio del Dr. Emilio Casanova Hevia en el *Center for Physiology and Pharmacology, Medical University of Vienna* (Viena, Austria). Parte de esta estancia estuvo financiada por el Programa IV, de Movilidad del Personal Investigador, Modalidad b, de la Universidad de Salamanca.

THESIS SUMMARY

GTPases are proteins that control a wide variety of cellular processes, such as proliferation, differentiation and apoptosis, among others. These proteins cycle between two states: one active or GTP-bound, and one inactive or GDP-bound. The exchange of GDP for GTP is catalysed by a group of proteins called GEF (Guanine nucleotide Exchange Factors), whereas GAP (GTPases activating proteins) participate in the inactivation of the GTPases. C3G is a GEF for several members of the Ras family of GTPases, mainly Rap1, R-Ras and TC21, and for the Rho family GTPase, TC10. Using mice overexpressing C3G (tgC3G) or a mutant form lacking the catalytic domain (tgC3G Δ Cat) specifically in megakaryocytes and platelets, we have previously shown that C3G promotes megakaryocyte (Mk) differentiation and regulates hemostatic functions of platelets. In particular, tgC3G platelets show a greater platelet activation and aggregation, which is correlated with lower bleeding times in tgC3G mice and increased thrombus formation *in vivo*. Moreover, C3G overexpression in platelets alters the release of platelet α -granules, characterized by the retention of vascular endothelial growth factor (VEGF) and thrombospondin-1 (TSP-1) inside the platelet, resulting in a net proangiogenic secretome. As a consequence, tgC3G expression in platelets promotes faster tumour growth in two models of heterotopic tumour cell implantation: 3LL (Lewis Lung carcinoma) cells and B16-F10 melanoma cells. Platelet C3G also promotes pulmonary metastasis of B16-F10 cells. However, transgenic C3G expression does not modify platelet counts in peripheral blood.

In my thesis, I have deepened into the role of C3G in megakaryopoiesis, ischemia-induced angiogenesis and tumour metastasis. For that, we developed an additional mouse model, in which C3G is specifically deleted in megakaryocytes (Rapgef1^{flox/flox}; PF4-Cre^{+/-}, hereinafter C3G-KO). C3G-KO mice did not show differences in the number of Mk in the bone marrow (BM) or in platelet count in peripheral blood, similar to what was observed in the tgC3G model. However, ablation of C3G promoted Mk maturation in BM cultured in medium supplemented with thrombopoietin (TPO) and a cocktail of cytokines, suggesting a possible role of C3G in pathological megakaryopoiesis.

Since platelet C3G showed no effect on megakaryopoiesis and thrombopoiesis in a physiological context, we analysed its role in two *in vivo* models of pathological megakaryopoiesis: TPO injection and 5-Fluorouracyl (5-FU)-induced myelosuppression. The intravenous injection of TPO stimulates megakaryopoiesis and increases platelet levels, while 5-FU induces platelet depletion around day 7 after injection, which is

followed by a profound increase in platelet numbers, known as platelet rebound, 10-15 days after treatment.

Surprisingly, TPO injection produced a more efficient increase in platelet levels in C3G-KO mice than in their controls. Moreover, after reaching the peak, the levels of C3G-KO platelets decreased slower than control platelets, suggesting an impaired downregulation. On the other hand, 5-FU injection resulted in significant lower platelet rebound in C3G-KO mice compared to their control. However, similar to the TPO-stimulation model, while control animals recovered normal platelet levels 20 days after the injection, platelet levels remained elevated in C3G-KO mice, indicating a defective downregulation. Opposite results were obtained in tgC3G mice, showing a greater rebound and a faster downregulation of platelet levels.

TPO is the major cytokine involved in megakaryopoiesis and platelet formation. TPO is constitutively produced in the liver and its plasma concentration varies inversely with the number of platelets, which remove it by clearance. In platelets, TPO binds to its receptor, c-Mpl, and induces its endocytosis, recycling and degradation. This mechanism is driven by the E3 ubiquitin ligase c-Cbl, responsible for the ubiquitination of c-Mpl and its degradation by the proteasome and lysosome systems. C3G and c-Cbl interaction has been detected previously in K562 cells, an erythro-megakaryoblastic cell line that acquires Mk markers upon stimulation with PMA. In this Thesis we demonstrated that C3G and c-Cbl also interact in platelets and that C3G is a mediator of c-Cbl phosphorylation and activation by kinases of the Src family. Indeed, C3G ablation in platelets completely impaired c-Cbl phosphorylation in response to TPO, due to a decreased interaction between Src and c-Cbl. This resulted in reduced c-Mpl internalization and degradation. In concordance, c-Mpl ubiquitination (measured by immunofluorescence as colocalization between c-Mpl and ubiquitin signal) was significantly decreased in TPO-stimulated C3G-KO platelets. Moreover, total ubiquitinated proteins levels dropped drastically in resting, thrombin- and TPO-stimulated C3G deficient platelets. Opposite results were obtained in tgC3G platelets exhibiting greater p-c-Cbl levels, correlated with a faster degradation and a greater ubiquitination of the c-Mpl receptor. In addition, *in vitro* TPO uptake was significantly decreased in C3G-KO platelets after 30 minutes incubation.

In summary, C3G-KO platelets are unable to regulate TPO plasma levels owing to a defective Src-mediated c-Cbl phosphorylation, which results in defective TPO-c-Mpl internalization and degradation. This could explain the sustained elevated platelet levels found in the pathological models.

All these results suggest the participation of C3G in the Src-c-Cbl pathway to regulate TPO levels and, hence platelet levels.

In the second part of the Thesis, we have studied the involvement of C3G in platelet-mediated angiogenesis. For that, we have used two models of ischemia-induced angiogenesis: tumour implantation and hind-limb ischemia. In response to hypoxia, VEGF, released by platelets and endothelial cells, induces platelet secretion of SDF-1 (stromal-derived factor, also known as CXCL12). VEGF and SDF-1 facilitate the recruitment of bone marrow-derived proangiogenic progenitor cells (BMDC) through interaction with their respective receptors, CXCR4 and VEGFR1. Then, these BMDC, also known as hemangiocytes, release angiogenic factors at the ischemic site that promote the incorporation and assembly of endothelial progenitor cells and the stabilization of new blood vessels. We found that C3G-KO mice showed a significant increase in the recruitment of hemangiocytes, in both ischemic models. In addition, C3G-KO mice exhibited larger and more vascularized tumours after 15 days of the injection of 3LL cells, and a slightly faster recovery of the blood flow after hind-limb ischemia, as compared to their control siblings. In contrast, lower number of hemangiocytes were detected in tgC3G mice in both ischemia models. In concordance with these *in vivo* results, C3G ablation resulted in increased SDF-1 secretion *in vitro*, whereas C3G overexpression resulted in an impaired SDF-1 release. In addition, C3G ablation increased VEGF release and TSP-1 retention, which, collectively results in a proangiogenic secretome and could explain the increased angiogenesis observed in the *in vivo* studies. These results suggest that platelet C3G has a role in hypoxia-induced BMDC recruitment through the modulation of SDF-1, VEGF and TSP-1 release.

In the third part of the Thesis, we have explored the role of C3G in platelet-mediated tumor metastasis. Previously, we described that transgenic expression of C3G in platelets promotes long-term metastasis of B16-F10 cells in the lungs. To further analyse this C3G function we developed a short-term metastasis model consisting in the injection of B16-F10 cells, expressing EGFP (green fluorescent protein), into the retroorbital sinus of the mouse and the count of EGFP-expressing cells in the lungs, by flow cytometry, 1 hour after the injection. TgC3G mice showed increased number of melanoma cells in the lungs, while C3G platelet ablation resulted in fewer short-term metastases. *In vitro* adhesion assays in poly-L-Lysine coverslips revealed increased adhesion of melanoma cells when they were incubated with tgC3G platelets. In contrast, melanoma cells incubated with C3G-KO platelets showed decreased adhesion. These results suggest that C3G enhances platelet ability to promote adhesion of tumor cells to the metastatic niche.

Since the metastatic potential of tumor cells *in vivo* correlates with their ability to aggregate platelets, we next studied the contribution of C3G to TCIPA (tumor cell induced platelet aggregation). TgC3G platelets incubated with B16-F10 cells showed significantly greater aggregation than control platelets, which was accompanied by a higher activation of integrin $\alpha\text{IIb}\beta\text{3}$ and correlated with an increased Rap1 activation. We did not find significant differences in TCIPA between C3G-KO platelets and their controls, in correlation with a similar activation of integrin $\alpha\text{IIb}\beta\text{3}$, although Rap1 activation was impaired in these platelets, as described in response to other stimuli.

All these results support the notion that C3G contributes to platelet-mediated tumor growth and metastasis, including cell adhesion to the metastatic niche and platelet-tumor cell communication, with a direct impact on metastases.

In conclusion, in this work we present evidence of a new role of C3G in the modulation of platelet levels through the regulation of c-Cbl-dependent c-Mpl ubiquitination and degradation. Furthermore, platelet C3G participates in hypoxia-induced angiogenesis by modulating hemangiocyte recruitment through the regulation of SDF-1 and VEGF release, as well as regulating TSP-1 release. Finally, we reveal a new function of C3G in TCIPA, facilitating metastatic cell homing and adhesion.

RESUMEN

Las GTPasas son proteínas que regulan una gran variedad de procesos celulares, entre los que cabe destacar la proliferación, la diferenciación celular y la apoptosis. Estas proteínas alternan entre dos conformaciones: una activa o unida a GTP y una inactiva o unida a GDP. El intercambio de GDP por GTP está catalizado por un grupo de proteínas denominadas GEF (factores intercambiadores de nucleótidos de guanina), mientras que las proteínas GAP (proteínas activadoras de la actividad GTPasa) inhiben a la GTPasa. C3G es un GEF para varias GTPasas de la familia de Ras, principalmente de Rap1, R-Ras y TC21, y para una GTPasa de la familia de Rho, TC10. Mediante el uso de modelos animales que expresan de manera específica en plaquetas y megacariocitos o bien C3G (tgC3G), o bien una forma mutante de C3G (caracterizada por la pérdida del dominio catalítico, tgC3G Δ Cat), nuestro grupo ha demostrado la participación de C3G en la diferenciación megacariocítica, así como en la regulación de la función hemostática de las plaquetas. En concreto, las plaquetas tgC3G presentan una mayor activación y agregación plaquetaria, que se correlaciona con tiempos de sangrado significativamente inferiores en los ratones tgC3G, además de un incremento en la formación de trombos en modelos *in vivo*. La sobreexpresión de C3G plaquetario, también genera una alteración en la secreción de los gránulos- α , caracterizada por la retención del factor de crecimiento del endotelio vascular (VEGF) y de trombospondina-1 (TSP-1) en el citoplasma de las plaquetas, dando lugar a un secretoma netamente proangiogénico. Como resultado de la mayor capacidad proangiogénica de las plaquetas que sobreexpresan C3G, los ratones tgC3G mostraron un crecimiento tumoral más rápido en dos modelos heterotópicos de implantación tumoral. Además, la proteína C3G plaquetaria promueve la metástasis pulmonar de células de melanoma (B16-F10). Sin embargo, la expresión transgénica de C3G no altera los recuentos plaquetarios en sangre periférica.

En esta Tesis, hemos profundizado en el papel de C3G en la megacariopoyesis, en la angiogénesis inducida por isquemia y en la metástasis tumoral. Para ello, hemos desarrollado un modelo animal adicional (C3G-KO), en el cual C3G se encuentra específicamente deletado en megacariocitos (Mk). Al igual que lo observado en ratones tgC3G, los animales C3G-KO tampoco mostraron diferencias ni en el número de Mk en médula ósea, ni en los recuentos plaquetarios en sangre periférica. Sin embargo, la delección de C3G resultó en una mayor maduración megacariocítica *in vitro* cuando las médulas óseas fueron cultivadas en medio enriquecido con trombopoietina

(TPO) junto con un *cocktail* de citocinas, sugiriendo un posible papel de C3G en una megacariopoyesis patológica.

En base a esto, hemos analizado el papel de C3G en dos modelos *in vivo* de megacariopoyesis patológica: la inyección de TPO y la mielosupresión inducida por 5-Fluoruracilo (5-FU). La inyección intravenosa de TPO estimula la megacariopoyesis, incrementando los niveles plaquetarios; mientras que el 5-FU induce la depleción de la médula ósea alrededor del séptimo día tras la inyección, lo que va seguido de un profundo incremento en el recuento plaquetario, proceso conocido como rebote plaquetario (*platelet rebound*) tras 10-15 días de tratamiento.

Sorprendentemente, tras la inyección con TPO, los animales C3G-KO mostraron un mayor incremento en los niveles plaquetarios que sus correspondientes controles. Además, tras alcanzar el pico máximo de producción de plaquetas, los recuentos plaquetarios de los ratones C3G-KO disminuyeron más lentamente que los de los animales silvestres. Por otro lado, la inyección de 5-FU, resultó en un rebote plaquetario significativamente inferior en los ratones C3G-KO. Sin embargo, de manera similar a lo observado en el modelo de inyección de TPO, mientras que los animales silvestres recuperaron niveles plaquetarios normales 20 días después del tratamiento con 5-FU, los recuentos de plaquetas en los animales C3G-KO permanecieron elevados, indicando un defecto en la recuperación de los niveles fisiológicos de plaquetas. Resultados opuestos se obtuvieron en los animales tgC3G, observándose un mayor rebote plaquetario y una recuperación más rápida de los niveles plaquetarios.

La TPO es la principal citocina implicada en la megacariopoyesis y en la formación de plaquetas. La TPO se produce de manera constitutiva en el hígado, y su concentración plasmática está inversamente relacionada con el número de plaquetas en sangre, las cuales se encargan de su aclaramiento. La TPO se une a su receptor, c-Mpl e induce su endocitosis, reciclamiento y degradación. Este mecanismo se encuentra dirigido por la E3 ubiquitina ligasa c-Cbl, responsable de la ubiquitinación de c-Mpl y de su degradación vía proteosoma y lisosoma. La interacción entre C3G y c-Cbl ha sido descrita previamente en células K562 (línea celular eritro-megacarioblástica que tras la estimulación con PMA (Forbol 12-Miristato 13-Acetato), adquieren marcadores megacariocíticos). En esta Tesis hemos demostrado la interacción de C3G y c-Cbl en plaquetas, así como, el requerimiento de C3G en la fosforilación y activación de c-Cbl mediada por kinasas de la familia de Src (SFK). La eliminación de C3G en plaquetas resultó en una alteración de la fosforilación de c-Cbl en respuesta a TPO debido a una menor interacción entre Src y c-Cbl, lo cual se tradujo en una reducción en la

internalización y la consiguiente degradación de c-Mpl. En este sentido, la ubiquitinación de c-Mpl (medida de forma indirecta, mediante inmunofluorescencia, como la colocalización entre c-Mpl y ubiquitina) se encuentra significativamente disminuida en plaquetas C3G-KO tras su estimulación con TPO. Además, la cantidad total de proteína ubiquitinada en plaquetas deficientes para C3G se encontró significativamente reducida en plaquetas en reposo, así como tras su estimulación con TPO y trombina. Por el contrario, las plaquetas tgC3G presentaron niveles de p-c-Cbl significativamente superiores, al igual que una mayor degradación y ubiquitinación de c-Mpl. Asimismo, tras 30 min de incubación, las plaquetas C3G-KO exhibieron una disminución en la captación *in vitro* de TPO.

En resumen, las plaquetas C3G-KO no realizan una correcta regulación de los niveles plasmáticos de TPO debido a un defecto en la fosforilación de c-Cbl mediada por Src, lo cual se traduce en una incorrecta internalización y degradación de c-Mpl tras la estimulación plaquetaria con TPO. Este hecho, explicaría el mantenimiento de los elevados niveles plaquetarios observados en ambos modelos de megacariopoyesis patológica.

Todos estos resultados sugieren la participación de C3G en la ruta de Src-c-Cbl encargada del aclaramiento de TPO plasmático y, por consiguiente, de la regulación de los recuentos plaquetarios.

En la segunda parte de esta Tesis, hemos analizado el papel de C3G en la angiogénesis mediada por plaquetas. Para ello, hemos utilizado dos modelos de angiogénesis inducida por isquemia: isquemia por implantación tumoral e isquemia de la extremidad posterior (*hind-limb*). La secreción de VEGF por parte de las plaquetas y de las células endoteliales promueve la liberación plaquetaria de SDF-1 (factor derivado del estroma-1, también conocido como CXCL12). Ambos factores, VEGF y SDF-1, a través de la unión a sus respectivos receptores CXCR4 y VEGFR1, participan en el reclutamiento de precursores de la médula ósea (BMDC). Las BMDCs, también conocidas como hemangiocitos, secretan diferentes factores que promueven la estabilización de los vasos sanguíneos. Los ratones C3G-KO, exhibieron un incremento significativo en el reclutamiento de hemangiocitos en ambos modelos isquémicos. En consonancia, los ratones C3G-KO presentaron tumores más grandes y más vascularizados 15 días después de la implantación de las células 3LL (*Lewis Lung Carcinoma*), y una aceleración en la recuperación del flujo sanguíneo tras la isquemia de la extremidad inferior, que sus hermanos silvestres. Por el contrario, los ratones tgC3G mostraron un menor reclutamiento de hemangiocitos en ambos modelos. De

acuerdo con estos resultados, la ablación de C3G promovió la liberación de SDF-1 *in vitro*, mientras que su sobreexpresión provocó su retención en el interior de la plaqueta. Asimismo, las plaquetas C3G-KO presentaron un incremento en la liberación de VEGF y en la retención de TSP-1 lo que, en conjunto, resultó en un secretoma proangiogénico, el cual explicaría la mayor angiogénesis observada *in vivo*. Estos resultados sugieren que C3G participa en el reclutamiento de hemangiocitos en respuesta a hipoxia, modulando la liberación de SDF-1, VEGF y TSP-1.

Por último, en la tercera parte de la Tesis, hemos explorado el papel de C3G en la metástasis mediada por las plaquetas. Previamente, nuestro grupo había descrito que la sobreexpresión de C3G en plaquetas promueve la metástasis a largo plazo de células de melanoma. Con el objetivo de profundizar sobre el papel de C3G en esta función plaquetaria llevamos a cabo un modelo de metástasis a corto plazo consistente en la inyección de células B16-F10-EGFP (expresan la proteína fluorescente verde) directamente en el seno retro-orbital de los ratones para, una hora más tarde, analizar mediante citometría de flujo el número de células EGFP positivas presentes en el pulmón. Los ratones tgC3G mostraron un mayor número de células de melanoma en los pulmones, mientras que los animales C3G-KO presentaron una reducción en el número de metástasis. Además, ensayos de adhesión sobre cubreobjetos pretratados con poli-L-Lisina revelaron una mayor adhesión de las células de melanoma después de haber sido incubadas con plaquetas tgC3G. Por el contrario, células de melanoma tratadas con plaquetas C3G-KO presentaron una menor capacidad de adhesión. Estos resultados sugieren que C3G promueve la capacidad de las plaquetas para promover la adhesión de las células tumorales al nicho metastásico.

Debido a que el potencial metastásico de un tumor depende de su capacidad para promover la agregación plaquetaria, decidimos estudiar la contribución de C3G al proceso de TCIPA (agregación plaquetaria inducida por la célula tumoral). Las plaquetas tgC3G incubadas con células B16-F10, mostraron una mayor agregación que sus correspondientes controles, acompañada de una mayor activación de la integrina $\alpha\text{IIb}\beta\text{3}$ y un incremento en los niveles de Rap1-GTP. Sin embargo, en plaquetas C3G-KO estimuladas con células B16-F10 no se observaron diferencias ni en TCIPA, ni en activación plaquetaria, aunque si observamos una menor activación de Rap1 que en las plaquetas control, al igual que lo observado con otros estímulos.

Todos estos resultados apoyan la idea de que C3G plaquetario contribuye al crecimiento tumoral y la metástasis, promoviendo la adhesión de las células tumorales

al nicho metastásico, así como participando activamente en la comunicación plaqueta-célula tumoral.

En conclusión, en este estudio hemos presentado varias evidencias que apoyan un nuevo papel de C3G en la modulación de los niveles plaquetarios a través de la regulación de la ubiquitinación y degradación de c-Mpl mediada por c-Cbl. Además, la proteína C3G plaquetaria participa en la angiogénesis inducida por hipoxia, regulando el reclutamiento de hemangiocitos a través de la liberación de SDF-1 y VEGF, así como de TSP-1. Finalmente, hemos revelado una nueva función de C3G en TCIPA, facilitando el reclutamiento y la adhesión de las células al nicho metastásico.

List of abbreviations

5-FU	5-Fluorouracil
A.u.	Arbitrary Units
AIR	Autoinhibitory Region
Ang-1	Angiopoietin-1
Atg	Autophagy Related Protein
bFGF	Basic Fibroblast Growth Factor
BFU-MK	Burst-Forming Unit Megakaryocyte
BM	Bone Marrow
BMC	Bone Marrow Cell
BMDC	Bone Marrow Derived Factor
BSA	Bovine Serum Albumin
C3G	Crk SH3-domain-binding Guanine-nucleotide-releasing factor
Cbl	Casitas B cell Lymphoma
CFU-MK	Colony-Forming Unit Megakaryocyte
CLP	Common Lymphoid Progenitor
CML	Chronic Myeloid Leukemia
CMP	Common Myeloid Progenitor
COX	Cyclooxygenase
Ct	Threshold Cycle
DAG	Diacylglycerol
DLL4	Delta-Like Ligand 4
DMEM	Dulbecco's Modified Eagle's Medium
DMSO	Dimethyl Sulfoxide
DRAM	Damage-Regulated Autophagy Modifier
DTS	Dense Tubular System
EC	Endothelial Cells
ECM	Extracellular Matrix
EGF	Epidermal Growth Factor
EGFP	Enhanced Green Fluorescent Protein
EMT	Epithelium-mesenchymal transition
EPO	Erythropoietin
ER	Endoplasmic Reticulum
ERK	Extracellular signal Regulated Kinase
FHL4	Familial Hemophagocytic Lymphohistiocytosis
FLK-1	Fetal Liver Kinase-1
GAP	GTPase Activating Protein
GEF	Guanine-nucleotide-Exchange Factor
GNRP	Guanine Nucleotide Releasing Factor
Gp	Glycoprotein
GST	Glutathione S-Transferase
H&E	Hematoxylin & Eosin
HCC	Hepatocellular Carcinoma
HGF	Hepatocyte Growth Factor
HSC	Hematopoietic Stem Cells
HUVEC	Human Umbilical Vein Endothelial Cell
IGF	Insulin-like Growth Factor
IHC	Immunohistochemistry
IL	Interleukin
JAK	Janus Kinase
KO	knockout
LIF	Leukemia Inhibitory Factor
LRP-1	Lipoprotein receptor-related protein 1
LSK	Lin-Sca1 ⁺ c-Kit ⁺
LT-HSC	Long-term Hematopoietic Stem Cell
MAPK	Mitogen-Activated Protein Kinase
MEF	Mouse Embryonic Fibroblast

MEP	Megakaryocyte-Erythroid Progenitor
mESCs	Mouse Embryonic Stem Cells
MFI	Mean Fluorescent Intensity
Mk	Megakaryocyte
MkP	Megakaryocyte progenitor
MMP	Multipotent Progenitor
MMP	Matrix Metalloproteinase
NFDM	Non-Fat Dry Mil
NF-kB	Nuclear-Factor kB
NK	Natural Killer
NO	Nitric Oxide
o/n	Overnight
OCS	Open Canicular System
PAI-1	Plasminogen Activator Inhibitor
PD-ECGF	Platelet-Derived Endothelial Cell Growth Factor
PDGF	Platelet Derived Growth Factor
PF4	Platelet Factor 4
PFA	Paraformaldehyde
PI	Propidium Iodide
PI3K	Phosphoinositol-3-Kinase
PRP	Platelet Rich Plasma
PS	Phosphatidylserine
PVDF	Polyvinylidene Fluoride
qPCR	Quantitative PCR
RBC	Red Blood Cell
RBD	Rap-Binding Domain
REM	Ras Exchange Motif
RPMI	Roswell Park Memorial Institute
RT	Room Temperature
RT	Reverse Transcription
SCF	Stem Cell Factor
SD	Standard Deviation
SDF-1	Stromal Derived Factor-1
SEM	Standard Error of the Mean
SFK	Src Family Kinases
SH3b	SH3-binding domain
SNAP	Synaptosome Associated Protein
SNARES	Soluble N-ethylmaleimide-sensitive factor Attachment Protein Receptor
STAT	Signal-Transducer and Activator of Transcription
ST-HSC	Short-term Hematopoietic Stem Cell
Syk	Spleen Tyrosine Kinase
t-	Target
TCIPA	Tumor Cell-Induced Platelet Aggregation
Tg	transgenic
TH	Thrombin
TIMP	Tissue Inhibitors of MMPs
TPO	Thrombopoietin
TSP	Thrombospondin
TXA₂	Thromboxane A ₂
Ub	Ubiquitin
UBL	Ubiquitin-Like domain
UPR	Unfolded Protein Response
UPS	Ubiquitin-Proteasome System
v-	Vesicle
VAMP	Vesicular Associated Membrane Protein
VEGF	Vascular Endothelial Growth Factor
vWF	Von Willebrand Factor
Wt	Wild-type

TABLE OF CONTENTS

INTRODUCTION	3
1. C3G	3
1.1. Generalities.....	3
1.2. C3G as a GEF	3
1.3. Structure.....	4
1.4. C3G functions	5
1.4.1. <i>C3G in embryonic development.</i>	5
1.4.2. <i>C3G in cancer</i>	5
1.4.3. <i>C3G in cell differentiation</i>	6
1.4.4. <i>C3G in platelet biology</i>	7
2. Megakaryopoiesis	7
2.1. TPO triggers megakaryocyte differentiation through different pathways	9
2.1.1. <i>Negative regulation of TPO/c-Mpl signaling</i>	10
2.2. Other cytokines involved in Mk differentiation	11
3. Platelets	11
3.1. Platelets and hemostasia	13
3.2. C3G contributes to platelet activation and aggregation	14
3.3. Platelet and angiogenesis	16
3.3.1. <i>Angiogenesis</i>	16
3.3.2. <i>Platelets store a variety of angiogenic factors.</i>	18
3.4. Platelets regulates their own mass by modulating TPO endocytosis.....	21
3.4.1. <i>c-Cbl is essential for c-Mpl internalization and ubiquitination in platelets</i>	21
3.4.2. <i>Platelet proteasome</i>	23
3.4.3. <i>Lysosome-protein degradation</i>	24
3.4.4. <i>Proteasome and lysosome crosstalk</i>	24
3.5. Platelets promote tumor growth	25
3.6. Platelets are required for metastasis.....	26
AIMS OF THE THESIS	31
OBJETIVOS	32
MATERIALS & METHODS	35
1. Mouse models	35
1.1. DNA extraction and genotyping.....	35
2. Cell lines and culture conditions.....	36
3. Bone Marrow isolation and culture	36

3.1.	Megakaryocyte differentiation	37
3.2.	Megakaryocyte purification	37
4.	Platelet purification	37
4.1.	Platelet activation	38
4.2.	Isolation of platelet releasate	38
5.	Analysis of platelet releasates using a Mouse Angiogenesis Array	39
6.	Capillary tube formation assay	39
7.	Analysis of platelet proteome.....	39
8.	Flow Cytometry Analysis.....	40
8.1.	Platelet count by flow cytometry.....	40
8.2.	Detection of hemangiocytes in peripheral blood and bone marrow.....	41
8.3.	Analysis of platelet activation	41
8.4.	Platelet aggregation assay	41
8.5.	Detection of Megakaryocytes by analysis of cell surface markers.....	42
8.6.	Analysis of DNA ploidy	42
8.7.	Analysis of c-Mpl internalization.....	42
9.	<i>In vivo</i> experiments.....	43
9.1.	Tail-bleeding assays	43
9.2.	Acute pulmonary thromboembolism	43
9.2.1.	<i>Lethal dose</i>	43
9.2.2.	<i>Sublethal-dose</i>	44
9.3.	Induction of ischemia by tumor cell implantation	44
9.3.1.	<i>Analysis of hemangiocyte recruitment</i>	44
9.3.2.	<i>Histological analysis</i>	45
9.4.	Induction of unilateral hind-limb ischemia	45
9.4.1.	<i>Doppler imaging and hemangiocyte recruitment</i>	46
9.5.	Intravenous injection of TPO.	47
9.6.	5-Fluorouracil-induced myelosuppression	48
9.6.1.	<i>Plasma TPO levels</i>	49
9.7.	Short- term metastasis model	49
10.	<i>In vitro</i> detection of TPO uptake by platelets	49
11.	RNA analysis.....	50
11.1.	RNA isolation from tissue	50
11.2.	RNA isolation from platelets and Megakaryocytes	50
11.3.	cDNA synthesis	50
11.4.	Quantitative PCR.....	51

11.4.1.	qPCR data analysis	51
12.	Immunodetection of proteins by Western Blot.....	52
12.1.	Sample preparation	52
12.2.	Protein Quantification and denaturalization	52
12.3.	SDS-Polyacrylamide gel electrophoresis.....	53
12.4.	Transfer of proteins to PVDF membranes	53
12.5.	Immunodetection	53
12.6.	Membrane stripping	54
13.	Confocal Microscopy	55
14.	B16-F10 Adhesion Assay.....	56
15.	Rap activation assay.....	56
15.1.	Platelet Rap1 activation induced by B16-F10 cells	56
15.2.	Detection of Rap1-GTP	57
16.	Co-Immunoprecipitation assay.....	57
16.1.	Detection of co-immunoprecipitated proteins	57
17.	c-Mpl degradation	57
18.	Statistical Analysis.....	57
19.	Ethical Considerations	58
RESULTS	61
1.	Characterization of Rapgef1 ^{fllox/fllox} ; Pf4-Cre ^{+/-} mice	61
1.1.	Successful deletion of C3G in megakaryocytes and platelets in Rapgef1 ^{fllox/fllox} ; PF4-Cre ^{+/-} mice.....	61
1.2.	C3G ablation from platelets alters hemostasis	63
1.3.	C3G ablation did not result in differences in platelet count or megakaryocyte number in bone marrow.....	64
1.4.	C3G ablation promotes Mk differentiation <i>in vitro</i>	66
2.	Role of C3G in pathological megakaryopoiesis	67
2.1.	C3G ablation promotes an increase in the number of platelets after TPO intravenous injection.	67
2.2.	C3G controls platelet rebound after 5-FU-induced myelosuppression, and is essential to maintain homeostatic platelet levels.	68
2.3.	C3G regulates c-Mpl levels.	70
2.4.	Platelet C3G controls c-Mpl internalization and degradation upon TPO stimulation 72	
2.5.	C3G deletion in platelets alter plasma TPO levels	74
2.6.	C3G-KO platelets fail to uptake TPO <i>in vitro</i>	74
2.7.	C3G interacts with c-Cbl in platelets.....	75

2.8.	C3G regulates Cbl phosphorylation.	77
2.9.	C3G controls c-Mpl ubiquitination.....	81
2.10.	C3G participates in UPS-Lysosome crosstalk	84
2.11.	C3G ablation alters the 19S regulatory proteasome regulatory particle.	87
3.	Role of C3G in ischemia induced angiogenesis.....	89
3.1.	C3G controls hemangiocyte recruitment to hypoxia sites.....	89
3.2.	Platelet C3G regulates SDF-1 release.....	95
3.3.	C3G ablation affects the release of VEGF and TSP-1 from platelets.	97
3.4.	C3G-KO secretome stimulates angiogenesis <i>in vitro</i>	100
4.	Role of platelet C3G in melanoma metastasis	101
4.1.	Platelet C3G promotes short-term melanoma metastasis	101
4.2.	C3G promotes melanoma cell adhesion.....	102
4.3.	C3G overexpression in platelets promotes tumor cell-induced platelet activation and aggregation.....	104
	DISCUSSION	109
1.	C3G plays a role in platelet hemostasis.	109
2.	C3G plays a role in the regulation of pathological megakaryopoiesis	110
3.	C3G controls protein ubiquitination in platelets.....	115
4.	Platelet C3G differentially regulates the release of pro- and antiangiogenic factors, leading to hemangiocyte recruitment in response to hypoxia.	116
5.	C3G participates in platelet-tumor cell communication, facilitating metastasis	118
6.	Conclusion	119
	CONCLUSIONS	123
	CONCLUSIONES	124
	REFERENCES	127

LIST OF FIGURES

INTRODUCTION

Figure I-1. Rap1b activation and deactivation cycle.....	3
Figure I-2. C3G primary structure.....	4
Figure I-3. Megakaryocyte maturation and differentiation.....	8
Figure I-4. Signaling pathways induced by TPO-c-Mpl.....	10
Figure I-5. Platelet regulates their own mas by modulating TPO plasma levels.....	11
Figure I-6. Platelet ultrastructure.....	12
Figure I-7. Platelets and hemostasia.....	13
Figure I-8. C3G regulates platelet activation and aggregation by controlling major signaling pathways.....	15
Figure I-9. Angiogenesis.....	18
Figure I-10. Granule secretion in platelets.....	21
Figure I-11. c-Cbl regulates TPO clearance from plasma.....	23
Figure I-12. Platelets induces metastasis at different levels.....	28

MATERIALS & METHODS

Figure M-1. Tumor-induced ischemia model.....	45
Figure M-2. Induction of ischemia in the hind-limb.....	46
Figure M-3. Hind-limb ischemia model.....	47
Figure M-4. In vivo model of TPO-induced megakaryopoiesis.....	47
Figure M-5. In vivo model of myeloablation and megakaryopoiesis induced by 5-FU.....	48

RESULTS

Figure R-1. Successful deletion of C3G in platelets and megakaryocytes from C3G-KO mice.....	62
Figure R-2. C3G ablation in platelets results in impaired platelet coagulation, causing bleeding diathesis.....	64
Figure R-3. C3G ablation do not alter basal levels of platelets in PB or Mk in BM.....	65
Figure R-4. C3G ablation promotes MK differentiation <i>in vitro</i>	66

Figure R-5. C3G-KO mice respond more efficiently to TPO intravenous injection than control mice.....	68
Figure R-6. C3G ablation produces a delay in platelet rebound and failed to downregulate platelet levels after 5-FU-induced myelosuppression.....	69
Figure R-7. C3G overexpression promoted platelet rebound after 5-FU-induced myelosuppression and produced faster downregulation of platelet levels.....	70
Figure R-8. C3G regulates c-Mpl in Mks and platelets.....	71
Figure R-9. Platelet C3G expression levels and activity controls c-Mpl degradation upon TPO stimulation.....	72
Figure R-10. Platelet C3G is necessary for c-Mpl internalization upon TPO stimulation.....	73
Figure R-11. C3G-KO mice showed lower levels of TPO in plasma after TPO administration.....	74
Figure R-12. C3G-KO platelets fails to uptake TPO <i>in vitro</i>	75
Figure R-13. c-Cbl immunoprecipitates with C3G in resting platelets and upon ADP and TPO stimulation.....	75
Figure R-14. C3G colocalizes with c-Cbl in platelets.....	76
Figure R-15. C3G promotes c-Cbl phosphorylation.....	77
Figure R-16. C3G promotes c-Cbl phosphorylation by Src in response to TPO.....	79
Figure R-17. C3G regulates c-Cbl phosphorylation by Src and c-Mpl ubiquitination and degradation.....	80
Figure R-18. C3G regulates c-Mpl ubiquitination.....	82
Figure R-19. C3G overexpression increases c-Mpl ubiquitination in TPO-stimulated platelets.....	84
Figure R-20. Proteasome inhibition triggers accumulation c-Mpl and ubiquitinated proteins in C3G-KO platelets.....	85
Figure R-21. Lysosome inhibition results in accumulation c-Mpl and ubiquitinated proteins in C3G-KO platelets.....	86
Figure R-22. Platelet C3G is necessary for the correct c-Mpl degradation by the proteasome and lysosome systems.....	87
Figure R-23. Platelet C3G regulates hemangiocyte recruitment in response to tumor cell growth.....	90
Figure R-24. C3G ablation in platelets promotes tumor growth and angiogenesis.....	91
Figure R-25. C3G overexpression in platelets promotes blood flow recovery after hind-limb ischemia but diminished hemangiocyte recruitment.....	92
Figure R-26. C3G overexpression in platelets increased <i>Sdf1</i> and <i>Cd31</i> mRNA expression in ischemic muscle.....	93

Figure R-27. Platelet C3G ablation promotes blood flow recovery and hemangiocyte recruitment after hind-limb ischemia.....	93
Figure R-28. Platelet C3G ablation promotes neovascularization after hind-limb ischemia.....	94
Figure R-29. Platelet C3G controls hemangiocyte recruitment through the release of SDF-1.....	96
Figure R-30. C3G regulates the release of SDF-1 from platelets.....	97
Figure R-31. C3G-KO platelets show increased VEGF release and TSP1 retention in response to thrombin.....	98
Figure R-32. Platelet C3G regulates the release of VEGF and TSP-1.....	99
Figure R-33. Releasate from thrombin-stimulated C3G-KO platelets promotes a higher formation of capillary networks in HUVEC.....	101
Figure R-34. C3G regulates short-term metastasis.....	102
Figure R-35. C3G overexpression promotes melanoma cell adhesion.....	103
Figure R-36. Platelet C3G ablation diminished melanoma cell adhesion.....	104
Figure R-37. C3G regulates platelet activation in response to melanoma cells.....	105
Figure R-38. C3G contributes to TCIPA induced by B16-F10 cells.....	106

DISCUSSION

Figure D-1. The C3G-Src-c-Cbl pathway is essential for c-Mpl internalization and the maintenance of hemostatic TPO plasma levels.....	113
Figure D-2. Schematic representation of the participation of platelet C3G in hemangiocyte recruitment in response to ischemia.....	117

LIST OF TABLES

Materials & Methods

Table M-1. Primers used in the genotyping of the mouse models used in this work.....	35
Table M-2. Cell lines used in this work.....	36
Table M-3. Cytokines used for the differentiation of BMC into megakaryocyte, indicating working concentration and suppliers.....	37
Table M-4. Platelet agonist used.....	38
Table M-5. Inhibitors of SFK, proteasome and lysosome used.....	38
Table M-6. Fluorochrome-conjugated antibodies for flow cytometry.....	40
Table M-7. Sequence of primers used in qPCR.....	51
Table M-8. SDS-PAGE stacking and separating gel composition.....	53
Table M-9. Primary and secondary antibodies used for western blot.....	54
Table M-10. Primary and secondary antibodies used for immunofluorescence.....	55

Results

Table R-1. C3G ablation did not modify platelet count or platelet parameters.....	65
Table R-2. C3G-KO platelets showed a significant decrease in Rpn1 abundance.....	88

INTRODUCTION

INTRODUCTION

1. C3G

1.1. Generalities

C3G (Crk SH3-domain-binding guanine-nucleotide-releasing factor) is a ubiquitously expressed protein that functions as a GEF (**G**uanine **N**ucleotide **E**xchange **F**actor) for several members of the Ras family of GTPases: Rap1, R-Ras and TC21, and for the member of the Rho family, TC10 (S. H. Chiang *et al.*, 2001; Gotoh *et al.*, 1995, 1997; Ohba *et al.*, 2000). C3G was firstly isolated and described in 1994 by the group of Mitsushiro Matsuda as a Crk SH3-binding protein (Tanaka *et al.*, 1994) and later identified as a Rap1 GEF (Gotoh *et al.*, 1995). Alternative names for C3G are Rapgef1 (the canonical name) and Grf2.

1.2. C3G as a GEF

Small GTPases are proteins that regulate a variety of cellular processes, including proliferation, differentiation, and vesicular trafficking. These proteins function as molecular switches, cycling between two conformational states: one active (GTP-bound) and one inactive (GDP-bound). GEFs catalyze the exchange of GDP to GTP, they promote the release of bound GDP and its replacement by GTP. Conversely, there are other group of proteins, known as GTPases Activating Proteins (GAPs) which activate the hydrolysis of GTP to GDP, resulting in the inactivation of the GTPases (Bos *et al.*, 2007). **Figure I-1** shows the activation/deactivation cycle of Rap1b, the main target of C3G in platelets.

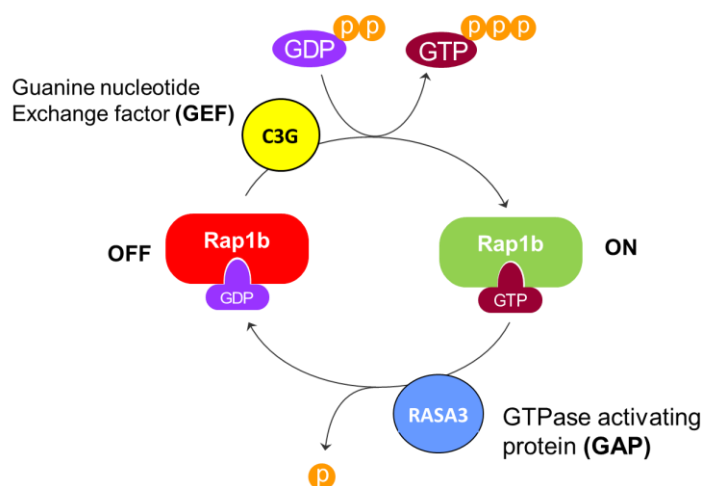


Figure I-1. Rap1b activation and deactivation cycle. GTPases acts as molecular switches cycling between two states: one active or GTP-bound and one inactive or GDP-bound. The exchange of GDP to GTP is catalyzed by GEF proteins, while GAPs, such as RASA3 promotes the hydrolysis of GTP and hence, the inactivation of the GTPase.

1.3. Structure

C3G is a 140 kDa protein with multiple well-defined functional and structural domains (**Figure I-2**).

The C-terminal region of C3G contains the catalytic domain, which is common to all Ras protein activators. This region, also known as CDC25-H, for its homology with the CDC25 protein of *S. cerevisiae*, comprises 224 aa and is responsible for the exchange of GDP to GTP. Upstream the catalytic domain is the REM (Ras Exchange Motif) domain, which participates in the exchange reaction. The central region contains five proline-rich sequences that follow the Pro-Pro-X-X-Pro-X-K/R consensus sequence (Knudsen *et al.*, 1994). This domain interacts with SH3 motifs present in several proteins, including Crk, Hck, p130Cas, c-Abl and the oncoprotein Bcr-Abl (Gutiérrez-Berzal *et al.*, 2006; Kirsch *et al.*, 1998; Maia *et al.*, 2013; Radha *et al.*, 2007; Shivakrupa *et al.*, 2003; Tanaka *et al.*, 1994; Wu *et al.*, 1995) and is therefore called SH3-binding domain (SH3b). Furthermore, our group has recently discovered the existence of an autoinhibitory region (AIR) within the SH3b domain, which binds to, and inhibits the CDC25-H catalytic domain (Carabias *et al.*, 2020). Interestingly, two missense mutations (Y554H and M555K) in AIR have been described in Hodgkin's non-lymphomas. These mutations disrupt the interaction between the AIR and the catalytic domain, blocking the autoinhibitory mechanism and leading to an hyperactive protein (Carabias *et al.*, 2020). The N-terminal region harbors an E-cadherin binding domain, through which C3G participates in the recruitment of E-cadherin during the initial steps of junction formation (Hogan *et al.*, 2004). The N-terminal domain also participates in the catalytic activity of C3G through its binding to the REM domain (Carabias *et al.*, 2020).

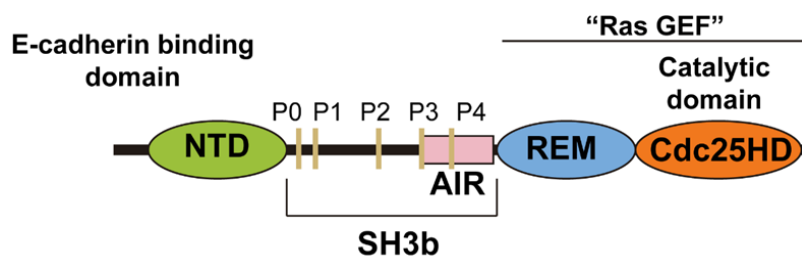


Figure I-2. C3G primary structure. The different domains composing C3G are indicated. NTD: N-terminal domain, SH3b: SH3-binding domain, P: prolin, AIR: autoinhibitory region, REM: Ras-exchange motif.

1.4. C3G functions

C3G has a role in a wide range of cellular processes such as proliferation, differentiation, cellular migration, adhesion, apoptosis and cell-cell interaction (Radha *et al.*, 2011). These functions can be mediated by its GEF activity or by the SH3-binding domain. Some of these functions are detailed below.

1.4.1. C3G in embryonic development.

C3G-dependent Rap1 activation was described as critical for embryonic development (Ohba *et al.*, 2001). C3G knock out mice (C3G^{-/-}) perish before embryonic day 7.5 (E7.5) development. The analysis of the embryos between E7.5 and E8.5 revealed the lack of a conventional placenta or fetal structure. Although embryonic fibroblasts (MEFs) from these mice showed a morphology that was indistinguishable from wild-type MEFs, cell adhesion and spreading were hindered in C3G^{-/-} MEFs, and cell migration was accelerated. The embryonic lethality of C3G^{-/-} mice was explained by these abnormalities. Reexpression of human C3G in the C3G null MEFs reversed the phenotype, confirming the relevance of C3G-Rap1 pathway in the regulation of adhesion and migration. C3G is also essential to maintain pluripotency of MEFs through the regulation of STAT and ERK pathways (Vishnu *et al.*, 2021).

The role of C3G during brain development has been studied in detail. The C3G-Rap1 pathway controls the size of brain precursors through inhibition of proliferative pathways β -catenin, Akt, and Ras-ERKs (Voss *et al.*, 2006) and is required for neural precursor migration and differentiation (Voss *et al.*, 2008). Furthermore, C3G is required for the transition of multipolar neural to a bipolar morphology during cortical development (Shah *et al.*, 2016).

C3G also participates in the regulation of centrosome duplication. C3G colocalizes with sub-distal appendages of mother centrioles in interphase cells and is required for maintenance of primary cilia length. Regulation of centrosome duplication and preservation of cilia homeostasis may be crucial for the role of C3G in embryonic development (S. C. Nayak & Radha, 2020).

1.4.2. C3G in cancer

The tumor suppressor properties of C3G have been well documented over the past years. C3G suppresses malignant transformation of NIH3T3 cells caused by overexpression of several oncogenes, such as *sis*, *ras*, *v-raf*, *dbl* and *R-ras* (Guerrero *et al.*, 1998). This is achieved through its SH3b domain, and involves PP2A-mediated

inhibition of ERK phosphorylation, resulting in loss of the anchorage-independent growth ability of the oncogenic cells (Guerrero *et al.*, 2004; Martín-Encabo *et al.*, 2007). According to this tumor suppression role, C3G expression is decreased in squamous cell carcinoma (Okino *et al.*, 2006) and C3G downregulation is linked to increased migration and aggressiveness of glioblastoma cells (Manzano *et al.*, 2021).

On the other hand, C3G can also function as a tumor promoter. C3G is overexpressed in non-small cell lung cancer (Okino *et al.*, 2006). Furthermore, in some gastrointestinal and gynecological cancers, the first intron of the *RAPGEF1* gene shows a somatic demethylation, which is linked to increased expression (Samuelsson *et al.*, 2011). C3G is a key player in the growth and progression of hepatocellular carcinoma (HCC) tumors, but its downregulation is required for HCC invasion (Sequera *et al.*, 2020). This dual effect of C3G is also found in colorectal cancer, inhibiting migration and invasion via Rap1-mediated p38 α downregulation, while increasing tumor growth through a p38 α independent mechanism (Priego *et al.*, 2016).

Furthermore, primary cells from Chronic Myeloid Leukemia (CML) patients express a shorter C3G isoform, p87C3G, that lacks the most amino terminal region of the canonical protein. p87C3G co-immunoprecipitates with p210-Bcr-Abl and is phosphorylated *in vitro* by this kinase, suggesting that p87C3G is involved in the development of CML (Gutiérrez-Berzal *et al.*, 2006). In addition, C3G downregulation in CML cells has a dual effect, enhancing STI-571 (a specific inhibitor of p210-Bcr-Abl)-induced apoptosis, by abrogation of the inhibitory effect of Rap1 on p38, and promoting survival through Rap1 independent mechanisms (Maia *et al.*, 2009).

1.4.3. C3G in cell differentiation

In the last few years, several publications have demonstrated the role of C3G in the modulation of cell differentiation in a variety of cell types. C3G ablation in embryonic mouse stem cells (mESCs) induces persistent self-renewal and resistance to differentiation, in response to cytokine leukaemia inhibitory factor (LIF) withdrawal, (Vishnu *et al.*, 2021). In addition, C3G overexpression in mouse mesenchymal cells increases survival and myogenic differentiation controlling the activity of Akt (Sasi Kumar *et al.*, 2015).

Furthermore, a novel isoform of C3G, 175 kDa, has been described to be the only one detected in post-natal brain (Sriram *et al.*, 2020). In addition, C3G participates in neuroblastoma cell differentiation by inducing the expression of cell cycle inhibitor p21 (Sasi Kumar *et al.*, 2015).

The expression of a constitutively active version of C3G in hematopoietic stem cells (HSC) hindered long-term hematopoiesis via Rap1 activation, through promoting increased proliferation and differentiation of HSC (Imai *et al.*, 2019). C3G overexpression enhances megakaryocyte (Mk) differentiation and proplatelet formation *in vitro* and *in vivo*. However, overexpression of C3G in mice does not correlate with an increase in platelet number (Ortiz-Rivero *et al.*, 2018).

1.4.4. C3G in platelet biology

Rap1b GTPase plays an important role in the regulation of platelet function. C3G, which is expressed on human and mouse platelets, mediates platelet activity triggered by thrombin, PMA, ADP and collagen through the activation of Rap1b (Gutiérrez-Herrero *et al.*, 2012, 2020). The role of C3G in platelet biology is explained in depth in **Section 3.3**.

2. Megakaryopoiesis

Megakaryopoiesis is the process by which HSC differentiate into Mk (Yu & Cantor, 2012). This is a complex process affected by multiple cytokines and other environmental factors. HSC is enriched in a population of Lin⁻Sca1⁺c-Kit⁺ (LSK) cells. This population is divided into three groups based on their self-renewal capacity: (i) long-term hematopoietic stem cell (LT-HSC, LSK CD34⁺Flt3⁻), responsible for the maintenance of the stem cell pool; (ii) short-term hematopoietic stem cell (ST-HSC, LSK CD34⁺Flt3⁺) that can only sustain hematopoiesis for a short period of time (Morrison & Weissman, 1994; Seita & Weissman, 2010; Yang *et al.*, 2005); (iii) multipotent progenitors (MPPs), a group of non-renewing lineage-biased progenitor cells that differentiate into the common lymphoid progenitor (CLP) and the common myeloid progenitor (CMP), the latter of which will give rise to the megakaryocyte-erythrocyte progenitor (MEP) (Noetzli *et al.*, 2019). MEPs develop into megakaryocyte progenitors (MkP), which comprise the burst-forming unit-megakaryocyte (BFU-Mk) and the colony-forming unit-megakaryocyte (CFU-Mks) progenitors. BFU-Mk is the most primitive MkP, and is able to produce produce in response to environmental factors or cytokines, a significant number of CFU-Mks, which are a more differentiated MkP CFU-Mks mature into immature megakaryocytes or megakaryoblasts, which undergo endomitosis and increase in size and DNA content to become a mature Mk (Vainchenker *et al.*, 2021). An alternative model of megakaryocyte differentiation has been proposed, in which HSCs derive directly into Mk, bypassing the classical Mk progenitors CMP and MEP (**Figure I-3**) (Woolthuis & Park, 2016).

Megakaryocytes are the largest (50-100 μm) cells in the bone marrow (BM). They represent 0.01% of nucleated cells and are responsible for the formation of platelets. During their maturation process, Mks increase in size, accumulate specific granules and cytoskeletal proteins, develop the invaginated membrane system (also known as Demarcation Membrane System or DMS (Radley & Haller, 1982) and acquire Mk-specific cell surface markers. Finally, mature Mks extend long protrusions, known as proplatelets, into the marrow intravascular sinusoidal space where, under shear and turbulent flow, platelets are produced and released into the blood stream (Machlus & Italiano, 2013). Although the BM has been proposed to be the primary site of platelet formation, the lungs has recently been described as a substantial source of platelet biogenesis (Lefrançois *et al.*, 2017).

The expression of Mk-specific cell surface markers changes throughout Mk maturation. MEP cells are characterized by $\text{Lin}^{-}\text{Sca1}^{-}\text{c-Kit}^{+}\text{CD34}^{+}$ cell surface markers phenotype (Akashi *et al.*, 2000). CD41 or glycoprotein IIb (GPIIb) is one of the Mk-specific cell surface markers that is already present in MEPs. When MEPs differentiate into megakaryoblasts, they lose the expression of CD34 and begin to express CD61 (GPIIIa). Finally, at later stages of Mk differentiation, CD42 expression emerges, which is associated with a marked increase in the expression of c-Mpl, GPVI (collagen receptor), integrin $\alpha 2\beta 1$ and specific α -granule proteins, such as PF4 (Platelet Factor 4) and von Willebrand Factor (vWF) (Chang *et al.*, 2007, **Figure I-3**).

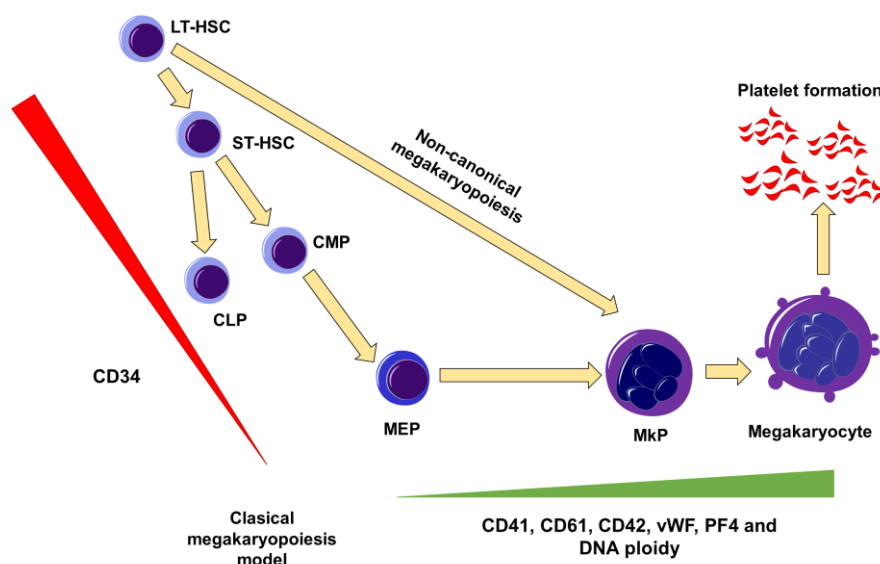


Figure I-3. Megakaryocyte maturation and differentiation. The figure illustrates the development of mature Mks and platelets from HSC, showing the classical model, with the transition from HSC to CMP and MEP, and the non-canonical megakaryopoiesis in which HSC gives rise directly to MkPs. Associated surface markers are shown to indicate the Mk stage in which they are expressed.

The transition from HSC to mature Mk is regulated by several cytokines, thrombopoietin (TPO) being the most important (Hitchcock & Kaushansky, 2014).

2.1. TPO triggers megakaryocyte differentiation through different pathways

As previously stated, TPO is the main cytokine involved in Mk differentiation, and capable of direct megakaryopoiesis on its own. TPO is constitutively expressed in the liver, and its expression is also found in the kidney, smooth muscle and a variety of other organs (Hitchcock & Kaushansky, 2014; S. Qian *et al.*, 1998). To promote megakaryopoiesis, TPO binds to its receptor c-Mpl, which is expressed on the surface of Mk, Mk progenitors and platelets. TPO binding to c-Mpl stimulates receptor dimerization, which activates Janus Kinase 2 (Jak2). When Jak2 is active, it phosphorylates c-Mpl, allowing the recruitment of proteins implicated in numerous signaling pathways that regulate the expression of genes involved in Mk differentiation and platelet formation. JAK-STAT, mitogen-activated protein kinase (MAPK) and phosphatidylinositol-3-kinase (PI3K) are the main pathways triggered by TPO (**Figure I-4**) (Hitchcock & Kaushansky, 2014).

During Mk differentiation, PMA and TPO stimulates the Ras/Raf/MEK/ERK pathway. The fast activation of extracellular signal-regulated kinases 1 and 2 (ERK 1/2) in K562 cells following treatment with PMA is linked to Mk differentiation (Herrera *et al.*, 1998). TPO stimulation of the c-Mpl receptor causes Ras activation by recruiting Sos (Rouyez *et al.*, 1997). However, TPO-induced Ras pathway leads to a transient ERK 1/2 activation, whereas Mk differentiation and maturation requires a sustained activation of ERKs, which is provided by the activation of Rap1/b-B-Raf (Stork & Dillon, 2005). Although there is no confirmation about the GEF involved in Rap1 activation in response to TPO, an association of the CrkL/C3G complex with the c-Mpl receptor has been described (**Figure I-4**) (Oda, Miyakawa, *et al.*, 1996; Reedquist *et al.*, 1996; Stork & Dillon, 2005).

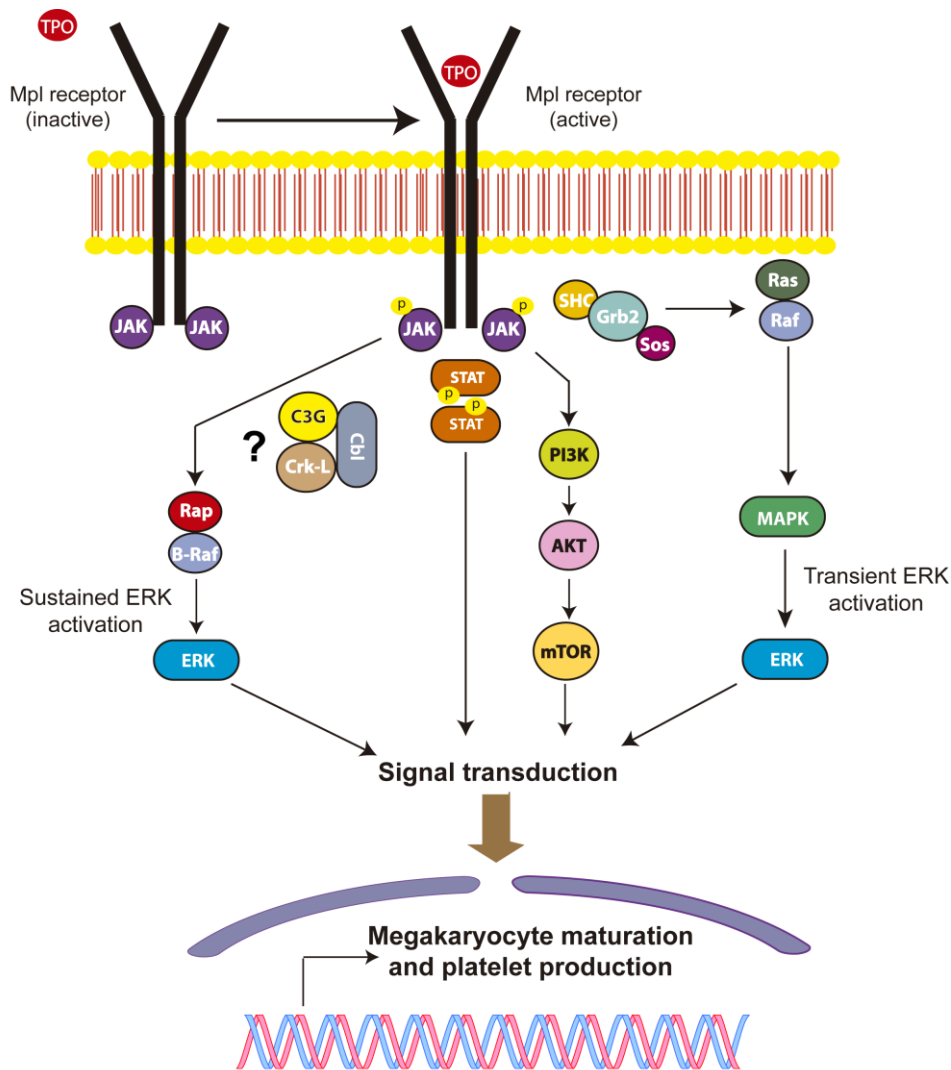


Figure I-4. Signaling pathways induced by TPO-c-Mpl. In Mks TPO binds to its receptor, c-Mpl, and initiates the activation of several signaling pathways, including JAK-STAT, Ras/Raf/MAPK/ERK, PI3K/AKT/mTOR and Rap1/B-Raf/ERK. The GEF involved in Rap1 activation in response to TPO remains unknown, although it has been proposed that C3G participates in the sustained activation of ERK via Rap1, essential for Mk differentiation (Stork & Dillon, 2005).

2.1.1. Negative regulation of TPO/c-Mpl signaling

TPO is constitutively expressed in hepatocytes, therefore, there is no change in TPO mRNA levels in the liver. To prevent excessive platelet formation and subsequent myeloproliferative disorders, it is critical to maintain adequate plasma TPO levels (**Figure I-5**). TPO levels are controlled by platelet mass; when TPO binds to c-Mpl on the surface of platelets, the TPO/c-Mpl complex is internalized and degraded by the proteasome and lysosome. Therefore, platelets act as a TPO sink, removing excess TPO from plasma (Fielder *et al.*, 1996). In fact, there is an inverse correlation between plasma TPO levels and the number of platelets (Kuter & Rosenberg, 1995). TPO is rapidly internalized in a

situation of high number of platelets in the blood, or thrombocytosis, preventing it from reaching the BM and thus, avoiding Mk differentiation. In contrast, when there is a low platelet count or thrombocytopenia, little TPO is cleared from the circulation, so it reaches the bone marrow, where it stimulates Mk maturation and platelet formation (Hitchcock *et al.*, 2021).

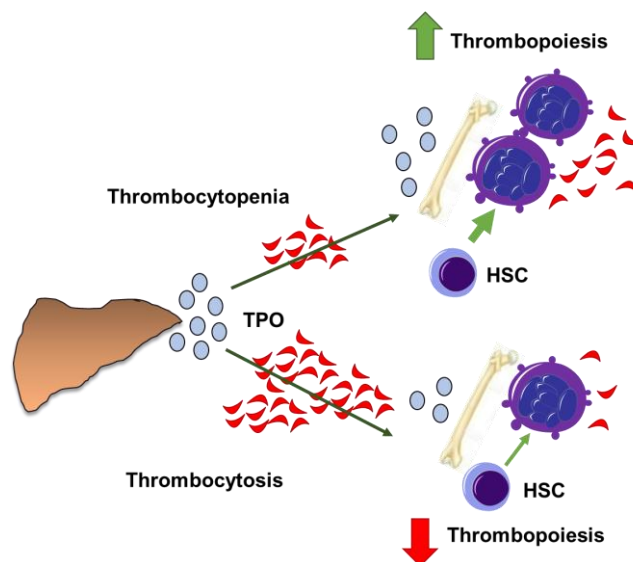


Figure I-5. Platelet regulates their own mass by modulating plasma TPO levels. TPO is constitutively produced in the liver. Platelets performed TPO clearance from plasma to maintain TPO homeostatic levels. In the situation of low platelet count (thrombocytopenia), TPO can not be removed from plasma and arrive to the BM, where it drives Mk differentiation and platelet formation. In contrast, high platelet count (thrombocytosis), rapidly eliminate TPO from plasma, leading to low levels of TPO signaling in Mks.

2.2. Other cytokines involved in Mk differentiation

Although TPO is sufficient to carry out megakaryopoiesis, there are other cytokines that participate in certain phases of Mk differentiation (Behrens & Alexander, 2018). Interleukin (IL)-6 and IL-11 increase Mk size *in vitro* and platelet production *in vivo*. Furthermore, SCF (Stem Cell Factor) works synergistically with TPO to enhance MkP proliferation. *In vitro*, IL-3 also promotes MkP cell proliferation (Metcalf *et al.*, 1986), however it does not increase platelet count when administered *in vivo* (Ishibashi *et al.*, 1990).

3. Platelets

Platelets are anucleate cell pieces approximately 2-5 μm in size produced by Mk cytoplasmatic fragmentation. Once platelets are released into the blood stream, they have a lifespan of 5 days in mice (Lebois & Josefsson, 2016) and around 7 days in humans (Harker, 1977). Despite their small size, several organelles are found in

platelets, including the open canicular system (OCS), which is formed by cytoplasmic membrane invaginations; the dense tubular system (DTS), which stores calcium and enzymes involved in platelet activation, and three different types of granules: α -granules, δ -granules and lysosomes (**Figure I-6**) (Rendu & Brohard-Bohn, 2001; Thon & Italiano, 2012).

α -granules are the most abundant and largest granules inside platelets (50-80 per platelet (Frojmovic & Milton, 1982)). They store a wide range of factors that participate in several processes, including hemostasis, inflammation, wound healing and angiogenesis. The most relevant angiogenic factors of platelets are the proangiogenic factor VEGF (vascular endothelial growth factor) and the antiangiogenic factor TSP-1 (thrombospondin) (Flaumenhaft & Sharda, 2018).

δ -granules (or dense bodies) are less abundant in platelets than α -granules, with only 3-8 dense granules per human platelet. Dense bodies, which contains serotonin, calcium, pyrophosphate, and a non-metabolic pool of ADP and ATP, assist platelet activation and recruitment at the site of vascular damage (Y. Chen *et al.*, 2018; McNicol & Israels, 1999).

Platelets also contain lysosomes, which are the rarest granules in platelets. They carry a variety of digestive enzymes that are active in acidic environments (Bentfeld-Barker & Bainton, 1982).

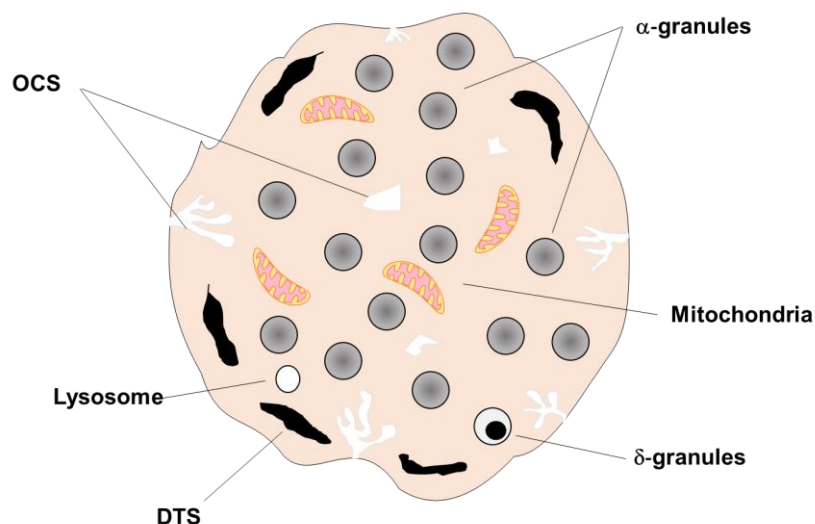


Figure I-6. Platelet ultrastructure. Schematic representation of platelet organelles. The different platelet-granules, mitochondria, Dense Tubular System (DTS) and Open Canicular System (OCS) are represented.

Platelets are best known for their role in hemostasis, but the large amount of substances they contain allows them to control a wide range of physiological and pathological processes, including angiogenesis (Battinelli *et al.*, 2011), inflammation (Bakogiannis *et al.*, 2019), tumor development (Ji & Kwon, 2017), and metastasis (Schlesinger, 2018).

3.1. Platelets and hemostasia

Platelets are the main regulators of hemostasis. When there is no vascular injury, endothelial cells (ECs) prevent platelet activation by releasing nitric oxide (NO) and endothelial prostaglandins, keeping platelets in a quiescent state (**Figure I-7**) (Smolenski, 2012).

Damage to the vasculature wall exposes different extracellular matrix proteins, mainly collagen and vWF, which interact with their receptors on the platelet surface. This interaction causes platelet adhesion to the damage area, resulting in the activation of different signaling pathways involved in cytoskeleton reorganization. Hence, platelets extend over the damage area and release factors like ADP and thromboxane A2 (TXA₂), which activates adjacent platelets amplifying the signal (Stalker *et al.*, 2013). Furthermore, platelet activation entails a series of events that culminate in a conformational change in integrin αIIbβ₃, resulting in its activation. The inactive form of integrin αIIbβ₃ has low affinity for its ligand fibrinogen, but this affinity increases when platelets are activated. Because fibrinogen may connect to receptors on several platelets at the same time, it forms fibrinogen “bridges” that start the platelet aggregation process and the formation of the platelet plug (**Figure I-7**) (Y. Q. Ma *et al.*, 2007).

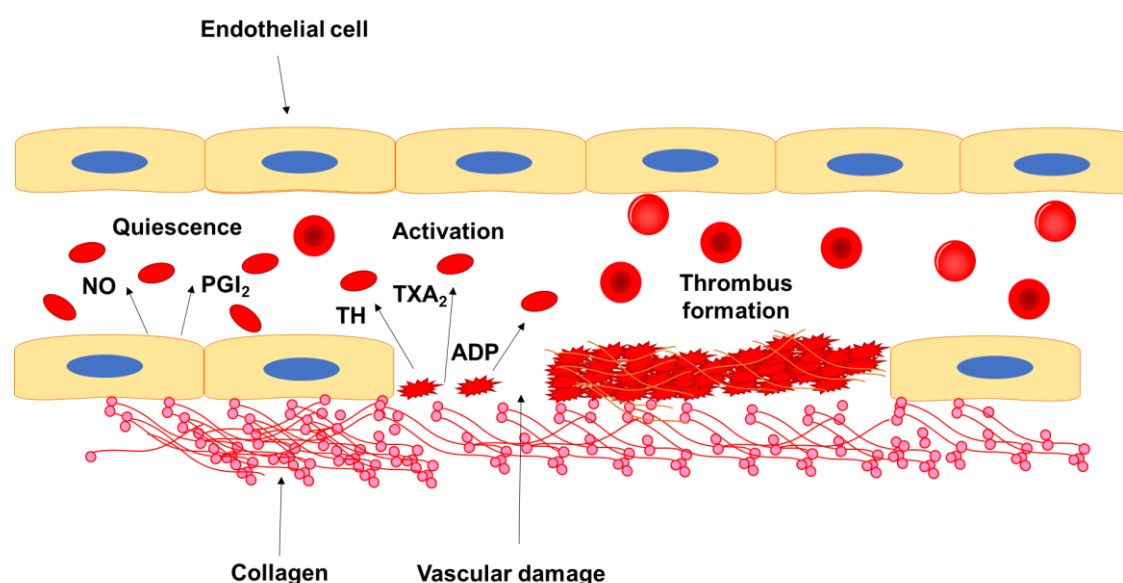


Figure I-7. Platelets and hemostasia. In absence of vascular damage, platelets are inhibited by ECs (endothelial cells) through the release of NO and PGI₂. When the vasculature wall is disrupted, components of the ECM (extracellular matrix) become exposed (collagen, vWF) and activate platelets. Active platelets release several hemostatic factors that trigger the coagulation cascade and the formation of the thrombus.

Although a large number of platelets can create this first plug, it is not yet stable enough. The transformation of fibrinogen into fibrin, a fibrillar protein that creates tridimensional networks that help clot formation, is required to strengthen the plug. This process is controlled by the activation of the extrinsic and intrinsic coagulation cascades. Both signaling pathways, which include a variety of enzymes, lead to the activation of the Xa factor, which stimulates the conversion of fibrinogen to fibrin. As a result, the clot is finally formed to stop bleeding (Shibata *et al.*, 2008).

Eventually, the clots are reabsorbed by a process known as fibrinolysis, driven primarily by plasmin, a proteolytic protein involved in the degradation of fibrinogen and the fibrin network, which results in the removal of the clot and the end of the coagulation process (Kanji *et al.*, 2021).

3.2. C3G contributes to platelet activation and aggregation

Platelet function is primarily controlled by the GTPase Rap1b, whose activation is triggered by a variety of stimuli. Rap1b is activated by several GEFs, being CalDAG-GEFI (RasGRP2) the main platelet GEF of Rap1b (Franke *et al.*, 1997; Stefanini & Bergmeier, 2016). CalDAG-GEFI knock out mice exhibit a deficient inside-out signaling, which results in an impaired aggregation, in response to several platelet agonists. However, platelet aggregation is not affected by high doses of thrombin or diacylglycerol (DAG) analog, phorbol 12-myristate 13-acetate (PMA), suggesting the existence of another Rap1 GEF involved in platelet function (Crittenden *et al.*, 2004).

C3G expression has been detected in human (Burkhart *et al.*, 2012; Rowley *et al.*, 2011) and mouse platelets (Rowley *et al.*, 2011; Zeiler *et al.*, 2014). Using mouse models that overexpress C3G (tgC3G mice) or a mutant form of C3G which lacks the catalytic domain (tgC3G Δ Cat), specifically in Mk and platelets our group previously demonstrated the participation of C3G in platelet activation and function. Indeed, tgC3G mice show increased platelet activation and aggregation, which correlated with decreased bleeding time. Conversely, tgC3G Δ Cat mice showed bleeding diathesis as a result of defective platelet activation and aggregation (Gutiérrez-Herrero *et al.*, 2012). Elimination of C3G in Mks and platelets confirmed the role of C3G in platelet hemostasis (Gutiérrez-Herrero *et al.*, 2020).

Platelets show a fast Rap1b activation in response to thrombin that is mediated through calcium-CaLDAG-GEFI (Harper *et al.*, 2010; Rosado & Sage, 2000). Thrombin induces a second wave of Rap1b activation independent on CaLDAG-GEFI, in which C3G is involved (Franke *et al.*, 2000; Gutiérrez-Herrero *et al.*, 2012). Regarding this latter signaling pathway, it has been shown that the binding of thrombin to its receptor stimulates PKC, which phosphorylates Src, which in turn phosphorylates and activates C3G. Thrombin also activates p38/ERK, which is involved on C3G activation by two different mechanisms. First, it stimulates TXA₂ production, which activates Src-C3G; second, it inhibits Shp2, the phosphatase that dephosphorylates and inhibits C3G. C3G also activates Rap1 via PI3K following ADP-P2Y₁₂ activation (**Figure I-8**) (Gutiérrez-Herrero *et al.*, 2020).

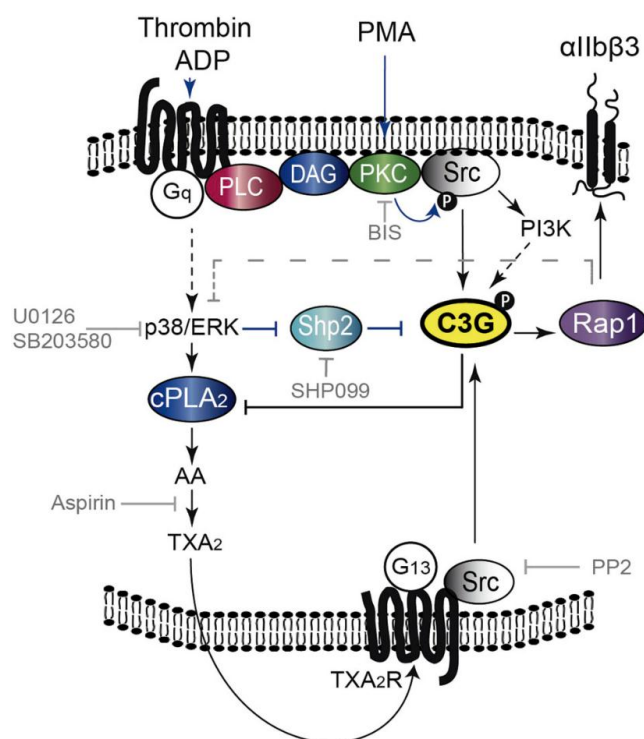


Figure I-8. C3G regulates platelet activation and aggregation by controlling major signaling pathways. C3G participates in the second wave of Rap1 activation induced by thrombin, which leads to its activation by phosphorylation at Tyr504 through the PKC-Src pathway. C3G phosphorylation is also regulated by ERKs and p38 MAPKs: ERKs inhibit the Shp2 tyrosine phosphatase, allowing C3G phosphorylation, and both MAPK control the production of TXA₂. C3G, via Rap1-dependent and -independent mechanism, regulates TXA₂ synthesis through a negative feedback loop involving the inhibition of cPLA₂. PLC: phospholipase A₂; DAG: diacylglycerol; AA: arachidonic acid; TXA₂: thromboxane A₂, TXA₂R: TXA₂ receptor; cPLA₂: cytosolic phospholipase A₂; BIS: bisindolylmaleimide, an inhibitor of PKC; PP2: a Src inhibitor; wortmannin: a PI3K inhibitor; SHP099: a Shp2 inhibitor; U0126: an ERK inhibitor; SB203580: a p38α/β MAPK inhibitor; aspirin: a cyclooxygenase inhibitor. Dashed grey lines indicate a hypothetical Rap1-dependent pathway that could regulate the activation of ERKs and p38 MAPKs Gutiérrez-Herrero *et al.*, 2020

3.3. Platelet and angiogenesis

3.3.1. Angiogenesis

Vasculogenesis is the process of generation of a primary vascular plexus from endothelial cell progenitors during the early stages of embryonic development. Angiogenesis, on the other hand, is the process of forming new blood vessels from pre-existing ones, and it is involved in both healthy (embryonic development, tissue regeneration) and pathological (tumor growth and metastasis) vessel formation (Ozel *et al.*, 2022; Patan, 2004).

Angiogenesis is a tightly controlled process that encompasses cell proliferation, differentiation, migration, matrix adhesion and cell-cell contact (Potente *et al.*, 2011). During angiogenesis ECs develop, in response to a variety of stimuli, into an endothelial sprout, formed by tip and stalk cells (Adams & Alitalo, 2007; Eelen *et al.*, 2020).

Tip cells are found at the distal end of the endothelial sprout and direct the growth and development of the vasculature. Stalk cells are located downstream of the tip cell, present a high proliferative rate and create the lumen of the new blood vessel (Gerhardt *et al.*, 2003). The behavior of tip and stalk cells is finely regulated by VEGF-A gradients. In response to VEGF-A tip cells differentiate and proliferate (**Figure I-9 A**). In addition, when VEGF-A binds to its receptor VEGFR-2, also known as Flk1 (fetal liver kinase 1), tip cells produce Delta-like ligand 4 (DLL4). The binding of this ligand to its Notch receptor on the surface of stalk cells provoke the suppression of the tip phenotype, favoring the stalk one (**Figure I-9 A**) (Thurston & Kitajewski, 2008). DLL4 ablation causes excessive sprouting and EC hyperproliferation (Lobov *et al.*, 2007). In contrast, another Notch ligand, Jagged1, which is expressed more abundantly in stalk cells than in tip cells, inhibits DLL4-Notch signaling and promotes the tip cell phenotype (Benedito *et al.*, 2009).

In order to form the new vessel, the initial sprout grow in response to three mechanisms: (i) chemotaxis: the directional growth in response to a gradient of soluble chemoattractants; (ii) haptotaxis: the directional gradient in response to immobilized ligands; and (iii) mechanotaxis: the directional migration generated by mechanical forces (Lamallice *et al.*, 2007). The main regulators of chemotaxis are VEGF and basic Fibroblast Growth Factor (bFGF), while haptotaxis is controlled by the binding of integrins to the extracellular matrix (ECM) (Gerhardt *et al.*, 2003; Klemke *et al.*, 1997). Finally, cell migration is promoted and modulated by shear stress and the stiffness of the surrounding ECM (Kretschmer *et al.*, 2021; S. Li *et al.*, 2005).

VEGF is the master regulator of vascular development. The VEGF family in mammals is comprised of five secreted proteins, VEGF-A, B, C, D and placenta growth factor (PLGF), which bind to three different receptor tyrosine kinases: VEGFR-1, 2 and 3. VEGFR-1 and VEGFR-2 are essential for angiogenesis from ECs, while VEGFR-3 is more critical in lymphangiogenesis (Matsumoto & Ema, 2014). VEGF-A shows a higher affinity for VEGFR-1 than for VEGFR-2, although the signaling induced by the latter is the main mechanism by which VEGF-A governs EC migration (Koch & Claesson-Welsh, 2012). However, VEGFR-1 serves as a VEGF-trap, preventing VEGF-A from attaching to VEGFR-2 and its consequent activation (Ambati *et al.*, 2006).

VEGF-A induces the activation of Cdc42 in tip cells. Cdc42 is a member of the Rho family of small GTPases, involved in filopodia formation, membrane protrusions that function as VEGF sensors, guiding cell migration (**Figure I-9 B**) (Barry *et al.*, 2015). Filopodia participate in growth and migration of the sprout in response to a VEGF spatial gradient. In addition, several isoforms of VEGF-A are produced by alternative splicing from a single gene, differing in the length of their protein product, as well as in their bioavailability and interaction with the co-receptor Neuropilin-1 (Peach *et al.*, 2018). Indeed, one of these isoforms (VEGF₁₆₄ in mice or VEGF₁₆₅ in humans) binds to ECM heparan sulphate and acts as a chemoattractant signal that stimulates the polarized extension of tip-cell filopodia (Gerhardt *et al.*, 2003).

On the other hand, there is another group of molecules that counteracts the proangiogenic effect of VEGF. Among them, thrombospondin-1 (TSP-1) and TSP-2 are the most important angiogenesis inhibitors. These factors can antagonize VEGF signaling through different mechanisms: (i) inhibition of VEGF release from the ECM; (ii) direct contact with VEGF and (iii) inhibition of VEGF-triggered signal transduction. Moreover, TSP-1 induces EC apoptosis (Lawler & Lawler, 2012). TSP-1 limits VEGF release from the ECM by inhibiting matrix metalloproteinases (MMP) (Rodríguez-Manzaneque *et al.*, 2001). In addition, TSP-1 promotes VEGF clearance from the extracellular space, via low density lipoprotein receptor-related protein-1 (LRP-1), by interacting directly with VEGF (Greenaway *et al.*, 2007). Moreover, in the presence of TSP-1, VEGF-mediated VEGFR-2 phosphorylation is inhibited *in vivo* and *in vitro* (Zhang *et al.*, 2009).

The angiogenic process is completed with the encounter of two tips from different sprouts or when the tip meets a preexisting capillary (**Figure I-9 C**). At this point, the tip cell suppresses its motility, forms EC-EC contacts and increases the adhesive

interactions at the joining point. Finally, the development of a vascular lumen is required for the establishment of blood flow (**Figure I-9 D**) (Adams & Alitalo, 2007).

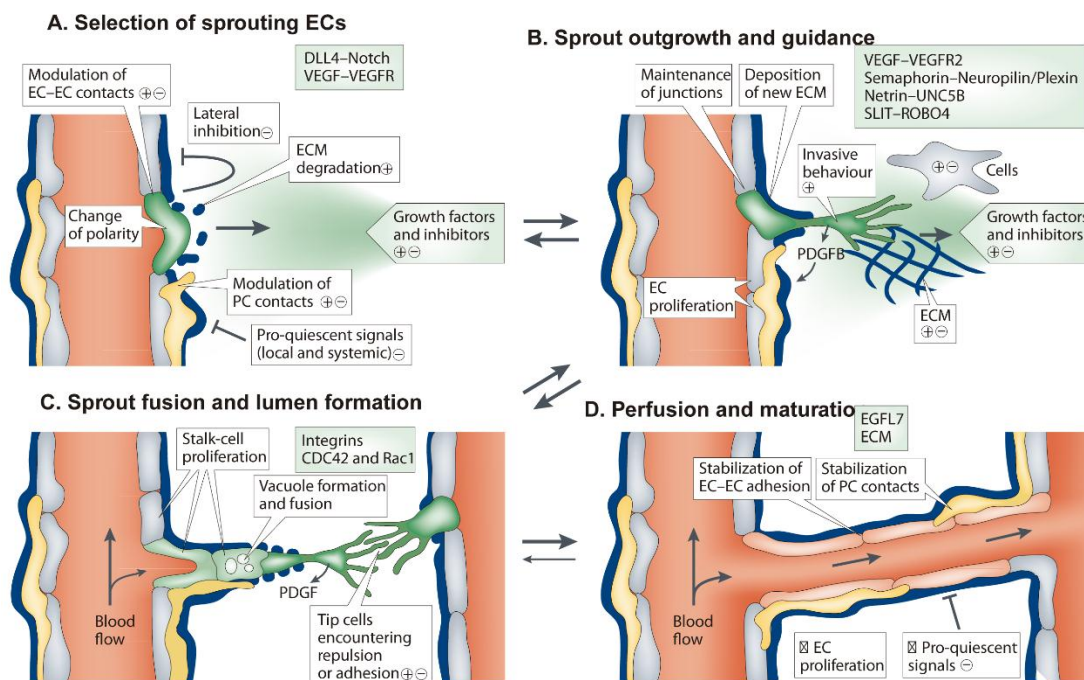


Figure I-9. Angiogenesis. Schematic representation of the formation of new vessels from a preexisting one. **(A)** In response to a gradient of proangiogenic factors (mainly VEGF), an endothelial cell acquires a tip cell phenotype, losing the interactions with the surrounding cells. At the same time, tip cell starts to release DLL4, that bind to its Notch receptor in the adjacent cells, inhibiting its transformation into a tip cell, and promoting its differentiation into a stalk cell. **(B)** The tip cell starts to invade the ECM and migrate in response to a gradient of proangiogenic factors. **(C)** The stalk cells begin to proliferate, to generate the body of the new blood vessel. The encounter of two tip cells, repress motility and promotes the interaction between the two tip cells. **(D)** The new blood vessel is finally developed with the formation of the lumen that is required for the establishment of the blood flow. Figure from (Adams & Alitalo, 2007)

3.3.2. Platelets store a variety of angiogenic factors.

Platelets play an essential role in angiogenesis; in fact, platelets induce ECs proliferation and tube formation *in vitro*, and promotes angiogenesis *in vivo* (Packham *et al.*, 2014; Pipili-Synetos *et al.*, 1998; Wojtukiewicz *et al.*, 2017). Platelets store a variety of proangiogenic and antiangiogenic substances in their α -granules, which are released in response to platelet activation (Sierko & Wojtukiewicz, 2004; Walsh *et al.*, 2015).

Among the proangiogenic factors found in platelets, we highlight VEGF (major proangiogenic factor), bFGF: promotes the migration, proliferation and differentiation of ECs, (Sufen *et al.*, 2011), HGF (Hepatocyte Growth Factor): stimulates the expression of VEGF in ECs (Tomita *et al.*, 2003), IGF (Insulin-like Growth Factor): mediates proteolytic events which are necessary during angiogenesis (Lee *et al.*, 2000), EGF

(Epidermal Growth Factor): increases the expression of VEGF mRNA levels *in vitro* and promotes angiogenesis in some cancer types, (Ravindranath *et al.*, 2001), PD-ECGF (Platelet Derived Endothelial Cell Growth Factor): promotes the release of angiogenic factors such as VEGF and the synthesis of matrix metalloproteinases-1, MMP-1 (Gotanda *et al.*, 2006), PDGF (Platelet Derived Growth Factor): triggers the expression of VEGF and the recruitment of pericytes to newly formed vessels, (Guo *et al.*, 2003), Ang-1 (Angiopoietin-1): acts a vascular stability factor, Augustin *et al.*, 2009) and PAI-1 (Plasminogen activator inhibitor-1): promotes angiogenesis although it was considered as an antiangiogenic factor (Ismail *et al.*, 2021).

Furthermore, platelets are the main source of Stromal Derived Factor-1 (SDF-1), also known as CXCL12, the main chemoattractant for hemangiocytes, a type of Bone Marrow Derived Cells (BMDC). In response to hypoxia, SDF-1 is released from platelets and ischemic tissue and, together with VEGF (released by platelets and ECs), promotes the recruitment of hemangiocytes, through interaction with their respective receptors, CXCR-4 and VEGFR-1 (Jin *et al.*, 2006; Massberg *et al.*, 2006; Stellos & Gawaz, 2007). Hemangiocytes release different angiogenic factors at the hypoxic site, which stimulate the assembly of endothelial progenitor cells and contribute to the stability of the new blood vessel (Amano *et al.*, 2015; Feng *et al.*, 2011).

Platelets, on the other hand, contain angiogenesis suppressive factors (Walsh *et al.*, 2015). TSP-1 is the major antiangiogenic factor found in platelets, accounting for 20% of the protein content in α -granules (Aburima *et al.*, 2021). Platelets also include PF4, which inhibits angiogenesis by blocking the binding sites of heparin-binding endothelial growth factors on the surface of ECs (Pluda & Parkinson, 1996). Furthermore, platelets contain angiostatin, endostatin and tissue inhibitors of MMPs (TIMP-1 and -4) that prevent blood vessels formation (Ikenaka *et al.*, 2003; Jurasz *et al.*, 2003; L. Ma *et al.*, 2005).

The distribution within platelet α -granules of the aforementioned pro- and antiangiogenic factors is a controversial issue. According to some authors, pro- and antiangiogenic factors are stored in different α -granules and are released in response to different stimuli. For example, thrombin triggers the secretion of antiangiogenic factors, such as TSP-1, whereas ADP promotes the release of proangiogenic factors, such as VEGF (Battinelli *et al.*, 2011; Italiano *et al.*, 2008; Martín-Granado *et al.*, 2017; Sehgal & Storrie, 2007). Furthermore, during proplatelet extension and platelet formation, Mks sort and package α -granule contents into different α -granule subpopulations (Battinelli *et al.*, 2019). However, other authors suggest that pro- and antiangiogenic factors are stored

in the same type of α -granules and are released simultaneously (Jonnalagadda *et al.*, 2012; Kamykowski *et al.*, 2011).

3.3.3. Platelet secretion.

Regardless of how angiogenic factors are stored in platelets or what stimulus triggers their release, secretion of pro- and antiangiogenic factors first requires the fusion of the vesicle membrane with the plasma membrane. This process is controlled by Soluble N-ethylmaleimide-sensitive factor Attachment protein Receptors (SNAREs). Depending on their physical location, these proteins are classified as v-SNAREs for vesicle/granule- or t-SNAREs for target membrane-localized (**Figure I-10**). The association between v-SNAREs and t-SNAREs forms a coiled coil structure that links the two membranes together for fusion (**Figure I-10**) (Joshi & Whiteheart, 2017).

Vesicle Associated Membrane Proteins (VAMPs) are the largest group among v-SNAREs. Platelets contain a variety of v-SNARE isoforms, being VAMP-7 and VAMP-8 the most abundant in human platelets, whereas VAMP-2, VAMP-7 and VAMP-8 are the most abundant in mouse platelets. VAMP-2 ablation had no effect on platelet secretion (Ren *et al.*, 2007), while VAMP-7 knockout platelets display a defective α -granule exocytosis and a decreased capacity to spread (Koseoglu *et al.*, 2015). VAMP-8 is essential for a rapid and optimal platelet exocytosis; its ablation, similarly to VAMP-7, resulted in a hamper release of platelet granules (Ren *et al.*, 2007). Indeed, VAMP-8 knockout animals show slower recovery from hind-limb ischemia due to lack of BMDC recruitment at the site of hypoxia, suggesting that platelet VAMP-8 is crucial for ischemia outcome (Feng *et al.*, 2011).

Platelets, on the other hand, express a number of t-SNARE proteins, including Syntaxin 2, 4, 6, 7, 8, 11, 12, 16, 17, and 18, as well as SNAP (Synaptosome Associated Proteins) -23, 25, and 29. Syntaxin 2/4 single or double knockout platelets present normal platelet secretion. Nevertheless, a missense mutation in both copies of *STX11* gene triggers the Familiar Hemophagocytic Lymphohistiocytosis type 4 (FHL4). Platelets from these patients show defective platelet secretion (Ye *et al.*, 2012).

In addition to v- and t- SNAREs, other sets of proteins are needed to regulate the fusion of SNARE proteins in a specific and temporal manner (**Figure I-10**). These proteins can act as chaperones (Sec1/Munc18 proteins) for the trafficking syntaxins to their target membrane (Archbold *et al.*, 2014), while others (Rab27, Munc 13-4 or Synaptotagmin-Like) regulate platelet secretion by affecting docking/tethering of granules to site of exocytosis (Chicka *et al.*, 2016; Fukuda, 2013).

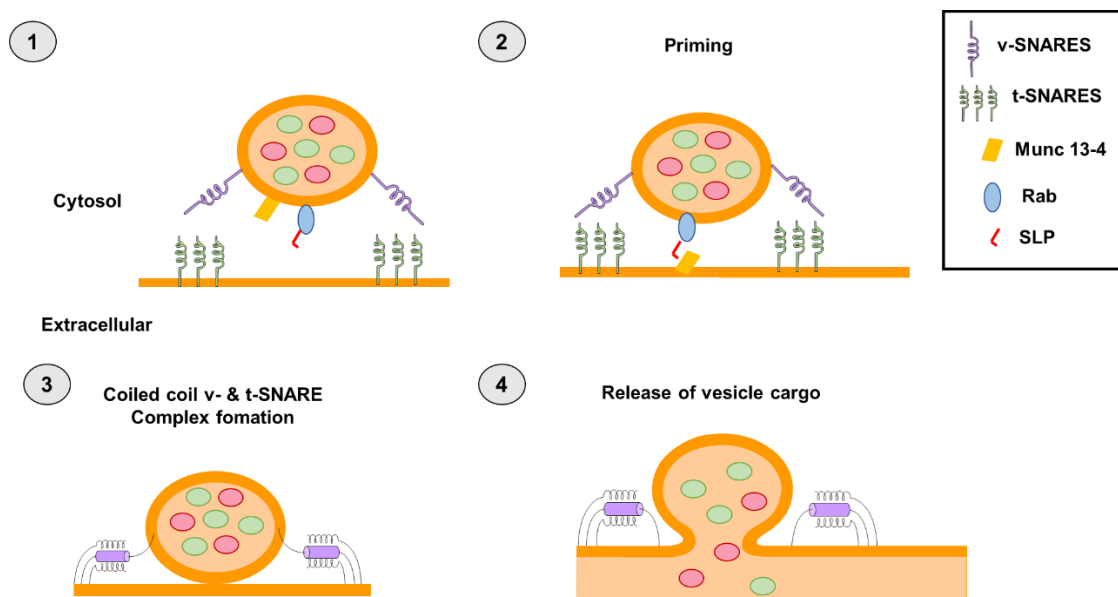


Figure I-10. Granule secretion in platelets. The release of vesicle cargo is a complex process in which several vesicle-proteins and platelet-membrane proteins are involved **(1)**. Rab, Munc 13-4 and SLP, regulates the tethering of the granule to the exocytosis site **(2)**, allowing the formation of a coiled coil v- and t- SNARE complex **(3)**, which leads to the fusion of the membranes and the release of platelet cargo **(4)**.

C3G is thought to have a role in α -granule release, and hence in the secretion of angiogenic factors. Indeed, C3G overexpression in platelets causes VEGF and TSP-1 retention inside the platelet, both at rest and under stimulation with thrombin, probably due to the interaction of C3G with VAMP-7 (Martín-Granado *et al.*, 2017). Preliminary results from our group suggest that C3G may act as a secretion brake, preventing the uncontrolled release of α -granules.

3.4. Platelets regulates their own mass by modulating TPO endocytosis.

As stated above, plasma TPO levels must be tightly regulated to avoid excessive platelet production and the development of myeloproliferative disorders (Ng *et al.*, 2014).

3.4.1. *c-Cbl is essential for c-Mpl internalization and ubiquitination in platelets*

The covalent binding of one (mono-ubiquitination), two (bi-ubiquitination), or multiple (polyubiquitination) units of ubiquitin (Ub) is known as ubiquitination. Three enzymes are involved in this process: Ub-activating enzyme (E1), Ub-conjugating enzyme (E2) and Ub-ligase (E3). The 26S proteasome complex, which consists of one or two 19S regulatory subunits and the 20S proteolytic subunit, performs the degradation of ubiquitinated-proteins. The 19S subunit is responsible for recognizing and unfolding ubiquitinated proteins, whereas the proteolytic process is carried out in the 20S complex.

Finally, ubiquitin is recycled by the deubiquitinating enzymes. Together, the ubiquitination enzymes (E1, E2 and E3), the 26S proteasome complex and the deubiquitinating enzymes form the Ubiquitin-Proteasome System (UPS) (Bard *et al.*, 2018; Hanna *et al.*, 2019).

The 26S multi-catalytic proteasome complex is made up of two 19S regulatory caps (750 kDa) and a core 20S catalytic subunit. Each 19S regulatory subunit is assembled by a “lid” (made by up to 10 non-ATPase subunits), a “base”, composed of 2 non-ATPase subunits and 6 homologous hexameric rings that form ATPases (PSMC2/1/4/6/3/5). The “base” regulates the assembly of the 19S regulatory subunits with the 20S catalytic subunits (Bard *et al.*, 2018; Colberg *et al.*, 2020).

Rpn1, a 19S base member, is involved in the identification of ubiquitin or proteins with ubiquitin-like domains (UBL). Inhibition of Rpn1 phosphorylation at Ser-361 leads to decreased mitochondrial function and cellular fitness, due to impaired proteasome assembly (Liu *et al.*, 2020).

The proteolytic 20S core protease activity complex is made up of 8 heterogeneous subunits organized into four rings: two beta rings on the inner side and two pore-forming non-catalytic alpha rings on the outer side. β -rings performed caspase-, trypsin-, and chymotrypsin-like proteolytic activities and are involved in the digestion of acid-, basic- and hydrophobic amino acids respectively (Colberg *et al.*, 2020).

Cbl (Casitas B cell lymphoma) is a family of proteins constituted by three different members: c-Cbl, Cbl-b and Cbl-c (Keane *et al.*, 1995; Kim *et al.*, 1999; Lupher *et al.*, 1998). These proteins are characterized for the presence of a RING domain in their structure, which is typical of E3 Ub-ligase enzymes, and function as both positive and negative regulators of different signaling pathways. For example, EPO-dependent proliferation and survival of F36-P cells were increased in c-Cbl knockout platelets owing to inhibition of proteasome-mediated Src-degradation (Shintani *et al.*, 2014).

In platelets, the expression of c-Cbl and Cbl-b has been described (Buitrago *et al.*, 2013; Oda, Ozaki, *et al.*, 1996). However, most of the studies are focused on c-Cbl. C-Cbl activation has been reported in response to a variety of stimuli. Stimulation of GPVI (collagen receptor) causes c-Cbl phosphorylation and activation via two members of the Src family of kinases (SFK) Fyn and Lyn, performing a negative regulation of the GPVI pathway (Auger *et al.*, 2003; Polgár *et al.*, 1997). Indeed, c-Cbl knockout platelets display hyperphosphorylation of several proteins downstream GPVI, including Spleen tyrosine kinase (Syk), which requires c-Cbl-mediated ubiquitination to regulate its activity

(Dangelmaier *et al.*, 2005). Furthermore, c-Cbl is phosphorylated in thrombin- and TPO-stimulated platelets (Oda, Ozaki, *et al.*, 1996; Saci *et al.*, 2000).

C3G is a well-known Src substrate (Radha *et al.*, 2004), and the interaction between C3G and c-Cbl has been established in a variety of cell types (Maia *et al.*, 2013; Uemura & Griffin, 1999). Indeed, it has been suggested that C3G and c-Cbl are recruited to the c-Mpl receptor after TPO-stimulated to activate the Rap1/Raf/ERK pathway (Stork & Dillon, 2005). Overall, this data suggests a possible role of C3G regulating c-Cbl activity.

Internalization and degradation of c-Mpl are regulated by c-Cbl (**Figure I-11**). In fact, c-Cbl ablation in Ba/F3 cells results in a constitutive activation of the TPO/c-Mpl pathway due to a defective c-Mpl degradation (Saur *et al.*, 2010). Furthermore, c-Cbl^{fl/fl};PF4^{Cre} mice, which present a specific deletion of c-Cbl in Mk, show microthrombocytosis and faster platelet turnover due to the inability of c-Cbl knockout platelets to internalize c-Mpl in response to TPO (Märklin *et al.*, 2020). Moreover, c-Cbl mutations are linked to lack of E3-Ub ligase activity, resulting in impaired c-Mpl/JAK2 degradation via the lysosome or proteasome (Grand *et al.*, 2009).

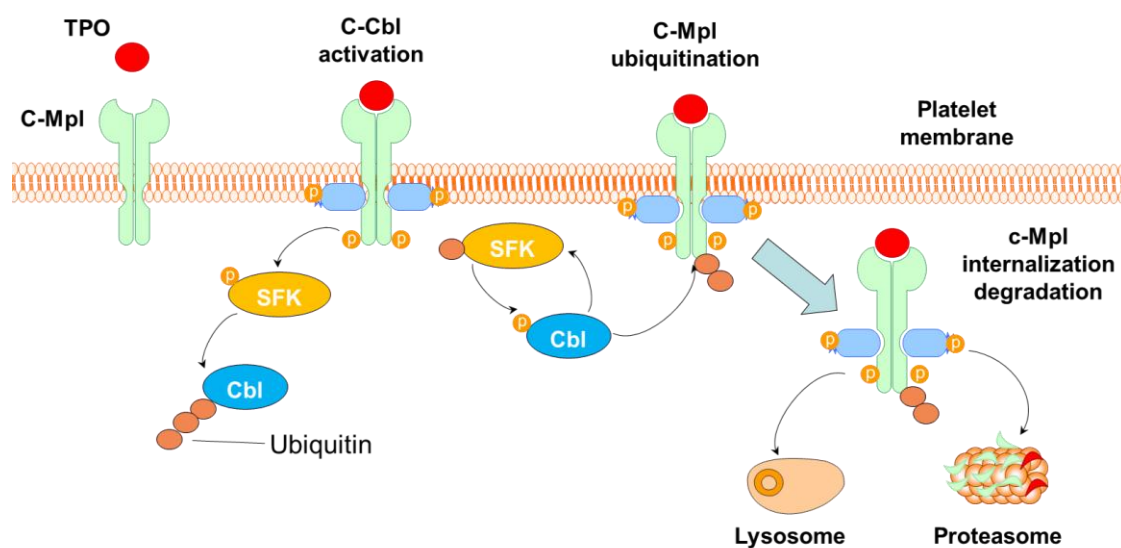


Figure I-11. c-Cbl regulates TPO clearance from plasma. TPO binding to its receptor c-Mpl induces c-Cbl activation and phosphorylation via SFKs. Active c-Cbl, performs ubiquitination of c-Mpl, which is crucial for its degradation through the proteasome and lysosome.

3.4.2. Platelet proteasome

Platelets perform a limited *de novo* protein production, including hemostatic and thrombo-inflammatory factors like COX-1 (cyclooxygenase-1), IL-1 β , NF- κ B (nuclear factor- κ B), among others. Surprisingly, despite their limited protein synthesis, platelets have a fully working protein degradation machinery (El-Kadiry & Merhi, 2021). 26S

proteasome complex is involved in platelet production and viability as well as in the modulation of platelet activation and function (El-Kadiry & Merhi, 2021).

In platelets, proteasome inhibition results in an accumulation of pro-apoptotic BAX proteins and enhances phosphatidylserine (PS) exposure, resulting in a decreased platelet count and increased clearance of platelets by macrophages (M. K. Nayak *et al.*, 2013). Furthermore, platelet production is also controlled by the proteasome; thus, Bortezomib (a proteasome inhibitor) increases active Rho levels, a negative regulator of platelet formation (Murai *et al.*, 2014).

In addition, proteasome inhibition diminishes platelet activity by preventing platelet aggregation and by causing the buildup of Talin-1 and Filamin-A, which results in decreased platelet adhesion and spreading (Gupta *et al.*, 2014). Moreover, platelets pretreated with MG132 (a proteasome inhibitor) and subsequently stimulated with subthreshold amounts of thrombin and/or collagen, exhibits decreased integrin $\alpha\text{IIb}\beta\text{3}$ activation (Karim *et al.*, 2015).

3.4.3. Lysosome-protein degradation

Lysosome protein degradation, also known as autophagy, performed the digestion of unfolded soluble proteins, protein complexes, aggregates, and oligomers. Autophagy requires the formation of phagophores, which enwrap certain proteins and create autophagosomes. Autophagosome development requires several proteins known as autophagy-related proteins (Atg), which are involved in autophagy initiation, nucleation, elongation, maturation, fusion, and degradation. Finally, autophagosomes are transported to the lysosome in a dynein-dependent way to degrade proteins (Korolchuk *et al.*, 2010).

3.4.4. Proteasome and lysosome crosstalk

Protein ubiquitination is a common step for protein degradation by the proteasome and lysosome systems. The relationship between the two systems has been investigated, and several evidences confirm that both protein degradation systems are in constant interplay (Ji & Kwon, 2017; Korolchuk *et al.*, 2010).

Proteasome suppression causes the activation of the lysosome/autophagy pathway through three different mechanisms: the activation of the unfolded protein response (UPR), the accumulation of misfolded proteins, and the buildup of p53. However, the fundamental mechanism behind this compensatory process remains unclear.

However, lysosome inhibition does not result in an increase in proteasome activity. Contrarywise, lysosome inhibition causes a reduction in proteasome activity and the accumulation of ubiquitinated proteins (Munch *et al.*, 2014). This effect is due to several processes. On the one hand, lysosome is in charge of degrading aging and inactive proteasome for the maintenance of the proteasome pool (Marshall *et al.*, 2016). However, in the absence of functional lysosomes, inactive proteasome are accumulated in the cytosol (Cohen-Kaplan *et al.*, 2017). Lysosome inhibition, on the other hand, stimulates the formation of protein aggregates in association with p62, which sequester ubiquitinated substrates for proteasomal degradation (Korolchuk *et al.*, 2009).

3.5. Platelets promote tumor growth

The platelet-cancer nexus has been well-established (Wojtukiewicz *et al.*, 2017). In 1865, Armand Trousseau showed a close relationship between unexpected or migratory thrombophlebitis and occult malignancy (Varki, 2007). Tumor cells release several cytokines (IL-6, TPO or granulocyte macrophage colony-stimulating factor, GM-CSF), that promotes megakaryocyte formation and platelet production (Estrov *et al.*, 1995; Gastl *et al.*, 1993; Kato *et al.*, 1999). Indeed, thrombocytosis is present in approximately 10-57% of cancer patients and correlates with a poor prognosis in colon (Costantini *et al.*, 1990), lung (Costantini *et al.*, 1990), gastric (Ikeda *et al.*, 2002), renal (Symbas *et al.*, 2000), prostatic (Ribeiro *et al.*, 1997), cervical (Lopes *et al.*, 1994), endometrial (Gücer *et al.*, 1998), ovarian cancer (Zeimet *et al.*, 1994) and in malignant mesothelioma (Nakano *et al.*, 1986).

The development of a tumor demands the formation of new blood vessels to ensure an adequate blood supply in order to obtain oxygen and nutrients to continue proliferating, as well as the removal of waste products from the tumor microenvironment. For this, tumors release several factors that favor vascularization. However, the development of a pro-angiogenic environment is not only driven by the tumoral cell, but is also supported by other players that stimulates the release of angiogenic factors, being platelets one of the most important.

Tumor-cells promote platelet activation through the release of several soluble mediators such as ADP, TXA₂, and thrombin (Steinert *et al.*, 1993; Zucchella *et al.*, 1989), which triggers granule release (Egan *et al.*, 2011), and, consequently, the secretion of pro-angiogenic factors, such as VEGF, PDGF and FGF2, resulting in a proangiogenic microenvironment that stimulates tumor growth and proliferation (Wojtukiewicz *et al.*, 2017). Indeed, VEGF from platelets promote proliferation of breast cancer cells, leading to enhanced tumor growth *in vivo* (Jiang *et al.*, 2017). In addition,

platelets perform the recruitment of hemangiocytes to the tumor vasculature, which release angiogenic factors, that in turns, enhances neovascularization and the stabilization of new blood vessels (Feng *et al.*, 2011).

Platelet-induced angiogenesis is not only mediated by the release of angiogenic factors (Braun *et al.*, 2021). Indeed, platelets can physically contact ECs and stimulate their proliferation. Platelets promote the formation of capillary-like structures *in vitro* independently of their granular content (Pipili-Synetos *et al.*, 1998). In this case, the proangiogenic capacity of platelets is mediated by the interaction of several platelet-surface proteins with the ECs. Indeed inhibition of the integrin $\alpha\text{IIb}\beta\text{3}$ or platelet tetraspanin CD151 suppresses angiogenesis and impairs tube formation of HUVEC cells on a Matrigel assay (Huang *et al.*, 2016; Varner *et al.*, 1999).

3.6. Platelets are required for metastasis

Metastasis is the process by which a tumor cell leaves its initial location, disseminates within the blood vessels and colonizes different areas of the body, eventually forming a new tumor. Initially, metastasis requires a tumor cell to break contact with adjacent tumor cells and undergo the epithelial-mesenchymal transition (EMT). EMT confers critical properties to the metastatic cell that enable it to invade, such as increased motility and a greater capacity to degrade ECM proteins. This is a critical stage in the metastasis process, since it allows tumor cells to escape from the primary tumor and enter into the bloodstream, where they must, not only withstand shear stress, but also scape from the immune system. In order to colonize a new tissue, the metastatic cell must escape the blood vessel. To this end, tumor cells are arrested at the endothelial wall and undergo extravasation. Through this process, malignant cells are able to infiltrate the parenchyma of distant organs and establish a secondary tumor (A. C. Chiang & Massagué, 2008; Lambert *et al.*, 2017).

Platelets are well recognized for their role in hemostasis, but they are also critical players in metastasis, facilitating several steps of the process. Once in the bloodstream, tumor cells activate platelets by releasing different platelet agonists (ADP, thrombin) (Zucchella *et al.*, 1989), which initiate different signaling pathways leading to platelet activation (Zucchella *et al.*, 1989), release of platelet granules and, eventually, P-selectin exposure (Yan & Jurasz, 2016).

Platelets release several factors (TGF- β , HGF and PDGF) in response to tumor cells that support the EMT process, and hence, stimulate metastasis (**Figure I-12 A**). Therefore, tumor-induced platelet activation, causes the establishment of platelet aggregates that surround tumoral cell, shielding it from the immune system, anoikis and

shear stress (**Figure I-12 B**). During this process, known as tumor cell-induced platelet aggregation (TCIPA), platelets form “bridges” with tumoral cells, due to the activation of integrin $\alpha\text{IIb}\beta\text{3}$ and the exposure of P-selectin (Schlesinger, 2018). In fact, ablation or inhibition (e.g. with heparin) of these proteins reduces the amount of disseminated cells *in vivo* (Erpenbeck *et al.*, 2010).

The arrest at the endothelium wall and the recruitment of BMDC are required for extravasation of metastatic cells (Fabricius *et al.*, 2021). Platelets that surround tumor cells can attach to ECs via P-selectin or integrin $\alpha\text{IIb}\beta\text{3}$, promoting the arrest of the tumor cell (Zuchtriegel *et al.*, 2016)(**Figure I-12 C**). Moreover, the release of platelet α -granules results in the accumulation of several chemoattractants, such as CXCL5 and CXCL7 (Labelle *et al.*, 2014), which are involved in the recruitment of granulocytes. In addition, platelets release ATP, which modulates endothelial barrier and ECs cytoskeleton remodeling, allowing the breakdown of the endothelial barrier and the extravasation of the metastatic cell (Schumacher *et al.*, 2013) (**Figure I-12 C**). Furthermore, platelets secrete a plethora of angiogenic factors that, together with ATP, stimulate the establishment of the new metastatic niche (N. Li, 2016).

We have previously mentioned that C3G controls platelet activation and aggregation in response to different platelet agonists. Thus, it is reasonable to think that C3G may controls platelet responses to tumor cells. C3G overexpression in platelets enhances P-selectin exposure, integrin $\alpha\text{IIb}\beta\text{3}$ activation, and platelet aggregation (Gutiérrez-Herrero *et al.*, 2012), all of which may contribute to the development of metastasis. Indeed, tgC3G mice exhibit higher number of lung metastases than wild-type mice, after intravenous injection of melanoma cells (Martín-Granado *et al.*, 2017). These results confirm that platelet C3G actively participates in the metastatic process, although the underlying molecular mechanisms remain unknown.

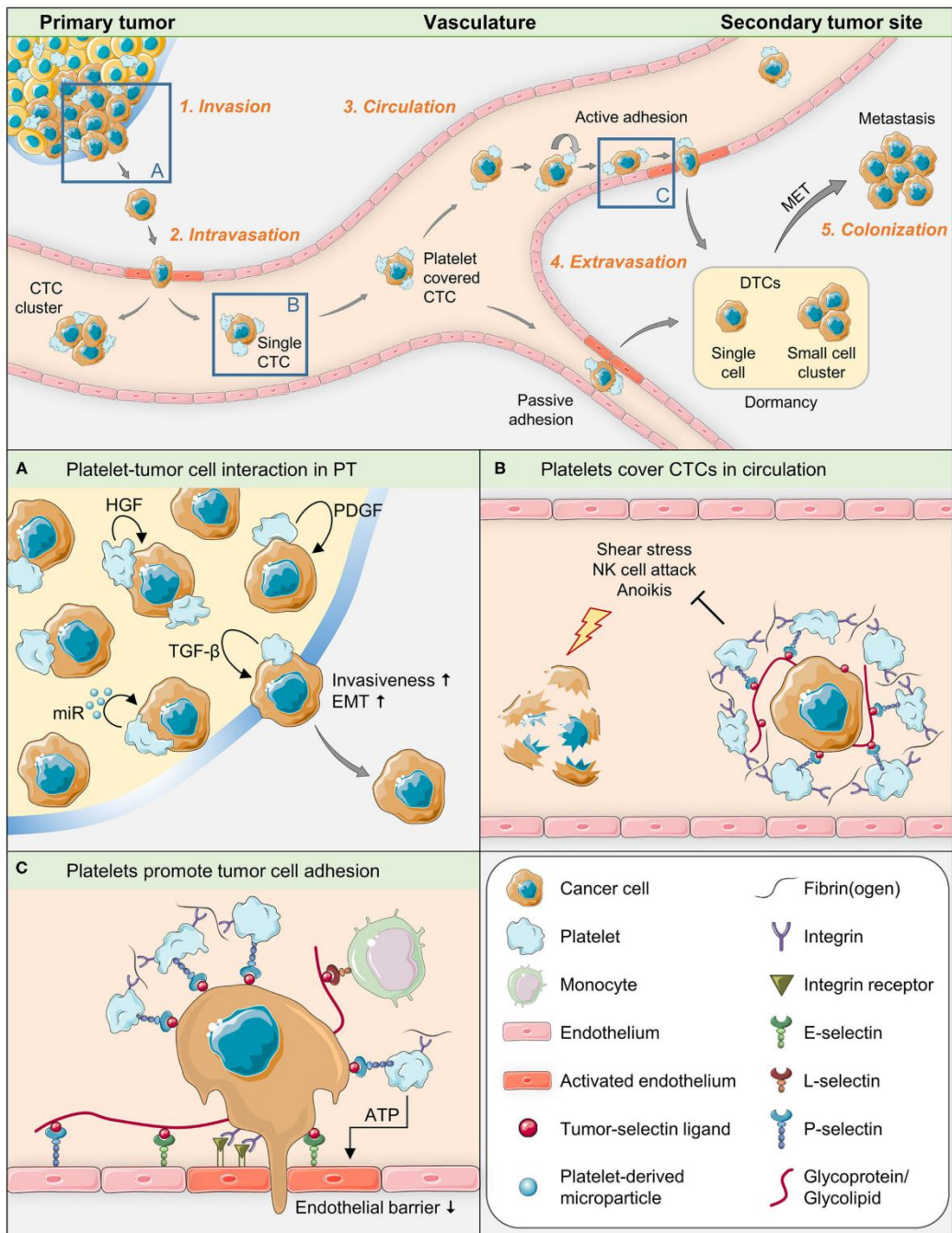


Figure I-12. Platelets induces metastasis at different levels. (A) At the primary tumor, platelets promote the release of several factors that support EMT. **(B)** Bloodstream tumor cells must protect themselves from shear stress, NK (Natural Killer) cell attack and anoikis. Tumor cells encourage the formation of platelet aggregates that surround the tumor cell and shield it from the aforementioned hazards, preventing cell death. **(C)** Platelets interact with ECs through P-selectin, causing the arrest of the tumor cell at the vasculature wall. Moreover, platelets secrete ATP and angiogenic factors, which enhance the extravasation and the establishment of the secondary tumor. Figure from Fabricius *et al.*, 2021.

AIMS/OBJETIVOS

AIMS OF THE THESIS

Using transgenic mouse models which specific overexpression of full-length C3G, or a catalytically inactive C3G mutant in Mks, our group has previously demonstrated a key role for C3G in Mk maturation, as well as, in various aspects of platelet function.

Therefore, the general objective of this Thesis is to deepen into the functions of C3G C3G functions in platelets, adding to our animal models a knockout mouse, in which C3G is specifically deleted in Mks and platelets. To achieve this goal, the following specific objectives have been addressed:

1. To generate a mouse model with specific deletion of C3G in Mks and platelets ($Rapgef1^{flox/flox};PF4-Cre^{+/-}$).
2. To analyze the effect of C3G deletion on platelet hemostatic function.
3. To study the role of C3G in pathological megakaryopoiesis.
4. To study the participation of platelet C3G in ischemia-induced angiogenesis.
5. To analyze the contribution of platelet C3G in melanoma metastasis.

OBJETIVOS

Utilizando modelos de ratón transgénicos con sobreexpresión específica de C3G, o un mutante catalíticamente inactivo, en Mks, nuestro grupo ha demostrado previamente un papel clave de C3G en la maduración de Mk, así como en varios aspectos de la función plaquetaria.

Por tanto, el objetivo general de esta Tesis es profundizar en las funciones de C3G en plaquetas, añadiendo a nuestros modelos animales un ratón *knockout*, en el que c3g está específicamente eliminado en Mk y plaquetas. Para lograr este objetivo, se han abordado los siguientes objetivos específicos:

1. Generar un modelo e ratón con delección específica de C3G en Mk y plaquetas (Rapgef1^{flox/flox};PF4-Cre^{+/-}).
2. Analizar el efecto de la delección de C3G en la función hemostática de las plaquetas.
3. Estudiar el papel de C3G tanto en la megacariopoyesis patológica.
4. Estudiar la participación de C3G plaquetario en la angiogénesis inducida por la isquemia.
5. Analizar la contribución de C3G plaquetario en la comunicación plaqueta-tumor durante la metástasis de células de melanoma.

MATERIALS & METHODS

MATERIALS & METHODS

1. Mouse models

In this work we have used two transgenic mouse models for C3G with specific expression in megakaryocytes and platelets: tgC3G (in which C3G full-length is overexpressed) and tgC3G Δ Cat (overexpressing a mutant form of C3G lacking the catalytic domain). In both models, the transgenes are expressed under the control of the PF4 gene promoter, specific for platelets and megakaryocytes (Gutiérrez-Herrero *et al.*, 2012).

We also developed a knockout model of C3G specific for platelets and megakaryocytes. Rapgef1^{fllox/fllox};PF4-Cre^{+/-} (hereinafter C3G-KO, (Gutiérrez-Herrero *et al.*, 2020)) mouse was obtained by crossing Rapgef1^{fllox/fllox} mice (in which exons 17 to 21 of C3G are flanked by LoxP sites (Shah *et al.*, 2016)) with PF4-Cre transgenic mice (expressing Cre recombinase under the control of the PF4 promoter (Tiedt *et al.*, 2007)). Rapgef1^{fllox/fllox};PF4-Cre^{-/-} (hereinafter C3G-wt) mice were used as controls.

1.1. DNA extraction and genotyping

A section of less than 5 mm was excised from the tail of the mice at the time of weaning. The tissue was digested overnight (o/n) at 55 °C in Tail Lysis Buffer (100 mM Tris pH 8.0, 5 mM EDTA pH 8.0, 200 mM NaCl and 0.2 mM SDS) supplemented with proteinase K (Recombinant PCR Grade, Roche, 03115844001). After digestion, DNA was isolated from the supernatant by precipitation with 5M NaCl and ethanol, following the protocol describe in (Miller *et al.*, 1988).

The primers used in the genotyping of each mouse model are described in **Table-M1**.

Table M-1. Primers used in the genotyping of the mouse models used in this work.

Mouse model genotype	Characteristics	Primer	Sequence
TgC3G TgC3G Δ Cat	C3G overexpression	Primer-A1	5'-ACCACATGGCAGTCAAACCTCACAGC-3'
		Primer-C1	5'-TCTTCTGCCTTTGAGACCTGGAAGC-3'
Rapgef1 x PF4-Cre	Conditional and Rapgef1 alleles	C3G-KO-LoxF	5'-AGCCTGTTGGCAAGTTTGG-3'
		LoxR	5'-CTGATGGAGAACCTAGCTGTGG-3'
	PF4-Cre and wild-type alleles	PF4-prom-F	5'-CCCATACAGCATACCTTTTG-3'

PF4-prom-Cre-R	5'-TGCACAGTCAGCAGGTT-3'
PF4-prom-WT2-R	5'-TTACAGCATCGCCTTCCCCT-3'

2. Cell lines and culture conditions

The cell lines used in this work are indicated in **Table M-2**:

Cell line	Organism	Tissue	Disease	Medium
B16-F10	<i>Mus musculus</i>	Skin	Melanoma	RPMI
B16-F10-EGFP	<i>Mus musculus</i>	Skin	Melanoma	RPMI
3LL	<i>Mus musculus</i>	Lung	Lewis Lung Carcinoma	DMEM
HUVEC	Human	Umbilical Vein	-	EBM™-BulletKit™ (Lonza)

Roswell Park Memorial Institute (RPMI, Gibco) and Dulbecco's modified Eagle's medium (DMEM, Gibco) media were supplemented with 10% Fetal Bovine Serum (FBS, Gibco), 2 mM Glutamine (Gibco) and 100 U/ml Penicillin/Streptomycin (Gibco). EBM-2 medium was supplemented with BulletKit™ (Lonza), containing hydrocortisone, hFGF-B, VEGF, R3-IGF-1, Ascorbic Acid, hEGF, GA-1000 and heparin.

Trypsin-EDTA (0.25%) was used to collect adherent cells (Gibco). To count cells Neubauer Chamber or Beckman Coulter Z2 particle counter were used. Complete media supplemented with 10% dimethyl sulfoxide (DMSO) was used to store cells in liquid nitrogen.

3. Bone Marrow isolation and culture

BM was isolated by flushing femurs and tibias with sterile PBS using a 25 G needle. BM was considered to have been completely expelled when the color of the bone changed from red to white. After a centrifugation step at 300 g, erythrocytes were lysed in Red Blood Cell Lysis Buffer (RBC, 0.155 M NH₄Cl, 10 mM KHCO₃, 10 mM EDTA, pH 7.4). BM cells (BMC) were cultured in DMEM with 20% Horse Serum, 100 U/mL Penicillin/Streptomycin, 1.4 mM L-Glutamine and 30 µg/mL Gentamicin. Specific culture conditions and subsequent procedures are described in the following sections.

3.1. Megakaryocyte differentiation

Mk differentiation from BMC was stimulated with the addition of TPO in combination with SCF, IL-3, IL-6 and IL-11 (**Table M-3**). BM was cultured for 6 days, changing medium every two days. Mk differentiation was analyzed by measuring surface expression of CD41, CD61 and CD42 by flow cytometry using BD Accuri™ C6 cytometer.

Table M-3. Cytokines used for the differentiation of BMC into megakaryocytes, indicating working concentration and Suppliers.

Name	Supplier and reference	Final Concentration
Mouse TPO	Innovative research (IMSTHPOCF100UG)	50 ng/mL
Mouse SCF	Miltenyi Biotech (130-094-074)	10 ng/mL
IL-3	Invitrogen (PMC0034)	10 ng/mL
IL-6	Miltenyi Biotech (130-094-065)	10 ng/mL
IL-11	Miltenyi Biotech (130-094-950)	10 ng/mL

3.2. Megakaryocyte purification

BM cultures were harvested at day 6, washed with cold PBS and centrifuged for 5 min at 300 g. Mk were isolated by bovine serum albumin (BSA) density gradient. Briefly, a density gradient was generated using different concentration of BSA. First 1 mL of 3% BSA was pipetted into a 15 mL conical tube. Then, the tube was carefully tilted and 1 mL of 1.5% BSA was slowly pipetted on top of the 3% BSA phase. Finally, BM resuspended in DMEM was pipetted over the 1.5% BSA layer. Cells were allowed to separate depending on its density for 30 min at 37 °C. Mk cells gather near the bottom of the conical tube because they are the largest hematopoietic cells. The cell pellet was declared pure Mk after 30 min.

4. Platelet purification

Blood obtained by cardiac puncture was collected in tubes containing sodium citrate as anticoagulant (Sarstedt®). Platelet rich plasma (PRP) was prepared by centrifuging blood twice for 4 min at 100 g. Platelets were isolated from PRP after a 5 min centrifugation step at 1200 g. Before activation, the platelet pellet was resuspended in Tyrode's Buffer (130 mM NaCl, 10 mM Trisodium citrate, 9 mM NaHCO₃, 6 mM dextrose,

0.9 mM MgCl₂, 0.81 mM KH₂PO₄, 10 mM Tris, pH 7.4) and allowed to rest at room temperature (RT) for at least 1 h.

4.1. Platelet activation

Platelets were activated following different protocols depending on the experiment. **Table M-4** and **Table M-5** list, respectively, the various agonists and inhibitors used in this study, as well as their concentrations.

Table M-4. Platelet agonist used. The name of the agonist, the platelet receptor, the time of stimulation, the working concentration and the supplier are indicated.

Agonist	Target	Assay	Concentration	Time	Supplier
Thrombin	PAR4 receptor	Western Blot	0.2 and 0.5 U/mL	1 and 5 min	Sigma
		Immunofluorescence	0.2 and 0.5 U/mL	1 and 5 min	
ADP	P2Y12 receptor	Western Blot	25 µM	5 min	Sigma
		Immunofluorescence	25 µM	5 min	
TPO	c-Mpl (TPO receptor)	Western Blot	25 and 100 ng/mL	5, 15, 30 and 60 min	Innovative Research
		Immunofluorescence	100 ng/mL	4 and 60 min	
		Mpl internalization	25 ng/mL	30 min	
		TPO uptake	2 ng/mL	30 min	
B16-F10 cells	Platelet	Activation	1 x 10 ⁶ cells	10 min	ATCC
		Aggregation	3 x 10 ⁴ cells	1, 2, 5 and 10 min	
		Rap1 activation	1 x 10 ³ cells	1, 2, 5 and 10 min	
		Adhesion	1 x 10 ⁴ cells	10 min	

Table M-5. Inhibitors of SFK, proteasome and lysosome used. The name of the inhibitor, its targets, the time of action, the working concentration and the supplier are listed.

Inhibitor	Target	Assay	Concentration	Time	Supplier
PP2	Src	Immunofluorescence	10 µM	5 min	Selleckchem
MG132	Proteasome	Western Blot	30 µM	60 min	Calbiochem
		Immunofluorescence			
NH ₄ Cl	Lysosome	Western Blot	20 mM	60 min	Acros Organics
		Immunofluorescence			

4.2. Isolation of platelet releasate

Platelets were activated with 0.2 U/mL thrombin for 5 min at 37 °C under stirring conditions. Reaction was stopped on ice. The samples were centrifuged at 2500 g for 10

min. Supernatants were considered platelet releasates, and were stored at -80 °C until needed.

5. Analysis of platelet releasates using a Mouse Angiogenesis Array

Proteins present in the secretome of thrombin-stimulated platelets (1×10^9) were analyzed using the Proteome Profiler Mouse Angiogenesis Array kit (R&D systems) following manufacturer's instructions. This kit contains membranes spotted with over 100 antibodies against various angiogenesis proteins. Briefly, proteins in the releasate were mixed with a cocktail of HRP-conjugated detection antibodies for 1 h and then, incubated with the membranes o/n at 4 °C. Next day, the HRP-conjugated antibodies, adsorbed in the membrane due to the binding of antibodies to specific target proteins in the secretomes, were visualized with a chemiluminescence reagent.

6. Capillary tube formation assay

Releasate from 2×10^8 platelet/mL were obtained as described in **Section 4.2** and stored at -80 °C until use. HUVEC cells were harvested and diluted 1:5 in PBS. 32.000 cells (resuspended in 37.5 μ L) were mixed with 15 μ L of platelet releasate diluted to a final volume of 37.5 μ L in PBS. The resultant mixture (75 μ L) were seeded onto Matrigel matrix in p-96 culture plates. Capillary tube was allowed to form at 37 °C and 5% CO₂. Capillary tube formation was recorded every hour using a THUNDER Image Live Cell 12899 microscope (Leica). The releasate angiogenic capacity was determined analyzing three parameters: number of master segment (segment bounded by two branches), total length of master segments and the number of internal meshes. All these parameters were acquired with the Skeleton Analyzer plug-in (Arganda-Carreras *et al.*, 2010) and the Angiogenesis Analyzer Macro (Carpentier, G., Angiogenesis Analyzer for ImageJ (2012) available online: <http://imagej.nih.gov/ij/macros/toolsets/Angiogenesis%20Analyzer.txt>).

7. Analysis of platelet proteome.

PRP was isolated as described in **Section 4**. Proteins were precipitated directly from samples using three parts of methanol and one of chloroform. Proteins were digested with trypsin and analyzed by liquid nano-chromatography (nano Easy-nLC, Thermo Scientific) coupled to a high-resolution mass spectrophotometer Q-Exactive HF (Thermo Scientific, Bremen, Germany). The Proteome Discoverer 2.4 software with the MASCOT search engine was used to analyze MS/MS spectra obtained on the samples. Proteins

were identified with the algorithm Percolator. Only proteins with quantification values for more than one peptide and at least present in two replicates were evaluated.

The proteomic analysis was performed in the Proteomic Unit of Complutense University of Madrid., a member of ProteoRed and is supported by grant PT17/0019, of the PE I+D+I 2013-2016. Funded by ISCIII and ERDF”.

8. Flow Cytometry Analysis

8.1. Platelet count by flow cytometry

Blood (15 μ L) was washed with 1 mL Tyrode’s buffer and resuspended in 800 μ L Tyrode’s buffer supplemented with 3% BSA. 30 μ L were collected and incubated 15 min at RT with 1 μ L anti-mouse CD41-FITC antibody (specific for platelets and Mk, **Table M-6**). Samples were washed with 500 μ L Tyrode’s buffer and excess of antibody removed by centrifuging at 1300 g for 5 min. Pellet was resuspended in 1 ml Tyrode’s buffer and 50 μ l analyzed with a BD Accuri™ C6 cytometer. Platelet concentration (per mL) was calculated from the number of platelets (CD41 positive cells) in the 50 μ L sample.

Table M-6. Fluorochrome-conjugated antibodies for flow cytometry. The name of the antibodies, as well as, its target, the assay in which were used, the working concentration and the supplier are listed.

Antibody	Target	Assay	Dilution	Supplier
PE Anti-Mouse CXCR4 (#247506 clone)	SDF-1 receptor	Recruitment of hemangiocytes	1:50	R&D Systems
APC Anti Mouse VEGFR (#141522 clone)	VEGF receptor	Recruitment of hemangiocytes	1:50	R&D Systems
FITC Anti-Mouse CD41 (MWRReg30 clone)	α II β integrin	Platelet count	1:50	eBiosciences (11-0411-82)
APC Anti-Mouse CD41 (MWRReg30 clone)	α II β integrin	Platelet activation	1:50	eBiosciences (17-0411-82)
Alexa Fluor 488-Fibrinogen	α II β 3 activated integrin	Platelet activation	1:30	Molecular Probes (F13191)
FITC Anti-Mouse CD9 (mz3 clone)	Platelet protein tetraspanin	Platelet aggregation	1:100	Biolegend (T22.124805)
PE Anti-Mouse CD9 (mz3 clone)	Platelet protein tetraspanin	Platelet aggregation	1:100	Biolegend (T22.124807)
PE Anti-Mouse CD61 (2C9.G3 clone)	Mouse Integrin β 3	MK differentiation	1:50	eBiosciences (12-0611)
FITC Anti-Mouse CD42 (Xia.H10 clone)	GPIb	MK differentiation	1:50	Emfret Analytics (#M041-1)

8.2. Detection of hemangiocytes in peripheral blood and bone marrow.

Blood (200 μ l) from the submandibular plexus was collected into EDTA-tubes (Sarstedt®). Erythrocytes were lysed with RBC buffer for 30 min at 4 °C. Blood, was then washed with PBS containing 5% FBS and resuspended in 50 μ l PBS with 0.5% FBS.

BM was collected as described in **Section 3**.

Both samples were incubated one hour with murine FC gamma RIII (CD16) antibody (1:50, R&D Systems) to block lymphocytes. Hemangiocytes were stained with anti-CXCR4-PE and anti-VEGFR-APC antibodies (**Table M-6**), for 15 min at 4 °C. The excess of antibody was removed by centrifugation at 300 g, and the cell pellet was resuspended in 300 μ L PBS for acquisition using FACSCalibur™ or FACS Aria™ cytometers.

8.3. Analysis of platelet activation

Platelets can be activated by substances released by tumor cells (thrombin, ADP, etc.). Platelet activation can be determined by measuring the amount of activated integrin α IIb β 3 present on platelet surface. To this end, 50 μ l of blood from the retro-orbital plexus was collected in tubes containing heparin as anticoagulant, washed with Tyrode's buffer and resuspended in 1 mL Tyrode's buffer. 30 μ L of diluted blood was incubated with 1×10^6 B16-F10 melanoma cells for 10 min at 37 °C in the presence of Fibrinogen-Alexa Fluor 488 (binds specifically to the activated form of integrin α IIb β 3 (**Table M-6**) and anti-CD41-FITC antibody (**Table M-6**). The percentage of activated platelets was assessed using a BD Accuri™ C6 cytometer.

8.4. Platelet aggregation assay

Platelet aggregation was measured as previously described in (De Cuyper *et al.*, 2013). To do so, 50 μ l of citrate-anticoagulated blood from the retro-orbital plexus was washed and resuspended in 1 mL Tyrode's buffer. Blood was then split into two populations. Each population was labeled with either anti-CD9-FITC or anti-CD9-PE antibodies (**Table M-6**) for 15 min (platelet surface glycoprotein CD9, or tetraspanin, does not participate in the aggregation process). After centrifugation at 2100 g for 5 min to remove the excess antibodies, the blood was suspended in Tyrode's-Hepes buffer and both populations were mixed and incubated with 3×10^4 B16-F10 melanoma cells at 37 °C to induce platelet aggregation. The reaction was halted at different times (0, 1, 2, 5 and 10 min) by the addition of 750 μ L 0.5% formaldehyde in PBS. Flow cytometry was used to determine the number of aggregates (percentage of double labeling events) using BD Accuri™ C6.

8.5. Detection of Megakaryocytes by analysis of cell surface markers

Isolated BM or differentiated Mks were washed once with PBS containing 5% BSA, centrifuged for 5 min at 300 g, and resuspended in 100 μ L PBS containing 0.5% BSA. Cells were incubated with anti-CD41-FITC and anti-CD61-PE or anti-CD42-FITC antibodies (**Table M-6**). After incubation, samples were washed in 500 μ L PBS and centrifuged at 300 g for 5 min. Cell pellets were resuspended in 300 μ L PBS before analyzed using a BD Accuri™ C6 cytometer.

8.6. Analysis of DNA ploidy

Propidium Iodide (PI) was used to quantify DNA in Mk. PI is a dye that intercalates between double-strand DNA producing a highly fluorescent signal when excited at 488 nm. Therefore, it is an accurate indicator of DNA ploidy.

Isolated BMC were washed in PBS, centrifuged at 300 g for 5 min and resuspended in 50 μ L PBS. Cells were fixed by the dropwise addition of 100 μ L 70 % ethanol, while vortexing to avoid cell aggregation, and maintained at 4 °C o/n. Then, cells were washed with 500 μ L PBS, centrifuged at 300 g for 5 min at 4 °C, and resuspended in 50 μ L PBS. Cells were labeled with anti-CD41-FITC (**Table M-6**) for 20 min and then incubated for 40 min at RT with 100 μ g/mL RNase A and 50 μ g/mL PI. Finally, samples were washed, centrifuged, and resuspended in 100 μ L PBS before being analyzed with BD Accuri™ C6 cytometer.

For the analysis, we first gated the CD41⁺ cell population. Cell doublets were excluded based on pulse-width vs pulse-area. These gates (CD41⁺ and single cells) were combined and the PI histogram plot (Cell count vs PI intensities) applied. The histogram plot is comprised of several peaks, each one representing a population of CD41⁺ cells with equal DNA content. The first peak corresponds to the population of diploid cells, the second correspond to tetraploid cells, and so on.

8.7. Analysis of c-Mpl internalization

Flow cytometry was used to track c-Mpl internalization. PRP was isolated as described in **Section 4**, and allowed to rest for at least 1 h. PRP was then stimulated with TPO at a concentration of 25 ng/mL for 30 min at 37 °C with no stirring. Platelets were fixed using 4 % paraformaldehyde (PFA, 15 min, RT) and incubated with anti-c-Mpl antibody (Merck, 06-944) at a concentration 1:50, for 1 h at RT. After removing excess antibodies by washing with 500 μ L PBS, samples were incubated with goat anti-rabbit-Cy5-conjugated (1:125, **Table M-10**) and anti-CD41-FITC antibodies (**Table M-6**).

Finally, platelets were centrifuged and resuspended in 200 μ L PBS before acquired using a BD Accuri™ C6 cytometer.

c-Mpl internalization was calculated as the percentage of c-Mpl labeled platelets in the CD41⁺ population. The percentage was calculated using the following equation, considering the MFI (mean fluorescent intensity) of C3G-wt samples at time 0 as the 100%.

$$\% \text{ cMpl on the surface} = \frac{\text{MFI C3Gwt } t(0) - \text{MFI sample}}{\text{MFI C3Gwt } t(0)} \times 100$$

9. *In vivo* experiments

9.1. Tail-bleeding assays

6-8-week-old mice were anesthetized with isoflurane. A section of 0.5 cm of the tail tip was transected and the tail was immersed in pre-warmed PBS at 37 °C to avoid vasoconstriction. Bleeding time was noted when the blood flow ceased. To avoid the death of the animal, experiment was stopped after 8 min of bleeding.

9.2. Acute pulmonary thromboembolism

Mice were anesthetized with a mixture of Ketamine/Valium (100 mg/kg of mouse body weight and 5 mg/kg of mouse body weight, respectively, in 0.9% NaCl). Once the adequate level of anesthesia was confirmed, jugular vein was exposed. Acute lung thromboembolism was induced by the injection of a mixture of 600 μ g of collagen (type I, Sigma, MO, USA) and 60 μ g of norepinephrine (Sigma)/kg of mouse body weight (lethal dose) or 150 μ g of collagen and 15 μ g of norepinephrine/kg of mouse body weight (sublethal dose) into the jugular vein.

9.2.1. *Lethal dose*

The injection of a lethal dose of collagen/norepinephrine produces a fast thrombi formation inside vessels. Thrombi end into the lungs, causing pulmonary obstruction and, as a result, animal death from respiratory failure. The time elapsed between the injection of collagen/norepinephrine and the death of the animal was recorded. Surviving animals were those that were still alive 20 min after injection.

Thrombi formation was confirmed in histological sections. To this end, lungs were collected and preserved in 4% formaldehyde at RT o/n. Histological processing (embedding, 3- μ m slice sections obtaining and hematoxylin-eosin staining (H&E)) was

performed by the Comparative Molecular Pathology Unit of the Cancer Research Center. Thrombi were detected as eosinophilic material with boundaries, with entire or partial involvement of the lumen of the small and medium size blood arteries situated mostly on the periphery of the pulmonary lobes, and were visualized under an optic microscope (Olympus BX51 with Olympus DP70 camera).

9.2.2. Sublethal-dose

A sublethal-dose of collagen/norepinephrine activates platelets and triggers platelet aggregation and coagulation, resulting in a drop in platelet count. The decrease in platelet number in peripheral blood can be used to track the development of thrombus. A volume of 100-200 μL of blood was collected from the jugular vein, before and after the sublethal injection, and platelets were labeled with anti-CD41-FITC antibodies (**Table M-6**), as described in **Section 8.1** to count them by flow cytometry. The percentage of platelet number reduction was calculated using the following equation:

$$\% \text{ decrease platelet number} = \frac{\text{Final Platelet Number}}{\text{Initial Platelet Number}} \times 100$$

9.3. Induction of ischemia by tumor cell implantation

To study the effect of C3G in platelet-mediated tumor growth, 5×10^5 3LL (Lewis Lung Carcinoma) cells were subcutaneously injected in the shaved flanks C3G-KO mice and their controls. Tumors were allowed to develop for 15 days before being removed.

9.3.1. Analysis of hemangiocyte recruitment

Ischemia induces the recruitment of hemangiocytes, proangiogenic progenitor cells from the bone marrow that express surface markers CXCR4 and VEGFR (Jin *et al.*, 2006). Hemangiocyte recruitment was monitored by flow cytometry as the number of double CXCR4/VEGFR positive cells (**Table M-6**) in peripheral blood, at days 0, 9 and 15 post ischemia, and in bone marrow at the final day of the experiment (**Figure M-1**).

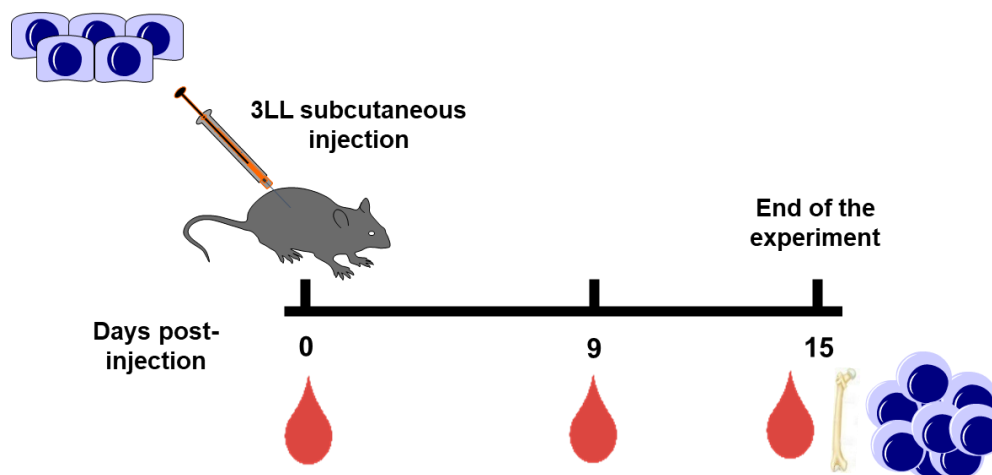


Figure M-1. Tumor-induced ischemia model. Diagram of blood and BM sample collection for the analysis of hemangiocyte recruitment following 3LL cells implantation. Blood was collected at days 0, 9 and 15. At the final day of the experiment, tumors were removed, weighted and fixed to analyze the number of vessels in tumor section by immunohistochemistry (IHC).

9.3.2. Histological analysis

Tumors were collected 15 days after the implantation to analyze vessel formation. Tissue was immersed in 4 % formaldehyde o/n at RT and processed for histological analysis. Slice sections (3- μ m) were stained with an anti-CD31 antibody (specific for endothelial cells, 1:25, Abcam). The immunohistochemistry staining was made with the automated system Discovery (Roche). Chromo Map Kit (Roche) was used to visualize the signal.

At least 5 fields per section were captured using the light microscope (Olympus BX51 with Olympus DP70 camera). The number of vessels were quantified using the ImageJ plug-in IHC tool-box following the indication of the developers.

9.4. Induction of unilateral hind-limb ischemia

A unilateral hind-limb ischemia was induced in mice following the methodology reported by (Niiyama *et al.*, 2009). Mice were anesthetized with 2 % isoflurane (Vetflurane®, Virbac) and placed in supine position in a heat pad at 37 °C. After ensuring the correct level of anesthesia, an incision of 1 cm was made from the knee towards the medial thigh. The neurovascular bundle was uncovered using tiny forceps and a fine pointed swab. The femoral nerve was separated from the femoral artery and vein to avoid damage. Double knots were used to occlude the femoral artery and vein at the proximal and distal location (**Figure M-2**). Ischemia was produced by transectioning the segment

between the proximal and distal knots. Finally, the incision was closed using silk suture and mice were removed from the anesthesia and placed in a heating pad until awake.

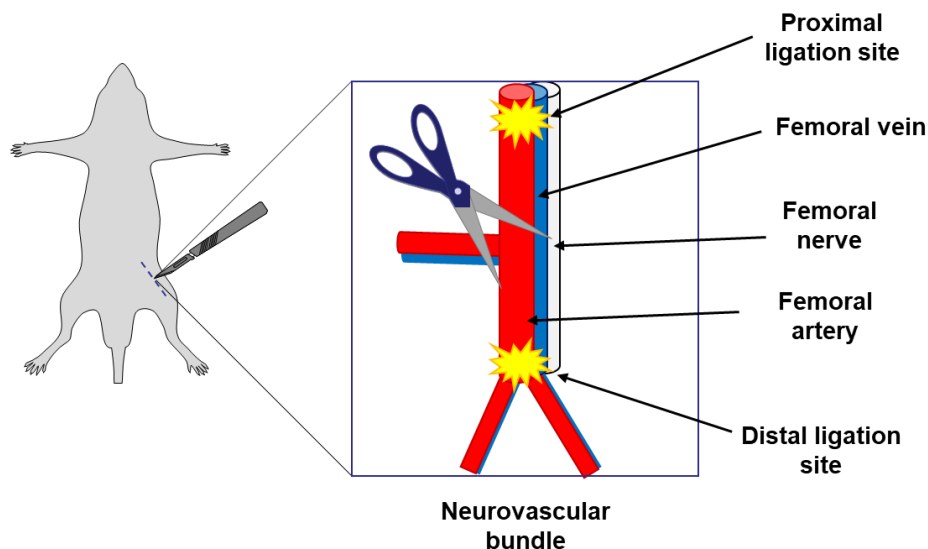


Figure M-2. Induction of ischemia in the hind-limb. After separating from the femoral nerve, two pair of knots were made to occlude femoral artery and vein. The ischemia was then induced by transecting the segment between the distal and proximal knots.

9.4.1. Doppler imaging and hemangiocyte recruitment

A Laser Doppler was used to assess blood flow on days 0, 1, 2, and 14 after inducing ischemia (**Figure M-3**). Mice were sedated with isoflurane and placed in a prone position on a light-absorbing surface that was non-reflective. Blood flow was measured at the same time in the ischemic and non-ischemic foot. Mice were then removed from anesthesia and placed in a heating pad for recovery. Blood from the submandibular plexus was collected at days 0,1,2 and 14 days after the surgery to analyze ischemic-induced hemangiocyte recruitment.

9.6. 5-Fluorouracil-induced myelosuppression

The uracil analogue 5-fluorouracil (5-FU) is a heterocyclic aromatic organic compound that interferes with nucleoside metabolism because it can be incorporated into DNA and RNA, producing cytotoxicity and cell death.

The subcutaneous administration of a sublethal dose of 5-FU in mice (150 mg per kg of body weight) causes BM ablation except for the HSC. This ablation is accompanied by a drop in platelet count until day 10 after injection, after which there is an exacerbated increase in platelet count, known as platelet rebound. These effects of 5-FU make it a suitable model to analyze the role of C3G in the production of megakaryocytes and platelets in a pathological situation.

Mice (6-10-week-old) were weighted before receiving a sublethal dose of 5-FU, and the appropriate amount of 5-FU was dissolved in saline serum containing 12.5% of DMSO, o/n at 37 °C under constant stirring. Once it was completely dissolved, 5-FU was injected intraperitoneally. Platelets were counted every 3-4 days for 21 days by flow cytometry (as described in **Section 8.1**) to monitor myelosuppression and platelet recovery (**Figure M-5**). At the end of the experiment, mice were sacrificed, and BM was collected, as described in **Section 3**, to determine the number of mature Mk and their ploidy status.

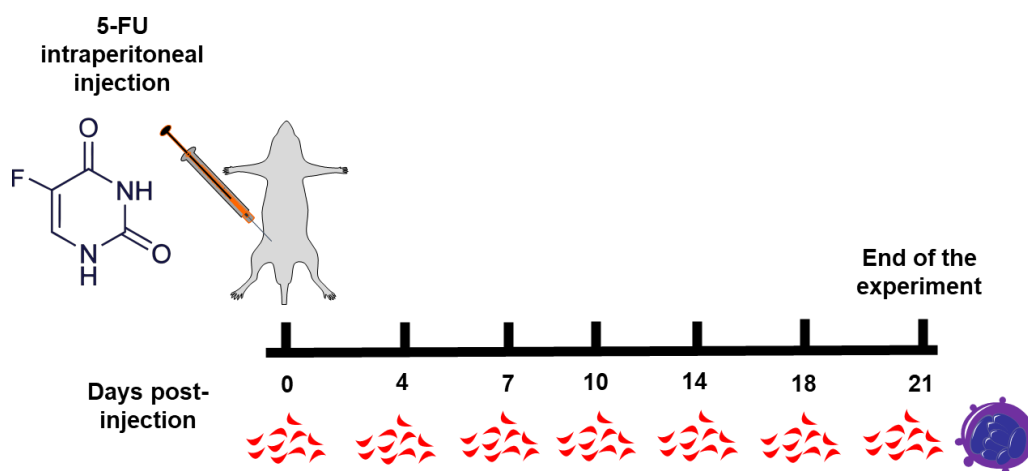


Figure M-5. *In vivo* model of myeloablation and megakaryopoiesis induced by 5-FU. Schedule of blood and bone marrow sample collection to analyze the number of platelets and mature Mk at different days, before and after the injection of a sublethal dose of 5-FU.

9.6.1. Plasma TPO levels

Blood from the submandibular plexus was collected into Microvette tubes (Sarstedt®) at days 0, 3, 6, and 9 after the injection of 0.5 µg TPO to examine the fluctuation in plasma TPO levels. Blood was centrifuged at 10000 g for 5 min, and plasma (supernatant) was immediately frozen at -20 °C until use.

TPO levels were tested using an ELISA kit (Quantikine;R&D). Briefly, samples were incubated for 2 h in wells precoated with monoclonal antibody against TPO. After washing (5 times) to eliminate non-bound substances, a peroxidase-linked antibody against TPO was added to the wells for 2 h at RT. Following washing to eliminate any unbound antibody-enzyme reagent, a substrate solution (comprised by hydrogen peroxide and tetramethylbenzidine) was added to the wells during 30 min. Finally, the reaction was stopped with the Stop Solution and the absorbance was measured at 540 nm using a TECAN (infinite M200 PRO) microplate reader. TPO concentration was calculated by generating a standard curve, plotting the mean absorbance for each standard against the concentration of each point.

9.7. Short-term metastasis model

B16-F10 murine melanoma cells (2×10^6), expressing the enhance green fluorescent protein (EGFP) were resuspended in 100 µL PBS and injected into the retro-orbital plexus of isoflurane-anesthetized mice. Lungs were extracted within one hour after injection and digested, with a lung digestion buffer (RPMI, 5% fetal calf serum (FCS), 150 U/mL collagenase I (Sigma) and 50 U/mL dispase type II (Sigma)), for 45 min at 37 °C under stirring. The digested suspension was filtered through a 70-µm cell strainer (Falcon) and treated with RBC lysis buffer to eliminate erythrocytes. Cells were then centrifuged at 300 g for 5 min at 4 °C and the resultant cell pellet was resuspended in 1 mL PBS. Flow cytometry was used to count the number of B16-F10-EGFP positive cells using a BD Accuri™ C6 cytometer.

10. *In vitro* detection of TPO uptake by platelets

Platelets were isolated as described in **Section 4** and allowed to settle for 1h. Then, 1×10^6 platelets were stimulated with 2000 pg/mL TPO for 30 min. Supernatants were extracted by centrifugation at 2100 g for 10 min at 4 °C and immediately used for TPO measurement by ELISA (Quantikine, R&D) following the protocol described in **Section 9.6.1**.

TPO uptake by platelets was measured using the following formula:

$$TPO \text{ uptake} = TPO \text{ pg/mL} (t_0) - TPO \text{ pg/mL} (t_{30})$$

11. RNA analysis

11.1. RNA isolation from tissue

Liver or Ischemic muscle (≈ 50 mg both), were dissected and homogenized in 1 mL of NZYol (NZYTech) using a GentleMACS dissociator (Miltenyi Biotec). RNA was isolated according to the manufacturer's instructions. Homogenates were incubated at RT for 5 min, and then mixed with 0.2 mL chloroform for 3 min at RT and centrifuged at 12000 *g* for 15 min at 4 °C. The samples were separated into three different phases: one lower-green phenol-chloroform phase, and interphase and an upper aqueous phase containing RNA. The upper phase was carefully transferred into a new tube and RNA was precipitated with cold isopropyl alcohol and then washed with 75% ethanol. After 12000 *g* 5 min centrifugation, supernatant were discarded and pellet were air dried for 5-10 min. Finally, pellets were resuspended in 30-50 μ L of DEPC-treated water.

11.2. RNA isolation from platelets and Megakaryocytes

The RNeasy Mini Kit (Qiagen) was used to isolate RNA from platelets and megakaryocytes following manufacture's instructions.

RNA capillary electrophoresis columns were used to determine the concentration and quality of the extracted RNA (Agilent Technologies, RNA 6000 Nanochips). RNA samples were kept at -80°C until they were needed.

11.3. cDNA synthesis

A reverse transcription (RT) reaction was conducted to synthesized cDNA. Briefly, 1 μ g RNA (from ischemic muscle) or 1 ng RNA (from platelets and megakaryocytes) was combined with 10 μ L NZYRT 2X Master Mix (which includes oligo(dT)₁₈, random hexamers, MgCl₂ and dNTPs), 2 μ L of NZYRT Enzyme mix (which includes NZY Reverse Transcriptase and NZY Ribonuclease inhibitor) and DEPC-treated water (NZYTech). The mixture was incubated for 10 min at 25 °C, followed by 30 min at 50 °C. The reaction was stopped by heating 5 min at 85 °C, and samples were chilled on ice. RNA was eliminated by incubating samples for 20 min at 37 °C with 1 μ L NZY RNase H. cDNA was stored at -20 °C.

11.4. Quantitative PCR

Quantitative PCR (qPCR) was used to assess gene expression in ischemic tissue, liver, platelets and Mk using specific primers listed in **Table M-7**. Reaction was performed by mixing 1 μ L cDNA with 2X NZYSpeedy qPCR green Master Mix (NZYTech), 10 μ M forward primer, 10 μ M reverse primer and RNase-free water. Gene expression levels were normalized against the housekeeping gene β -Actin in each experiment, which was done in triplicate.

Table M-7. Sequence of primers used in qPCR. The size of the amplicon is indicated

Gene	Forward primer (5'-3')	Reverse primer (5'-3')	Amplicon size (kb)
C3G N-Terminus	GTGAGCAAAGAGGCAAGAGA	CACAGCACTGGTGGACATAA	99
C3G C-Terminus	ATTTCCACAGCCACGAGATAG	CTCTTCTCCTCATTCTGCTCTT	115
Vegfa	GAGAGAGGCCGAAGTCCTTT	TTGGAACCGGCATCTTTATC	163
Vegfr	GTCTCCATCAGTGGCTCTACG	CCCGTTCTTGTTGTATTTG	104
Cd31	ACTTCTGAACTCCAACAGCGA	CCATGTTCTGGGGGTCGTAAT	80
Sdf-1	AGCCAACGTCAAGCATCT	GCACACTTGTCTGTTGTTGTT	130
Cxcr4	CTCTGAAGAAGTGGGTTCTGG	AAGTAGATGGTGGGCAGGAAG	100
Mpl	AGACTGCTTGGATCACCTTG	CGCAGGAAATTGCCACTTTAG	95
β-Actin	TAGACTTCGAGCAGGAGATGG	CAAGAAGGAAGGCTGGAAAG	122
Tpo	TTCAGTGTCACAGCCAGAAC	GGGACCTGGAGGTTTGATTTAG	100

11.4.1. qPCR data analysis

mRNA expression levels were analyzed using the $2^{-\Delta\Delta C_t}$ method (Livak & Schmittgen, 2001). C_t value (threshold cycle) is defined as the cycle at which the fluorescence signal of the amplification curves cross the threshold line. This value is inversely correlated with gene expression. C_t values were obtained from the real-time PCR equipment software QuantStudio3 and QuantStudio5 (Thermo Scientific). According to $2^{-\Delta\Delta C_t}$ method requisites, efficiency of primer pairs was analyzed by serial dilutions of the cDNA. Only primers that showed an efficiency between 80 and 120% were used.

12. Immunodetection of proteins by Western Blot

12.1. Sample preparation

Platelets were lysed under non-denaturing conditions with RIPA 1X (20 mM Tris pH 7.5, 150 mM NaCl, 1% Triton-X-100, 0.1% sodium deoxicolate, 0.1% SDS, 1 mM PMSF, 5 mM NaF, 1 mM Na₃VO₄ y 1X cOmplete® (Roche)) or modified RIPA 2X (100 mM Tris pH 7.5, 400 mM NaCl, 5 mM MgCl₂, 2% Igepal, 20% Glycerol, 1 mM PMSF, cOmplete® (Roche)) for 10 min at 4 °C. Lysates were centrifuged at 16000 g for 10 min at 4° C. The supernatants were considered as the cytosolic fraction, while the pellets were considered as the membrane fraction. Membranes were directly resuspended in 12 µl of Laemmli Buffer 2X (100 mM Tris pH 6.8, 20% Glycerol, 2% SDS, 2% β-Mercaptoethanol, 2% Bromophenol Blue) and boiled for 5 min at 95-100 °C. Supernatants were stored at -80 °C until use.

For some experiments, platelets were directly resuspended in 20 µL of Laemmli Buffer 2X and boiled 10 min at 95-100 °C. Samples were stored at -80 °C until use.

Mks obtained as described in **Section 3.2** were resuspended in RIPA buffer and maintained on ice for 20 min. Cells were sonicated using a Vibracell™ VCX750 Ultrasonic Cell Disrupter at 30% amplitude by applying pulses of 5 s, with 30 s on ice between each pulse. Lysates were cleared by centrifugation at 16000 g for 10 min at 4 °C. Samples were kept at -80 °C until use.

12.2. Protein Quantification and denaturalization

To determine protein concentration, 1 µl of lysate was diluted in 800 µl MiliQ water and incubated for 5 min at RT with 200 µl Bradford Reagent (0.25 mg/mL Coomassie Brilliant Blue G-250, 25% Methanol, 42.5% orthophosphoric acid). Protein concentration was detected by spectrophotometry at a wavelength of 595 nm. Different known concentration BSA (0 to 5 µg/µL) were used to create a standard curve by plotting the 595 nm values (y-axis) versus their concentration in µg/ml (x-axis). The concentration of the samples was determined using this standard curve.

The appropriate amount of protein (typically 30 µg) was denatured by boiling in 4X Laemmli Buffer.

12.3. SDS-Polyacrylamide gel electrophoresis

Proteins were separated using SDS-polyacrylamide gels. This technique allows protein separation based on their length and mass-to-charge ratio. The concentration of polyacrylamide depends on the molecular weight of the protein of interest, being inversely proportional to the size of the protein (**Table M-8**). Equal amount of denatured proteins was loaded onto polyacrylamide gels and the electrophoresis was performed in running buffer (25 mM Tris-HCl pH 8.3, 250 mM Glycine, 0.1% SDS) at constant voltage. The size of the proteins was determined using the pre-stained protein standard PageRuler™ Plus Prestained Protein Ladder (Thermo Fisher).

Table M-8. SDS-PAGE stacking and separating gel composition

	Stacking Gel	Separating Gel		
		7.5%	10%	12.5%
4X Upper Tris (pH 6.8)	0.625 mL	-	-	-
Lower Tris 4x (pH 8.8)	-	1.25 mL	1.25 mL	1.25 mL
Acrylamide 30 %/ Bis 3.3%	0.29 mL	1.25 mL	1.662 mL	2.083 mL
H ₂ O	1.555 mL	2.5 mL	2.062 mL	1.662 mL
Ammonium Persulphate (APS) 10%	25 µL	35 µL	35 µL	35 µL
TEMED	1.875 µL	2.5 µL	2.5 µL	2.5 µL

12.4. Transfer of proteins to PVDF membranes

After electrophoresis, proteins were transferred to methanol-pretreated Immobilon-P PVDF (Polyvinylidene fluoride) membranes (Merck Millipore) by wet transfer using Mini Trans Blot® System (Bio-Rad) and transfer buffer (66 mM Tris-HCl pH 8.3, 386 mM Glycine, 0.1% SDS, 20% methanol). Transfer was carried out at a constant amperage of 0.3 A for 2 or 3 h, depending on the thickness of the gel.

To minimize non-specific protein binding, membranes were incubated o/n at 4 °C in blocking buffer (5% non-fat dry milk (NFDM) in TTBS (10 mM Tris pH 7.3, 150 mM NaCl, 0.5% Tween-20)).

12.5. Immunodetection

Membranes were incubated with primary antibodies (**Table M-9**) for 1 h at RT or o/n at 4 °C in 2% BSA in TTBS. Next, membranes were washed three times with TTBS (10 min each) and incubated with secondary antibodies (**Table M-9**) for 50 min at RT in 5% of NFDM. Excess secondary antibodies were removed by washing three times with TTBS (10 min each).

For the detection by chemiluminescence, membranes were incubated with HRP-conjugated secondary antibodies, and proteins were detected using the reagents from the commercial kit, Clarity™ Western ECL Blotting Substrates (Bio-Rad) following the manufacturer’s instructions. For the detection by immunofluorescence, using Odyssey Infrared Imaging System (LI-COR), membranes were incubated with fluorochrome-conjugated secondary antibodies.

Table M-9. Primary and secondary antibodies used for western blot. Antibody target, host-species in which the antibodies were generated, supplier and reference, and working dilution are indicated.

Primary Antibodies					
Antibody	Target	Host	Supplier	REF	Dilution
VEGF (VG-1)	121, 165 and 189 VEGF isoforms	Mouse	Abcam	ab1316	1:500
TSP-1	Thrombospondin	Mouse	Thermo scientific	MA5-13398	1:1000
c-Cbl	c-Cbl	Rabbit	Cell Signalling	#2747	1:1000
Rap1	C-terminus of human Rap1	Rabbit	Santa Cruz	Sc-65	1:1000
c-Mpl	Amino acids 615-628 of TPOR/Mpl	Rabbit	Merck	06-944	1:1000
Ubiquitin (P4D1)	Amino acids 1-76 of Ubiquitin	Mouse	Santa Cruz	sc-8017	1:1000
β-Actin	β-Actin	Mouse	Merck	A5441	1:1000
β-Tubulin	β-Tubulin	Mouse	Merck	T5293	1:1000
Secondary Antibodies					
Antibody	Target	Host	Supplier	REF	Dilution
Anti-Mouse IgG HRP-linked	Anti-Mouse	Sheep	GE HealthCare	NXA931	1:5000
Anti-Rabbit IgG HRP-Linked	Anti-Rabbit	Goat	Santa Cruz	Sc-2004	1:5000
Goat Anti-Mouse IgG Dylight 680	Anti-Mouse	Goat	Thermo Fisher	35518	1:5000
Goat Anti-Mouse IgG Dylight 800	Anti-Mouse	Goat	Thermo Fisher	35521	1:5000
Goat Anti-Rabbit IgG Dylight 680	Anti-Rabbit	Goat	Thermo Fisher	35568	1:5000
Goat Anti-Rabbit IgG Dylight 800	Anti-Rabbit	Goat	Thermo Fisher	SA5-10036	1:5000

12.6. Membrane stripping

To reuse the immunoblotted membranes, antibodies were removed by two 10-min washes in Stripping Buffer (1.5% Glycine, 0.1% SDS, 1% Tween-20 in MilliQ water, pH

2.2), followed by three washes with TTBS. Prior incubation with the new antibody, membranes were blocked with 5% NFDM in TTBS, 1 h at RT.

13. Confocal Microscopy

Platelets were fixed with 4% PFA for 15 min at RT following activation. Platelets were seeded onto glass coverslips pre-coated with poli-L-lysine during 50 min at RT. Attached platelets were washed with PBS, permeabilized with 0.2% Triton™ X-100 (Sigma) and washed again with PBS. Coverslips were blocked with 1% BSA o/n. Primary antibodies were prepared in 1% BSA and incubated for 2 h at RT. Coverslips were rinsed three times in PBS and next incubated for 1 h at RT with secondary antibodies. Phalloidin-iFluor 488 (Abcam) was used to label the actin cytoskeleton. After staining, platelets were washed three times in PBS followed by one wash in MilliQ water. Finally, preparations were mounted with Prolong™ Diamond Antifade Mountant (Thermo Scientific). **Table-M10** shows all the antibodies used for immunofluorescence. Images were captured with a Leica SP8 confocal microscope and processed with FIJI Software (National Institutes of Health, Bethesda, MD, USA). Colocalization between two proteins was analyzed using Coloc2 plug-in (Dunn *et al.*, 2011; Peters *et al.*, 2012).

Table M-10. Primary and secondary antibodies used for immunofluorescence. Antibody target, host-species in which the antibodies were generated, supplier and reference and working dilution are indicated.

Primary Antibodies					
Antibody	Target	Host	Supplier	REF	Dilution
C3G 1008	SH3b-RemCat domain of human C3G	Rabbit	Guerrero <i>et al</i> 1998		1:50
c-Cbl	c-Cbl	Rabbit	Cell Signalling	#2747	1:100
pCbl (E-10)	pTyr 700 of Cbl	Mouse	Santa Cruz Biotechnology	sc-377571	1:100
pSrc Y418	pTyr 418	Rabbit	Abcam	ab4816	1:100
c-Mpl	Amino acids 615-628 of TPOR/Mpl	Rabbit	Merck	06-944	1:100
Ubiquitin (P4D1)	Amino acids 1-76 of Ubiquitin	Mouse	Santa Cruz Biotechnology	sc-8017	1:100
VEGF (VG-1)	121, 165 and 189 VEGF isoforms	Mouse	Abcam	ab1316	1:200
TSP-1	Thrombospondin	Mouse	Thermo Scientific	MA5-13398	1:200
SDF-1	CXCL12 α and CXCL12 β	Mouse	R&D systems	MAB350-100	1:100
P-selectin (C-20)	CD62P	Goat	Santa Cruz Biotechnology	Sc-6941	1:100
Secondary Antibodies					
Antibody	Target	Host	Supplier	REF	Dilution
Cy3-Affinity Pure IgG	Donkey	Goat	Jackson ImmunoResearch	705-165-147	1:50

Alexa Fluor-568 conjugated IgG	Goat	Rabbit	Thermo Scientific	A21236	1:500
Alexa Fluor-647 conjugated IgG	Goat	Mouse	Thermo Scientific	A11036	1:500

14. B16-F10 Adhesion Assay

B16-F10 melanoma cells (4×10^4) were incubated with 1×10^7 platelets from the different genotypes for 10 min at 37 °C to induce platelet-tumor cell interaction. Cells were then transferred to poly-L-lysine coated glass coverslips and maintained for 30 min at 37 °C. After washing out unbound cells with PBS, adhered cells were fixed with 4% PFA and blocked overnight with PBS containing 1% BSA. Platelets and B16-F10 cells were incubated with anti-P-selectin antibody (**Table M-10**) followed by anti-goat Cy3 antibodies (**Table M-10**) and Phalloidin-488. The number of B16-F10 adhered cells per field was analyzed with a Leica SP8 confocal microscope.

15. Rap activation assay

Pulldown assays were performed to assess Rap1 activation. This experiment is based on the interaction between activated Rap1 (GTP-bound) with the Rap-binding domain (RBD) of its target Ral-GDS fused to GST (glutathione S-transferase). Rap1-GTP binds to GST-RalGDS-RBD and can be precipitated by incubation with glutathione-Sepharose beads, which have a high affinity for GST.

15.1. Platelet Rap1 activation induced by B16-F10 cells

For each condition, 2×10^7 platelets were employed. Platelets were allowed to rest for at least 1 h before being stimulated at 37 °C with 1×10^3 B16-F10 cells. Platelets and tumor cells were incubated at various time points (0, 5, 10, 15 and 20 min) and the reaction stopped on ice. Samples were lysed with RIPA modified buffer and clarified by 10 min centrifugation (16000 g) at 4 °C. Each sample was split into two tubes: one for the analysis of total Rap1 and the other for Rap1-GTP pull down assay.

Samples for total Rap1 detection were supplemented with the necessary amount of 4X Laemmli buffer, boiled, and stored at -80 °C until use. Samples for Rap1-GTP detection were incubated 1 h at 4 °C with GST-RalGDS-RBD bound beads with gentle rotation. After the incubation, complexes were washed 3 times with RIPA buffer and then boiled with 2X Sample Buffer to separate proteins from the beads.

15.2. Detection of Rap1-GTP

Samples were charged onto 12.5% polyacrylamide gels and transferred into PVDF membranes as detailed in **Section 12.3** and **Section 12.4**. Total Rap1 and Rap1-GTP was detected using an anti-Rap1 antibody (**Table M-9**).

16. Co-Immunoprecipitation assay

Platelets were isolated and activated as described in **Section 4**. Platelets were centrifuged at 1200 *g* for 5 min before being lysed in 150 μ L RIPA buffer. Lysates were clarified by centrifugation (16000 *g*) for 10 min at 4 °C and 100 μ L of lysate was incubated o/n at 4 °C with the primary antibody C3G-G4 (**Table M-9**) under gentle rotation. Next, 100 μ L Agarose-G 4 beads (RapidRun®, ABT, which have a high affinity for IgG) were added to the samples and incubated for 1 h at 4 °C under gentle rotation. Unbound protein was removed by 3 washing steps with RIPA buffer. Finally, samples were boiled with 2X sample buffer to separate immunoprecipitated protein from the beads.

16.1. Detection of co-immunoprecipitated proteins

Samples were charged onto 10% polyacrylamide gels and transferred into PVDF membranes as describe in **Section 12.3** and **Section 12.4**. Cbl was detected using anti-Cbl antibody (**Table M-9**).

17. c-Mpl degradation

To analyze TPO-induced c-Mpl degradation, blood was collected in tubes containing citrate as anticoagulant, and platelets were isolated as detailed in **Section 4**. After 1 h rest, platelets were stimulated with 25 ng/mL TPO at different time points (0, 5, 15, 30 and 60 min) at 37 °C without shaking. Samples were centrifuged at 1300 *g* for 5 min at 4 °C and proteins extracted as described in **Section 12.1**. c-Mpl protein levels were detected by western blot using an anti-c-Mpl antibody (**Table M-9**).

18. Statistical Analysis

Data are represented as the mean \pm SD (standard deviation) or the mean \pm SEM (Standard Error of the Mean) as indicated. The Kolmogorov-Smirnov test was performed to determine if the data fit into a normal distribution. To compare between two experimental groups, unpaired Student's t-test was computed, when the data were normally distributed. The non-parametric Mann-Whitney U-test was used when the data did not fit a normal distribution. Both statistical methods were performed using Sigma

Plot v 11.0 and GraphPad Prism v8 software. Differences were considered significant when $p < 0.05$.

19. Ethical Considerations

This study was carried out in strict accordance with the EU Directive 2010/63/EU for animal experiments (http://ec.europa.eu/environment/chemicals/lab_animals/legislation_en.htm), including the “three Rs” rule. The protocols were approved by the Committee on the Ethics of Animal Experiments of the University of Salamanca (ID number: 639) and the Department of Agriculture, Livestock and Rural Development, Regional Government of Castilla y León, Spain. All procedures were performed under isoflurane anesthesia, and all efforts were made to minimize suffering.

RESULTS

RESULTS

1. Characterization of *Rapgef1*^{flox/flox}; *Pf4-Cre*^{+/-} mice

1.1. Successful deletion of C3G in megakaryocytes and platelets in *Rapgef1*^{flox/flox}; *Pf4-Cre*^{+/-} mice

We generated a mouse model with specific deletion of C3G in Mk and platelets, *Rapgef1*^{flox/flox}; *Pf4-Cre*^{+/-} (hereinafter C3G-KO). *Rapgef1*^{flox/flox}; *Pf4-Cre*^{-/-} mice (hereinafter C3G-wt) were used as negative controls. C3G ablation in C3G-KO Mk and platelets was validated at the DNA, RNA and protein level.

The primers used to detect the deletion in the genomic DNA should amplify, in the wild-type allele, a fragment longer than the maximum extension size allowed by the PCR technique, which explain why no PCR product was detected. Recombination between loxP sites in the *Rapgef1* gene, on the other hand, generated a 400-bp PCR product (**Figure R-1A**) that was detected in the genomic DNA of Mk from spleen and BM of C3G-KO mice (**Figure R-1B**), thus confirming the deletion.

To verify that this deletion resulted in the abrogation of C3G expression, we examined C3G expression by RT-qPCR in platelets and Mk from C3G-KO and C3G-wt mice. As shown in **Figure R-1C**, C3G mRNA was almost undetectable in Mk and platelets from C3G-KO mice. The residual expression detected in KO samples probably comes from contaminating cells.

Furthermore, we confirmed C3G ablation in platelets by immunofluorescence using anti-serum C3G #1008 (Guerrero *et al.*, 1998). C3G-KO platelets showed a substantial reduction in C3G signal, as compared to control platelets (**Figure R-1D**). C3G deletion was also verified in C3G-KO platelet lysates by western blot using the anti-mouse C3G G4 antibody (**Figure R-1E**).

All these data confirm the successful abrogation of C3G in C3G-KO Mk and platelets.

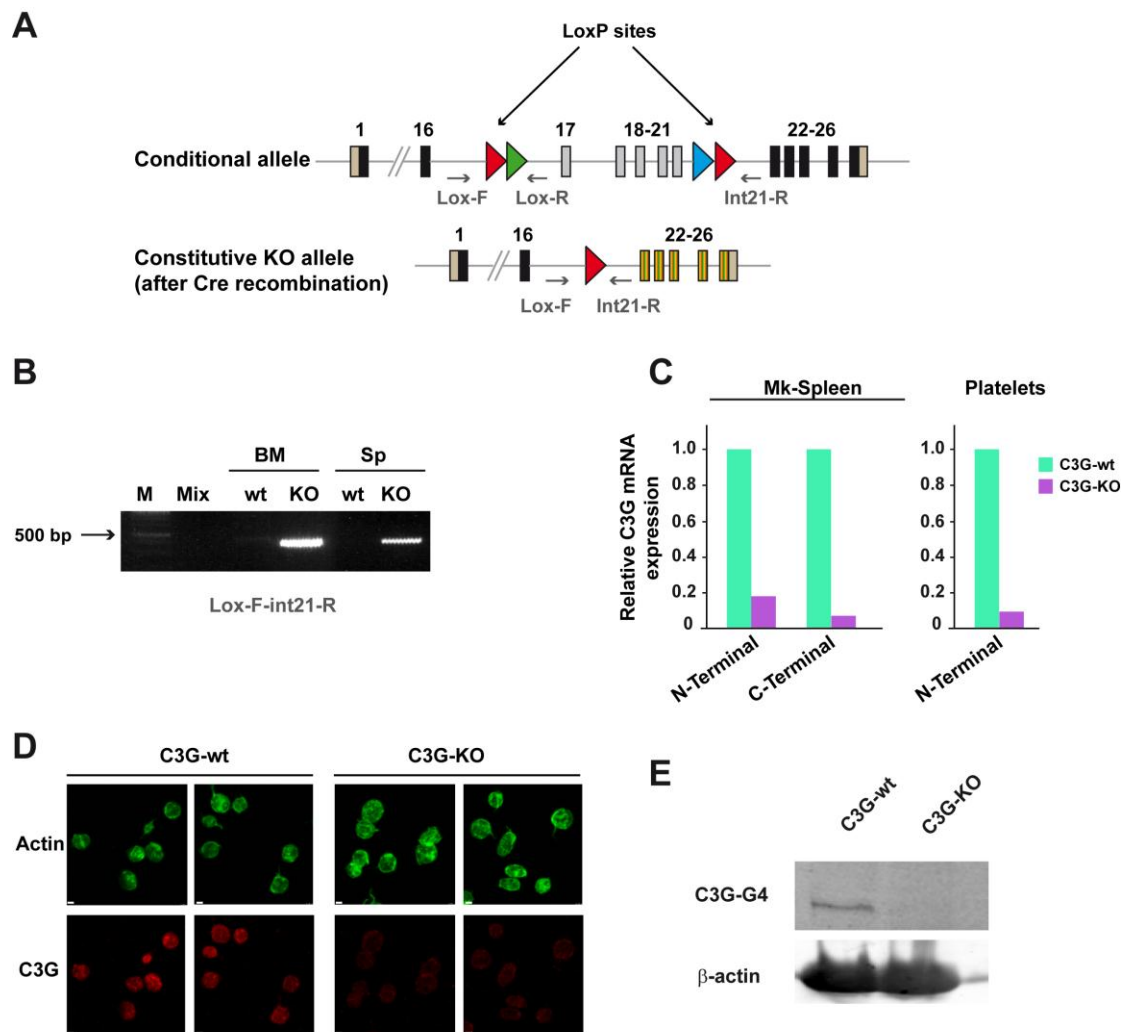


Figure R-1. Successful deletion of C3G in platelets and megakaryocytes from C3G-KO mice. (A) Schematic representation of the targeting strategy used to generate the *Rapgef1^{fllox/fllox}* conditional knockout (based on Shah *et al.*, 2016)). Cre-mediated recombination of exons 17-21 (which includes part of the catalytic domain), accompanied by a frame-shift from exon 16, result in inactivation of C3G. (B) PCR amplification, using primers Lox-F and int21R, of genomic megakaryocyte DNA obtained from bone marrow (BM) and spleen (Sp) of *Rapgef1^{fllox/fllox}; PF4-Cre^{+/-}* (KO) and control *Rapgef1^{fllox/fllox}; PF4-Cre^{-/-}* (wt) mice. The PCR mix was used as a negative control (Mix). M: Thermo Scientific™ GeneRuler™ 1kb Plus DNA Ladder. As expected, amplification of the ≈400 bp predicted band only occurred in the C3G-KO genomic DNA. (C) RT-qPCR analysis of C3G mRNA from spleen megakaryocytes and platelets of C3G-KO and C3G-wt mice. N-terminal amplicon: n190-n288; C-terminal amplicon: n2540-n2654 (NM_054050.2). (D) Representative immunofluorescence confocal microscopy images of C3G-KO and C3G-wt platelets stained with phalloidin and antibodies to C3G (rabbit antiserum #1008). Bar: 1 μm. (E) Analysis of C3G levels by western blot in platelets from both genotypes. β-actin was used as loading control. wt: wild-type, KO: knockout.

1.2. C3G ablation from platelets alters hemostasis

Previous data from our group demonstrated that C3G overexpression in platelets produces a significant decrease in bleeding time in a tail-bleeding assay. Conversely, tgC3G Δ Cat mice (transgenic mice overexpressing in Mk and platelets a mutant form of C3G lacking the catalytic domain) showed bleeding diathesis (Gutiérrez-Herrero *et al.*, 2012). To deep into this role of C3G in the control of hemostasis, tail-bleeding assays were performed in C3G-KO and C3G-wt mice at time of weaning. A significant bleeding diathesis was observed in C3G-KO mice, but not in their C3G-wt siblings (**Figure R-2A**), a phenotype similar to that of transgenic C3G Δ Cat mice (Gutiérrez-Herrero *et al.*, 2012).

To further demonstrate *in vivo* the involvement of platelet C3G in coagulation, we induced a pulmonary thromboembolism by injecting a mixture of collagen/norepinephrine into the jugular vein of C3G-KO and C3G-wt mice. A lethal dose of collagen/norepinephrine (600 μ g of collagen and 60 μ g of norepinephrine per kg of mouse body weight) causes a fast thrombi formation that ends up in the lungs, resulting in respiratory failure and animal death. C3G-KO mice showed a higher survival rate in response to collagen/norepinephrine injection, as seen by the higher number of mice surviving after 20 minutes, when compared with control littermates (**Figure R-2B**). Thrombus formation was confirmed by visualizing lung tissue sections stained with H&E. Thrombi were detected as eosinophilic material with borders, with total or partial affection of the lumen of the small and medium caliber blood vessels located mainly on the periphery of the pulmonary lobes (**Figure R-2C**).

Sublethal administration of collagen/norepinephrine (150 μ g of collagen and 15 μ g of norepinephrine per kg of mouse body weight) produces a decrease in platelet count in peripheral blood, indicating platelet aggregation. C3G-KO mice showed a significantly smaller decline in the number of circulating platelets, suggesting decreased aggregation in C3G null platelets (**Figure R-2D**).

Overall, the increased bleeding times and the lower thrombus formation seen in C3G-KO mice, together with the opposite phenotype observed in tgC3G mice (Gutiérrez-Herrero *et al.*, 2012) strongly suggest that C3G may be a key regulator of platelet hemostatic function.

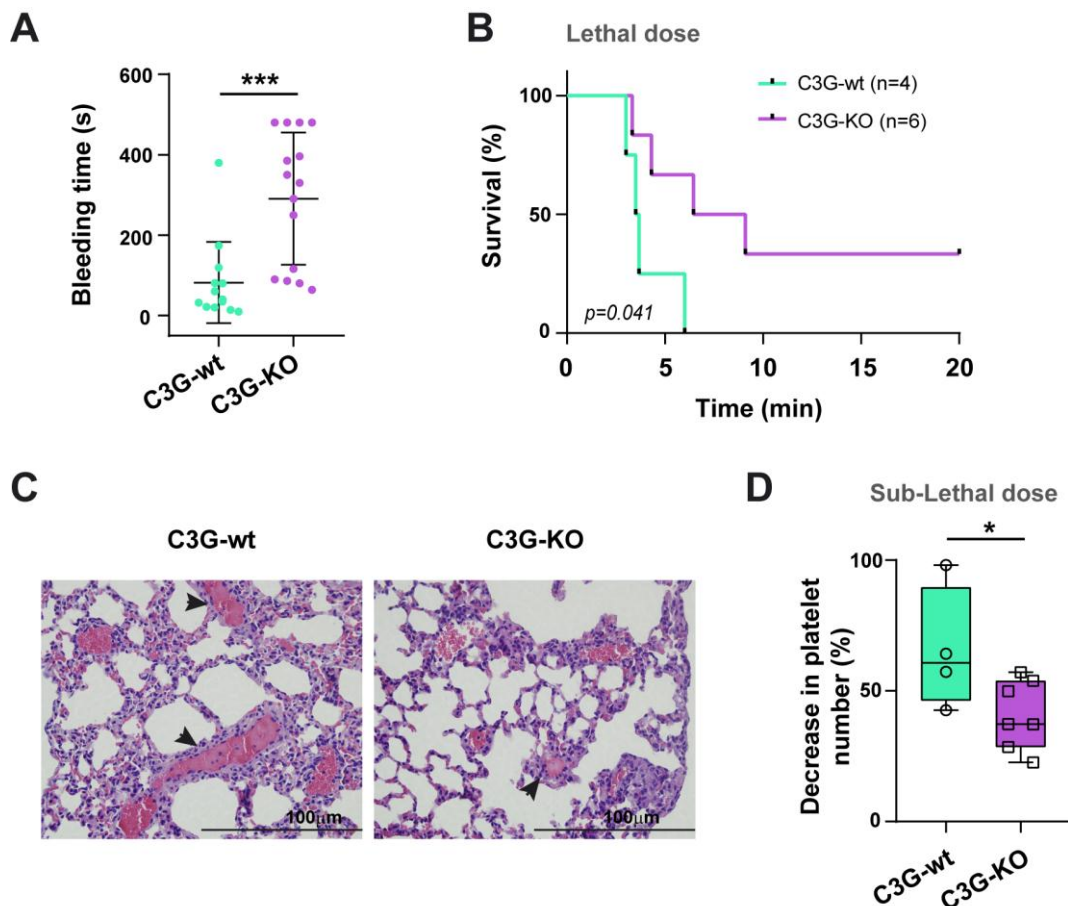


Figure R-2. C3G ablation in platelets results in impaired platelet coagulation, causing bleeding diathesis. (A) The scatter plot represents the mean \pm SD of bleeding time from 13-15 mice of each genotype at weaning. (B) A lethal dose of collagen/norepinephrine was injected into the jugular vein of C3G-KO and C3G-wt mice. Kaplan-Meier survival plots after induction of acute pulmonary thromboembolism. Long-Rank test ($p=0.0409$) was performed to analyze the difference in survival between both genotypes. Two out of six C3G-KO mice were alive 20 min after the stimulus. (C) Representative H&E staining images of lung sections from mice treated with a lethal dose of collagen/norepinephrine. Thrombi are indicated by arrowheads. Bar: 100 μ m (D) Boxplots show percentage (mean \pm SD) of platelet count reduction after injection of a sublethal dose of collagen/norepinephrine. * $p<0.05$, *** $p<0.001$. wt: wild-type, KO: knockout.

1.3. C3G ablation did not result in differences in platelet count or megakaryocyte number in bone marrow.

We previously demonstrated that C3G enhances Mk differentiation *in vivo* and *in vitro* (Ortiz-Rivero *et al.*, 2018). However, transgenic expression of C3G in Mk was not accompanied by an increase in platelet count in a physiological context (Ortiz-Rivero *et al.*, 2018). We used our C3G-KO model to fathom the role of C3G in megakaryopoiesis. First, we analyzed the number of circulating platelets and found no differences between C3G-KO and control mice, similar to what we observed in the tgC3G model (Figure R-3A). In correlation, C3G-KO mice did not present an alteration in the number of mature

Mk in BM (CD41⁺ cells, CD61⁺ cells or CD41/CD61 double positive cells), compared with control siblings (**Figure R-3B**). We also analyze platelet size and other platelet parameters with an Advia 120 Hematology Analyzer. Results showed that C3G-KO platelets were indistinguishable from control platelets (**Table R-1**). Overall, our data imply that C3G is not essential for Mk differentiation or platelet production in a physiological context.

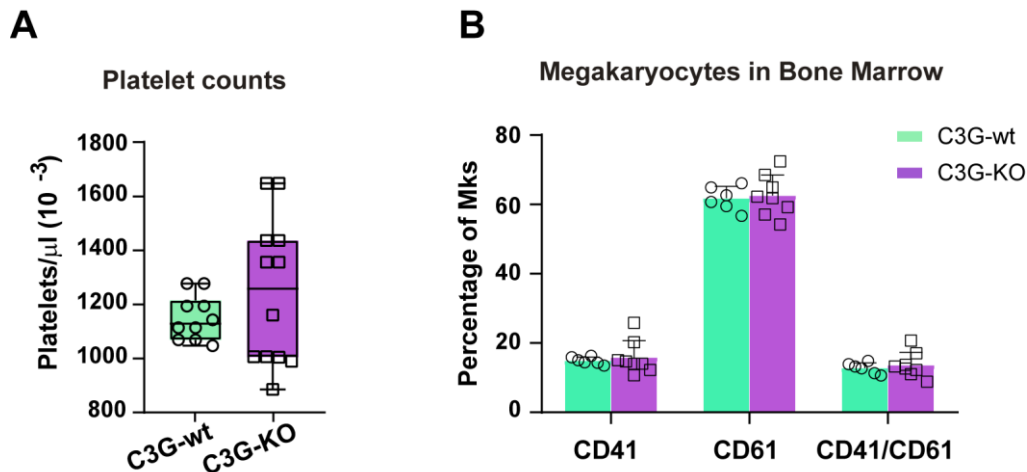


Figure R-3. C3G ablation do not alter basal levels of platelets in PB or Mk in BM. (A) Box plots represent median platelet counts in C3G-KO mice and their respective controls **(B)** Histogram represents mean \pm SD of the percentage of CD41⁺, CD61⁺ and CD41 and CD61 double positive cells in BM of C3G-wt and C3G-KO mice. wt: wild-type, KO: knockout.

Table R-1. C3G ablation did not modify platelet count or platelet parameters. Blood from five-week-old mice (n=5 per genotype and gender) was collected and analyzed using the Advia 120 Hematology Analyzer (Bayer). Values represent the mean of five animals separated into males and females. There were no significant differences between genotypes.

Parameter	Units	C3G-wt male	C3G-KO male	C3G-wt female	C3G-KO female
Platelet count	10^3 cells/ μl	1259.2	1179.4	1092	1160.25
Mean platelet volume (MPV)	fL	6.4	6.38	6.56	6.375
PDW (Platelet volume distribution width)	%	51.08	53.68	53.58	49.225
PCT (Platelet crit)	%	0.81	0.752	0.718	0.74
MPC (Mean platelet component) concentration	g/dl	21.74	21.94	21.78	22.125
PCDW (Platelet component concentration distribution width)	g/dl	6.9	7.14	7.12	7.05
MPM (Mean platelet (dry) mass)	pg	1.24	1.234	1.266	1.2675
PMDW (platelet dry mass distribution width)	pg	0.422	0.428	0.428	0.4225
Large PLT	10^3 cells/ μl	5	5.6	5	3

RBC fragments	10 ⁶ cells/ μ l	0.166	0.162	0.142	0.15
RBC ghosts	10 ⁶ cells/ μ l	0.05	0.044	0.056	0.055
Clumps counts		44.6	42.2	111.2	51.5

1.4. C3G ablation promotes Mk differentiation *in vitro*.

Previous results from our group showed that BM from mice with transgenic expression of C3G in Mk (tgC3G) cultured in TPO-supplemented medium produced an increase in the number of mature Mk, compared with BM cultures from wtC3G mice (Ortiz-Rivero *et al.*, 2018). Based on that, we sought to see if C3G deletion also impacts Mk differentiation *in vitro*. We isolated BM from C3G-KO and C3G-wt animals and cultured it in medium enriched with TPO plus an interleukin cocktail (SCF, IL-3, IL-6 and IL-11). The number of Mk (CD41⁺/CD61⁺) and mature Mk (CD42⁺) cells was analyzed by flow cytometry at various time points. C3G-KO BM cultures showed a higher percentage of double positive CD41/CD61 cells (**Figure R-4A**) and CD42⁺ cells (**Figure R-4B**) on the last day of the experiment than C3G-wt BM cultures. Therefore, C3G ablation would enhance megakaryopoiesis under non-physiological conditions.

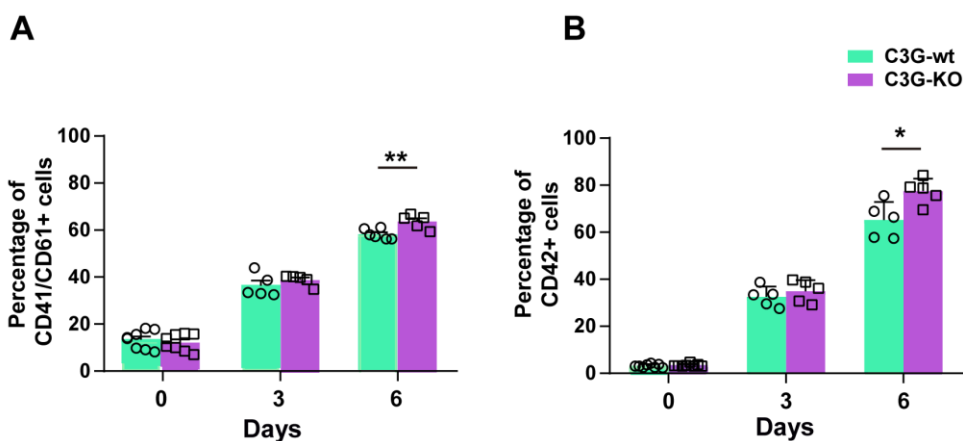


Figure R-4. C3G ablation promotes MK differentiation *in vitro*. Bone marrow was isolated and immediately cultured in medium enriched with TPO, SCF, IL-3, IL-6 and IL-11 for six days to promote Mk differentiation and maturation. **(A)** Histogram represents mean \pm SD of the percentage of megakaryocytes (CD41⁺/CD61⁺ cells) at different days after initiation of bone marrow culture. **(B)** Histogram represents mean \pm SD of the percentage of mature megakaryocytes (Mk expressing surface marker CD42). * $p < 0.05$, ** $p < 0.01$ wt: wild-type, KO: knockout.

2. Role of C3G in pathological megakaryopoiesis

The above results showed that, although C3G did not alter physiological MK and platelet counts, C3G ablation promoted Mk differentiation under strong stimuli, such as the mixture of TPO and interleukins. Thus, we hypothesized that C3G could participate in pathological megakaryopoiesis. In order to unveil this possible role of C3G, we developed two *in vivo* models of pathological megakaryopoiesis: TPO injection and 5-FU-induced myelosuppression.

2.1. C3G ablation promotes an increase in the number of platelets after TPO intravenous injection.

TPO intravenous injection stimulates Mk differentiation and platelet formation (Hitchcock & Kaushansky, 2014). Previous experiments showed that, after TPO injection, tgC3G mice presented a slightly higher platelet count than their controls. The opposite result was obtained with tgC3G Δ Cat animals, which showed a lower platelet count than their control siblings. However, these differences were not significant (Ortiz-Rivero *et al.*, 2018).

TPO (0.5 μ g) was injected into the lateral tail vein of C3G-KO and C3G-wt mice, and platelet count in PB was measured by flow cytometry every three days after injection during the nine days of the experiment. BM was collected on the last day to assess the number of mature Mk (CD41, CD61 and CD42 markers) as well as the ploidy status. Unexpectedly, three days after injection, C3G-KO mice showed a greater increase in platelet levels than control animals, suggesting a better response to TPO stimulation. Furthermore, after reaching a peak in platelet count, C3G-KO mice showed a slower decline in platelet levels, suggestive of impaired downregulation (**Figure R-5A-B**). We also checked the expression of mature-Mk specific markers (CD41, CD61 and CD42) and Mk ploidy in the BM of C3G-wt and C3G-KO mice, 21 days after the 5-FU injection. (**Figure R-5C-E**). Surprisingly, we found no changes in the number of mature Mk or in ploidy status.

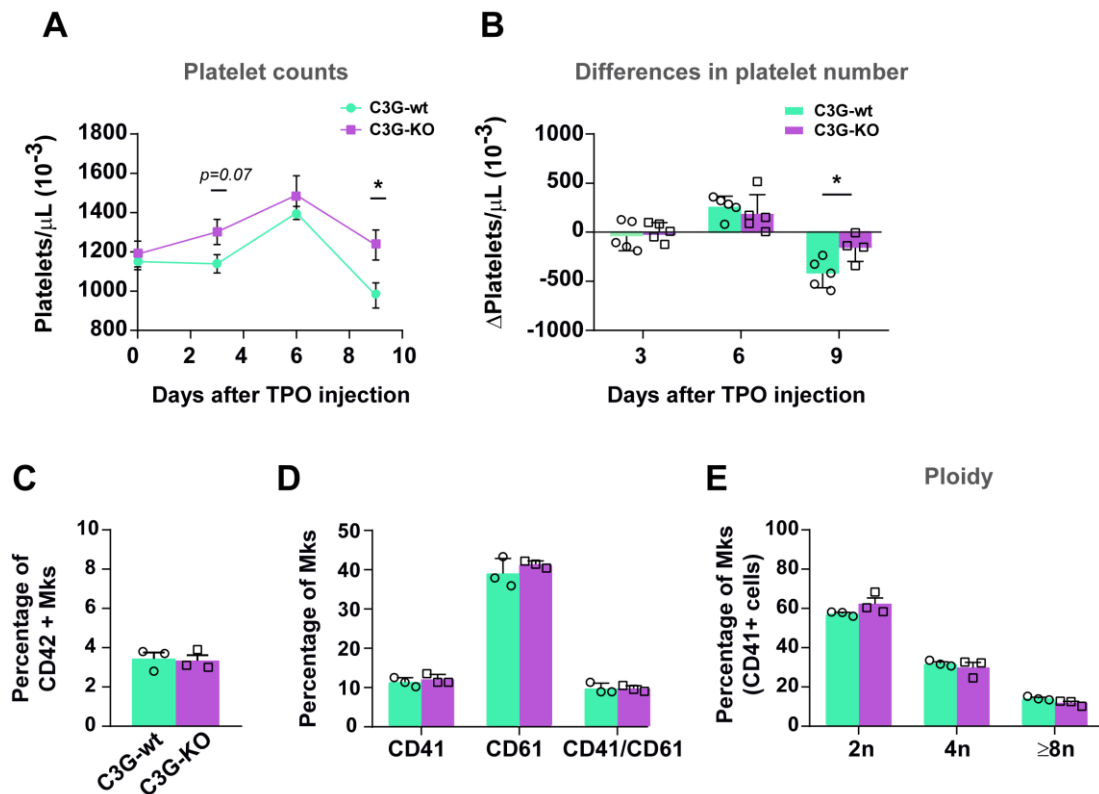


Figure R-5. C3G-KO mice respond more efficiently to TPO intravenous injection than control mice. TPO (0.5 μg) was intravenously injected and platelet count in PB was measured at different days after injection. Mk number and ploidy status were analyzed by flow cytometry on the final day of the experiment. **(A)** Scatter plot represents mean \pm SEM of platelet count in PB prior and after TPO injection ($n=9$ C3G-KO and C3G-wt). **(B)** Histogram represents mean \pm SD of differences in platelet number between two consecutive measurements in C3G-KO and C3G-wt mice as an indication of the increased or decreased rate. **(C, D, E)** Mk maturation was analyzed by measuring the expression of surface markers **(C)** CD42, **(D)** CD41 and CD61, and **(E)** ploidy status. Each graph represents mean \pm SD. * $p<0.05$ wt: wild-type, KO: knockout.

2.2. C3G controls platelet rebound after 5-FU-induced myelosuppression, and is essential to maintain homeostatic platelet levels.

To further analyze C3G participation in platelet production under pathological stimuli, we studied platelet rebound after 5-FU-induced myelosuppression in our C3G knockout and transgenic models. 5-FU is a chemotherapeutic drug that works by acting as an analogue of uracil. It is incorporated into DNA, preventing DNA synthesis and causing cell death, particularly in cells with a high rate of proliferation. A sublethal administration of 5-FU (150 mg per kg of body weight) triggers BM cell ablation, except for HSC due to its low proliferation rate. 5-FU induces platelet depletion around day seven after injection, followed by a profound increase in platelet number, known as platelet rebound, 10-15 days after treatment (X. Li & Slayton, 2013). Therefore, 5-FU-induced myelosuppression is an excellent model to study the participation of C3G in Mk and platelet recovery following bone marrow ablation. As shown in **Figure R-6A**, C3G-KO mice, injected

intraperitoneally with the appropriate dose of 5-FU, showed a lower platelet rebound than C3G-wt mice. Furthermore, after reaching the maximum platelet count, while control animals recovered normal platelet levels 20 days after injection, platelet levels remained elevated in C3G-KO mice, indicating defective downregulation (**Figure R-6A-B**). Twenty-one days after 5-FU injection, the number of mature Mk in BM was analyzed by flow cytometry. As in the TPO injection model, there were no alterations in CD42 (**Figure R-6C**), CD41/CD61 expression (**Figure R-6D**) or ploidy status (**Figure R-6E**).

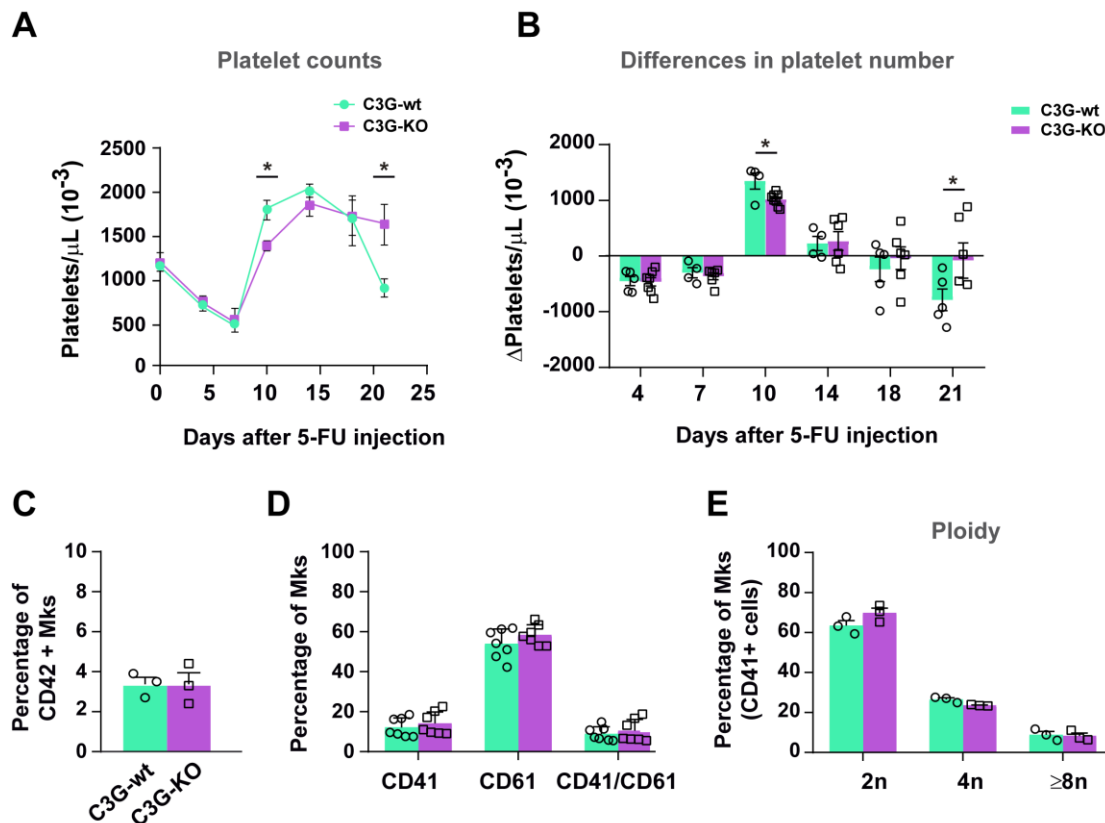


Figure R-6. C3G ablation produces a delay in platelet rebound and failed to downregulate platelet levels after 5-FU-induced myelosuppression. An intraperitoneal injection of 150 mg/kg body weight of 5-FU was administered to C3G-KO and C3G-wt mice. Platelet count was monitored at different days after injection. The mature Mk number and ploidy status were analyzed on the final day of the experiment. **(A)** Scatter plot represents mean \pm SEM of platelet count in PB prior and after 5-FU injection ($n=8$ C3G-KO and C3G-wt). **(B)** Differences in platelet number between two consecutive measurements as an indication of an increased or decreased rate. **(C, D, E)** Mk maturation was analyzed by measuring expression of surface markers **(C)** CD42, **(D)** CD41 and CD61 and **(E)** ploidy status. Each graph represents mean \pm SD. * $p<0.05$. wt: wild-type, KO: knockout.

To confirm these findings, we performed 5-FU-induced myelosuppression in tgC3G mice. Mice with C3G overexpression in platelets showed a higher platelet rebound and faster platelet downregulation than their control siblings, which is in concordance with

results in the C3G-KO model (**Figure R-7A-B**). Similar to C3G-KO mice, BM analyses did not show any differences in CD42 (**Figure R-7C**), CD41/CD61 expression, (**Figure R-7D**) or Mk ploidy (**Figure R-7E**).

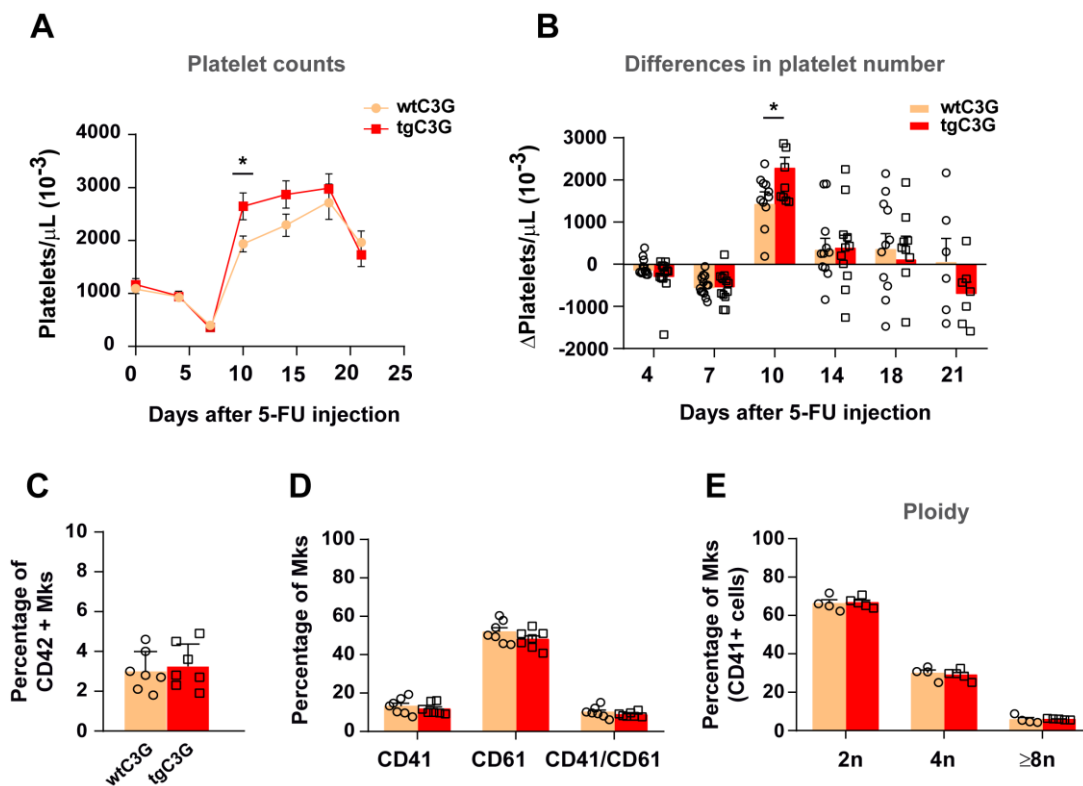


Figure R-7. C3G overexpression promoted platelet rebound after 5-FU-induced myelosuppression and produced faster downregulation of platelet levels. An intraperitoneal injection of 150 mg/kg body weight of 5-FU was administered to tgC3G and wtC3G mice. Platelet count was monitored at different days after injection. The mature Mk number and ploidy status were analyzed on the final day of the experiment. **(A)** Scatter plot represents mean \pm SEM of platelet count in PB prior and after 5-FU injection (n=12 tgC3G, n=13 wtC3G). **(B)** Differences in platelet number between two consecutive measurements as an indication of an increased or decreased rate. **(C, D, E)** Mk maturation was analyzed by measuring expression of the surface markers **(C)** CD42, **(D)** CD41 and CD61 and **(E)** ploidy status. Each graph represents mean \pm SD. *p<0.05. wt: wild-type, tg: transgenic.

Altogether, these data suggest that C3G could be required to maintain homeostatic platelet levels.

2.3. C3G regulates c-Mpl levels.

TPO is the major cytokine involved in megakaryopoiesis and platelet production. TPO activates multiple signaling pathways that promote the expression of genes involved in megakaryopoiesis and thrombopoiesis via its receptor c-Mpl (Kuter, 2013). TPO is endocytosed by platelets through a mechanism involving c-Cbl phosphorylation by SFKs, which leads to c-Mpl ubiquitination and degradation, as well as TPO removal from plasma (Märklin *et al.*, 2020; Murphy *et al.*, 2013; Saur *et al.*, 2010). Since C3G appears

to play a role in platelet maintenance, we first investigated whether it is involved in the regulation of c-Mpl levels in Mk and platelets.

According to RT-qPCR analysis, C3G ablation boosted c-Mpl mRNA expression in platelets and Mk. On the other hand, tgC3G Mk showed a substantial reduction in c-Mpl expression (**Figure R-8A**), whereas an increase in c-Mpl expression was found in tgC3G platelets (**Figure R-8B**).

To confirm these results, c-Mpl protein levels were analyzed by western blot. In contrast to RT-qPCR analyses, C3G ablation resulted in a reduction in c-Mpl levels in platelets and Mk when compared with their controls. C3G overexpression had no effect on c-Mpl protein levels in Mk, although a slight increase in c-Mpl was observed in tgC3G platelets (**Figure R-8C-D**). These results suggest that C3G regulates the expression of c-Mpl in platelets and Mk. The discordance between mRNA expression and protein levels is likely due to post-transcriptional and/or post-translational regulatory mechanisms.

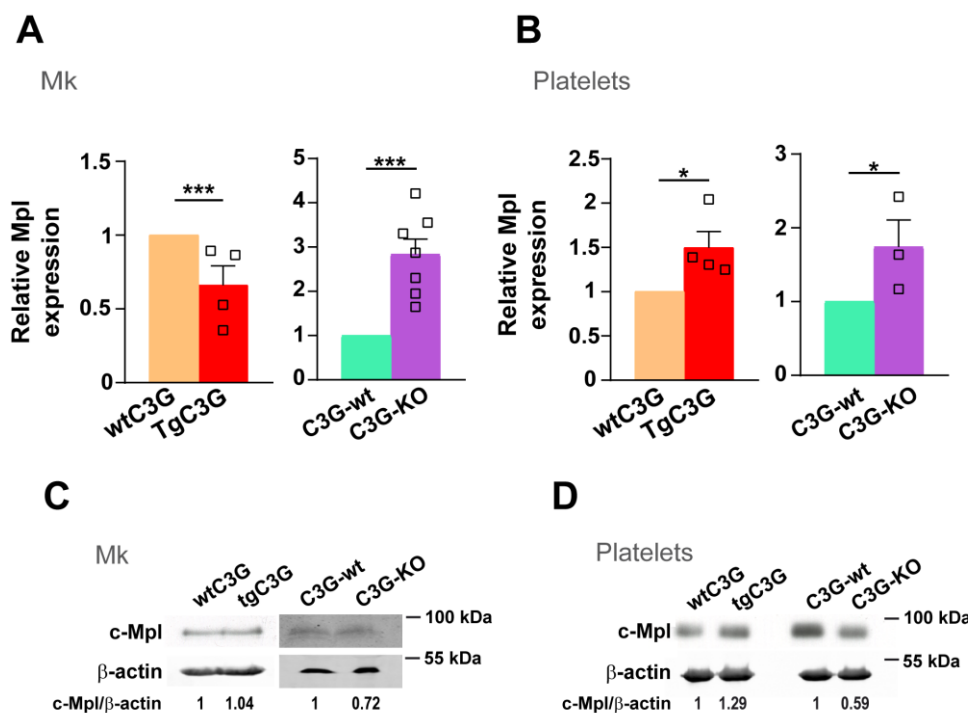


Figure R-8. C3G regulates c-Mpl in Mks and platelets. c-Mpl levels were analyzed in platelets and Mk at the RNA and protein levels. **(A, B)** Histograms represent mean \pm SD of the relative mRNA expression of c-Mpl in **(A)** Mk and **(B)** platelets, using β -actin as housekeeping gene. **(C, D)** Analysis of c-Mpl protein levels by western blot in **(C)** Mk and **(D)** platelets, Values are relative to β -actin expression and were normalized against those of each wild-type * $p < 0.05$ *** $p < 0.001$. wt: wild-type, tg: transgenic, KO: knockout, Mk: megakaryocyte.

2.4. Platelet C3G controls c-Mpl internalization and degradation upon TPO stimulation

As mentioned above, in platelets, TPO binds to its receptor, c-Mpl, and induces its endocytosis, recycling and degradation as a mechanism of TPO clearance from plasma. Based on the above results, indicating a role for C3G in the regulation of cMpl levels, we aimed to investigate whether C3G participates in TPO-induced c-Mpl degradation by performing a time course of TPO stimulation. Platelets were incubated with TPO (25 ng/ml for tgC3G; 100 ng/ml for C3G-KO) at different times and the levels of c-Mpl were analyzed by western blot. As expected, wild-type platelets exhibited a consistent time-dependent decrease in c-Mpl levels in response to TPO. However, tgC3G platelets showed a faster degradation of c-Mpl than their controls (**Figure R-9A**), whereas C3G-KO platelets presented a delay in c-Mpl degradation (**Figure R-9B**). No degradation of c-Mpl was observed in tgC3G Δ Cat platelets (**Figure R-9C**). These results suggest that changes in the levels and/or functionality of C3G disrupt the normal turnover of c-Mpl. According to these data, C3G GEF activity would play a positive role, promoting c-Mpl degradation, while C3G would play a negative role through its protein-protein interaction function.

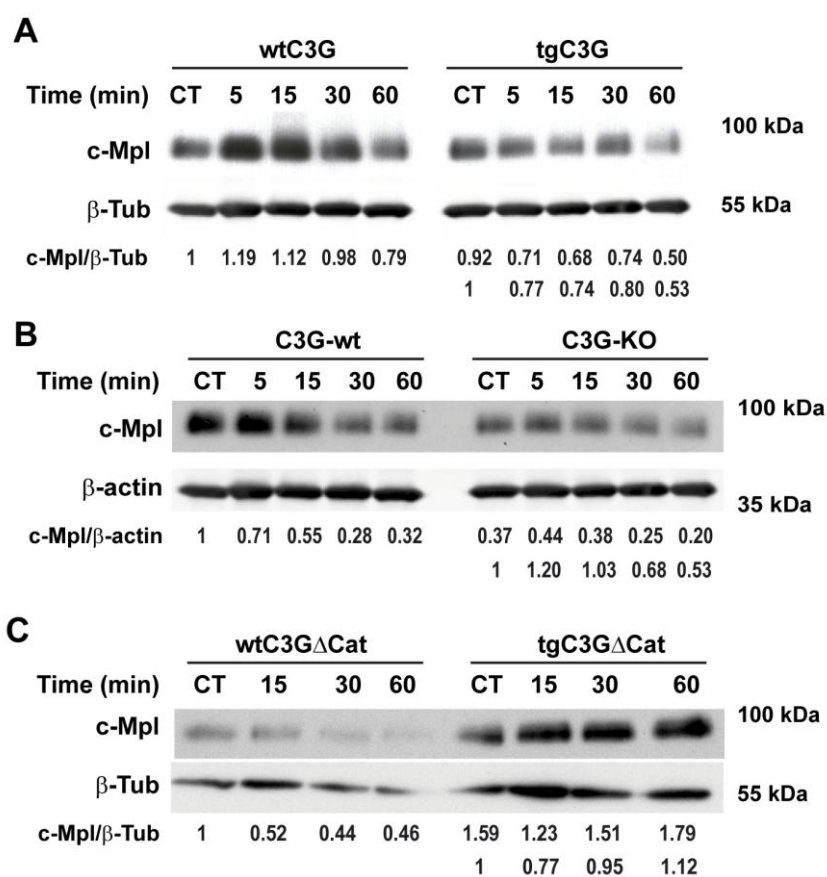


Figure R-9. Platelet C3G expression levels and activity controls c-Mpl degradation upon TPO stimulation. Platelets were stimulated with thrombopoietin (TPO, 25 ng/mL) at different time points to analyze c-Mpl degradation in tgC3G (A), C3G-KO (B) and tgC3G Δ Cat (C) platelets. Relative c-Mpl/ β -actin or c-Mpl/ β -tubulin levels are shown. Values were normalized against those of untreated wild-type platelets. For tgC3G, C3G-KO and tgC3G Δ Cat, the lower/second line of values shows normalization against their untreated sample. CT: control (0 min). wt: wild-type, tg: transgenic, KO: knockout.

Once we showed that platelet C3G regulates c-Mpl degradation, we next studied whether C3G is also involved in the internalization of the receptor. To this end, platelets were incubated with TPO for 30 minutes and the amount of receptor remaining on the platelet surface was measured by flow cytometry. On the one hand, under resting conditions, C3G-KO platelets showed lower levels of c-Mpl receptor on the surface than C3G-wt platelets (Figure R-10). On the other hand, after 30 min of TPO treatment, internalization of the c-Mpl receptor was found to be reduced in C3G-KO platelets compared with control platelets (Figure R-10). Interestingly, lower levels of c-Mpl on the surface and impaired c-Mpl internalization were also observed in c-Cbl-KO platelets (Märklin *et al.*, 2020).

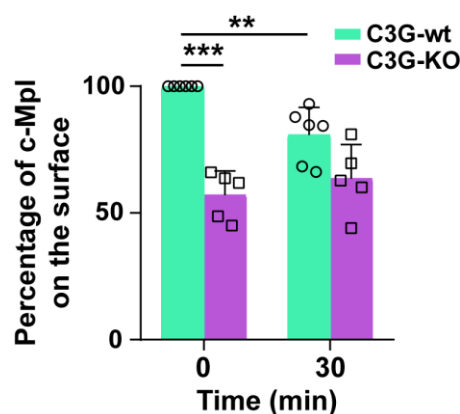


Figure R-10. Platelet C3G is necessary for c-Mpl internalization upon TPO stimulation. Platelets of C3G-KO and control mice were treated with TPO (25 ng/ml) for 30 min and c-Mpl surface levels measured by flow cytometry with anti-c-Mpl + anti-rabbit-Cy5 in the CD41-FITC⁺ population. The histograms represent the mean \pm SD of the percentage of double-labeled platelets. Values are relative to those of untreated C3G-wt platelets (100%). * $p < 0.05$, ** $p < 0.01$ wt: wild-type, KO: knockout.

Therefore, C3G modulates the exposure of c-Mpl on the surface and is required for its correct internalization and degradation. This novel role of C3G might explain the aberrant downregulation of platelet levels in C3G-KO mice observed in both *in vivo* models of pathological megakaryopoiesis.

2.5. C3G deletion in platelets alter plasma TPO levels

To further demonstrate the implication of C3G in the regulation of plasma TPO levels, we evaluated serum TPO content *in vivo* at different days after intravenous administration of 0.5 μ g TPO. Interestingly, C3G ablation had no effect on basal plasma TPO levels (**Figure R-11A**). Contrary to expectations, TPO administration did not induce a strong increase in plasma TPO levels at the time points of the experiment, likely due to rapid TPO metabolization. Moreover, C3G-KO mice showed a significant decrease in plasma TPO levels 6 days after the injection (**Figure R-11A**), which is consistent with the increased platelet count observed under the same experimental settings (**Figure R-5A**). As a control, we analyzed TPO expression in the liver to see if the lower plasma TPO levels found in C3G-KO mice were attributable to impaired TPO production. C3G-KO and C3G-wt mice showed similar liver TPO expression, according to RT-qPCR analyses (**Figure R-11B**).

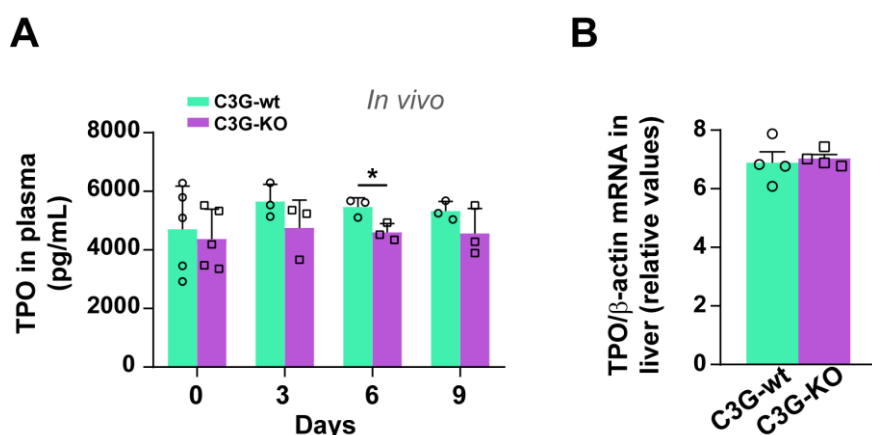


Figure R-11. C3G-KO mice showed lower levels of TPO in plasma after TPO administration. (A) Mice were injected with 0.5 μ g TPO in 100 μ L of PBS. Plasma from C3G-KO and C3G-wt mice was harvested at the indicated time points and TPO levels were measured by ELISA (mean \pm SD). (B) TPO mRNA levels in livers from C3G-KO and C3G-wt mice were analyzed by RT-qPCR and normalized to β -actin. Histograms represents mean \pm SD of relative TPO expression (Δ Ct). * $p < 0.05$. wt: wild-type, KO: knockout.

This data suggests that platelet C3G regulates plasma TPO levels under pathological conditions.

2.6. C3G-KO platelets fail to uptake TPO *in vitro*.

In the *in vivo* experiment in **Figure R-11A**, we only observed a modest increase in plasma TPO levels in our experimental conditions, probably due to the rapid internalization of TPO, less than 30 min (J. Li *et al.*, 1999; Stefanich *et al.*, 1997). Therefore, to investigate whether C3G participates in TPO-uptake, we performed an *in*

in vitro TPO uptake experiment. C3G-KO platelets were incubated with 2 pg/mL TPO for 30 min. The amount of TPO remaining in the supernatant was immediately measured by ELISA as an indirect indicator of platelet uptake. Compared with C3G-wt platelets, C3G null platelets exhibited a defective TPO-uptake, as evidenced by the significantly higher amount of TPO remaining in the supernatants. (**Figure R-12**).

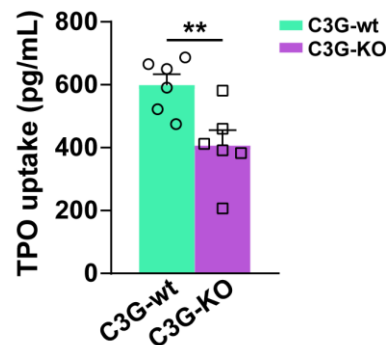


Figure R-12. C3G-KO platelets fails to uptake TPO *in vitro*. To determine the TPO uptake, platelets from C3G-KO and C3G-wt mice were harvested and stimulated with TPO (2 ng/mL) for 30 min. TPO levels in the supernatant were measured by ELISA and TPO uptake was calculated as follows: TPO pg/mL (t0) – TPO pg/mL (t30) (Mean \pm SEM). ** $p < 0.01$. wt: wild-type, KO: knockout.

This result indicates that C3G is required for TPO-induced c-Mpl internalization.

2.7. C3G interacts with c-Cbl in platelets.

Following internalization c-Mpl is ubiquitinated by the E3 ubiquitin-ligase c-Cbl (Saur *et al.*, 2010). C3G forms complexes with c-Cbl at focal adhesions in K562, an erythromegakaryoblastic cell line that acquires Mk markers upon stimulation with PMA (Maia *et al.*, 2013). Based on this and the results described above, suggesting a role for C3G in c-Mpl internalization, we investigated whether C3G interacts with c-Cbl in platelets. Immunoprecipitation assays revealed that C3G interacts with c-Cbl in resting, TPO- (100 ng/mL, 5 min) and ADP- (25 μ M, 5 min) activated platelets (**Figure R-13**). Under thrombin stimulation (0.5 U/ml, 1 min), this association was not detectable, however this is likely owing to a faster activation rate in this condition, resulting in signaling desensitization (**Figure R-13**).

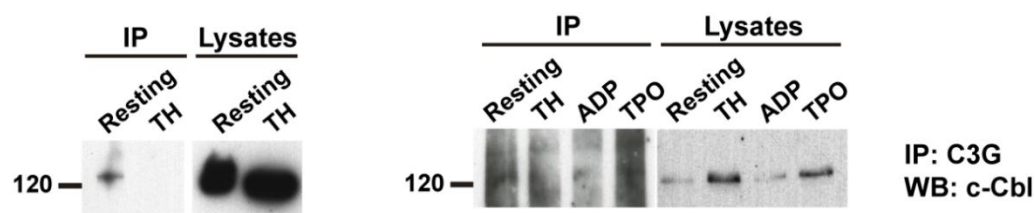


Figure R-13. c-Cbl immunoprecipitates with C3G in resting platelets and upon ADP and TPO stimulation. Lysates from tgC3G platelets, untreated or treated with thrombin (TH, 0.5U/mL, 1 min), ADP (25 μ M, 5 min) and thrombopoietin (TPO, 100 ng/mL, 5 min) were immunoprecipitated with anti-C3G antibody and the levels of c-Cbl were detected by western blot. IP: immunoprecipitation, WB: western blot.

To further support these results, we analyzed C3G-Cbl colocalization by immunofluorescence. As in the immunoprecipitation assay, stimulation with TPO and ADP increased the interaction between both proteins, while this interaction was not detected under thrombin stimulation (**Figure R-14**).

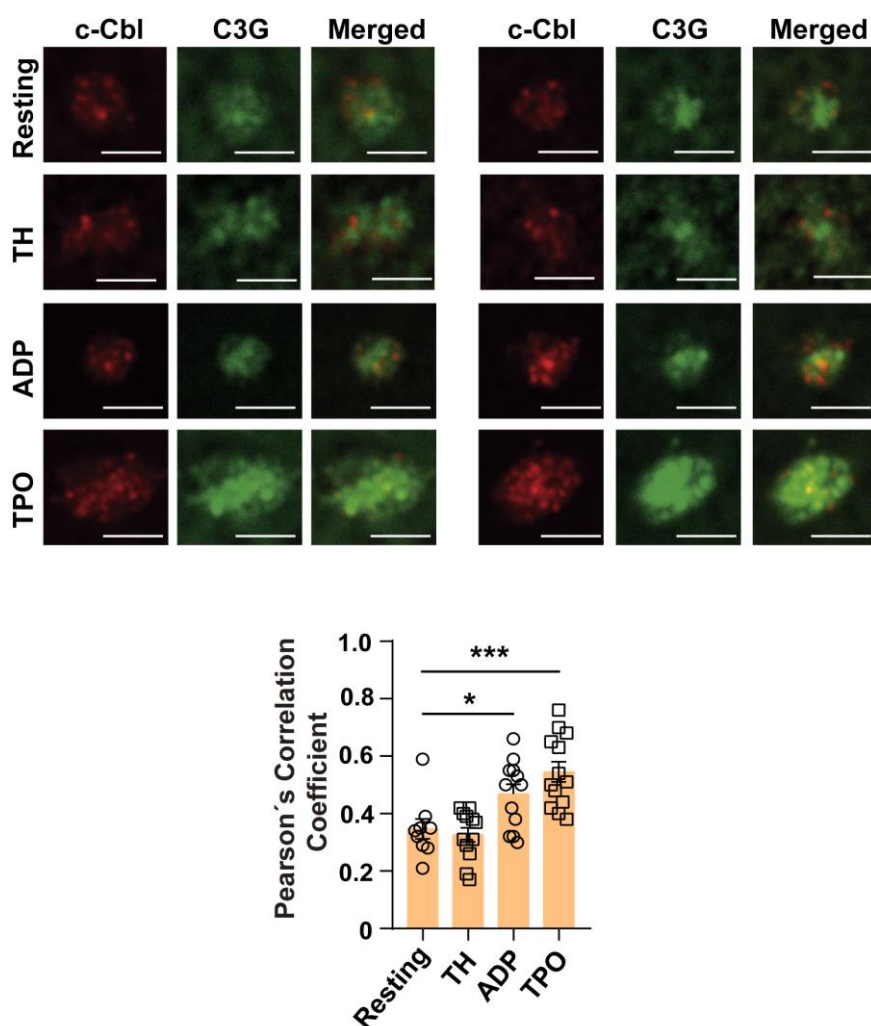


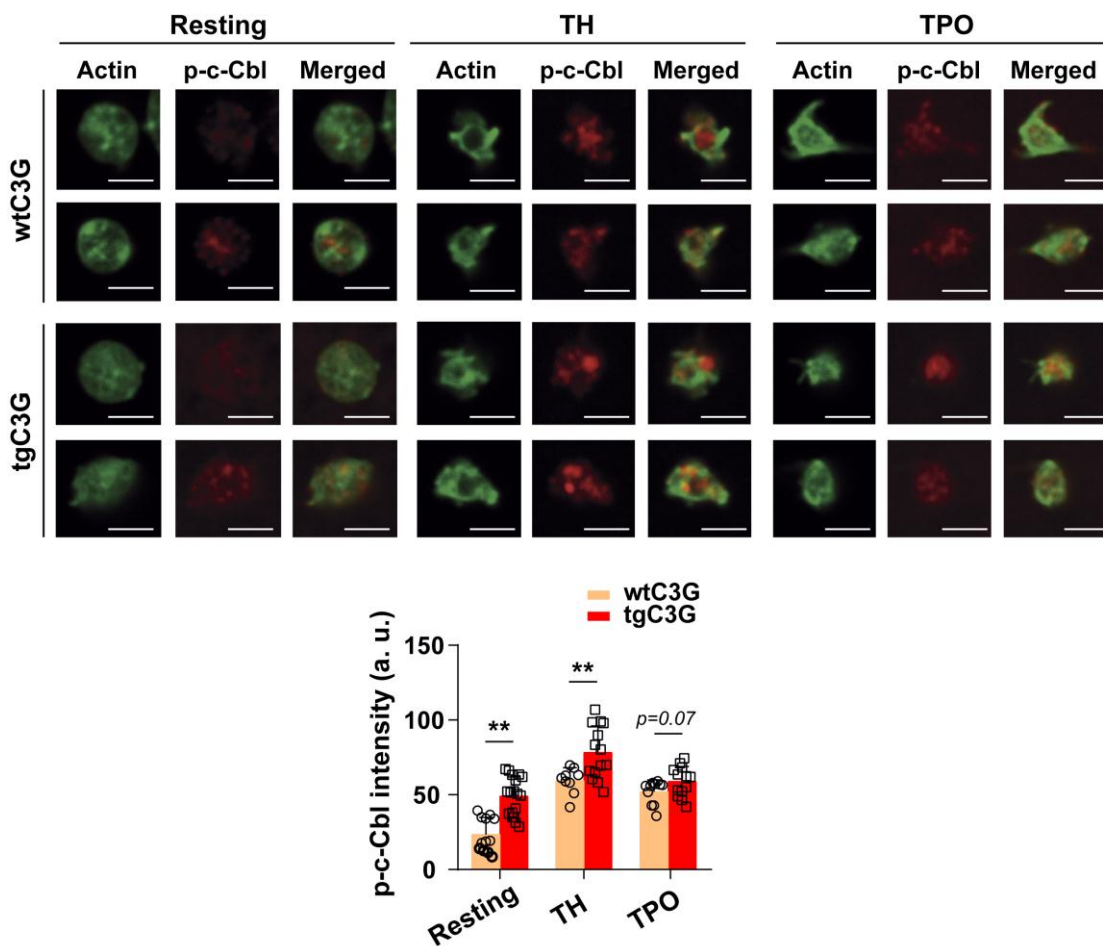
Figure R-14. C3G colocalizes with c-Cbl in platelets. TPO induces C3G and c-Cbl colocalization. Representative immunofluorescence confocal microscopy images of tgC3G platelets treated with thrombin (TH, 0.5 U/mL, 1 min), ADP (25 μ M, 5 min) or TPO (100 ng/mL, 5 min) and labeled with anti-c-Cbl + Alexa Fluor™-568 (red) and anti-C3G + Alexa Fluor™-647 (green). The histograms show the Pearson's Correlation Coefficients (mean \pm SD) of C3G and c-Cbl. * p <0.05, *** p <0.001. Bar: 2.5 μ m.

This result suggests the participation of C3G in c-Cbl actions in platelets.

2.8. C3G regulates Cbl phosphorylation.

To become activated and conduct its ubiquitin-ligase function, c-Cbl must be phosphorylated (Tsygankov *et al.*, 2001). Based on the interaction between C3G and c-Cbl in platelets, we next studied whether C3G is involved in c-Cbl activation. We measured phospho-c-Cbl (p-c-Cbl) levels in platelets at rest and treated with thrombin or TPO. TgC3G platelets exhibited a significant increase in p-c-Cbl levels, both at rest and after stimulation with thrombin (0.5 U/mL, 1 min) and TPO (100 mg/mL, 5 min), compared with wtC3G platelets (**Figure R-15A**). In contrast, C3G ablation in platelets almost completely impaired c-Cbl phosphorylation, under stimulation with thrombin or TPO (**Figure R-15B**).

A



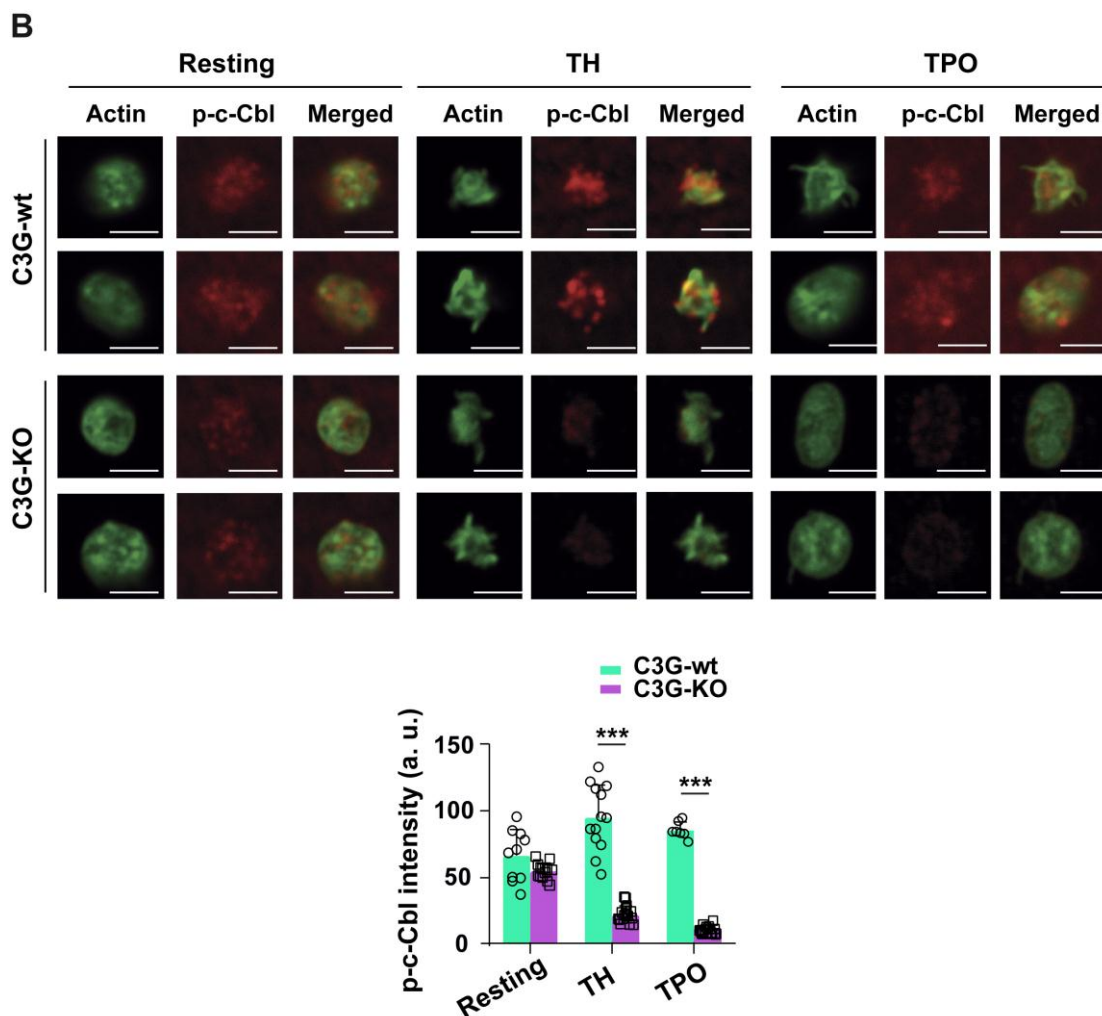


Figure R-15. C3G promotes c-Cbl phosphorylation. Representative immunofluorescence confocal microscopy images of tgC3G (A), C3G-KO (B) and their control platelets treated with thrombin (TH, 0.5 U/mL, 1 min) or TPO (100 ng/mL) and labeled with anti-phospho-c-Cbl + Alexa Fluor™-647 (red) and Phalloidin (green). All images were taken at the same exposure time. Bar: 2.5 μ m. Histograms represent the mean \pm SD of the fluorescence intensities (arbitrary units) of p-c-Cbl in the indicated genotypes. ** $p < 0.01$, *** $p < 0.001$. wt: wild-type, KO: knockout, a.u.: arbitrary units.

Phosphorylation of c-Cbl is mediated by SFKs (Hunter *et al.*, 1999; Murphy *et al.*, 2013; Yokouchi *et al.*, 2001). On the other hand, we have previously demonstrated a functional relationship between C3G and Src in platelets (Gutiérrez-Herrero *et al.*, 2020). Thus, we investigated whether C3G is a mediator of c-Cbl phosphorylation by Src. Transgenic C3G expression in platelets increased p-Src levels (Figure R-16A-B) upon TPO stimulation. Furthermore, p-c-Cbl-p-Src colocalization was significantly increased in tgC3G platelets compared with their controls (Figure R-16B). TPO-stimulated C3G-KO platelets, on the other hand, displayed lower levels of p-Src (Figure R-16C-D), accompanied by a considerable reduction in p-c-Cbl-p-Src colocalization (Figure R-16D).

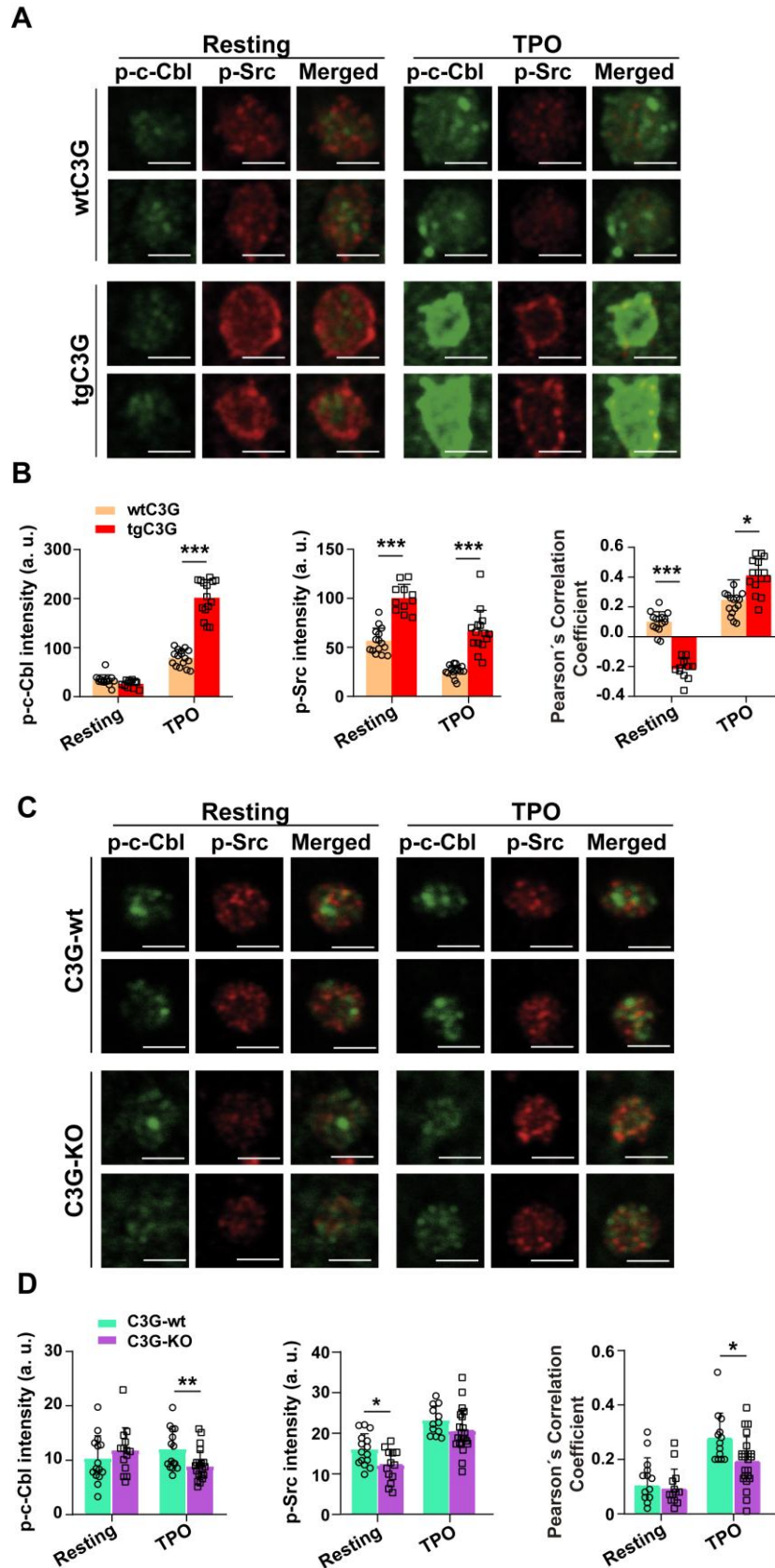
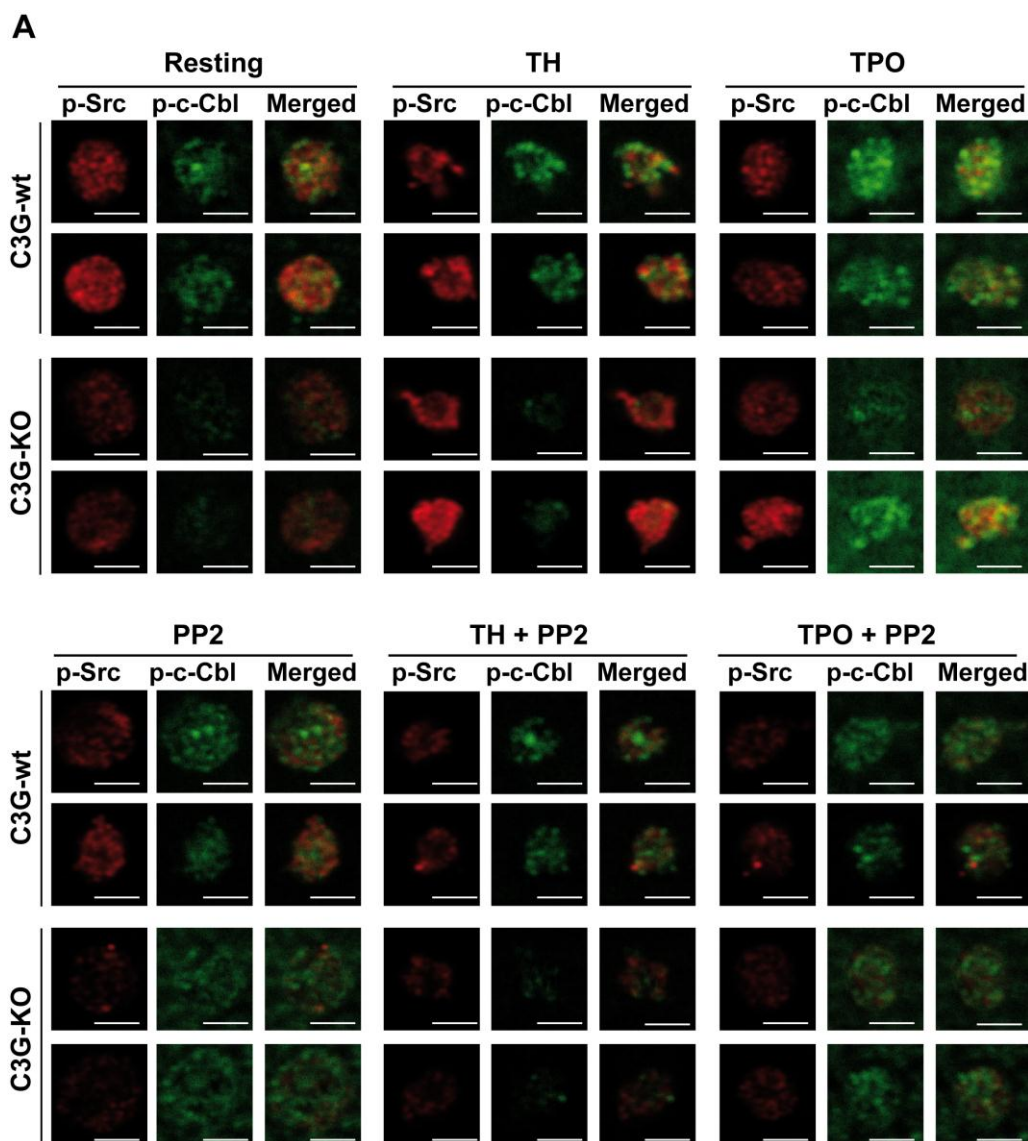


Figure R-16. C3G promotes c-Cbl phosphorylation by Src in response to TPO. Representative immunofluorescence confocal microscopy images of tgC3G (A), C3G-KO (C) and control platelets treated with TPO (100 ng/mL, 5 min) and labeled with anti-phospho-c-Cbl + Alexa Fluor™-647 (green) and anti-phospho-Src + Alexa Fluor™-568 (red). All images were

taken at the same exposure time. Bar: 2.5 μm . **(B, D)** Histograms represents the mean \pm SD of fluorescence intensities (arbitrary units) of phospho-c-Cbl and phospho-Src, as well as the Pearson's Correlation Coefficient (mean \pm SD) of phospho-c-Cbl and phospho-Src in the indicated genotypes under the specified experimental conditions. * $p < 0.05$, ** $p < 0.01$, *** $p < 0.001$. wt: wild-type, KO: knockout, a.u.: arbitrary units.

To confirm the involvement of C3G in Src-dependent c-Cbl phosphorylation, we analyzed p-c-Cbl and p-Src levels in tgC3G, C3G-KO and control platelets pretreated with PP2 (SFK pan-inhibitor), before thrombin or TPO stimulation. As expected, PP2 decreased p-Src levels, but also p-c-Cbl levels (**Figure R-17A-B**), supporting a Src-dependent c-Cbl phosphorylation. Furthermore, PP2 inhibitory effect was enhanced in C3G-KO platelets in all experimental conditions, and induced a drastic reduction in p-c-Cbl-p-Src interaction in these platelets (**Figure R-17C**), suggesting that C3G is a mediator of c-Cbl phosphorylation by Src.



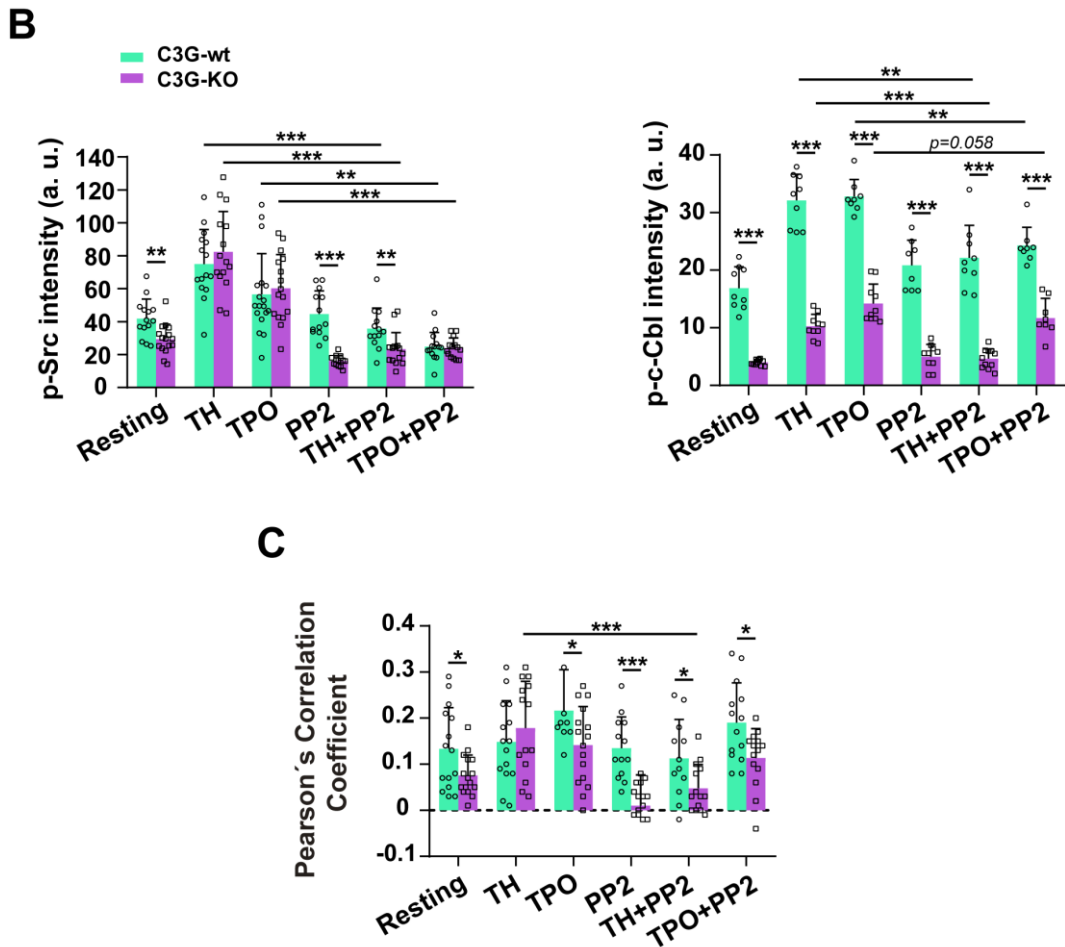
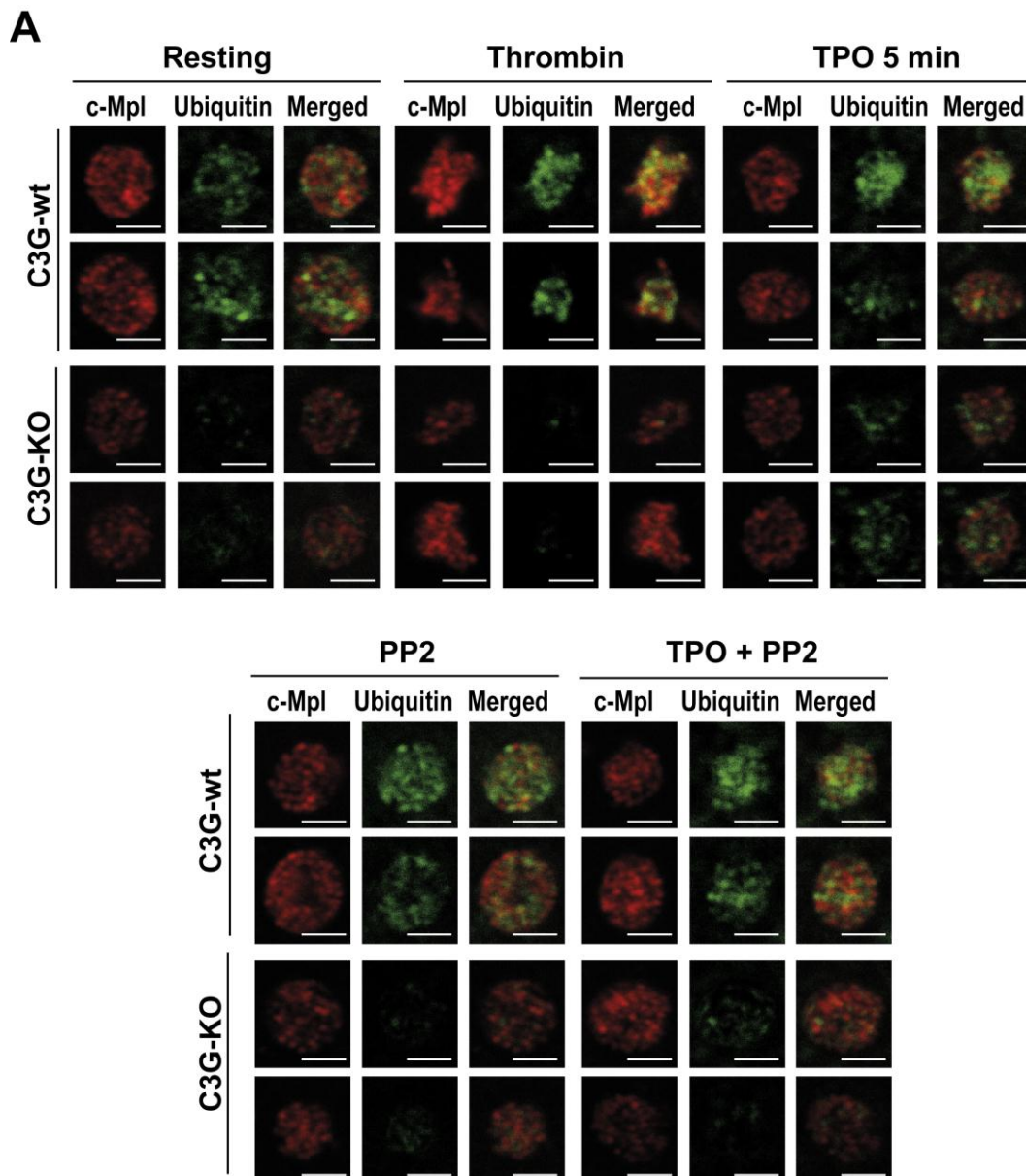


Figure R-17. C3G regulates c-Cbl phosphorylation by Src and c-Mpl ubiquitination and degradation. (A) Representative immunofluorescence confocal microscopy images of C3G-KO platelets and their controls treated with TH (0.5 U/mL, 5 min) or TPO (100 ng/mL, 5 min), in the presence or absence of PP2 (10 μ M) and labeled with anti-phospho-c-Cbl + Alexa FluorTM-647 (green) and anti-phospho-Src + Alexa FluorTM-568 and. Bar: 2.5 μ m. (B) Histogram represents mean \pm SD of the fluorescence intensity of phospho-Src (left panel) and phospho-c-Cbl (right panel) under the indicated treatment. (C) Graph showing the Pearson's Correlation Coefficients (mean \pm SD) of phospho-c-Cbl and phospho-Src under the indicated experimental conditions. * $p < 0.05$, ** $p < 0.01$ *** $p < 0.001$. wt: wild-type, KO: knockout, a.u.: arbitrary units.

2.9. C3G controls c-Mpl ubiquitination

As previously mentioned, c-Mpl is ubiquitinated and degraded upon TPO binding. Since C3G participates in c-Mpl degradation and c-Cbl activation, our next question was whether C3G could modulate c-Mpl ubiquitination. To this end, we analyzed by immunofluorescence c-Mpl levels, ubiquitinated protein levels and the colocalization between c-Mpl and ubiquitin (as an indicator of c-Mpl ubiquitination) in platelets from the different genotypes at rest and after stimulation with thrombin (0.5 U/mL, 1 min, positive control of ubiquitination) and TPO (100 ng/mL, 5 min). Platelets were also pretreated with PP2 before stimulation with TPO (100 ng/mL, 5 min).

C3G-KO platelets exhibited a strong reduction in ubiquitin signal, both at rest and under stimulation with TPO and thrombin, compared to control platelets (**Figure R-18A-B**). Colocalization between c-Mpl and ubiquitin was also lower in TPO-stimulated C3G-KO platelets than in their controls. On the other hand, PP2 pre-treatment further decreased ubiquitination, mainly in C3G null platelets, including c-Mpl ubiquitination (**Figure R-18C**), probably due to an additive effect. This suggests that C3G and Src participate in a common pathway that regulates c-Mpl receptor ubiquitination.



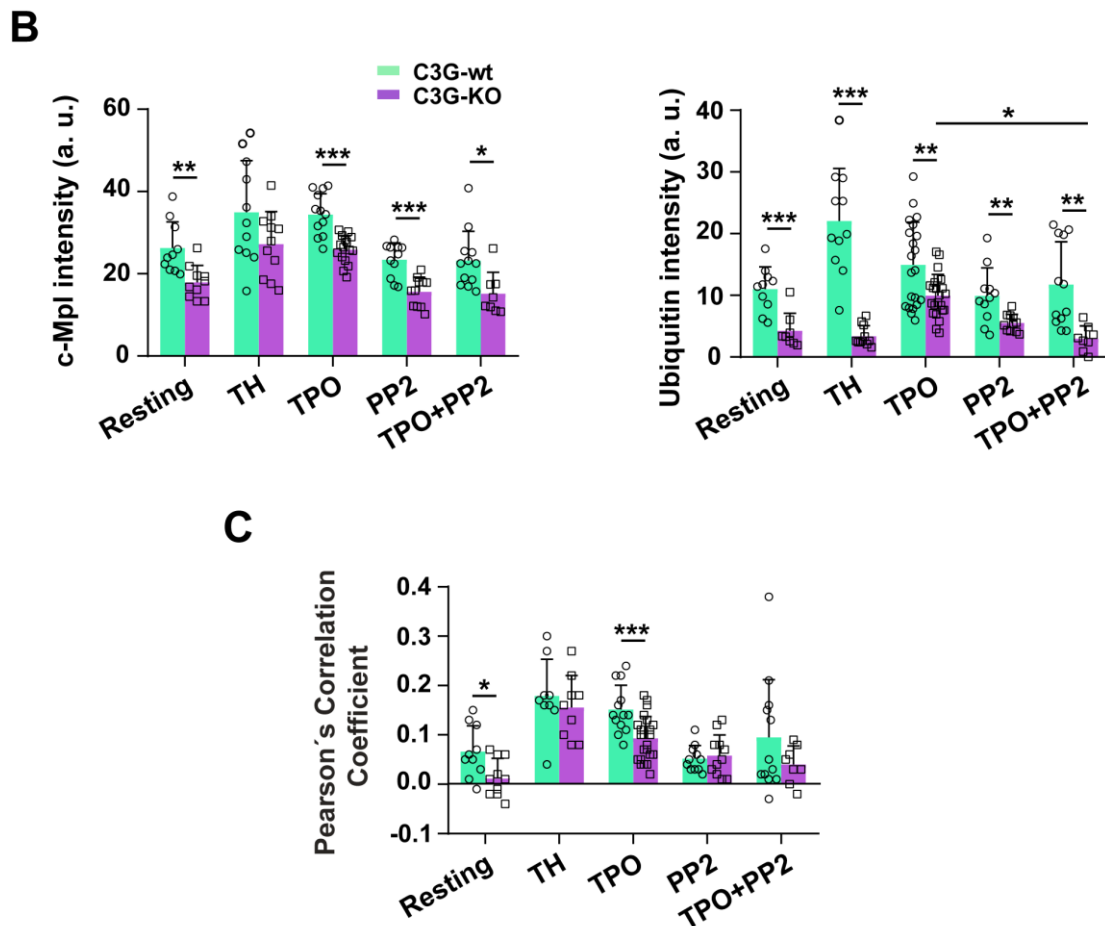


Figure R-18. C3G regulates c-Mpl ubiquitination. C3G-KO and C3G-wt platelets were treated with thrombin (TH, 0.5 U/mL, 1 min) or TPO (100 ng/mL, 5 min) in the presence or absence of the Src inhibitor PP2 (10 μ M) and labeled with anti-c-Mpl + Alexa FluorTM-568 (red) or anti-Ubiquitin + Alexa FluorTM-647 (green). **(A)** Representative immunofluorescence confocal microscopy images of platelets of each genotype under each treatment condition, taken at the same exposure time. Bar: 2.5 μ m. **(B)** Histograms represent the mean \pm SD of the fluorescence intensities (arbitrary units) of c-Mpl (left panel) or ubiquitin (right panel). **(C)** The graph shows the Pearson's Correlation Coefficient's (mean \pm SD) of c-Mpl and ubiquitin under the indicated experimental conditions. * p <0.05, ** p <0.01, *** p <0.001. wt: wild-type, KO: knockout, a.u.: arbitrary units.

To confirm the above findings, we analyzed c-Mpl ubiquitination in tgC3G platelets. Ubiquitin signal was significantly higher in TPO-stimulated tgC3G platelets than in wtC3G platelets, further suggesting a novel role for C3G in protein ubiquitination in platelets (**Figure R-19A-B**). This correlated with increased c-Mpl-ubiquitin colocalization (**Figure R-19C**). PP2 completely abolished the increased c-Mpl ubiquitination found in TPO-stimulated tgC3G platelets, which confirms the participation of Src and C3G in a common pathway (**Figure R-19A-B**).

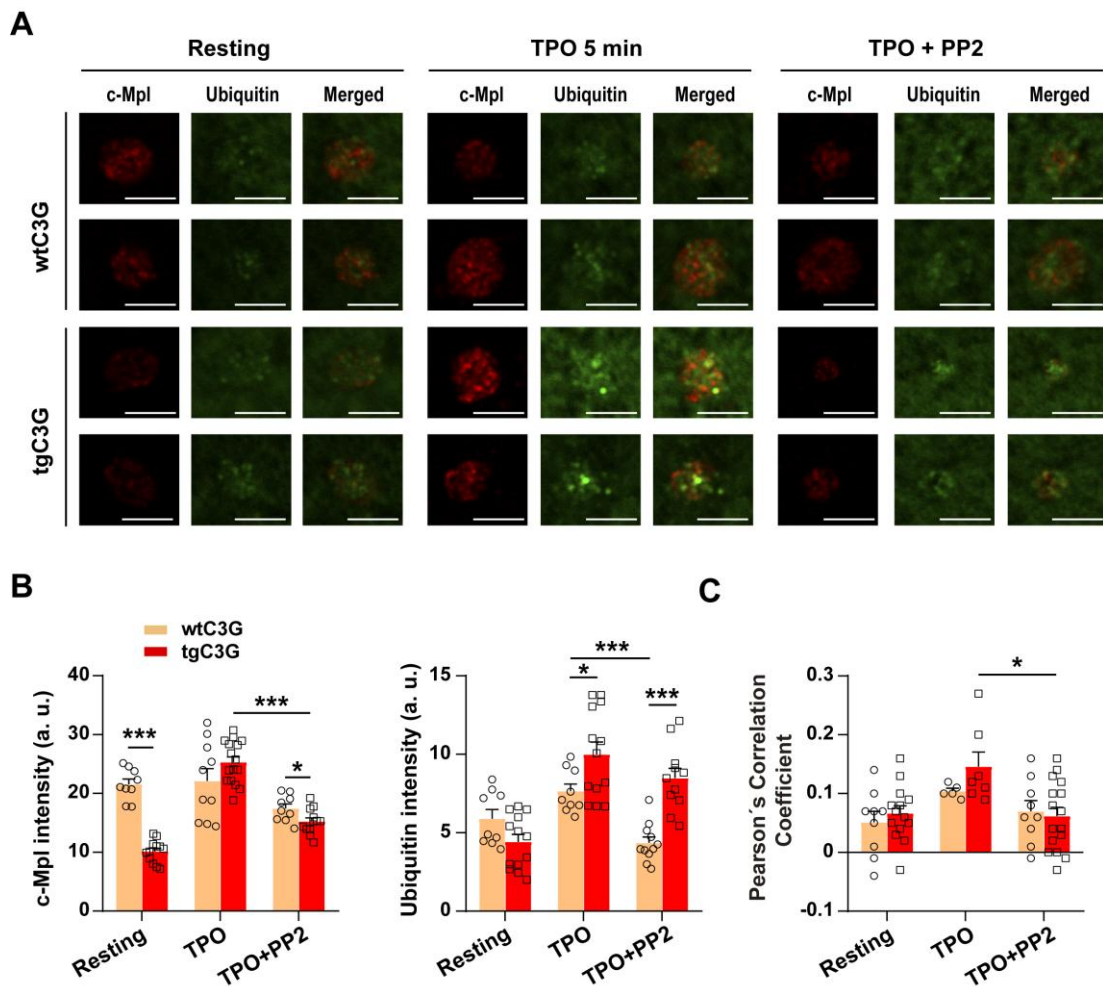


Figure R-19. C3G overexpression increases c-Mpl ubiquitination in TPO-stimulated platelets. tgC3G and wtC3G platelets were treated with TPO (100 ng/mL, 5 min) in the presence or absence of the Src inhibitor PP2 (10 μ M) and labeled with anti-c-Mpl + Alexa FluorTM-568 (red) or anti-Ubiquitin + Alexa FluorTM-647 (green). **(A)** Representative confocal microscopy images of platelets of each genotype under each treatment condition, taken at the same exposure time. Bar: 2.5 μ m. **(B)** Histograms represents the mean \pm SD of the fluorescence intensities of c-Mpl (left) or ubiquitin (right). **(C)** The graph shows the Pearson's Correlation Coefficients (mean \pm SD) of c-Mpl and Ubiquitin under the indicated experimental conditions. * p <0.05, *** p <0.001. wt: wild-type, tg: transgenic, a.u.: arbitrary units.

Overall, these results points to the existence of a C3G-Src-c-Cbl pathway that leads to c-Mpl ubiquitination and degradation in response to TPO.

2.10. C3G participates in UPS-Lysosome crosstalk

In platelets, ubiquitination of c-Mpl, caused by TPO stimulation of c-Cbl, resulted in its destruction via the proteasome (UPS, from Ubiquitin Proteasome System) and the lysosome (Märklin *et al.*, 2020; Saur *et al.*, 2010). It has been proposed that both systems cooperate to remove proteins. In fact, hyperactivation of lysosome-mediated degradation induced by UPS inhibition has been reported (Ji & Kwon, 2017; Korolchuk *et al.*, 2009). Since C3G affects c-Mpl degradation, we investigated the effect of C3G ablation on UPS

and lysosome activities. Total ubiquitination and c-Mpl levels were analyzed by western blot in TPO-stimulated (100 ng/mL) platelets in the presence or absence of the proteasome inhibitor MG132 (30 μ M) or the lysosome inhibitor NH₄Cl (20 mM). As expected, MG132 prevented, at least in part, TPO-induced c-Mpl degradation in wild-type platelets, which correlated with an accumulation of ubiquitinated proteins. This effect was more pronounced in C3G-KO platelets, showing a higher accumulation of c-Mpl and ubiquitinated proteins (**Figure R-20A-B**). These results suggest that the lysosome degradation mechanism in C3G-KO platelets may be hampered.

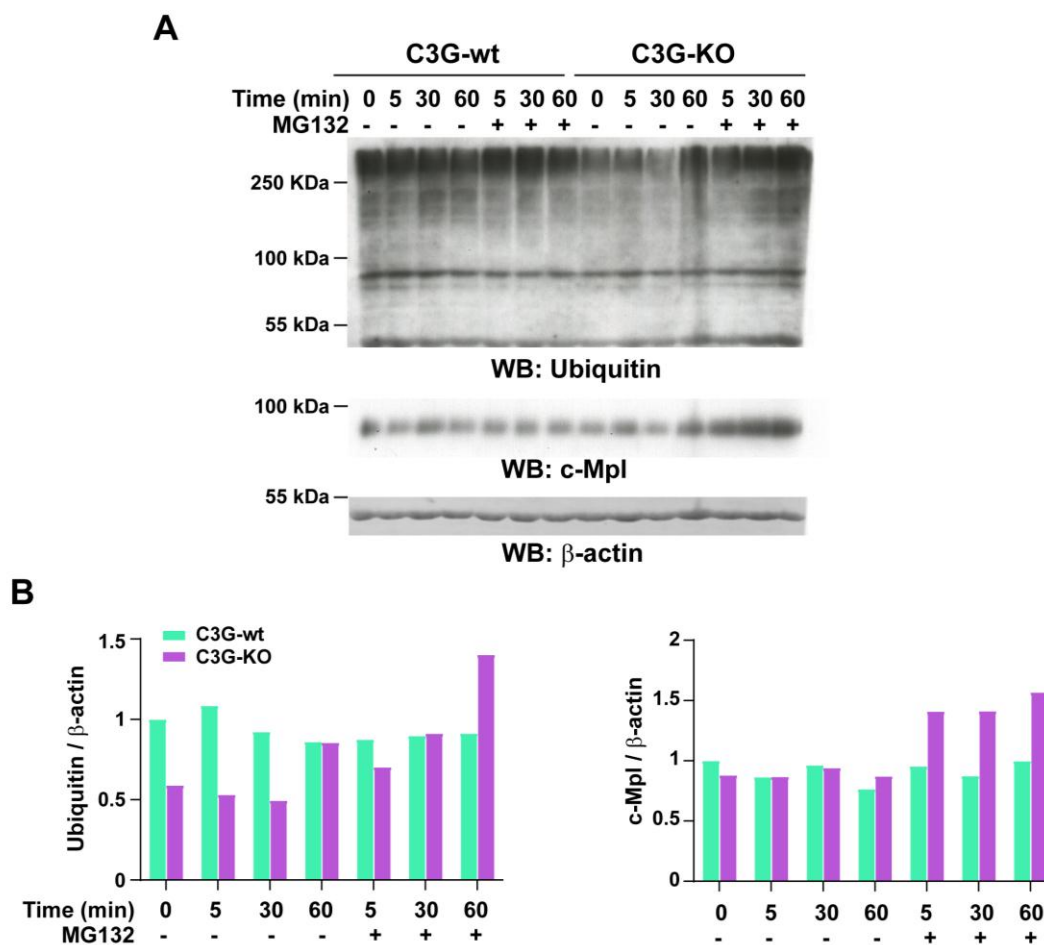


Figure R-20. Proteasome inhibition triggers accumulation c-Mpl and ubiquitinated proteins in C3G-KO platelets. (A) Platelets from C3G-KO and C3G-wt mice were pre-treated 1 h with 30 μ M MG132 prior the incubation with 100 ng/mL TPO for the indicated times. The levels of ubiquitinated proteins and c-Mpl were measured by western blot using β -actin as the loading control. **(B)** Histograms represents the quantification of ubiquitinated proteins (left panel) and c-Mpl levels (right panel) relative to β -actin and normalized against the T0 value of C3G-wt. wt: wild-type, KO: knockout.

On the other hand, lysosome inhibition did not substantially affect c-Mpl degradation in C3G-wt platelets, but induced a strong accumulation of ubiquitinated proteins and c-Mpl in C3G-KO platelets (**Figure R-21A-B**), even greater than that observed with

proteasome inhibition (**Figure R-20A-B**). These results indicate that UPS is the main responsible for c-Mpl degradation in platelets, although the lysosome could also contribute. In addition, our results suggest that C3G ablation in platelets could cause proteasome and lysosome dysfunction.

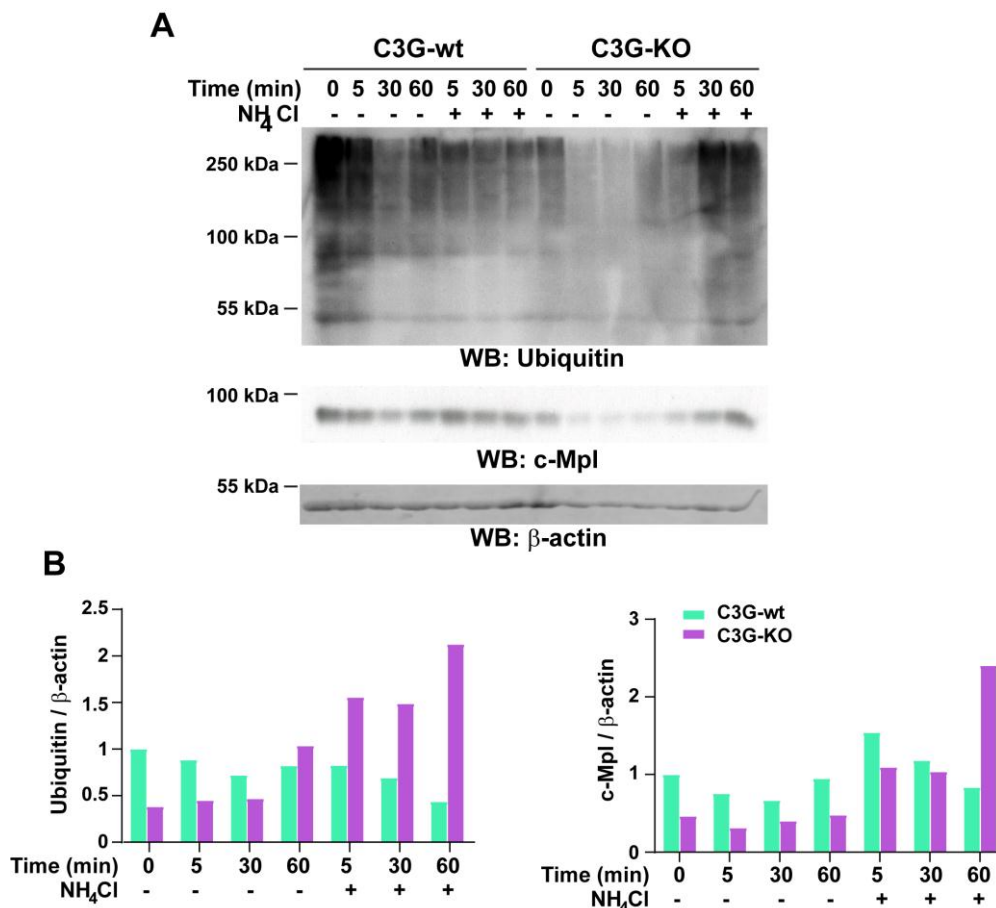


Figure R-21. Lysosome inhibition results in accumulation c-Mpl and ubiquitinated proteins in C3G-KO platelets. (A) Platelets from C3G-KO and C3G-wt mice were pre-treated 1 h with 20 mM NH₄Cl prior incubation with 100 ng/mL TPO for the indicated times. The levels of ubiquitinated proteins and c-Mpl were measured by western blot using β -actin as the loading control. (B) Histograms represent the quantification of ubiquitinated proteins (left panel) and c-Mpl levels (right panel) relative to β -actin and normalized against the T0 value of C3G-wt. wt: wild-type, KO: knockout.

All these data suggest that C3G may be involved in the degradation of c-Mpl by the UPS and lysosome systems. In addition, the fact that in both experiments the accumulation of c-Mpl coincided with that of ubiquitination suggests that c-Mpl is one of the ubiquitinated proteins. To confirm this hypothesis, we analyzed c-Mpl ubiquitination by immunofluorescence in platelets treated with TPO (100 ng/mL, 60 min), in the presence or absence of MG132 (30 μ M) or NH₄Cl (20 mM) inhibitors. The results showed a higher accumulation of ubiquitinated-c-Mpl in C3G-deficient platelets than in their controls (**Figure R-22**), suggesting proteasome failure in the C3G null platelets.

These results are indicative of a putative role for C3G in proteasome and lysosome activities.

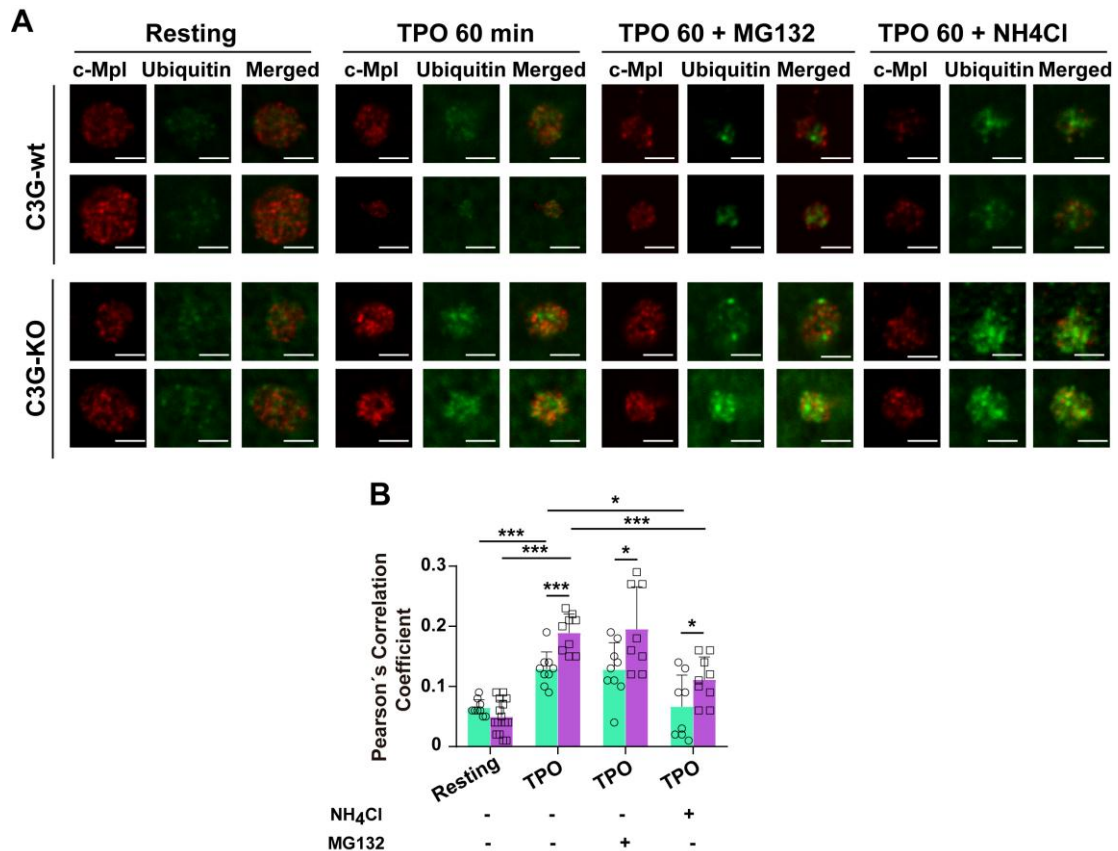


Figure R-22. Platelet C3G is necessary for the correct c-Mpl degradation by the proteasome and lysosome systems. C3G-KO and control platelets were treated with 100 ng/mL TPO for 60 min, after 1 h pre-treatment with 30 μ M MG132 or 20 mM NH₄Cl, and labeled with anti-c-Mpl + Alexa Fluor™-568 (red) or anti-Ubiquitin + Alexa Fluor™-647 (green). (A) Representative immunofluorescence confocal microscopy images of platelets of each genotype under each treatment condition, taken at the same exposure time. Bar: 2.5 μ m. (B) The graph shows the Pearson's Correlation Coefficients (mean \pm SD) of c-Mpl and Ubiquitin under the indicated experimental conditions. * p <0.05, *** p <0.001. wt: wild-type, KO: knockout.

2.11. C3G ablation alters the 19S regulatory proteasome regulatory particle.

The aforementioned results suggest that removing C3G from platelets could impair proteasome function. Thus, we used proteomics to perform a preliminary analysis of whether C3G deficiency would affect proteasome composition, in order to find alterations that could explain the reduced proteasome activity in C3G-KO platelets. C3G-KO platelets showed lower levels of the majority of 20S core subunits, although these variations were not statistically significant. (Table R-2). However, we found that Rpn1 (26S proteasome non-ATPase regulatory subunit 2 or PSMD2), a critical component of the 19S proteasome regulatory particle, was severely downregulated in C3G-KO platelets (Table R-2). Rpn1 is a ubiquitin receptor required for the correct assembly and

function of the 26S proteasome complex. Indeed, lack of Rpn1 phosphorylation resulted in impaired proteasome assembly and function (Liu *et al.*, 2020). This finding might explain the lower proteasome activity observed in C3G-KO platelets, resulting in the accumulation of c-Mpl and ubiquitinated proteins.

Table R-2. C3G-KO platelets showed a significant decrease in Rpn1 abundance. Quantification of different proteasome subunits by proteomics. Results are shown as C3G-KO/C3G-wt abundance ratio.

Protein	Abundance Ratio KO/wt	p-Value	Proteasome Localization
Proteasome endopeptidase complex OS=Mus musculus OX=10090 GN= <i>Psm1</i> PE=1 SV=1	0.855	0.556168553	20S
Proteasome subunit alpha type-2 OS=Mus musculus OX=10090 GN= <i>Psm2</i> PE=1 SV=3	0.789	0.40723091	20S
Proteasome subunit alpha type-3 OS=Mus musculus OX=10090 GN= <i>Psm3</i> PE=1 SV=3	0.975	0.843706076	20S
Proteasome subunit alpha type-4 OS=Mus musculus OX=10090 GN= <i>Psm4</i> PE=1 SV=1	0.845	0.531681827	20S
Proteasome subunit alpha type-6 OS=Mus musculus OX=10090 GN= <i>Psm6</i> PE=1 SV=1	0.835	0.508566389	20S
Proteasome subunit alpha type-7 OS=Mus musculus OX=10090 GN= <i>Psm7</i> PE=1 SV=1	0.905	0.673075913	20S
Proteasome subunit beta type-1 OS=Mus musculus OX=10090 GN= <i>Psb1</i> PE=1 SV=1	1.043	0.99794806	20S
Proteasome subunit beta type-2 OS=Mus musculus OX=10090 GN= <i>Psb2</i> PE=1 SV=1	0.766	0.35972284	20S
Proteasome subunit beta type-3 OS=Mus musculus OX=10090 GN= <i>Psb3</i> PE=1 SV=1	0.733	0.29440268	20S
Proteasome subunit beta type-4 OS=Mus musculus OX=10090 GN= <i>Psb4</i> PE=1 SV=1	0.674	0.19462892	20S
Proteasome subunit beta type-5 OS=Mus musculus OX=10090 GN= <i>Psb5</i> PE=1 SV=3	0.754	0.33432672	20S
Proteasome subunit beta type-7 OS=Mus musculus OX=10090 GN= <i>Psb7</i> PE=1 SV=1	1.047	0.99008031	20S
Proteasome subunit beta type-8 OS=Mus musculus OX=10090 GN= <i>Psb8</i> PE=1 SV=2	1.111	0.85006348	20S
Proteasome subunit beta type-10 OS=Mus musculus OX=10090 GN= <i>Psb10</i> PE=1 SV=1	1.206	0.66474158	20S
Proteasome activator complex subunit 2 OS=Mus musculus OX=10090 GN= <i>Pse2</i> PE=1 SV=4	1.133	0.80405915	19S

26S proteasome non-ATPase regulatory subunit 2 (Fragment) OS=Mus musculus OX=10090 GN=<i>Psmc2</i> PE=1 SV=1	0.01	1E-17	19S
---	-------------	--------------	------------

In summary, C3G-KO platelets are unable to regulate plasma TPO levels due to defective Src-mediated c-Cbl phosphorylation, leading to impaired TPO-c-Mpl internalization and degradation. Moreover, C3G-deficient platelets displayed an accumulation of c-Mpl and ubiquitinated proteins after one-hour of TPO-stimulation, indicating reduced proteasome activity. The gross deficiency in Rpn1 expression found in C3G null platelets could, at least in part, explain the defective function of the proteasome in these platelets.

3. Role of C3G in ischemia induced angiogenesis

3.1. C3G controls hemangiocyte recruitment to hypoxia sites

Ischemia is the temporary or permanent decrease in blood supply to a part of the body, caused by a normal or pathological alteration of the artery or arteries afferent to it. VEGF, which is released from platelets and endothelial cells, induces SDF-1 (CXCL12) secretion from platelets. Both VEGF and SDF-1 promote the recruitment of proangiogenic progenitor cells from the BM through interaction with their respective receptors, CXCR4 and VEGFR1. Then, these cells, known as bone marrow-derived cells (BMDC) or hemangiocytes, release angiogenic factors at the ischemic site that promote the incorporation and assembly of endothelial progenitor cells and the stabilization of new blood vessels, stimulating angiogenesis and recovery of blood flow (Feng *et al.*, 2011; Jin *et al.*, 2006; Massberg *et al.*, 2006; Stellos & Gawaz, 2007).

We have previously demonstrated that transgenic expression of C3G in platelets promotes the release of a net proangiogenic secretome. Indeed, in two *in vivo* models of syngeneic heterotopic tumor cell transplantation, tgC3G mice exhibited increased neovascularization (Martín-Granado *et al.*, 2017). To deep into the mechanism by which C3G might regulate angiogenesis, we sought to see if platelet C3G was involved in the recruitment of hemangiocytes in response to ischemia. To this end, we developed two models of ischemia-induced angiogenesis: tumor cell implantation and hind-limb ischemia, which were applied to our transgenic and knockout mouse models.

The tumor implantation model consisted of subcutaneous injection of 5×10^5 murine Lewis Lung (3LL) carcinoma cells. Flow cytometry was used to examine the recruitment of hemangiocytes in PB, before and after 3LL implantation, by quantifying the percentage of CXCR4⁺ and VEGFR1⁺ cells. TgC3G mice showed lower hemangiocyte recruitment

than wtC3G mice, particularly on the last day of the study, although differences were not significant (**Figure R-23A**). Moreover, at day 15, tgC3G mice showed increased levels of hemangiocytes in BM than wtC3G mice, which correlates with the decrease observed in PB (**Figure R-23B**). In contrast, platelet C3G ablation resulted in a greater recruitment of CXCR4/VEGFR-double positive cells to PB, compared with their controls (**Figure R-23C**), with no variations in the number of hemangiocytes in BM on the last day of the experiment (**Figure R-23D**).

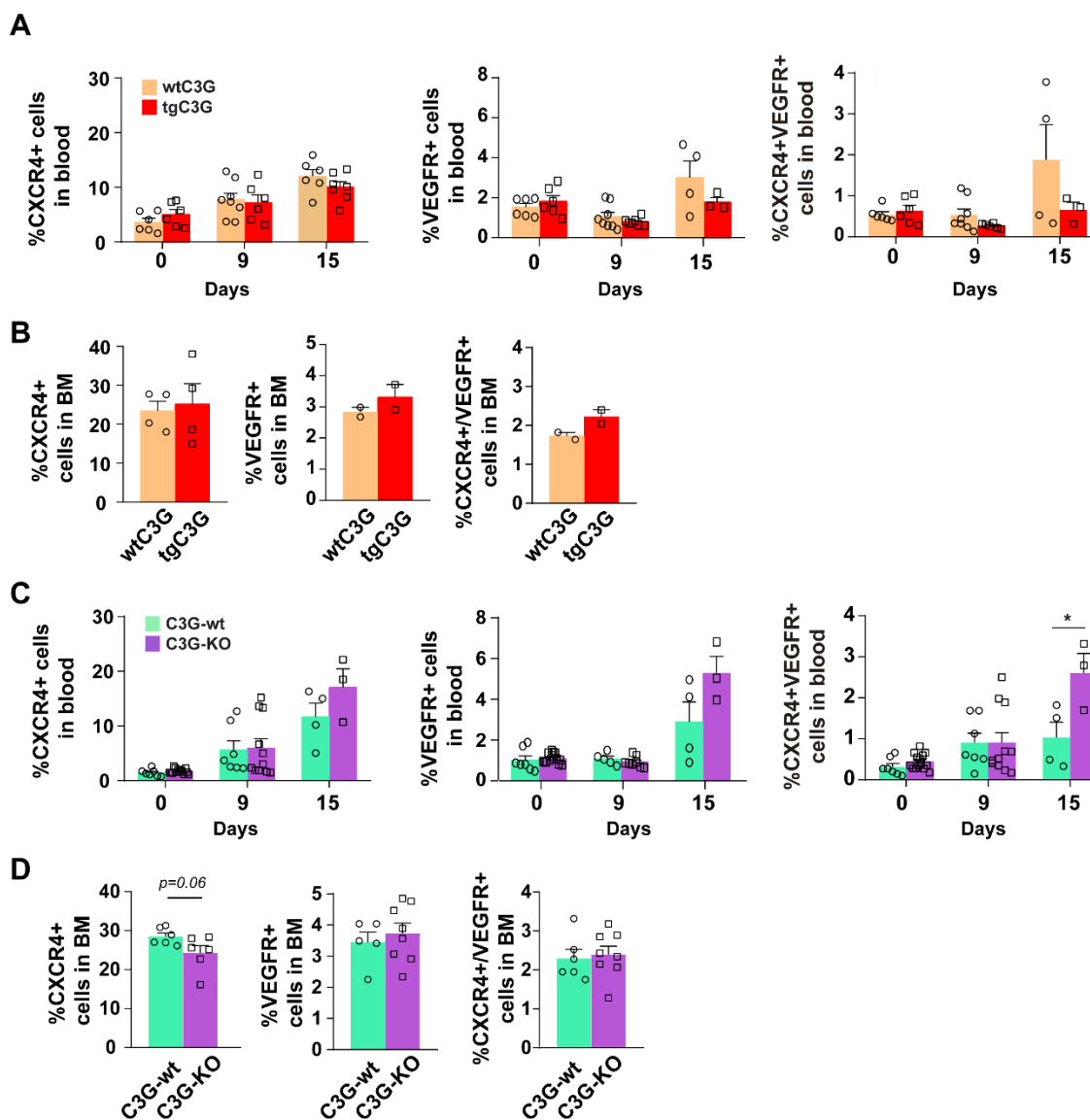


Figure R-23. Platelet C3G regulates hemangiocyte recruitment in response to tumor cell growth. Blood collected at the indicated days after the implantation of 3LL cells in tgC3G, C3G-KO mice and their controls was incubated with anti-CXCR4-PE and anti-VEGFR-APC antibodies to determine the percentage of hemangiocytes. The histograms represent the mean \pm SEM of the percentage of CXCR4⁺, VEGFR⁺ and double CXCR4⁺/VEGFR⁺ cells in (**A, C**) peripheral blood or (**B, D**) BM (day 15 post-ischemia) from wtC3G and tgC3G mice (**A, B**) or from C3G-wt and C3G-KO mice (**C, D**). * $p < 0.05$. wt: wild-type, KO: knockout, tg: transgenic, BM: bone marrow.

To delve into the role of C3G in angiogenesis, tumors in C3G-KO and C3G-wt mice were removed, weighed and processed to analyze vessel formation by immunohistochemistry (**Figure R-24A**) using anti-CD31 antibody (a specific marker of endothelial cells). Consistent with the increased hemangiocyte recruitment observed, C3G-KO mice developed larger (**Figure R-24B**) and more vascularized tumors (**Figure R-24A,C**) than control mice, similar to that observed in tgC3G mice (Martín-Granado *et al.*, 2017).

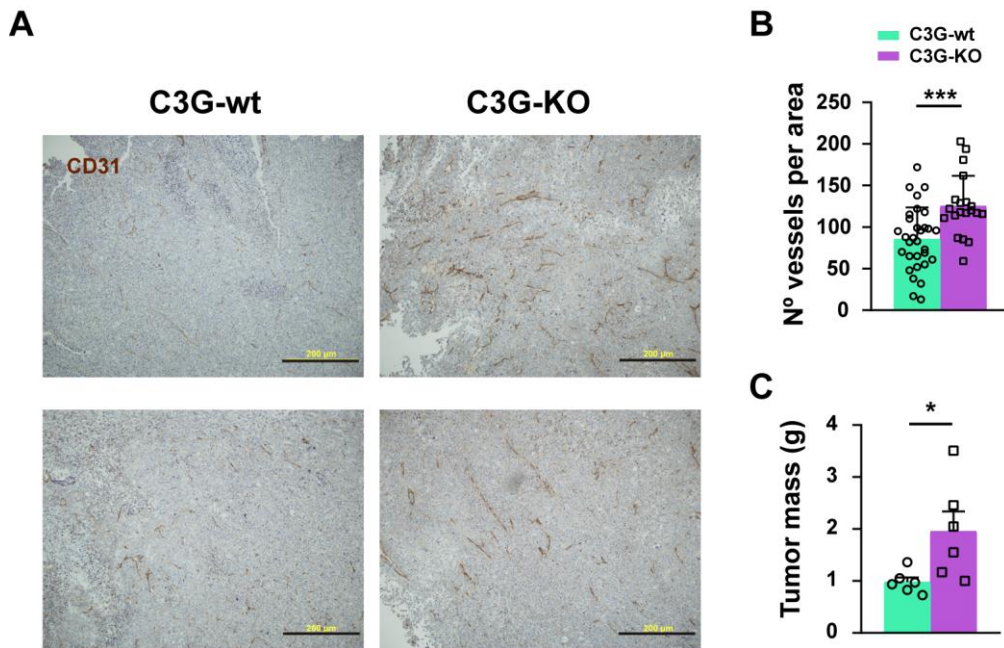


Figure R-24. C3G ablation in platelets promotes tumor growth and angiogenesis. (A) Representative images of 3LL tumor sections, from C3G-wt and C3G-KO mice, showing vessel density detected by CD31 staining. Bar: 200 μm. Quantification of the number of vessels per area in tumor sections (**B**) and tumor mass (**C**) from the indicated genotypes. * $p < 0.05$, $p^{***} < 0.001$. wt: wild-type, KO: knockout.

To corroborate these findings, we analyzed hemangiocyte recruitment in a model of hind-limb ischemia. In this model, ischemia was generated in the hind leg of mice by sectioning the femoral artery, as detailed in M & M Section, and blood flow recovery was monitored by Laser Doppler (**Figure R-25A** (Niiyama *et al.*, 2009)). Recruitment of hemangiocytes to PB was quantified by flow cytometry, 14 days after ischemia.

TgC3G mice showed a faster recovery of blood flow than their controls (**Figure R-25B**). We found no differences in hemangiocyte recruitment to PB, compared to wtC3G mice (**Figure R-25C**); however, the number of VEGF-positive BMDCs in BM on the final day of the experiment was significantly increased in tgC3G mice, compared to control siblings (**Figure R-25D**).

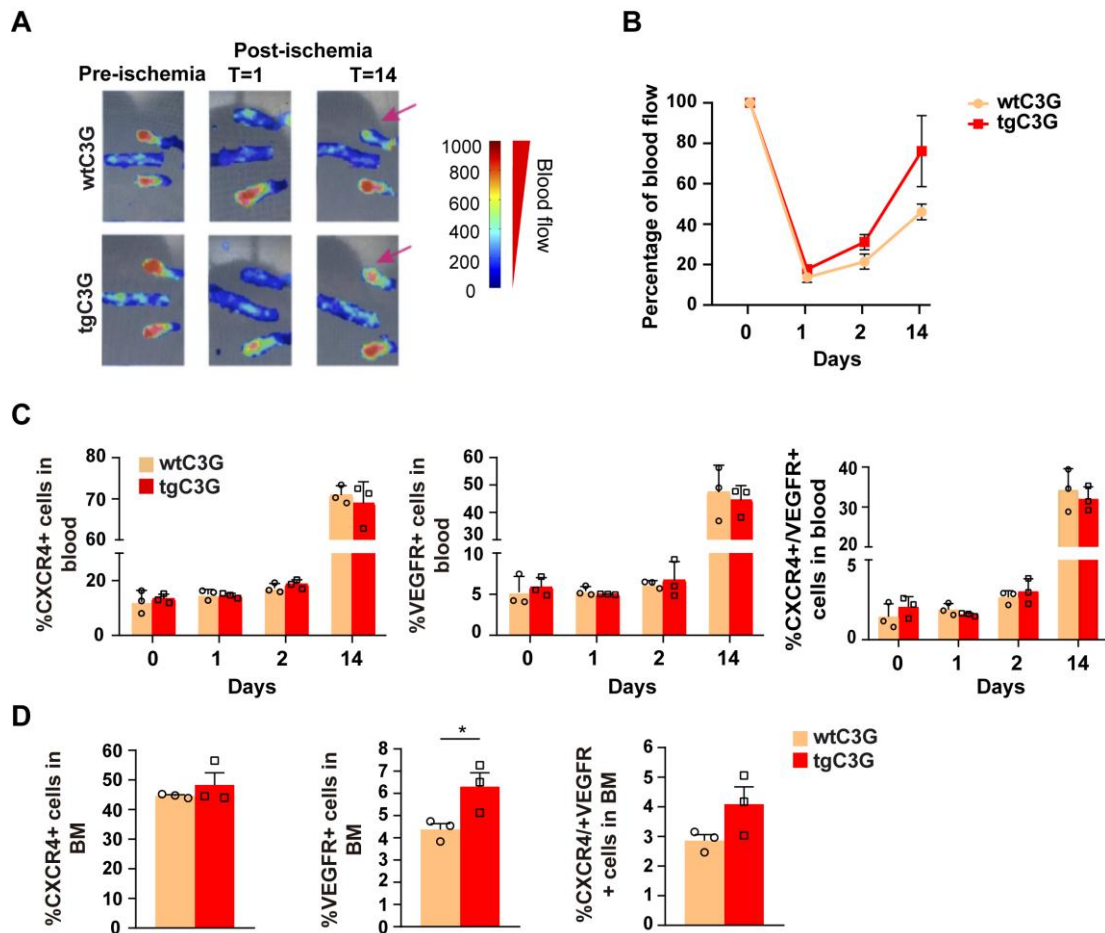


Figure R-25. C3G overexpression in platelets promotes blood flow recovery after hind-limb ischemia but diminished hemangiocyte recruitment. (A) Representative Doppler images at the indicated times are depicted. The color scale represents the blood flow values. **(B)** Doppler values represented as the mean \pm SEM of the percentage of blood flow ($n=6$ tgC3G and wtC3G). **(C, D)** The histograms represents the mean \pm SEM of the percentage of CXCR4⁺ (upper), VEGFR⁺ (middle) and CXCR4⁺/VEGFR⁺ (lower) cells in **(C)** blood or **(D)** bone marrow (15 days after the induction of the ischemia) from tgC3G and their control, collected at the indicated times post-ischemia. * $p<0.05$. wt: wildtype, tg: transgenic.

To further investigate ischemia recovery, RNA was isolated from ischemic and non-ischemic muscle, and the expression of several angiogenic markers (*Vegfr*, *Vegfa*, *Sdf1*, *Cxcr4*, *Sdf1*, *Cd31*) was assessed by RT-qPCR. A decreasing trend in *Cd31*, *Vegfa* and *Cxcr4* mRNA expression was found in tgC3G ischemic muscle, 7 days after surgery, while *Vegfr* expression appeared to increase, although none of these changes were statistically significant. However, at day 14 post-ischemia, ischemic muscle from tgC3G mice showed a significant higher expression of *Cd31* and *Sdf1* than control muscle (**Figure R-26**). These findings are consistent with the faster blood flow recovery in tgC3G animals following ischemia induction.

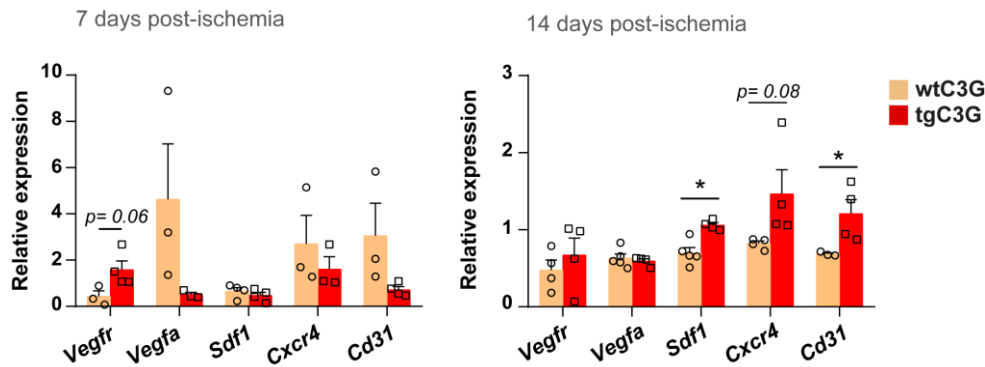


Figure R-26. C3G overexpression in platelets increased *Sdf1* and *Cd31* mRNA expression in ischemic muscle. RT-qPCR analysis of *Vegfr*, *Vegfa*, *Sdf1*, *Cxcr4* and *Cd31* mRNA expression in homogenates of murine muscle from tgC3G and wtC3G mice at day 7- (left panel) and 14- (right panel) post-ischemia. Values are relative to β -actin expression and were normalized against the corresponding value in the contralateral (non-ischemic) leg. * $p<0.05$. wt: wildtype, tg: transgenic.

Similarly to the tumor implantation model, C3G-KO mice showed a greater recruitment of hemangiocytes and other VEGFR⁺ cells, to peripheral blood 2 days after the induction of hind-limb ischemia (**Figure R-27A**). Consistently, C3G-KO mice presented a faster blood flow recovery compared with their controls (**Figure R-27B**). However, C3G-KO mice did not present differences in the proportions of CXCR4⁺, VEGFR⁺ and CXCR4/VEGFR-double positive cells in BM 14 days after the induction of the ischemia (**Figure R-27C**).

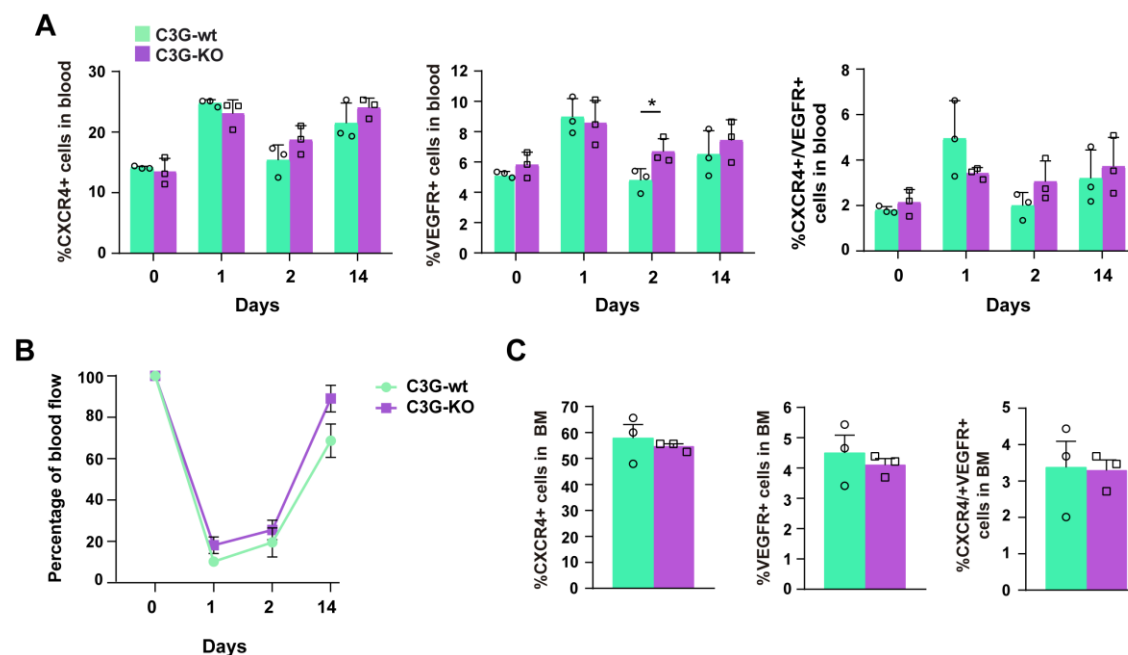


Figure R-27. Platelet C3G ablation promotes blood flow recovery and hemangiocyte recruitment after hind-limb ischemia. (A) The histograms represents the mean \pm SEM of the percentage of CXCR4⁺ (left), VEGFR⁺ (middle) and double CXCR4⁺/VEGFR⁺ (right) cells in

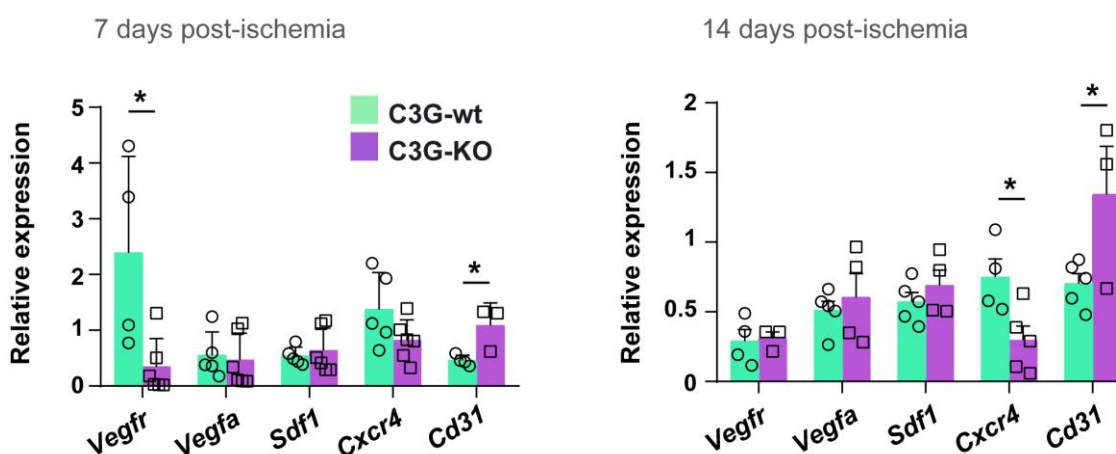
blood from C3G-KO and their control mice, collected at the indicated times post-ischemia. **(B)** Doppler values represented as the mean \pm SEM of the percentage of blood flow (n=3 C3G-KO and C3G-wt). **(C)** The histograms represent the mean \pm SEM of the percentage of CXCR4-positive (left), VEGFR-positive (middle) and CXCR4/VEGFR-double-positive (right) cells in bone marrow from C3G-wt and C3G-KO mice, 14 days after the induction of the ischemia. *p<0.05. wt: wild-type, KO: knockout.

Furthermore, we used RT-qPCR to examine the expression of angiogenic markers in ischemic muscle homogenates, just as we did with tgC3G animals. C3G-KO mice had lower *Vegfr* expression and higher *Cd31* expression 7 days after ischemia than control siblings. This increase in *Cd31* expression was also found 14 days after ischemia induction, and was accompanied by a drop in *Cxcr4* expression (**Figure R-28A**).

The histological analysis of the ischemic muscle showed a considerably larger vessel area in animals deficient in platelet C3G than in control mice, in agreement with the higher hemangiocyte recruitment and *Cd31* expression, and in consonance with the greater angiogenesis found in the tumor ischemia model (**Figure R-28B, C**).

These data, along with those from tumor implantation, suggest that C3G ablation facilitates recovery from ischemia by increasing platelet-mediated angiogenesis, likely through increased hemangiocyte recruitment. Overexpression of C3G in platelets also promoted ischemia-induced angiogenesis, albeit by a different mechanism.

A



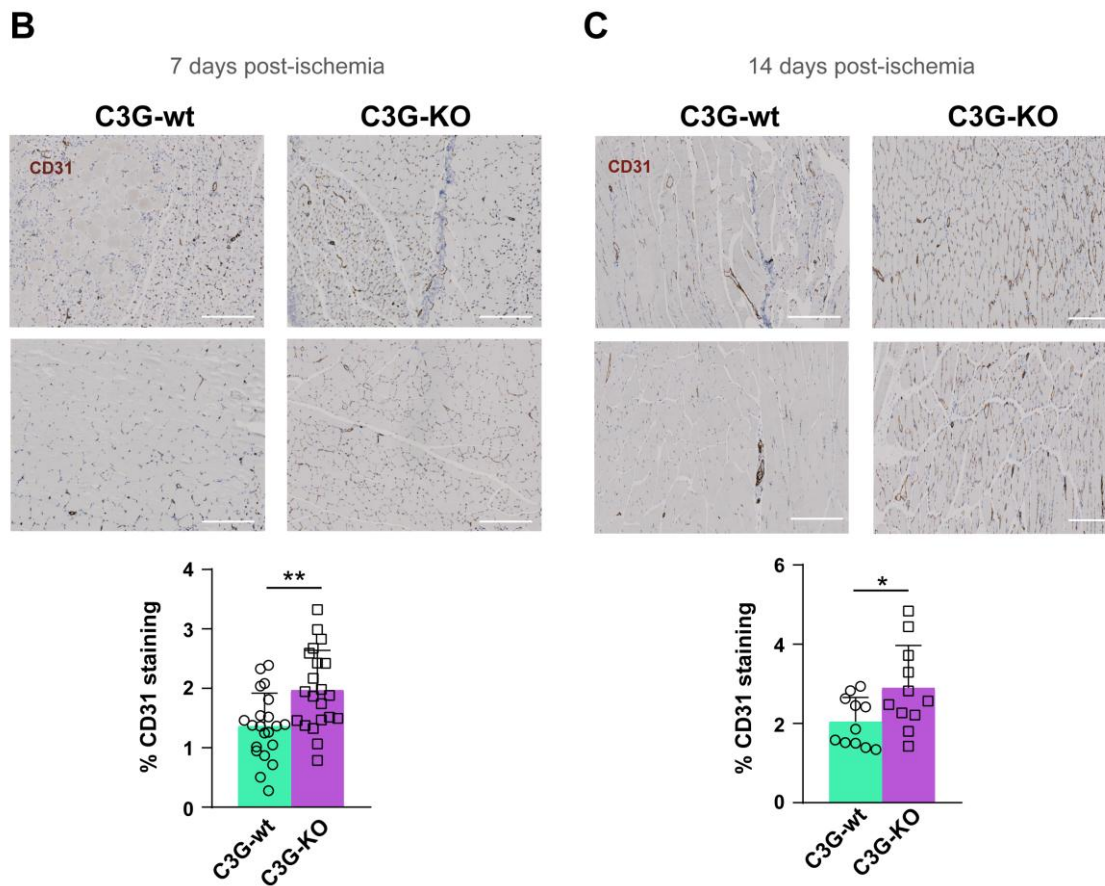


Figure R-28. Platelet C3G ablation promotes neovascularization after hind-limb ischemia. (A) RT-qPCR analysis of *Vegfr*, *Vegfa*, *Sdf1*, *Cxcr4* and *Cd31* mRNA expression in homogenates of murine muscle from C3G-KO and C3G-wt mice at day 7- (left panel) and 14- (right panel) post-ischemia. Values are relative to β -actin expression and were normalized against the corresponding value in the contralateral (non-ischemic) leg. **(B, C)** Representative images of ischemic leg sections of C3G-wt and C3G-KO mice, showing vessel density detected by CD31 staining, **(B)** 7- (left panel) and **(C)** 14-days (right panel) post ischemia. The histograms represent the mean \pm SD of the percentage of positive pixels for CD31 staining, relative to the total number of pixels. * $p < 0.05$, ** $p < 0.01$. wt: wild-type, KO: knockout.

3.2. Platelet C3G regulates SDF-1 release

The above findings suggest that C3G might regulate the recruitment of hemangiocytes in response to distal hypoxia. Since SDF-1 is the main cytokine involved in hemangiocyte chemoattraction, we evaluated whether C3G is involved in the release of SDF-1 from platelets.

Thus, using immunofluorescence confocal microscopy, we analyzed SDF-1 release from platelets in response to thrombin (0.2 U/mL, 5 min) or ADP (25 μ M, 5 min). Thrombin stimulation led to a significantly higher SDF-1 release from C3G-KO platelets than from C3G-wt platelets, which is consistent with the increased hemangiocyte recruitment observed in the *in vivo* models. Conversely, in concordance with the lower levels of hemangiocytes found in PB from tgC3G mice after ischemia, thrombin induced significantly lower SDF-1 release from tgC3G platelets, compared to their wild-types

(Figure R-29). No differences in SDF-1 release were observed in C3G-KO or tgC3G platelets after ADP stimulation.

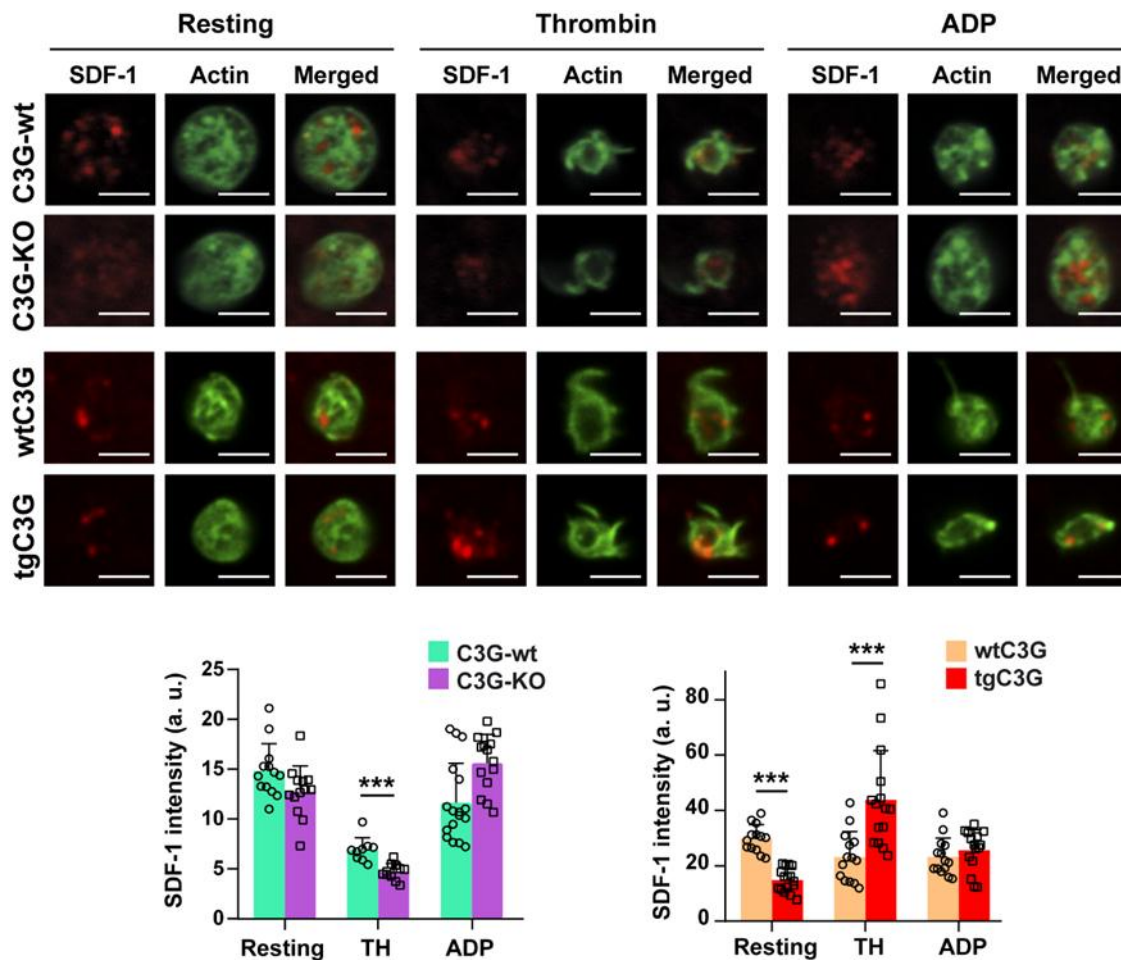


Figure R-29. Platelet C3G controls hemangiocyte recruitment through the release of SDF-1. (A) Representative immunofluorescence confocal microscopy images of tgC3G, C3G-KO platelets and their controls, untreated or treated 5 min with thrombin (TH, 0.2 U/mL) or ADP (25 μ M) and stained with anti-SDF-1 + Alexa Fluor™.647 (red) and phalloidin-488 (green). The histograms represent the mean \pm SD of SDF-1 fluorescence intensity under the indicated experimental condition. *** p <0.001, a.u.: arbitrary units.

To further analyze the involvement of platelet C3G in SDF-1 release, we examined SDF-1 levels in thrombin-induced (0.2 U/mL, 5 min) platelet releasates using the Proteome Profiler Mouse Angiogenesis Array Kit (R&D systems). In line with the immunofluorescences in Figure R-29, C3G-KO platelet secretomes showed an increase in the amount of SDF-1, whereas secretomes from tgC3G platelets showed lower levels of SDF-1 than their controls (**Figure R-30**).

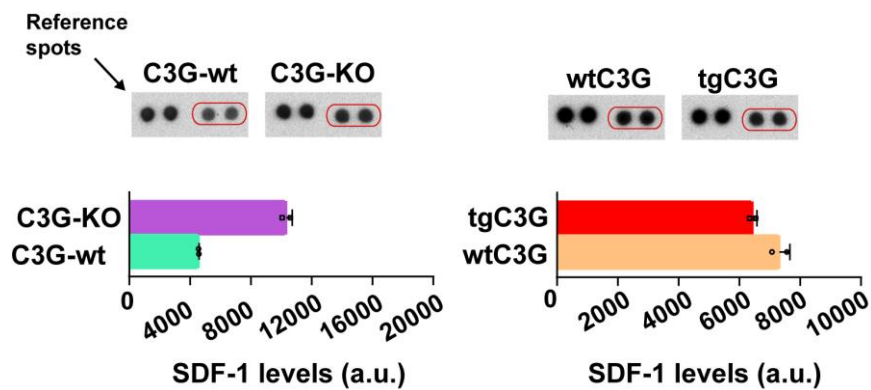


Figure R-30. C3G regulates the release of SDF-1 from platelets. Histograms represent the quantification of SDF-1 levels in thrombin-induced secretome from tgC3G, C3G-KO platelets and their controls, using a Mouse Angiogenesis Array Kit (n=2, each per duplicate). Representative images of the arrays are depicted in the upper panels. SDF-1 spots are marked with red boxes. Reference spots, which are not suitable for quantification, are indicated. Wt: wild-type, KO: knockout, tg: transgenic, a.u.: arbitrary units.

These results confirm a role for C3G in the regulation of SDF-1 secretion, and explain the differential recruitment of hemangiocytes between tgC3G and C3G-KO mice observed in the ischemia models.

3.3. C3G ablation affects the release of VEGF and TSP-1 from platelets.

Previous results from our group demonstrated that C3G overexpression in platelets induced retention of TSP-1 and VEGF, following thrombin stimulation, resulting in a net proangiogenic secretome both *in vivo* and *in vitro* (Martín-Granado *et al.*, 2017). This could explain the increased angiogenesis observed, despite the lower recruitment of hemangiocytes. Hence, we sought to investigate, whether C3G ablation also affects the release of VEGF and TSP-1.

In contrast to tgC3G platelets, thrombin-stimulated C3G-KO platelets released a significantly higher amount of VEGF, than their controls. However, as with tgC3G platelets, C3G-KO platelets showed a clear retention of TSP-1 upon thrombin stimulation (**Figure R-31**).

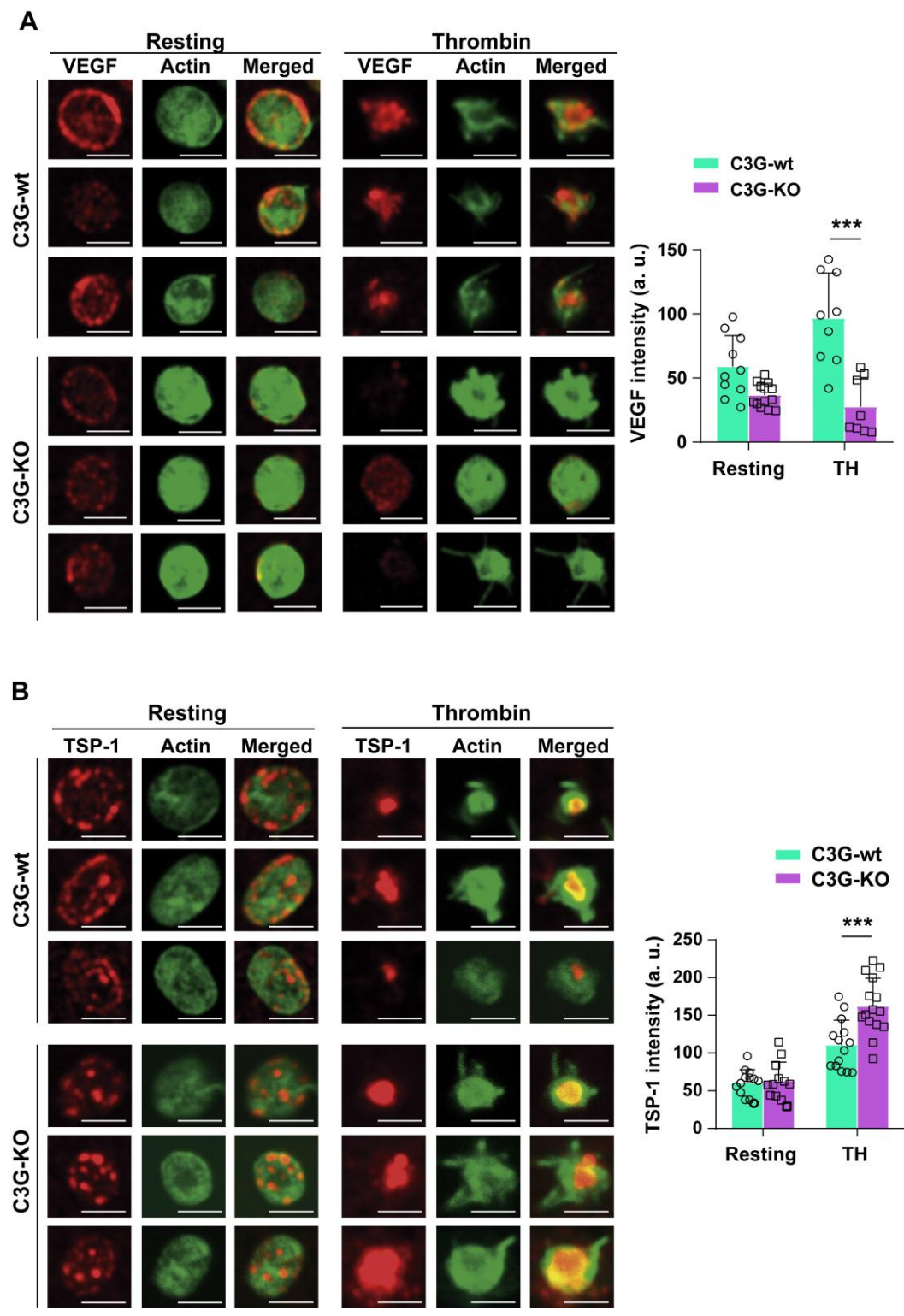


Figure R-31. C3G-KO platelets show increased VEGF release and TSP1 retention in response to thrombin. Representative immunofluorescence confocal microscopy images of C3G-KO platelets and their wt controls, untreated or treated with thrombin (TH, 0.2 U/mL) and stained with anti-TSP-1 + Alexa Fluor™-647 (red) or anti-VEGF + Alexa Fluor™-647 (red) and phalloidin-488 (green), as indicated. All images were taken at the same exposure time. Bar: 2.5 μm. The histograms show the mean ± SD of VEGF (left) and TSP-1 (right) fluorescence intensity (a.u.: arbitrary units). ***p<0.001. wt: wild-type, KO: knockout.

The secretion of VEGF and TSP-1 in response to thrombin or ADP (which also promotes the differential release of angiogenic factors) was also evaluated by western blot in cytosolic and membrane fractions from platelets of the different genotypes. Lower levels of VEGF were detected in the cytosolic fraction of thrombin-stimulated C3G-KO platelets, suggesting an increased release of VEGF. Lower levels of TSP-1 were also detected in the cytosolic fraction of C3G-KO platelets, suggesting a greater release of this antiangiogenic factor. However, analysis of the membrane fraction showed that TSP-1 was retained in the membrane, mainly in C3G null platelets (**Figure R-32**), consistent with the fluorescence microscopy results. C3G-KO platelets also showed decreased TSP-1 release and increased VEGF release in response to ADP, compared to their controls (**Figure R-32**).

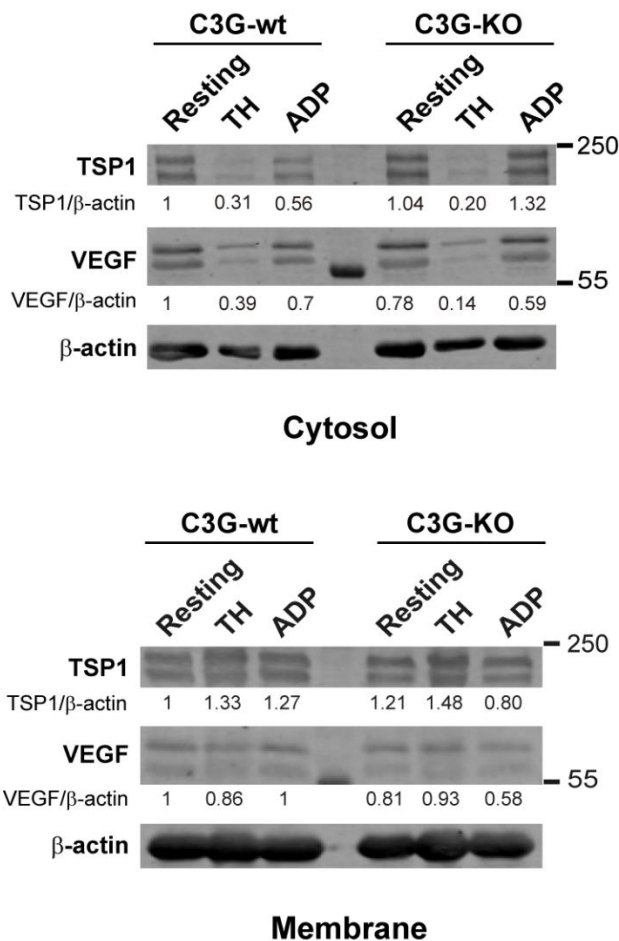


Figure R-32. Platelet C3G regulates the release of VEGF and TSP-1. Western blot analysis of TSP-1 and VEGF levels in cytosolic (upper) and membrane (lower) fractions from resting, thrombin- (TH, 0.2 U/mL, 5 min) or ADP- (25 μM, 5 min) stimulated C3G-KO or C3G-wt platelets. β-actin was used as a loading control. Values were normalized against to those of resting C3G-wt platelets. wt: wild-type, KO: knockout.

In conclusion, ablation of C3G in platelets increases the release of the proangiogenic factors SDF-1 and VEGF, while retaining the major antiangiogenic factor, TSP-1, further

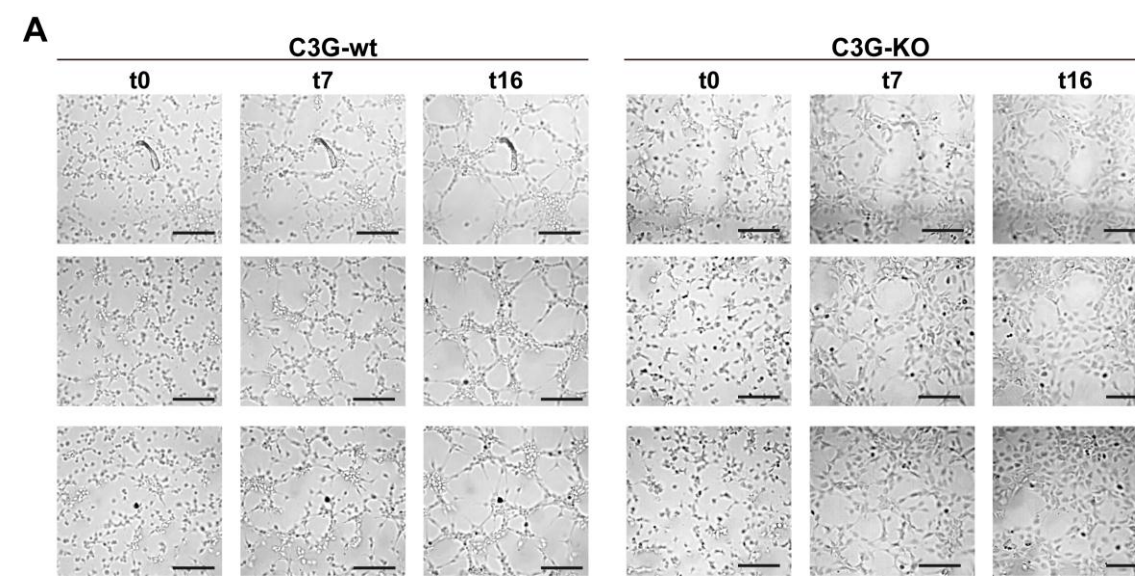
contributing to a net proangiogenic platelet secretome, in agreement with the enhanced angiogenesis found in C3G-KO animals in the ischemia models.

3.4. C3G-KO secretome stimulates angiogenesis *in vitro*

To further validate the proangiogenic characteristics of C3G-KO platelet secretomes, we used an *in vitro* capillary tube formation assay in HUVECs (Human Umbilical Vein Endothelial Cell). Cells were treated with secretomes from C3G-KO or C3G-wt platelet stimulated with thrombin. We analyzed three parameters of the capillary network: the number of master segments, the overall length of master segments, and the number of internal meshes.

Treatment of HUVECs with platelet secretomes caused the development of capillary tubes, as previously documented (Martín-Granado *et al.*, 2017). In addition, HUVECs stimulated with C3G-KO releasates generated a significantly higher number of longer master segments, compared to HUVECs treated with control secretomes. We also found that C3G-KO secretomes promoted the formation of capillary networks with a greater number of internal meshes than control secretomes. Furthermore, C3G-KO secretomes seemed to promote greater HUVEC proliferation, as evidenced by the lower cell-free space observed at the end of the experiment (**Figure R-33**).

Overall, our findings support the proangiogenic features of C3G-KO platelet secretomes following thrombin activation, which is probably due to enhanced release of SDF-1 and VEGF, accompanied by increased retention of TSP-1.



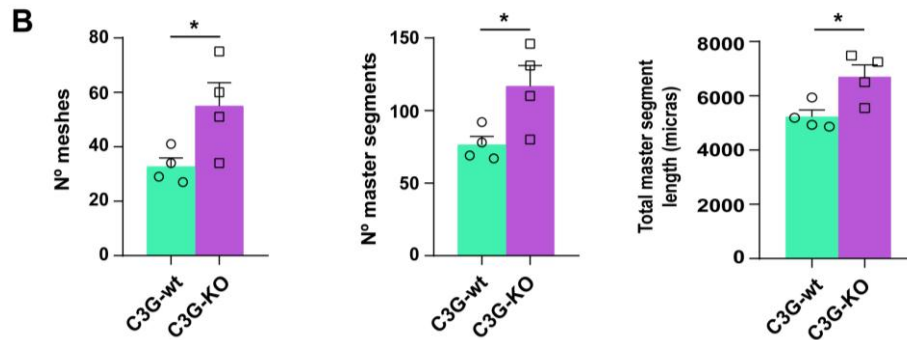


Figure R-33. Releasate from thrombin-stimulated C3G-KO platelets promotes a higher formation of capillary networks in HUVEC. (A) Presentative images showing the capillary-like structures formed by HUVECs seeded onto basement membrane matrix and supplemented with releasates from thrombin-stimulated C3G-KO and C3G-wt platelets. Images were taken every 15 min for 17 intervals. Intervals, t₀, t₇ and t₁₆ are shown, t₀ corresponds to 1.5 h after releasate supplementation. Scale bars: 200 μ m. (B) Graphics show the mean \pm SEM of different network characteristics determined at 2.5 h. 2 independent experiments were performed. * $p < 0.05$.

4. Role of platelet C3G in melanoma metastasis

4.1. Platelet C3G promotes short-term melanoma metastasis

Our group previously demonstrated that C3G overexpression in platelets enhances pulmonary metastasis of B16-F10 melanoma cells (Martín-Granado *et al.*, 2017). The release of angiogenic factors from platelets is a well-known phase in the promotion of metastasis. To gain in-depth knowledge about the role of platelet C3G in melanoma metastasis, we developed a short-term metastasis model (Erpenbeck *et al.*, 2010), in which 2×10^6 B16-F10 cells expressing EGFP (B16-F10-EGFP) were injected into the retro-orbital plexus of tgC3G, C3G-KO, and their control mice. After one hour, lungs were harvested for flow cytometry analysis to determine the number of green cells (EGFP positive) in the lungs, as an indicator of metastatic homing (**Figure R-34A**).

In accordance with previous results, tgC3G mice showed a greater number of metastatic cells in the lungs, compared with the control group (**Figure R-34B**). C3G-KO mice, conversely, presented a lower number of green cells retained in the lung compared with C3G-wt mice (**Figure R-34C**), although differences were not significant. The implantation of B16-F10-EGFP cells was validated by immunohistochemistry (**Figure R-34D**).

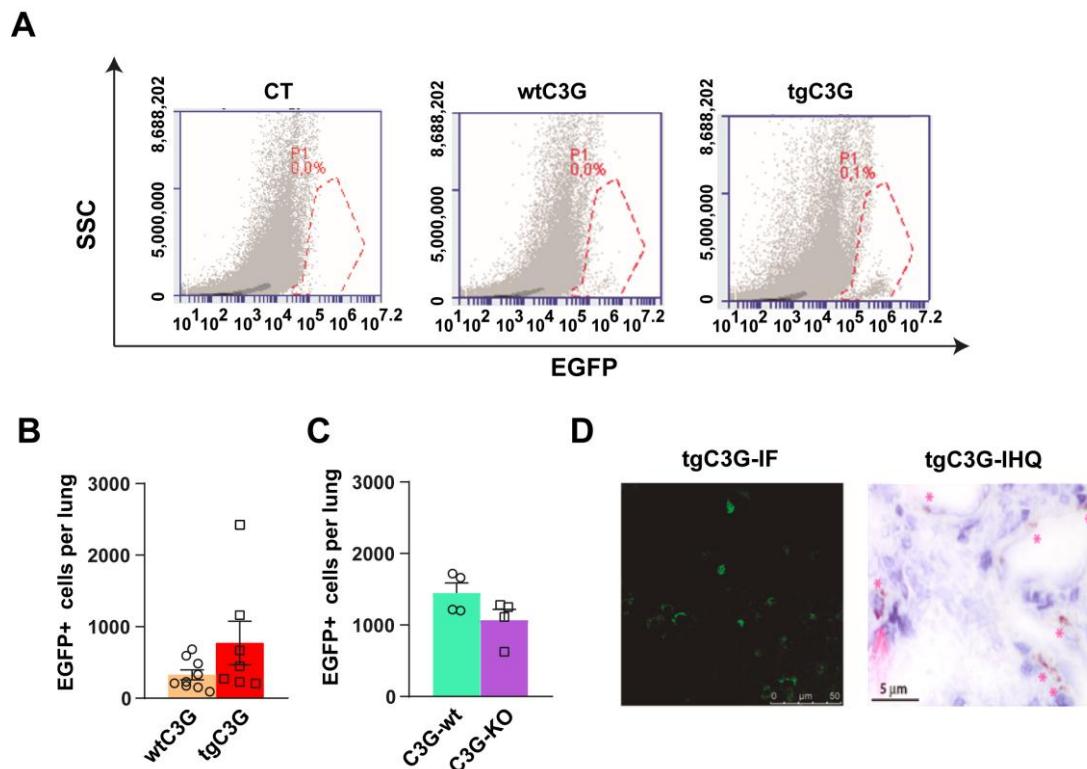


Figure R-34. C3G regulates short-term metastasis. The presence of EGFP-expressing B16-F10 melanoma cells in lung homogenates of tgC3G, C3G-KO mice and their controls was analyzed by flow cytometry. **(A)** Representative flow cytometry plots of samples from wtC3G and tgC3G animals. CT: lung homogenates from untreated mice. The histograms represent the mean \pm SEM of the number of EGFP⁺ cells in 1,000,000 lung cells of tgC3G **(B)**, C3G-KO **(C)** and their corresponding control siblings. **(D)** Representative sections of lung tissue from tgC3G mice analyzed by immunofluorescence (IF, left) or immunohistochemistry (IHQ) with anti-GFP antibodies (right). Presence of B16-F10 cells is indicated with asterisks. Bar 5 μ m. wt: wild-type, tg: transgenic, KO: knockout.

This result suggests that the higher metastatic potential of platelets overexpressing C3G could be due to a better implantation of the melanoma cells in the metastatic niche.

4.2. C3G promotes melanoma cell adhesion.

Platelets secrete a variety of factors that promote tumor cell adherence during the development of a new metastatic niche (Schlesinger, 2018). Since C3G overexpression promotes short-term metastasis, we wanted to know whether platelet C3G impacts melanoma cell adhesion. B16-F10 melanoma cells were co-cultured with tgC3G, C3G-KO or control platelets for 10 min at 37 °C before allowing them to attach to poli-L-Lysine-coated coverslips for 30 min. The number of attached cells was counted by immunofluorescence confocal microscopy using anti-P-selectin antibodies to visualize platelets and Phalloidin to detect melanoma cell.

The analysis of the images revealed a significantly higher number of tumor cells adhered to the substrate when they were stimulated with tgC3G platelets *versus* wtC3G

platelets (**Figure R-35A**). No differences were found in the size of the melanoma cells or in the number of platelets bound to them (**Figure R-35B**).

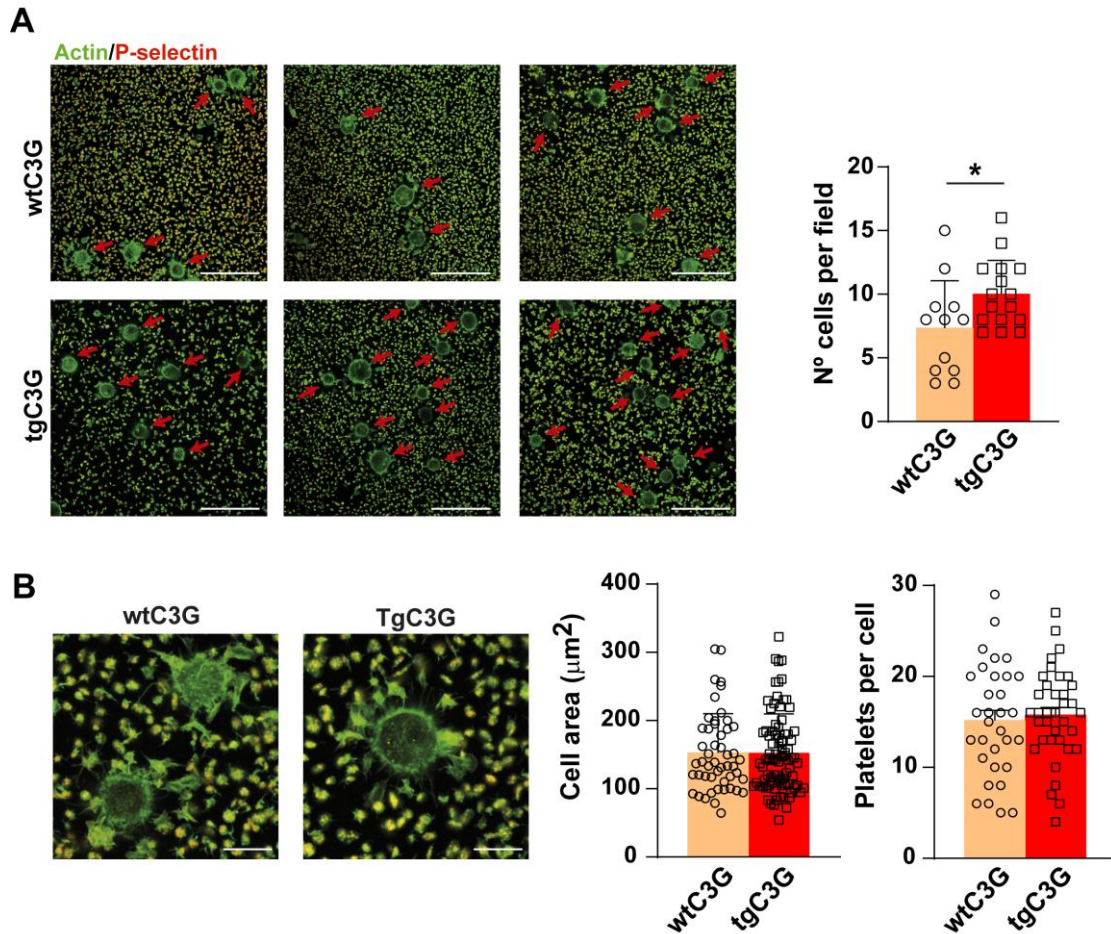


Figure R-35. C3G overexpression promotes melanoma cell adhesion. (A) Representative immunofluorescence confocal microscopy images of B16-F10 melanoma cells adhered to poly-L-Lysine-coated coverslips, after stimulation with tgC3G or wtC3G platelets and stained with anti-P-selectin + Cy3 (to visualize platelets) and phalloidin-488 to detect actin. Arrows indicate the presence of B16-F10 cells. The histogram represents the mean \pm SD of the number of B16-F10 cells per field. Bar: 50 μm . (B) Representative enlarged images of B16-F10 melanoma cells and platelet adhered to them. Histograms represent the mean \pm SD of the size (area) of the melanoma cells (left) and the number of platelets bound to individual cells (right). * $p < 0.05$. wt: wild-type, tg: transgenic.

In contrast, we found fewer melanoma cells adhered to poly-L-Lysine when they were incubated with C3G-KO platelets, compared to wt-C3G platelets (**Figure R-36**).

All these findings suggest a role for platelet C3G in the early stages of metastasis, favoring the adhesion of tumor cells to the metastatic niche.

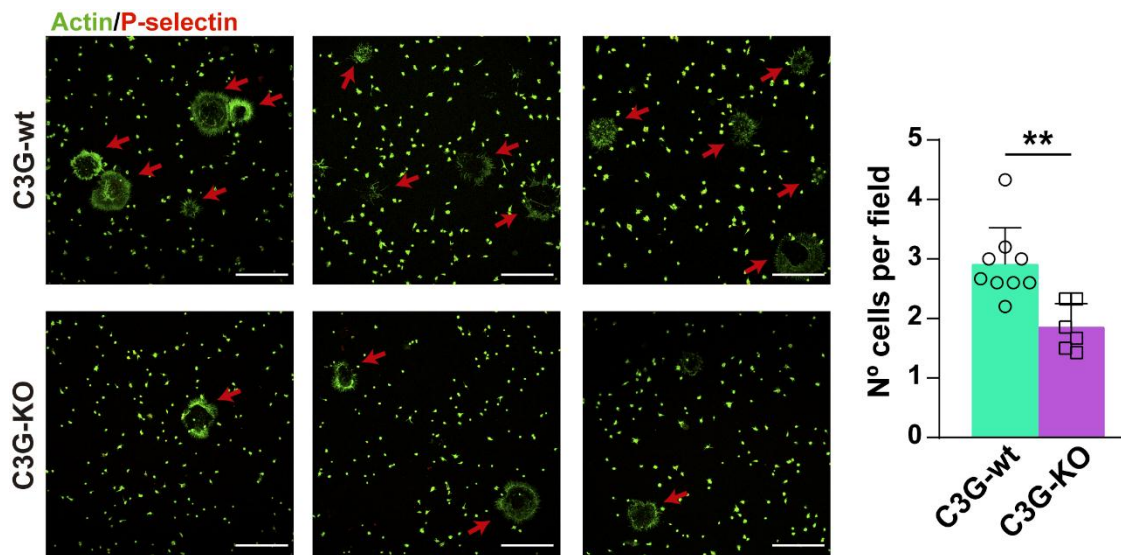


Figure R-36. Platelet C3G ablation diminished melanoma cell adhesion. Representative immunofluorescence confocal microscopy images of B16-F10 melanoma cells adhered to poly-L-Lysine-coated coverslips, after stimulation with C3G-KO or C3G-wt platelets and stained with anti-P-selectin + Cy3 (to visualize platelets) and phalloidin-488 to detect actin. Arrows indicate the presence of B16-F10 cells. The histogram represents the mean \pm SD of the number of B16-F10 cells per field. Bar: 50 μ . ** p <0.01. wt: wild-type, KO: knockout.

4.3. C3G overexpression in platelets promotes tumor cell-induced platelet activation and aggregation.

Platelets release several factors that aid the metastatic process. However, platelet activation is required first and it has been shown that this activation can be promoted by the tumor cell itself (Boukerche *et al.*, 1994; Meikle *et al.*, 2017). Since tgC3G mice showed a higher number of B16-F10 cell metastases in both the long-term (Martín-Granado *et al.*, 2017) and short-term models, and the opposite was found in C3G-KO mice, we wanted to know whether platelet C3G participates in tumor cell-induced platelet activation.

Platelets were incubated with melanoma cells for 10 min at 37 °C. Then, platelets were labelled with Alexa-488-Fibrinogen, which specifically binds to the active form of integrin α IIb β 3, a marker of platelet activation. In the presence of melanoma cells, tgC3G platelets became significantly more active than their controls (**Figure R-37A**). In correlation, melanoma cells also induced greater and faster Rap1 activation in tgC3G platelets than in wtC3G platelets (**Figure R-37B**).

In contrast, C3G ablation in platelets had no effect on platelet activation in response to melanoma cells (**Figure R-37C**), despite finding lower levels of active Rap1 in C3G-KO platelets than in their controls (**Figure R-37D**).

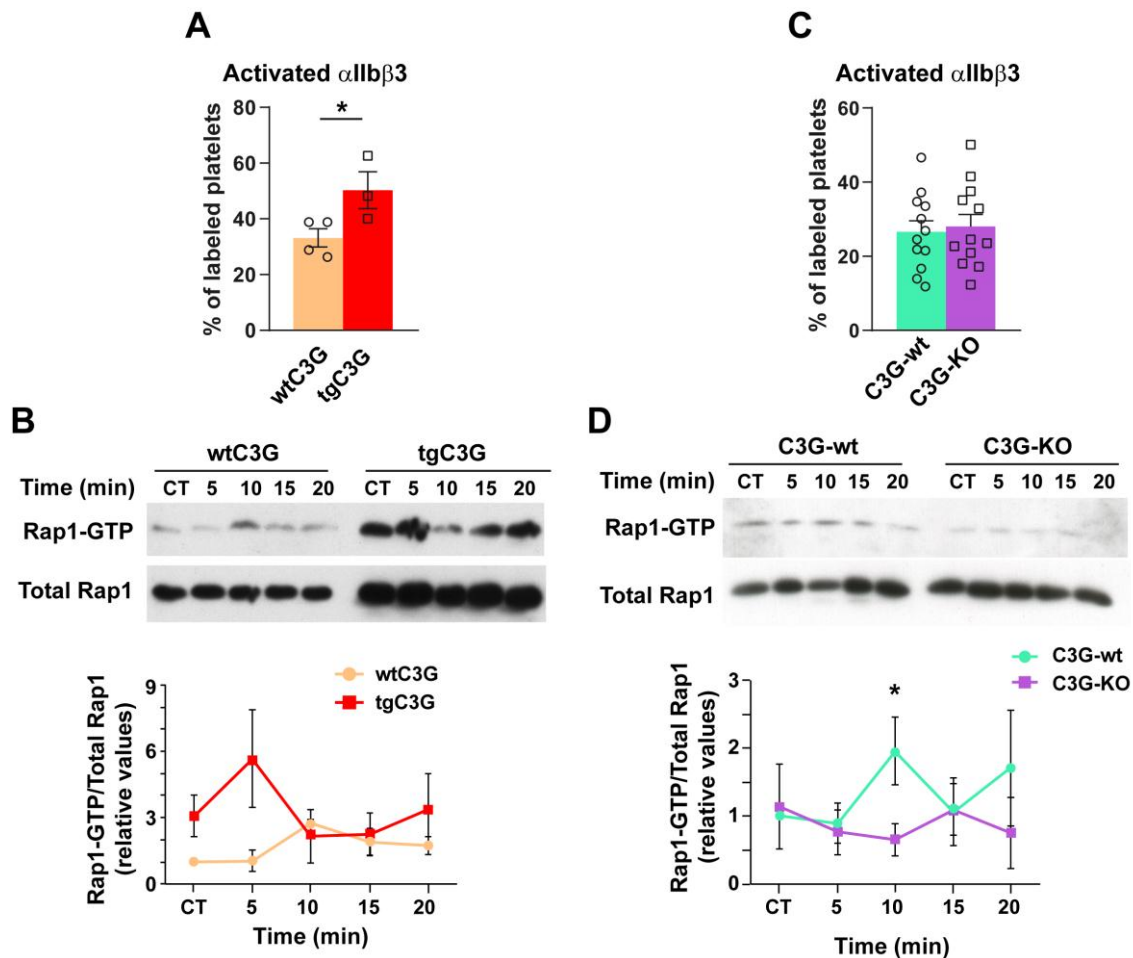


Figure R-37. C3G regulates platelet activation in response to melanoma cells. (A, C) Washed blood from tgC3G and wtC3G (A) or C3G-KO and C3G-wt platelets (C) was stimulated with 1×10^6 B16-F10 cells in combination with Alexa 488-fibrinogen, and labeled platelets (with activated integrin α IIb β 3) were detected by flow cytometry. The histograms represent the mean \pm SEM of the percentage of labeled platelets. (B, D) Platelets from tgC3G and wtC3G mice (B) or C3G-KO and C3G-wt mice (D) were stimulated with 1×10^3 B16-F10 cells. The levels of Rap1-GTP were determined by pull-down assay and immunoblotting using a Rap1 antibody. Upper panels: representative western blots of tgC3G, C3G-KO and their corresponding controls are shown. Lower panels: line/scatter plot of Rap1-GTP levels ($n=3$). Values (mean \pm SEM) are relative to those in unstimulated wild-type platelets and were normalized to total Rap1 levels. * $p < 0.05$. wt: wildtype, tg: transgenic, KO: knockout.

Finally, since tgC3G platelets showed increased activation upon B16-F10 cell stimulation we wanted to know whether platelet C3G also contributes to TCIPA (tumor cell-induced platelet aggregation). Platelets were incubated with melanoma cells under aggregating conditions and the number of aggregates measured by flow cytometry. As expected, tgC3G platelets exhibited significantly greater aggregation than control platelets (Figure R-38A). No differences were found in the aggregation capacity between C3G-KO and C3G-wt platelets, in line with the activation results (Figure R-38B).

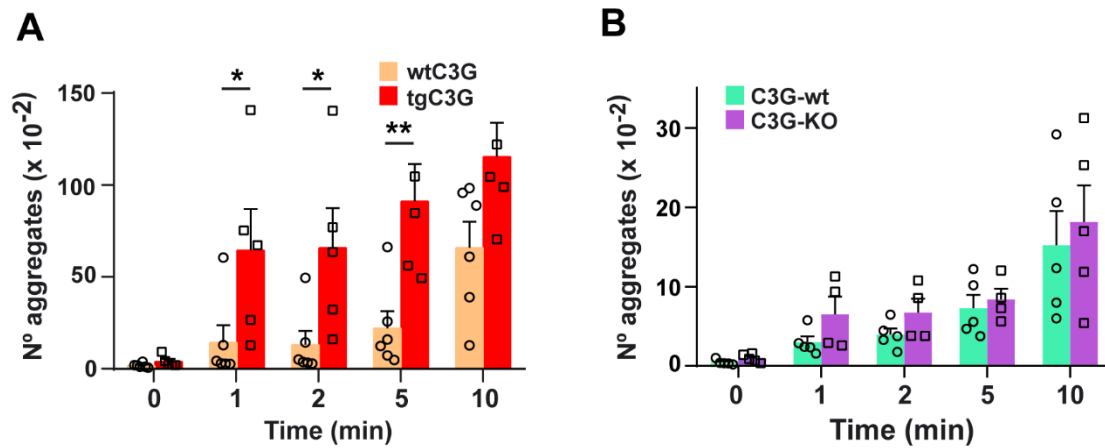


Figure R-38. C3G contributes to TCIPA induced by B16-F10 cells. (A, B) Histograms represent the mean \pm SEM of the number of platelet aggregates formed upon stimulation of tgC3G and wtC3G platelets **(A)** or C3G-KO and C3G-wt platelets **(B)** from 50 μ L of washed blood, with 3×10^4 B16-F10 cells (in 30 μ L volume) for the indicated time periods. * $p < 0.05$, ** $p < 0.01$. wt: wild-type, tg: transgenic, KO: knockout.

All these results support the notion that C3G contributes to platelet-mediated tumor growth and metastasis, including cell adhesion to the metastatic niche and platelet-tumor cell communication, in agreement with previous findings (Martín-Granado *et al.*, 2017).

DISCUSSION

DISCUSSION

In the present work we have investigated the implication of C3G in thrombopoiesis and in the maintenance of homeostatic platelet levels, discovering a new important function of C3G in the regulation of plasma TPO levels. Using two *in vivo* models of ischemia (hind-limb ischemia and 3LL tumor cell implantation), we have also unveiled a new mechanism through which platelet C3G participates in ischemia-induced angiogenesis. Finally, we have demonstrated a role for platelet C3G in TCIPA and its implication in metastatic cell adhesion.

1. C3G plays a role in platelet hemostasis.

To achieve this work we have used two transgenic mouse models, already available in the lab, specific for platelets and Mks: tgC3G (overexpressing C3G full-length) and tgC3G Δ Cat (overexpressing a mutant form of C3G lacking the catalytic domain) (Gutiérrez-Herrero *et al.*, 2012). In addition, during this thesis work, we have developed a knockout model, in which C3G is specifically ablated in platelets and Mks (Gutiérrez-Herrero *et al.*, 2020).

Previous result from the group showed that overexpression of C3G in platelets increases platelet activation and aggregation (Gutiérrez-Herrero *et al.*, 2012). The C3G null model confirmed this role of C3G in the hemostatic function of platelets, since C3G ablation led to a significant bleeding diathesis in mice subjected to a tail bleeding assay. This phenotype was associated with decreased platelet aggregation and increased survival rate in a model of pulmonary thromboembolism. These results were in concordance with results in tgC3G mice, which present the opposite phenotype: a significant decrease in bleeding times (Gutiérrez-Herrero *et al.*, 2012) and a greater thrombus formation in the thromboembolism model (Gutiérrez-Herrero, 2018).

Rap1b is the predominant GTPase that regulates platelet activity in response to a variety of agonists (e.g., thrombin, ADP), including activation of the integrin α IIb β 3 and platelet granule release, two critical steps in the coagulation process (Chrzanowska-Wodnicka *et al.*, 2005; Stefanini *et al.*, 2018). Rap1b is activated primarily by CalDAG-GEFI, an essential Rap1b GEF in platelets in response to many agonists (Crittenden *et al.*, 2004). Similarly, C3G actions on platelet activation and aggregation are mediated through its GEF activity on Rap1b (Gutiérrez-Herrero *et al.*, 2012, 2020). As mentioned, previous results on C3G function in platelets were based on mouse models of C3G overexpression (Gutiérrez-Herrero *et al.*, 2012). However, endogenous C3G expression

in platelets is very low (Burkhart *et al.*, 2012; Rowley *et al.*, 2011; Zeiler *et al.*, 2014), raising the question whether the phenotype observed in tgC3G platelets is mainly due to the artificial increase in C3G expression, which causes these platelets to become “addict” to C3G. However, the hemorrhagic phenotype observed in C3G-KO mice, together with the increased survival in the pulmonary thromboembolism model, accompanied by decreased thrombus formation, confirmed a physiological role of C3G in platelets. Altogether, we have demonstrated that, despite its modest expression in platelets, C3G is an alternative GEF for Rap1b, contributing to the maintenance of adequate platelet function.

2. C3G plays a role in the regulation of pathological megakaryopoiesis

C3G overexpression in Mks result in increased maturation and differentiation, both *in vitro* and *in vivo*. Specifically, transgenic C3G expression favors the acquisition of Mk surface markers, increases polyploidization, drives migration to the vascular niche and enhances Mk proplatelet formation ability (Ortiz-Rivero *et al.*, 2018). Nevertheless, this effect of tgC3G expression on Mk maturation does not modify the physiological number of Mks in BM nor does it translate into a higher number of platelets in peripheral blood. Similarly, we found no difference in the number of mature Mks in the BM or in the number of platelets in the circulation between C3G-KO mice and their controls, a phenotype similar to that observed in single Rap1a and Rap1b platelet-specific knockouts (Stefanini *et al.*, 2018). Hence, C3G seems not to be necessary for physiological megakaryopoiesis. In contrast, a modest increase in platelet count was observed in tgC3G animals after intravenous injection of TPO (Ortiz-Rivero *et al.*, 2018), leading us to consider a possible role of C3G in pathological megakaryopoiesis.

In fact, culture of BMCs from C3G-KO mice in the presence of TPO plus a cocktail of interleukins resulted in greater Mk maturation, when compared to C3G-wt controls, suggesting that C3G could play a negative regulatory function in Mk development. This hypothesis was confirmed in the *in vivo* TPO intravenous, showing a greater rise in platelet count in the C3G null animals. Furthermore, the inability to downregulate platelet levels after 5-FU-induced platelet rebound (which is also TPO-dependent (Li *et al.*, 2013)) suggested that C3G might play a role in the negative feed back mechanism mediated by TPO that controls platelet mass (De Graaf & Metcalf, 2011). This hypothesis was supported by the opposite phenotype found in the tgC3G model, showing platelet levels below normal after 5-FU-induced rebound.

This data in agreement with the described role of C3G-Rap1 in the regulation of long-term hematopoiesis (Imai *et al.*, 2019). C3G, through the activation of Rap1, is essential for the maintenance of HSCs in a quiescence state, thus hyperactivation of the pathway induces HSC proliferation and differentiation, leading to exhaustion of the progenitor pool (Imai *et al.*, 2019).

All these data are in favor of a role for C3G in the regulation of hemostatic platelet levels in pathological settings.

Regulation of platelet levels and platelet production is mainly controlled by the TPO/c-Mpl pathway (Hitchcock & Kaushansky, 2014). Therefore, we have investigated whether C3G could be part of it. Firstly, we observed that c-Mpl mRNA expression in Mks was regulated by C3G levels; increased in C3G null platelets and decreased in C3G overexpressing platelets, although increased c-Mpl expression was found in platelets of both genotypes. However, at the protein levels, we found opposite results: increased amount of the receptor in tgC3G Mk and platelets and decreased c-Mpl protein levels in defective C3G Mk and platelets. This is probably due to post-transcriptional or post-translational compensatory mechanisms. In this sense, C3G has been shown to play a role in gene expression regulation; C3G knockout clones of C2C12 (mouse myoblast) and MDA-MB-231 (human breast cancer) cells show lower protein levels of various splicing factors, implying that C3G regulates RNA alternative splicing (Shakyawar *et al.*, 2018).

Furthermore, consistent with the lower c-Mpl protein levels observed in C3G-KO platelets, flow cytometry analysis revealed reduced c-Mpl levels on the surface. Lower levels of c-Mpl have also been found in a PF4-c-Cbl-KO mouse model (Märklin *et al.*, 2020).

Regulation of plasma TPO levels requires internalization, ubiquitination and, eventually degradation of the c-Mpl receptor via the proteasome and lysosome. This process is tightly regulated by the E3 ubiquitin ligase c-Cbl (Saur *et al.*, 2010). TPO-induced c-Mpl degradation was impaired in C3G-KO and tgC3G Δ Cat platelets, whereas C3G overexpression resulted in increased c-Mpl degradation. In addition, C3G-KO platelets were defective in c-Mpl internalization. Similarly, c-Cbl null platelets also exhibit an impaired platelet-mediated uptake of TPO (Märklin *et al.*, 2020). This suggests that C3G could be a mediator of c-Cbl action on c-Mpl. Indeed, results showing C3G colocalization/co-immunoprecipitation with c-Cbl in TPO-stimulated platelets, as well as previous findings on a functional relationship in CML cells (Maia *et al.*, 2013) supports

this hypothesis. Moreover, in this study we discovered that C3G enhances c-Cbl phosphorylation and activation by promoting the colocalization of c-Cbl with the SFK Src. In fact, C3G deficiency resulted in abrogation of Src-mediated c-Cbl phosphorylation. C-Cbl phosphorylation and activation through Src also occurs after the stimulation of erythropoietin receptor, in which Src and c-Cbl regulate each other's activity (Shintani *et al.*, 2014). In addition, other kinases have also been reported to phosphorylate c-Cbl in platelets in response to TPO (Hunter *et al.*, 1999; Murphy *et al.*, 2013).

The fact that C3G-KO and tgC3G Δ Cat platelets display different phenotypes with respect c-Mpl degradation in response to c-Mpl degradation in response to TPO (slower degradation in C3G-KO *versus* no degradation in tgC3G Δ Cat), opposite to that of tgC3G platelets, suggests that the SH3-binding domain might also be involved in the role of C3G in c-Mpl regulation. This is in agreement with the interaction between C3G and c-Cbl through their C3G-SH3b and c-Cbl-SH3 domains described (Maia *et al.*, 2013).

The impaired c-Cbl phosphorylation by Src in TPO-stimulated C3G-KO platelets, led to a deficient c-Mpl ubiquitination and degradation, which would result in elevated plasma TPO levels. This is in contradiction with the lower TPO levels detected after 3-9 days of TPO injection *in vivo*. One possible explanation is that TPO uptake by Mks is very fast, so excess TPO would rapidly disappear from the circulation and not be reflected in our experiment. Impaired TPO internalization by C3G-KO platelets would favor increased TPO uptake by Mks leading to increased megakaryopoiesis. In favor of this hypothesis, we showed increased platelet mass in C3G-KO mice at the same time points after TPO injection. **Figure D-1** shows a proposed model of C3G-mediated c-Cbl regulation during TPO-induced c-Mpl internalization and degradation.

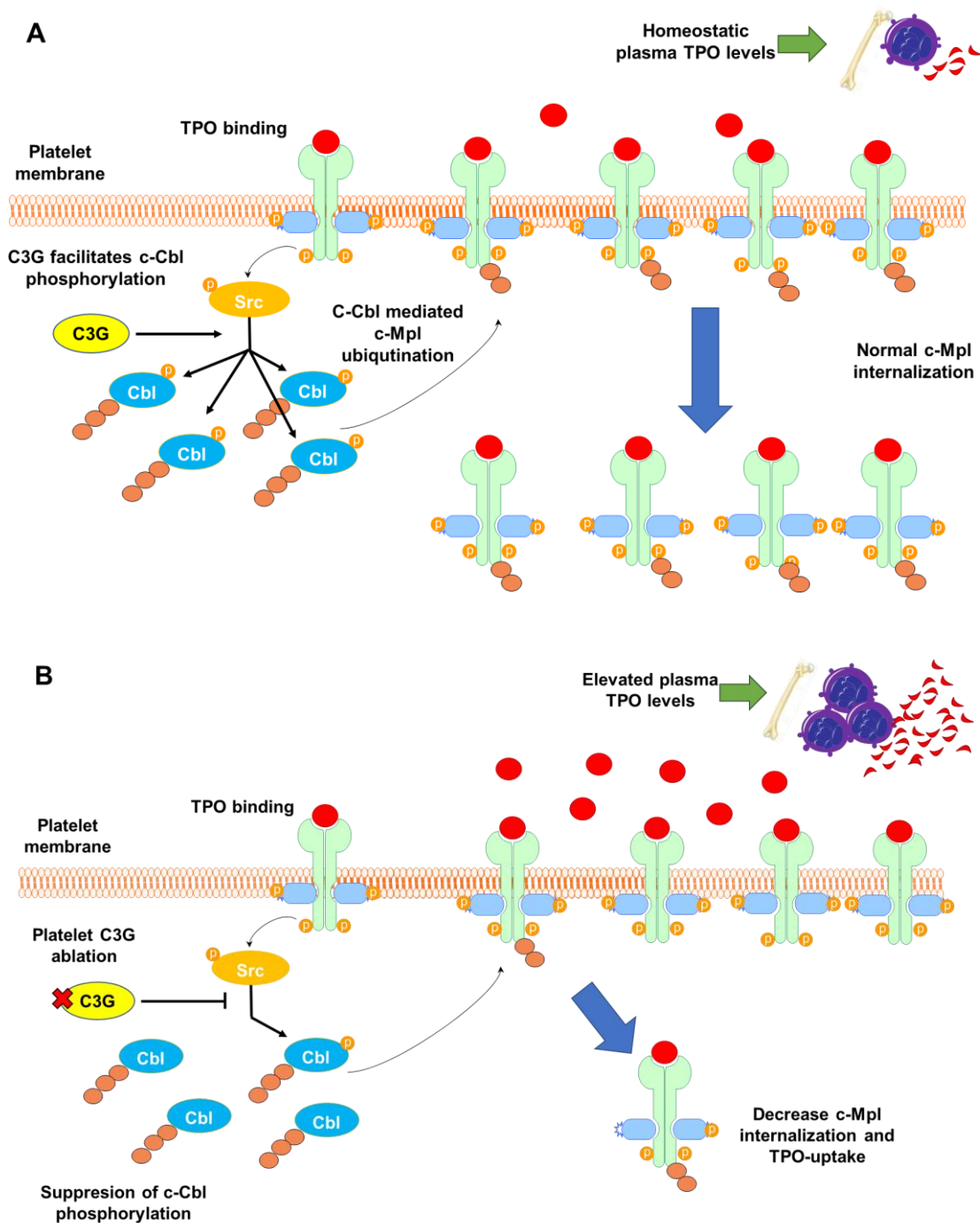


Figure D-1. The C3G-Src-c-Cbl pathway is essential for c-Mpl internalization and the maintenance of hemostatic plasma TPO levels. (A) Binding of TPO to its receptor c-Mpl triggers activation of Src, which mediates the phosphorylation and activation of c-Cbl in a C3G-dependent process. Activated c-Cbl undergoes ubiquitination of c-Mpl leading to its internalization and degradation, which keeps plasma TPO levels under control to prevent excessive platelet formation. **(B)** C3G ablation in platelets results in the abrogation of Src-mediated c-Cbl phosphorylation, leading to decreased c-Mpl ubiquitination and subsequent internalization. This would lead to elevated plasma TPO levels that would promote Mk maturation and platelet formation.

In addition to its involvement in Mk differentiation and platelet formation, TPO is required for the maintenance of a healthy pool of HSCs (Qian *et al.*, 2007). Indeed,

defects in c-Mpl expression trigger higher plasma TPO levels, which correlates with a increased risk in the development of myeloproliferative disorders (Ng *et al.*, 2014). Based on the defective internalization of TPO from C3G-KO platelets, we hypothesized that, following a pathological rise in plasma TPO levels, C3G-KO mice could be at higher risk of developing myeloproliferative diseases. For this reason, it would be interesting to analyze the HSC population in C3G-KO mice in response to TPO injection, to study whether platelet C3G affects HSC differentiation.

During Mk differentiation, TPO-induced c-Mpl activation engages the c-Cbl-Rap1-B-Raf-ERK pathway, involved in sustained ERK activation (Garcia *et al.*, 2001; Stork & Dillon, 2005). However, the GEF that activates Rap1b in Mks has yet to be identified, although C3G has been suggested (Stork & Dillon, 2005), based on its participation in neuronal differentiation via the same pathway (York *et al.*, 1998). In addition, CrkL, an adaptor protein essential for C3G activation through its recruitment to the plasma membrane (Tanaka *et al.*, 1994, 1997), is constitutively phosphorylated in platelets from CML patients, and is significantly activated in response to TPO phosphorylation (Oda, Miyakawa, *et al.*, 1996).

Further evidence that C3G is the GEF of Rap1 in this pathway is that C3G forms complexes with c-Cbl and CrkL at focal adhesions in K562 cells (Maia *et al.*, 2013), an erythromegakaryoblastic cell line that differentiates to Mks in response to PMA (Jacquel *et al.*, 2006).

Therefore, our findings, together with the literature, suggest that TPO-induced c-Mpl activation causes CrkL-mediated recruitment of C3G to the c-Mpl receptor, leading to the interaction of C3G with Src and c-Cbl, most likely via the SH3b domain of C3G, which facilitates Src-mediated c-Cbl phosphorylation.

According to the above, C3G would be essential for Mk maturation through the TPO-Cbl-C3G-Rap1 pathway (Garcia *et al.*, 2001; Stork & Dillon, 2005). However, Mk differentiation occurred in C3G-KO mice, where it even increased. Therefore, we speculate that an alternative Rap1b GEF must be upregulated in this context to fulfill the role of C3G. Indeed, increased expression of CalDAG-GEFI has been observed in C3G-KO Mks (data not shown), suggesting that the lack of C3G must be compensated by overexpression of other GEFs to maintain Rap1 activation levels during megakaryopoiesis.

Overall, our result supports the idea of an important role of C3G in megakaryopoiesis and platelet function, despite its low expression levels observed in these systems.

3. C3G controls protein ubiquitination in platelets

As mentioned above, a functional TPO-c-Mpl-C3G-Src-c-Cbl pathway is indispensable to regulate c-Mpl levels through the regulation of c-Mpl internalization, which involves ubiquitination by c-Cbl (Märklin *et al.*, 2020; Saur *et al.*, 2010). In addition to its role in c-Cbl activation, in this work we present evidence on a role of C3G in the regulation of the ubiquitination machinery.

Ubiquitination is the covalent binding of ubiquitin units to proteins to be degraded by UPS or lysosome, although ubiquitination can also operate as an inactivation signal (Dangelmaier *et al.*, 2005). Mks and platelets show a complete UPS system that is required for thrombopoiesis and proper platelet function (El-Kadiry & Merhi, 2021; Gupta *et al.*, 2014; Karim *et al.*, 2015; Murai *et al.*, 2014; M. K. Nayak *et al.*, 2013).

As an E3 ubiquitin-ligase, c-Cbl is involved in the ubiquitination of other proteins, apart from c-Mpl. Since C3G controls c-Cbl activation, it is reasonable to speculate that C3G might play a more general role in ubiquitination. In fact, C3G ablation caused a dramatic decrease of ubiquitinated proteins shortly after TPO activation. However, C3G-KO platelets displayed an accumulation of ubiquitinated proteins one hour after TPO stimulation, suggesting impaired proteasome function. This new putative role of C3G in proteasome regulation is supported by the reduced levels of Rpn1 found in C3G null platelets. Rpn1 is a ubiquitin receptor necessary for a correct proteasome assembly and activity. Lack of Rpn1-Ser361 phosphorylation reduces proteasome activity, impairs cell proliferation and promotes mitochondrial malfunction, leading to oxidative stress (Liu *et al.*, 2020). According to this, C3G would be required for a correct proteasome assembly and activity, with a direct impact on the degradation of ubiquitinated proteins. This putative role of C3G, which requires future investigation, might explain, why, despite having less c-Cbl activity, C3G-KO platelets accumulate ubiquitinated proteins including c-Mpl after prolonged exposure to TPO.

Proteasome or lysosome blockade in wild-type platelets only results in a partial increase in c-Mpl and ubiquitinated proteins due to compensatory activation of the alternative system Saur *et al.*, 2010. However, in our experiments, platelets (especially C3G-KO platelets) treated with the proteasome inhibitor MG132 accumulated more c-Mpl, than platelets treated with the lysosome inhibitor NH₄Cl, suggesting that c-Mpl degradation occurs primarily in the proteasome. This contradicts the findings of Saur *et*

al (Saur *et al.*, 2010), showing degradation of c-Mpl by both systems. It is worth noting, though, that this group has only reported c-Mpl degradation in Mks and BaF cells, but not in platelets. In addition, the stronger accumulation of ubiquitinated proteins, including Ub-c-Mpl, observed in C3G-KO platelets treated with proteasome and lysosome inhibitors, suggest the participation of C3G in the crosstalk between both systems.

Hence, results from this Thesis, suggest a novel role for C3G in the control of protein degradation in platelets through several mechanism: (i) C3G might be required for the correct assembly of the 26S proteasome complex. (ii), C3G, might participate in the crosstalk between proteasome and lysosome systems. This opens a new research field that might help us to fully understand the role of C3G in platelet function.

4. Platelet C3G differentially regulates the release of pro- and antiangiogenic factors leading to hemangiocyte recruitment in response to hypoxia.

We have previously demonstrated that transgenic expression of C3G in platelets promotes tumor-induced angiogenesis. This was due to the retention of TSP-1 inside platelets, generating a net proangiogenic secretome (Martín-Granado *et al.*, 2017). To deepen the role of platelet C3G in angiogenesis, we added to the tumor implantation model, another type of ischemia-induced angiogenesis, the hind-limb ischemia model (Niiyama *et al.*, 2009). Surprisingly, we found that C3G ablation in platelets also promoted angiogenesis in both experimental models. In particular, we observed a greater vascular density in tumors and ischemic muscles from C3G-KO mice, compared to their controls, which correlated with increased hemangiocyte recruitment. However, angiogenesis induced by C3G overexpression in platelets was not due to hemangiocyte recruitment, which, in fact, was decreased, indicating that C3G regulates platelet-mediated angiogenesis through multiple mechanisms.

C3G overexpression limits the release of α -granules and their cargo, by interfering with proteins of the secretory machinery (Martín-Granado *et al.*, 2017). Specifically, interaction of C3G with VAMP-7 leads to the retention of TSP-1, VEGF and bFGF (Martín-Granado *et al.*, 2017). Consistent with this, we showed that SDF-1 was also retained in tgC3G platelets, which explains the decreased hemangiocyte recruitment observed in the ischemia models. It is worth mentioning that SDF-1 was found accumulated at the platelet surface, suggesting that it could also contribute to a more local recruitment of endothelial progenitor cells at the ischemic site (Massberg *et al.*, 2006, **Figure D-2**). Moreover, the increased expression of SDF-1 in the ischemic muscle of these mice could also explain the greater recovery of tgC3G mice under hind-limb ischemia. In addition, since platelet C3G promotes larger aggregation and thrombus

formation, this extra SDF-1 in the muscle could be produced by enhanced vascular injury-induced thrombus (Massberg *et al.*, 2006, **Figure D-2**). Furthermore, it has been proposed that the expression of P-selectin on the platelet surface is involved in the interaction with BM progenitor cells during vascular repair (Massberg *et al.*, 2006), and that integrin $\alpha\text{IIb}\beta\text{3}$ activation induces the exposure and release of SDF-1 both, P-selectin and $\alpha\text{IIb}\beta\text{3}$, being more abundant on the surface of tgC3G platelets (Gutiérrez-Herrero *et al.*, 2012, 2020, **Figure D-2**).

Unlike tgC3G platelets, C3G-defective platelets showed increased release of VEGF and SDF-1 *in vitro*, explaining the higher hemangiocyte recruitment found *in vivo* (**Figure D-2**). Furthermore, TSP-1 was also retained within C3G-KO platelets, further contributing to the proangiogenic character of C3G-KO platelet secretome. This was confirmed by the increased capillary tube formation, and cell proliferation of HUVECs.

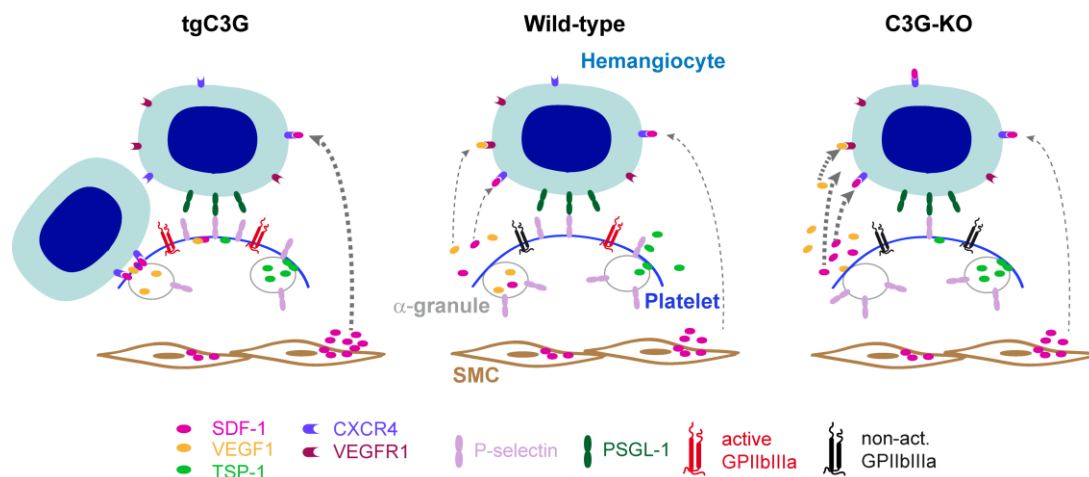


Figure D-2. Schematic representation of the participation of platelet C3G in hemangiocyte recruitment in response to ischemia. Platelets actively participate in hemangiocyte recruitment, through a variety of mechanism. Platelets release SDF-1, a key hemangiocyte chemoattractant, and participates in cell arrest via P-selectin and active integrin $\alpha\text{IIb}\beta\text{3}$. SDF-1 is retained in the platelet membrane of tgC3G platelets, which promotes local hemangiocyte recruitment. Furthermore, C3G overexpression resulted in a greater P-selectin exposure and $\alpha\text{IIb}\beta\text{3}$ activation, that, in turns, contribute to the recruitment of bone marrow precursors. In addition, the ability of tgC3G platelets to generate thrombus promotes increased expression of SDF-1 in the ischemic muscle. Conversely, C3G-KO platelets, show increased SDF-1 release, which promotes hemangiocyte recruitment, despite lower $\alpha\text{IIb}\beta\text{3}$ activation and P-selectin exposure.

The above results suggest that C3G could act as a “break” of platelet secretion. Indeed, C3G-KO platelets showed higher release of VEGF even at rest. However, this does not explain the retention of TSP-1 observed in these platelets.

The existence of different types of α -granules within platelets is controversial. Some authors defend that proangiogenic and antiangiogenic factors are stored in different α -

granules (Battinelli *et al.*, 2011, 2019; Italiano *et al.*, 2008; Martín-Granado *et al.*, 2017; Sehgal & Storrie, 2007), while others suggest that angiogenic factors are randomly distributed (Jonnalagadda *et al.*, 2012; Kamykowski *et al.*, 2011). C3G has been implicated in the differential secretion of pro- and antiangiogenic factors, which is thought to be related to its interaction with VAMP-7, a v-SNARE protein that decorates VEGF-containing α -granules and is essential for proper α -granule exocytosis (Martín-Granado *et al.*, 2017). Thereby, C3G inhibits the release of proangiogenic factors, whereas the proper release of antiangiogenic factors may be affected by changes in normal C3G levels. Moreover, hemangiocyte recruitment is dependent on VAMP-8 protein, since VAMP-8 ablation in platelets decreases hemangiocyte recruitment and revascularization after ischemia (Feng *et al.*, 2011). The increased release of SDF-1 in C3G-KO platelets and the inhibition found in tgC3G platelets suggest that C3G might play a role in the mechanism that control SDF-1 release. In fact, preliminary results from the group have detected an interaction between C3G and VAMP-8 in mouse platelets. Therefore, our findings, indicate that distinct regulatory mechanism would be involved in the release of pro- and antiangiogenic factors, which is consistent with the storage of these factors in different populations of α -granules within platelets, both in mice (Martín-Granado *et al.*, 2017) and humans (Chatterjee *et al.*, 2011; Italiano *et al.*, 2008).

PKC proteins, which mediate C3G phosphorylation in platelets (Gutiérrez-Herrero *et al.*, 2020), regulate α -granule release by phosphorylating proteins of the secretory machinery. Specifically, PKC δ inhibits GPVI-dependent degranulation and release of proangiogenic factors, while it activates PAR-dependent secretion, mainly composed of antiangiogenic factors (Chatterjee *et al.*, 2011; Harper & Poole, 2010). Therefore, PKC-C3G pathway might inhibit the release of the proangiogenic α -granules, whereas a separate signaling pathway also involving C3G, which deserves further investigation, would regulate the release of antiangiogenic α -granules.

5. C3G participates in platelet-tumor cell communication, facilitating metastasis

Platelets are essential in metastasis. Platelets, in fact, promote EMT, protect tumor cells from the immune system and shear stress in the blood stream and facilitate the establishment of a secondary tumor (Schlesinger, 2018). In addition, exposure of P-selectin on the surface and activation of integrin α IIb β 3 are essential to establish platelet-tumor cell interactions during metastasis (M. Chen & Geng, 2006; Erpenbeck *et al.*, 2010; Erpenbeck & Schön, 2010). Indeed, ablation of integrin α IIb β 3, results in a strong decrease in metastasis (Erpenbeck *et al.*, 2010). Previous findings of our group demonstrated the participation of platelet C3G in lung metastasis of melanoma B16-F10

cells injected into the lateral tail vein, an experiment that mimics long-term metastasis (Martín-Granado *et al.*, 2017). In this work, using a model of short-term metastasis, we have found that C3G facilitates the arrest of cells into the metastatic niche. This could be explained by the activation of the integrin $\alpha\text{IIb}\beta\text{3}$ and the expression of P-selectin on the surface promoted by C3G expression (Gutiérrez-Herrero *et al.*, 2012). In addition, the enhanced adhesion of B16-F10 cells cultured with tgC3G platelets would also contribute to the increased metastasis observed in tgC3G animals.

Platelet *also* contribute to metastasis through the release of a plethora of factors, e.g., SDF-1, that facilitate the migration of cancer cells to the metastatic (Rezaeeyan *et al.*, 2018). However, this does not appear to be the mechanism by which C3G regulates platelet-mediated metastasis, since C3G-KO mice showed less metastasis and decreased adhesion of B16-F10 melanoma cells, despite the greater release of angiogenic factors, specially SDF-1, by C3G-KO platelets.

Hence, these findings suggest that platelet C3G modulates melanoma cell metastasis by enhancing tumor cell adhesion to the metastatic niche.

Platelet-tumor cell interaction is a reciprocal phenomenon, so that to adhere to tumor cells, platelets must first be activated by them (N. Li, 2016). Our results indicated that C3G contributes to platelet activation and aggregation (TCIPA) by B16-F10 melanoma cells. However, we found no differences in TCIPA between C3G-KO and control platelets, despite a considerable reduction in Rap1 activation in C3G-KO platelets. This indicates that platelet C3G contributes to TCIPA but it is not essential, and that probably most important contribution of platelet C3G to the metastatic process is its ability to stimulate melanoma cell adhesion.

6. Conclusion

In conclusion, in this work we present evidence for the involvement of C3G in pathological megakaryopoiesis. This is supported by the increased platelet count observed in C3G-KO mice upon TPO injection or 5-FU-induced myelosuppression. The fact that neither C3G overexpression nor ablation modifies physiological platelet count is compatible with a dual role of C3G: it would induce c-Mpl degradation in platelets, regulating TPO levels, and would participate in c-Mpl signaling in Mks leading to platelet production. Therefore, similar to c-Mpl, the expression of C3G in platelets and Mks could play a role in the prevention of megakaryocytosis, thrombocytosis and myeloproliferative disorders. In addition, our findings demonstrate the involvement of C3G in ischemia-

induced platelet-dependent angiogenesis, as well as additional data corroborating prior findings on the role of platelet C3G in melanoma cell lung metastasis.

CONCLUSIONS/ CONCLUSIONES

CONCLUSIONS

1. Deletion of platelet C3G in Mks causes increased bleeding times and decreased thrombus formation *in vivo*, underscoring the important role of C3G for normal platelet function.
2. C3G contributes to the optimal clearance of TPO in plasma and plays a negative role in the modulation of platelet levels after a pathological increase in plasma TPO levels.
3. C3G plays a positive role in Src-mediated c-Cbl phosphorylation, which affects c-Mpl ubiquitination, internalization, and degradation via proteasome and lysosome.
4. C3G is required for an optimal proteasome activity, and is likely involved proteasome-lysosome crosstalk
5. Platelet C3G modulates ischemia-induced angiogenesis through regulation of the secretion of angiogenic factors, which have an impact on hemangiocyte recruitment to sites of ischemia.
 - C3G ablation promotes the release of SDF-1, and VEGF, both involved in hemangiocyte chemoattraction, and the retention of TSP-1, leading to a pro-angiogenic secretome.
 - C3G overexpression induces SDF-1 retention, resulting in inhibition of hemangiocyte recruitment, but also promotes angiogenesis, due to the retention of TSP-1, previously demonstrated.
6. Platelet C3G promotes melanoma cell adhesion and TCIPA, through its GEF activity on Rap1b.

CONCLUSIONES

1. La delección de C3G en Mk provoca un aumento de los tiempos de sangrado y una disminución de la formación de trombos *in vivo*, lo que subraya el importante papel de C3G para la función plaquetaria.
2. C3G contribuye a la correcta eliminación de la TPO del plasma y desempeña un papel negativo en la modulación de los niveles de plaquetas tras un aumento patológico de los niveles de TPO en el plasma.
3. C3G desempeña un papel positivo en la fosforilación de c-Cbl mediada por Src que afecta a la ubiquitinación, internalización y degradación de c-Mpl a través del proteasoma y lisosoma.
4. C3G es necesario para una actividad óptima del proteasoma y probablemente esté implicado en la conexión entre proteasoma y lisosoma.
5. C3G plaquetario modula la angiogénesis inducida por la isquemia regulando la secreción de factores angiogénicos. Que repercuten en el reclutamiento de hemangiocitos a los lugares de hipoxia:
 - La ablación de C3G promueve la liberación de SDF-1 y VEGF, ambos implicados en la quimioatracción de los hemangiocitos, y la retención de TSP-1, lo que conduce a un secretoma proangiogénico.
 - La sobreexpresión de C3G induce la retención de SDF-1, lo que resulta en la inhibición del reclutamiento de hemangiocitos, pero también promueve la angiogénesis, debido a la retención de TSP-1, previamente demostrada.
6. C3G plaquetario promueve la adhesión de células de melanoma y el TCIPA, a través de su actividad GEF sobre Rap1b.

REFERENCES

REFERENCES

- W., & Naseem, K. M. Thrombospondin-1 promotes hemostasis through modulation of cAMP signaling in blood platelets. *Blood* **137**(5): 678–689, 2021. DOI: 10.1182/blood.2020005382.
- Adams, R. H., & Alitalo, K. Molecular regulation of angiogenesis and lymphangiogenesis. *Nat. Rev. Mol. Cell Biol.* **8**(6): 464–478, 2007. DOI: 10.1038/nrm2183.
- Akashi, K., Traver, D., Miyamoto, T., & Weissman, I. L. A clonogenic common myeloid progenitor that gives rise to all myeloid lineages. *Nature* **404**(6774): 193–197, 2000. DOI: 10.1038/35004599.
- Amano, H., Kato, S., Ito, Y., Eshima, K., Ogawa, F., Takahashi, R., Sekiguchi, K., Tamaki, H., Sakagami, H., Shibuya, M., & Majima, M. The Role of Vascular Endothelial Growth Factor Receptor-1 Signaling in the Recovery from Ischemia. *PLoS One* **10**(7), 2015. DOI: 10.1371/journal.pone.0131445.
- Ambati, B. K., Nozaki, M., Singh, N., Takeda, A., Jani, P. D., Suthar, T., Albuquerque, R. J. C., Richter, E., Sakurai, E., Newcomb, M. T., Kleinman, M. E., Caldwell, R. B., Lin, Q., Ogura, Y., Orecchia, A., Samuelson, D. A., Agnew, D. W., St. Leger, J., Green, W. R., Mahasreshti, P. J., Curiel, D. T., Kwan, D., Marsh, H., Ikeda, S., Leiper, L. J., Collinson, J. M., Bogdanovich, S., Khurana, T. S., Shibuya, M., Baldwin, M. E., Ferrara, N., Gerber, H. P., De Falco, S., Witta, J., Baffi, J. Z., Raisler, B. J., & Ambati, J. Corneal avascularity is due to soluble VEGF receptor-1. *Nature* **443**(7114): 993–997, 2006 DOI: 10.1038/nature05249
- Archbold, J. K., Whitten, A. E., Hu, S. H., Collins, B. M., & Martin, J. L. SNARE-ing the structures of Sec1/Munc18 proteins. *Curr. Opin. Struct. Biol.* **29**: 44–51, 2014. DOI: 10.1016/j.sbi.2014.09.003.
- Arganda-Carreras, I., Fernández-González, R., Muñoz-Barrutia, A., & Ortiz-De-Solorzano, C. 3D reconstruction of histological sections: Application to mammary gland tissue. *Microsc. Res. Tech.* **73**(11): 1019–1029, 2010. DOI: 10.1002/jemt.20829.
- Auger, J. M., Best, D., Snell, D. C., Wilde, J., & Watson, S. P. c-Cbl negatively regulates platelet activation by glycoprotein VI. *J. Thromb. Haemost.* **1**(11): 2419–2426, 2003. DOI: 10.1046/j.1538-7836.2003.00464.x.
- Augustin, H. G., Young Koh, G., Thurston, G., & Alitalo, K. Control of vascular morphogenesis and homeostasis through the angiopoietin-Tie system. *Nat. Rev. Mol. Cell Biol.* **10**(3): 165–177, 2009. DOI: 10.1038/nrm2639.
- Bakogiannis, C., Sachse, M., Stamatelopoulos, K., & Stellos, K. Platelet-derived chemokines in inflammation and atherosclerosis. *Cytokine* **122**: 154157, 2019 DOI: 10.1016/j.cyto.2017.09.013.
- Bard, J. A. M., Goodall, E. A., Greene, E. R., Jonsson, E., Dong, K. C., & Martin, A. Structure and Function of the 26S Proteasome. *Annu. Rev. Biochem.* **87**: 697–724, 2018. DOI: 10.1146/annurev-biochem-062917-011931.
- Barry, D. M., Xu, K., Meadows, S. M., Zheng, Y., Norden, P. R., Davis, G. E., & Cleaver, O. Cdc42 is required for cytoskeletal support of endothelial cell adhesion during blood vessel formation in mice. *Development* **142**(17): 3058–3070, 2015. DOI: 10.1242/dev.125260.
- Battinelli, E. M., Markens, B. A., & Italiano, J. E. Release of angiogenesis regulatory proteins from platelet α granules: modulation of physiologic and pathologic angiogenesis. *Blood* **118**(5): 1359–1369, 2011. DOI: 10.1182/blood-2011-02-334524.

- Battinelli, E. M., Thon, J. N., Okazaki, R., Peters, C. G., Vijey, P., Wilkie, A. R., Noetzli, L. J., Flaumenhaft, R., & Italiano, J. E. Megakaryocytes package contents into separate α -granules that are differentially distributed in platelets. *Blood Adv.* **3**(20), 3092-3098, 2019. DOI: 10.1182/bloodadvances.2018020834.
- Behrens, K., & Alexander, W. S. Cytokine control of megakaryopoiesis. *Growth Factors* **36**(3-4): 89-103, 2018. DOI: 10.1080/08977194.2018.1498487.
- Benedito, R., Roca, C., Sørensen, I., Adams, S., Gossler, A., Fruttiger, M., & Adams, R. H. The Notch Ligands Dll4 and Jagged1 Have Opposing Effects on Angiogenesis. *Cell* **137**(6): 1124-1135, 2009. DOI: 10.1016/j.cell.2009.03.025.
- Bentfeld-Barker, M., & Bainton, D. (1982). Identification of Primary Lysosomes in Human Megakaryocytes and Platelets. *Blood* **59**(3): 472-481, 1982. DOI: org/10.1182/BLOOD.V59.3.472.472.
- Bos, J. L., Rehmann, H., & Wittinghofer, A. GEFs and GAPs: critical elements in the control of small G proteins. *Cell*, **129**(5): 865-877, 2007. DOI: 10.1016/j.cell.2007.05.018.
- Boukerche, H., Berthier-Vergnes, O., Penin, F., Tabone, E., Lizard, G., Bailly, M., & McGregor, J. L. Human melanoma cell lines differ in their capacity to release ADP and aggregate platelets. *Br. J. Haematol.* **87**(4): 763-772, 1994. DOI: 10.1111/J.1365-2141.1994.tb06736.x.
- Braun, A., Anders, H. J., Gudermann, T., & Mammadova-Bach, E. Platelet-Cancer Interplay: Molecular Mechanisms and New Therapeutic Avenues. *Front. Oncol.* **11**: 665534, 2021. DOI: 10.3389/fonc.2021.665534.
- Buitrago, L., Tsygankov, A., Sanjay, A., & Kunapuli, S. P. Cbl proteins in platelet activation. *Platelets* **24**(6), 419-427, 2013. DOI: 10.3109/09537104.2012.715216.
- Burkhart, J. M., Vaudel, M., Gambaryan, S., Radau, S., Walter, U., Martens, L., Geiger, J., Sickmann, A., & Zahedi, R. P. The first comprehensive and quantitative analysis of human platelet protein composition allows the comparative analysis of structural and functional pathways. *Blood* **120**(15): e73-82, 2012. DOI: 10.1182/blood-2012-04-416594.
- Carabias, A., Gómez-Hernández, M., de Cima, S., Rodríguez-Blázquez, A., Morán-Vaquero, A., González-Sáenz, P., Guerrero, C., & de Pereda, J. M. Mechanisms of autoregulation of C3G, activator of the GTPase Rap1, and its catalytic deregulation in lymphomas. *Sci. Signal.* **13**(647): eabb7075, 2020. DOI: 10.1126/scisignal.abb7075.
- Chang, Y., Bluteau, D., Debili, N., & Vainchenker, W. From hematopoietic stem cells to platelets. *J. Thromb. Haemost.* **5 Suppl 1**: 318-327, 2007. DOI: 10.1111/j.1538-7836.2007.02472.x.
- Chatterjee, M., Huang, Z., Zhang, W., Jiang, L., Hultenby, K., Zhu, L., Hu, H., Nilsson, G. P., & Li, N. Distinct platelet packaging, release, and surface expression of proangiogenic and antiangiogenic factors on different platelet stimuli. *Blood* **117**(14): 3907-3911, 2011. DOI: 10.1182/blood-2010-12-327007.
- Chen, M., & Geng, J. G. P-selectin mediates adhesion of leukocytes, platelets, and cancer cells in inflammation, thrombosis, and cancer growth and metastasis. *Arch. Immunol. Ther. Exp. (Warsz)*. **54**(2), 75-84, 2006. DOI: 10.1007/S00005-006-0010-6.
- Chen, Y., Yuan, Y., & Li, W. Sorting machineries: how platelet-dense granules differ from α -granules. *Biosci. Rep.* **38**(5): BSR2018458, 2018. DOI: 10.1042/BSR20180458.
- Chiang, A. C., & Massagué, J. Molecular basis of metastasis. *N. Engl. J. Med.* **359**(26): 2814-2823, 2008. DOI: 10.1056/NEJMra0805239.

- Chiang, S. H., Baumann, C. A., Kanzaki, M., Thurmond, D. C., Watson, R. T., Neudauer, C. L., Macara, I. G., Pessin, J. E., & Saltiel, A. R. Insulin-stimulated GLUT4 translocation requires the CAP-dependent activation of TC10. *Nature* **410**(6831): 944–948, 2001. DOI: 10.1038/35073608.
- Chicka, M. C., Ren, Q., Richards, D., Hellman, L. M., Zhang, J., Fried, M. G., & Whiteheart, S. W. Role of Munc13-4 as a Ca²⁺-dependent tether during platelet secretion. *Biochem. J.* **473**(5): 627–639, 2016. DOI: 10.1042/BJ20151150.
- Chrzanowska-Wodnicka, M., Smyth, S. S., Schoenwaelder, S. M., Fischer, T. H., & White, G. C. Rap1b is required for normal platelet function and hemostasis in mice. *J. Clin. Invest.* **115**(3): 680–687, 2005. DOI: 10.1172/JCI22973.
- Cohen-Kaplan, V., Ciechanover, A., & Livneh, I. Stress-induced polyubiquitination of proteasomal ubiquitin receptors targets the proteolytic complex for autophagic degradation. *Autophagy* **13**(4): 759–760, 2017. DOI: 10.1080/15548627.2016.1278327.
- Colberg, L., Cammann, C., Greinacher, A., & Seifert, U. Structure and function of the ubiquitin-proteasome system in platelets. *J. Thromb. Haemost.* **18**(4): 771–780, 2020. DOI: 10.1111/jth.14730.
- Costantini, V., Zacharski, L. R., Moritz, T. E., & Edwards, R. L. The platelet count in carcinoma of the lung and colon. *Thromb. Haemost.* **64**(4): 501–505, 1990.
- Crittenden, J. R., Bergmeier, W., Zhang, Y., Piffath, C. L., Liang, Y., Wagner, D. D., Housman, D. E., & Graybiel, A. M. CalDAG-GEFI integrates signaling for platelet aggregation and thrombus formation. *Nat. Med.* **10**(9): 982–986, 2004. DOI: 10.1038/nm1098.
- Dangelmaier, C. A., Quinter, P. G., Jin, J., Tsygankov, A. Y., Kunapuli, S. P., & Daniel, J. L. Rapid ubiquitination of Syk following GPVI activation in platelets. *Blood* **105**(10): 3918–3924, 2005. DOI: 10.1182/blood-2004-09-3689.
- De Cuyper, I. M., Meinders, M., Van De Vijver, E., De Korte, D., Porcelijn, L., De Haas, M., Eble, J. A., Seeger, K., Rutella, S., Pagliara, D., Kuijpers, T. W., Verhoeven, A. J., Van Den Berg, T. K., & Gutiérrez, L. A novel flow cytometry-based platelet aggregation assay. *Blood* **121**(10): e70-80, 2013. DOI: 10.1182/blood-2012-06-437723.
- De Graaf, C. A., & Metcalf, D. Thrombopoietin and hematopoietic stem cells. *Cell Cycle* **10**(10): 1582–1589, 2011. DOI: 10.4161/cc.10.10.15619.
- Drachman, J. G., Sabath, D. F., Fox, N. E., & Kaushansky, K. Thrombopoietin signal transduction in purified murine megakaryocytes. *Blood* **89**(2): 483–492, 1997. DOI: 10.1182/blood.v89.2.483.
- Dunn, K. W., Kamocka, M. M., & McDonald, J. H. A practical guide to evaluating colocalization in biological microscopy. *Am. J. Physiol. Cell Physiol.* **300**(4): C723-C742, 2011. DOI: 10.1152/ajpcell.00462.2010.
- Eelen, G., Treppe, L., Li, X., & Carmeliet, P. Basic and Therapeutic Aspects of Angiogenesis Updated. *Circ. Res.* **127**(2): 310–329, 2020. DOI: 10.1161/CIRCRESAHA.120.316851
- Egan, K., Crowley, D., Smyth, P., O'Toole, S., Spillane, C., Martin, C., Gallagher, M., Canney, A., Norris, L., Conlon, N., McEvoy, L., Ffrench, B., Stordal, B., Keegan, H., Finn, S., McEneaney, V., Laios, A., Ducrée, J., Dunne, E., Smith, L., Berndt, M., Sheils, O., Kenny, D., & O'Leary, J. Platelet adhesion and degranulation induce pro-survival and pro-angiogenic signalling in ovarian cancer cells. *PLoS One* **6**(10): e26125, 2011. DOI: 10.1371/journal.pone.0026125.
- El-Kadiry, A. E. H., & Merhi, Y. The Role of the Proteasome in Platelet Function. *Int. J. Mol. Sci.* **22**(8): 3999, 2021. DOI: 10.3390/ijms22083999.

- Erpenbeck, L., Nieswandt, B., Schön, M., Pozgajova, M., & Schön, M. P. Inhibition of platelet GPIb alpha and promotion of melanoma metastasis. *J. Invest. Dermatol.* **130**(2): 576–586, 2010. DOI: 10.1038/jid.2009.278.
- Erpenbeck, L., & Schön, M. P. Deadly allies: the fatal interplay between platelets and metastasizing cancer cells. *Blood* **115**(17): 3427–3436, 2010. DOI: 10.1182/blood-2009-10-247296.
- Estrov, Z., Talpaz, M., Mavligit, G., Pazdur, R., Harris, D., Greenberg, S. M., & Kurzrock, R. Elevated plasma thrombopoietic activity in patients with metastatic cancer-related thrombocytosis. *Am. J. Med.* **98**(6): 551–558, 1995. DOI: 10.1016/s0002-9343(99)80013-8.
- Fabricius, H. Å., Starzonek, S., & Lange, T. The Role of Platelet Cell Surface P-Selectin for the Direct Platelet-Tumor Cell Contact During Metastasis Formation in Human Tumors. *Front. Oncol.* **11**: 642761, 2021. DOI: 10.3389/fonc.2021.642761.
- Feng, W., Madajka, M., Kerr, B. A., Mahabeleshwar, G. H., Whiteheart, S. W., & Byzova, T. V. A novel role for platelet secretion in angiogenesis: mediating bone marrow-derived cell mobilization and homing. *Blood* **117**(14): 3893–3902, 2011. DOI: 10.1182/blood-2010-08-304808.
- Fielder, P. J., Gurney, A. L., Stefanich, E., Marian, M., Moore, M. W., Carver-Moore, K., & De Sauvage, F. J. Regulation of thrombopoietin levels by c-mpl-mediated binding to platelets. *Blood* **87**(6): 2154–2161, 1996. DOI: blood.v87.6.2154.bloodjournal8762154.
- Flaumenhaft, R., & Sharda, A. The life cycle of platelet granules. *F1000Research* **7**: 236, 2018. DOI: 10.12688/f1000research.13283.1.
- Franke, B., Akkerman, J. W. N., & Bos, J. L. Rapid Ca²⁺-mediated activation of Rap1 in human platelets. *EMBO J.* **16**(2): 252–259. DOI: 10.1093/emboj/16.2.252.
- Franke, B., van Triest, M., de Bruijn, K. M. T., van Willigen, G., Nieuwenhuis, H. K., Negrier, C., Akkerman, J.-W. N., & Bos, J. L. Sequential regulation of the small GTPase Rap1 in human platelets. *Mol. Cell. Biol.* **20**(3): 779–785, 2000. DOI: 10.1128/MCB.20.3.779-785.2000.
- Frojmovic, M. M., & Milton, J. G. Human platelet size, shape, and related functions in health and disease. *Physiol. Rev.* **62**(1): 185–261, 1982. DOI: 10.1152/physrev.1982.62.1.185.
- Fukuda, M. Rab27 effectors, pleiotropic regulators in secretory pathways. *Traffic* **14**(9): 949–963, 2013. DOI: 10.1111/tra.12083.
- Furie B., Furie B.C. Mechanisms of thrombus formation. *N. Engl. J. Med.*, **359**(9), 938-949. DOI: 10.1056/NEJMRA0801082.
- Garcia, J., de Gunzburg, J., Eychène, A., Gisselbrecht, S., & Porteu, F. Thrombopoietin-mediated sustained activation of extracellular signal-regulated kinase in UT7-Mpl cells requires both Ras-Raf-1- and Rap1-B-Raf-dependent pathways. *Mol. Cell. Biol.* **21**(8): 2659–2670, 2001. DOI: 10.1128/MCB.21.8.2659-2670.2001.
- Gastl, G., Plante, M., Finstad, C. L., Wong, G. Y., Federici, M. G., Bander, N. H., & Rubin, S. C. High IL-6 levels in ascitic fluid correlate with reactive thrombocytosis in patients with epithelial ovarian cancer. *Br. J. Haematol.* **83**(3): 433–441, 1993. DOI: 10.1111/j.1365-2141.1993.tb04668.x.
- Gerhardt, H., Golding, M., Fruttiger, M., Ruhrberg, C., Lundkvist, A., Abramsson, A., Jeltsch, M., Mitchell, C., Alitalo, K., Shima, D., & Betsholtz, C. VEGF guides angiogenic sprouting utilizing endothelial tip cell filopodia. *J. Cell Biol.* **161**(6): 1163–1177, 2003. DOI: 10.1083/jcb.200302047.

- Gotanda, T., Haraguchi, M., Tachiwada, T., Shinkura, R., Koriyama, C., Akiba, S., Kawahara, M., Nishiyama, K., Sumizawa, T., Furukawa, T., Mimata, H., Nomura, Y., Akiyama, S. I., & Nakagawa, M. Molecular basis for the involvement of thymidine phosphorylase in cancer invasion. *Int. J. Mol. Med.* **17**(6), 1085–1091, 2006. DOI: 10.3892/ijmm.17.6.1085.
- Gotoh, T., Hattori, S., Nakamura, S., Kitayama, H., Noda, M., Takai, Y., Kaibuchi, K., Matsui, H., Hatase, O., Takahashi, H., Kurata, T., & Matsuda, M. Identification of Rap1 as a Target for the Crk SH3 Domain-Binding Guanine Nucleotide-Releasing Factor C3G. *Mol. Cell Biol.* **15**(12): 6746–6753, 1995. DOI: 0.1128/MCB.15.12.6746.
- Gotoh, T., Niino, Y., Tokuda, M., Hatase, O., Nakamura, S., Matsuda, M., & Hattori, S. Activation of R-Ras by Ras-guanine nucleotide-releasing factor. *J. Biol. Chem.* **272**(30): 18602–18607, 1997. DOI: 10.1074/jbc.272.30.18602.
- Grand, F. H., Hidalgo-Curtis, C. E., Ernst, T., Zoi, K., Zoi, C., McGuire, C., Kreil, S., Jones, A., Score, J., Metzgeroth, G., Oscier, D., Hall, A., Brandts, C., Serve, H., Reiter, A., Chase, A. J., & Cross, N. C. P. Frequent CBL mutations associated with 11q acquired uniparental disomy in myeloproliferative neoplasms. *Blood* **113**(24): 6182–6192, 2009. DOI: 10.1182/blood-2008-12-194548.
- Greenaway, J., Lawler, J., Moorehead, R., Bornstein, P., Lamarre, J., & Petrik, J. Thrombospondin-1 inhibits VEGF levels in the ovary directly by binding and internalization via the low density lipoprotein receptor-related protein-1 (LRP-1). *J. Cell. Physiol.* **210**(3): 807–818, 2007. DOI10.1002/jcp.20904.
- Gücer, F., Moser, F., Tamussino, K., Reich, O., Haas, J., Arikan, G., Petru, E., & Winter, R. Thrombocytosis as a prognostic factor in endometrial carcinoma. *Gynecol. Oncol.* **70**(2): 210–214, 1998. DOI: 10.1006/gyno.1998.5078.
- Guerrero, C., Fernandez-Medarde, A., Rojas, J. M., Font De Mora, J., Esteban, L. M., & Santos, E. Transformation suppressor activity of C3G is independent of its CDC25-homology domain. *Oncogene* **16**(5): 613–624, 1998. DOI: 10.1038/sj.onc.1201569.
- Guerrero, C., Martín-Encabo, S., Fernández-Medarde, A., & Santos, E. C3G-mediated suppression of oncogene-induced focus formation in fibroblasts involves inhibition of ERK activation, cyclin A expression and alterations of anchorage-independent growth. *Oncogene* **23**(28): 4885–4893, 2004. DOI: 10.1038/sj.onc.1207622.
- Guo, P., Hu, B., Gu, W., Xu, L., Wang, D., Huang, H. J. S., Cavenee, W. K., & Cheng, S. Y. Platelet-derived growth factor-B enhances glioma angiogenesis by stimulating vascular endothelial growth factor expression in tumor endothelia and by promoting pericyte recruitment. *Am. J. Pathol.* **162**(4): 1083–1093, 2003. DOI: 10.1016/S0002-9440(10)63905-3.
- Gupta, N., Li, W., Willard, B., Silverstein, R. L., & McIntyre, T. M. Proteasome proteolysis supports stimulated platelet function and thrombosis. *Arterioscler. Thromb. Vasc. Biol.* **34**(1): 160–168, 2014. DOI10.1161/ATVBAHA.113.302116.
- Gutiérrez-Berzal, J., Castellano, E., Martín-Encabo, S., Gutiérrez-Cianca, N., Hernández, J. M., Santos, E., & Guerrero, C. Characterization of p87C3G, a novel, truncated C3G isoform that is overexpressed in chronic myeloid leukemia and interacts with Bcr-Abl. *Exp. Cell Res.* **312**(6): 938–948, 2006. DOI10.1016/j.yexcr.2005.12.007.
- Gutiérrez-Herrero, S., Fernández-Infante, C., Hernández-Cano, L., Ortiz-Rivero, S., Guijas, C., Martín-Granado, V., Ramón González-Porras, J., Balsinde, J., Porras, A., & Guerrero, C. C3G contributes to platelet activation and aggregation by regulating major signaling pathways. *Signal Transduct. Target. Ther.* **5**(1): 29, 2020. DOI: 10.1038/s41392-020-0119-9.

- Gutiérrez-Herrero, S. (2018). Función de C3G en la señalización plaquetaria utilizando modelos de ratón transgénicos. Tesis Doctoral. Universidad de Salamanca. Salamanca.
- Gutiérrez-Herrero, S., Maia, V., Gutiérrez-Berzal, J., Calzada, N., Sanz, M., González-Manchón, C., Pericacho, M., Ortiz-Rivero, S., González-Porras, J. R., Arechederra, M., Porras, A., & Guerrero, C. C3G transgenic mouse models with specific expression in platelets reveal a new role for C3G in platelet clotting through its GEF activity. *BBA Mol. Cell Res.* **1823**(8): 1366–1377, 2012. DOI: 10.1016/j.bbamcr.2012.05.021.
- Hanna, J., Guerra-Moreno, A., Ang, J., & Micoogullari, Y. Protein Degradation and the Pathologic Basis of Disease. *Am. J. Pathol.* **189**(1): 94–103, 2019. DOI: 10.1016/j.ajpath.2018.09.004.
- Harker, L. A. The kinetics of platelet production and destruction in man. *Clin. Haematol.* **6**(3): 671–693, 1977.
- Harper, M. T., Mason, M. J., Sage, S. O., & Harper, A. G. S. Phorbol ester-evoked Ca²⁺ signaling in human platelets is via autocrine activation of P(2X1) receptors, not a novel non-capacitative Ca²⁺ entry. *J. Thromb. Haemost.* **8**(7): 1604–1613, 2010. DOI: 10.1111/j.1538-7836.2010.03867.x.
- Harper, M. T., & Poole, A. W. Diverse functions of protein kinase C isoforms in platelet activation and thrombus formation. *J. Thromb. Haemost.* **8**(3): 454–462, 2010. DOI: 10.1111/j.1538-7836.2009.03722.x.
- Herrera, R., Hubbell, S., Decker, S., & Petruzzelli, L. A role for the MEK/MAPK pathway in PMA-induced cell cycle arrest: modulation of megakaryocytic differentiation of K562 cells. *Exp. Cell Res.* **238**(2): 407–414, 1998. DOI: 10.1006/excr.1997.3847.
- Hitchcock, I. S., Hafer, M., Sangkhae, V., & Tucker, J. A. The thrombopoietin receptor: revisiting the master regulator of platelet production. *Platelets* **32**(6): 770–778, 2021. DOI: 10.1080/09537104.2021.1925102.
- Hitchcock, I. S., & Kaushansky, K. Thrombopoietin from beginning to end. *Br. J. Haematol.* **165**(2): 259–268, 2014. DOI: 10.1111/bjh.12772.
- Hogan, C., Serpente, N., Cogram, P., Hosking, C. R., Bialucha, C. U., Feller, S. M., Braga, V. M. M., Birchmeier, W., & Fujita, Y. Rap1 regulates the formation of E-cadherin-based cell-cell contacts. *Mol. Cell. Biol.* **24**(15): 6690–6700, 2004. DOI: 10.1128/MCB.24.15.6690-6700.2004.
- Huang, Z., Miao, X., Patarroyo, M., Nilsson, G. P., Pernow, J., & Li, N. Tetraspanin CD151 and integrin $\alpha 6 \beta 1$ mediate platelet-enhanced endothelial colony forming cell angiogenesis. *J. Thromb. Haemost.* **14**(3): 606–618, 2016. DOI: 10.1111/jth.13248.
- Hunter, S., Burton, E. A., Wu, S. C., & Anderson, S. M. Fyn associates with Cbl and phosphorylates tyrosine 731 in Cbl, a binding site for phosphatidylinositol 3-kinase. *J. Biol. Chem.* **274**(4): 2097–2106, 1999. DOI: 10.1074/jbc.274.4.2097.
- Ikeda, M., Furukawa, H., Imamura, H., Shimizu, J., Ishida, H., Masutani, S., Tatsuta, M., & Satomi, T. Poor prognosis associated with thrombocytosis in patients with gastric cancer. *Ann. Surg. Oncol.* **9**(3): 287–291, 2002. DOI: 10.1007/BF02573067.
- Ikenaka, Y., Yoshiji, H., Kuriyama, S., Yoshii, J., Noguchi, R., Tsujinoue, H., Yanase, K., Namisaki, T., Imazu, H., Masaki, T., & Fukui, H. Tissue inhibitor of metalloproteinases-1 (TIMP-1) inhibits tumor growth and angiogenesis in the TIMP-1 transgenic mouse model. *Int. J. Cancer* **105**(3): 340–346, 2003. DOI: 10.1002/ijc.11094.
- Imai, T., Tanaka, H., Hamazaki, Y., & Minato, N. Rap1 signal modulators control the maintenance of hematopoietic progenitors in bone marrow and adult long-term hematopoiesis. *Cancer Sci.* **110**(4): 1317–1330, 2019. DOI: 10.1111/cas.13974.

- Ishibashi, T., Kimura, H., Shikama, Y., Uchida, T., Kariyone, S., & Maruyama, Y. Effect of recombinant granulocyte-macrophage colony-stimulating factor on murine thrombocytopoiesis in vitro and in vivo. *Blood* **75**(7): 1433–1438, 1990. DOI: 10.1182/blood.v75.7.1433.1433.
- Ismail, A. A., Shaker, B. T., & Bajou, K. The Plasminogen-Activator Plasmin System in Physiological and Pathophysiological Angiogenesis. *Int. J. Mol. Sci.* **23**(1): 337, 2021. DOI: 10.3390/IJMS23010337.
- Italiano, J. E., Richardson, J. L., Patel-Hett, S., Battinelli, E., Zaslavsky, A., Short, S., Ryeom, S., Folkman, J., & Klement, G. L. Angiogenesis is regulated by a novel mechanism: pro- and antiangiogenic proteins are organized into separate platelet α granules and differentially released. *Blood* **111**(3): 1227–1233, 2008. DOI: 10.1182/blood-2007-09-113837.
- Jacquel, A., Herrant, M., Defamie, V., Belhacene, N., Colosetti, P., Marchetti, S., Legros, L., Deckert, M., Mari, B., Cassuto, J. P., Hofman, P., & Auberger, P. A survey of the signaling pathways involved in megakaryocytic differentiation of the human K562 leukemia cell line by molecular and c-DNA array analysis. *Oncogene* **25**(5): 781–794, 2006. DOI: 10.1038/sj.onc.1209119.
- Ji, C. H., & Kwon, Y. T. Crosstalk and Interplay between the Ubiquitin-Proteasome System and Autophagy. *Mol. Cells* **40**(7): 441–449, 2017. DOI: 10.14348/molcells.2017.0115.
- Jiang, L., Luan, Y., Miao, X., Sun, C., Li, K., Huang, Z., Xu, D., Zhang, M., Kong, F., & Li, N. Platelet releasate promotes breast cancer growth and angiogenesis via VEGF-integrin cooperative signalling. *Br. J. Cancer* **117**(5): 695–703, 2017. DOI: 10.1038/bjc.2017.214.
- Jin, D. K., Shido, K., Kopp, H. G., Petit, I., Shmelkov, S. V., Young, L. M., Hooper, A. T., Amano, H., Avecilla, S. T., Heissig, B., Hattori, K., Zhang, F., Hicklin, D. J., Wu, Y., Zhu, Z., Dunn, A., Salari, H., Werb, Z., Hackett, N. R., Crystal, R. G., Lyden, D., & Rafii, S. Cytokine-mediated deployment of SDF-1 induces revascularization through recruitment of CXCR4+ hemangiocytes. *Nat. Med.* **12**(5): 557–567, 2006. DOI: 10.1038/nm1400.
- Jonnalagadda, D., Izu, L. T., & Whiteheart, S. W. Platelet secretion is kinetically heterogeneous in an agonist-responsive manner. *Blood* **120**(26): 5209–5216, 2012 DOI: 10.1182/blood-2012-07-445080.
- Joshi, S., & Whiteheart, S. W. The nuts and bolts of the platelet release reaction. *Platelets* **28**(2): 129–137, 2017. DOI: 10.1080/09537104.2016.1240768.
- Jurasz, P., Alonso, D., Castro-Blanco, S., Murad, F., & Radomski, M. W. Generation and role of angiostatin in human platelets. *Blood* **102**(9): 3217–3223, DOI: 10.1182/blood-2003-02-0378.
- Kamykowski, J., Carlton, P., Sehgal, S., & Storrie, B. Quantitative immunofluorescence mapping reveals little functional coclustering of proteins within platelet α -granules. *Blood* **118**(5): 1370–1373, 2011. DOI: 10.1182/blood-2011-01-330910.
- Kanji, R., Gue, Y. X., Memtsas, V., & Gorog, D. A. Fibrinolysis in Platelet Thrombi. *Int. J. Mol. Sci.* **22**(10): 5135, 2021. DOI: 10.3390/ijms22105135.
- Karim, Z. A., Vemana, H. P., & Khasawneh, F. T. MALT1-ubiquitination triggers non-genomic NF- κ B/IKK signaling upon platelet activation. *PLoS One* **10**(3): e0119363, 2015. DOI: 10.1371/journal.pone.0119363.
- Kato, N., Yasukawa, K., Onozuka, T., & Kimura, K. Paraneoplastic syndromes of leukocytosis, thrombocytosis, and hypercalcemia associated with squamous cell carcinoma. *J. Dermatol.* **26**(6): 352–358, 1999. DOI: 10.1111/j.1346-8138.1999.tb03487.x.

- Keane, M. M., Rivero-Lezcano, O. M., Mitchell, J. A., Robbins, K. C., & Lipkowitz, S. Cloning and characterization of cbl-b: A SH3 binding protein with homology to the c-cbl proto-oncogene. *Oncogene* **10**(12): 2367–2377, 1995.
- Kim, M., Tezuka, T., Suzuki, Y., Sugano, S., Hirai, M., & Yamamoto, T. Molecular cloning and characterization of a novel cbl-family gene, cbl-c. *Gene* **239**(1): 145–154, 1999. DOI: 10.1016/s0378-1119(99)00356-x.
- Kirsch, K. H., Georgescu, M. M., & Hanafusa, H. (1998). Direct binding of p130(Cas) to the guanine nucleotide exchange factor C3G. *J. Biol. Chem.* **273**(40): 25673–25679, 1998. DOI: 10.1074/jbc.273.40.25673.
- Klemke, R. L., Cai, S., Giannini, A. L., Gallagher, P. J., De Lanerolle, P., & Cheresch, D. A. (1997). Regulation of cell motility by mitogen-activated protein kinase. *J. Cell Biol.* **137**(2): 481–492, 1997. DOI: 10.1083/jcb.137.2.481.
- Knudsen, B. S., Feller, S. M., & Hanafusa, H. Four proline-rich sequences of the guanine-nucleotide exchange factor C3G bind with unique specificity to the first Src homology 3 domain of Crk. *J. Biol. Chem.* **269**(52): 32781–32787, 1994.
- Koch, S., & Claesson-Welsh, L. Signal transduction by vascular endothelial growth factor receptors. *Cold Spring Harb. Perspect. Med.* **2**(7): a006502, 2012. DOI: 10.1101/cshperspect.a006502.
- Korolchuk, V. I., Mansilla, A., Menzies, F. M., & Rubinsztein, D. C. Autophagy inhibition compromises degradation of ubiquitin-proteasome pathway substrates. *Mol. Cell* **33**(4): 517–527, 2009. DOI: 10.1016/j.molcel.2009.01.021.
- Korolchuk, V. I., Menzies, F. M., & Rubinsztein, D. C. Mechanisms of cross-talk between the ubiquitin-proteasome and autophagy-lysosome systems. *FEBS Lett.* **584**(7), 1393–1398, 2010. DOI: 10.1016/j.febslet.2009.12.047.
- Koseoglu, S., Peters, C. G., Fitch-Tewfik, J. L., Aisiku, O., Danglot, L., Galli, T., & Flaumenhaft, R. VAMP-7 links granule exocytosis to actin reorganization during platelet activation. *Blood* **126**(5): 651-660, 2015. DOI: 10.1182/blood-2014-12-618744.
- Kretschmer, M., Rüdiger, D., & Zahler, S. Mechanical Aspects of Angiogenesis. *Cancers (Basel)* **13**(19): 4987, 2021. DOI: 10.3390/cancers13194987.
- Kuter, D. J. The biology of thrombopoietin and thrombopoietin receptor agonists. *Int. J. Hematol.* **98**(1): 10–23, 2013. DOI: 10.1007/s12185-013-1382.
- Kuter, D. J., & Rosenberg, R. D. The Reciprocal Relationship of Thrombopoietin (c-Mpl Ligand) to Changes in the Platelet Mass During Busulfan-Induced Thrombocytopenia in the Rabbit. *Blood* **85**(10): 2720–2730, 1995. DOI: 10.1182/blood.V85.10.2720.bloodjournal85102720.
- Labelle, M., Begum, S., & Hynes, R. O. Platelets guide the formation of early metastatic niches. *Proc. Natl. Acad. Sci. U.S.A.* **111**(30): E3053-3061, 2014. DOI: 10.1073/pnas.1411082111.
- Lamallice, L., Le Boeuf, F., & Huot, J. Endothelial cell migration during angiogenesis. *Circ. Res.* **100**(6): 782–794, 2007. DOI: 10.1161/01.RES.0000259593.07661.1e.
- Lambert, A. W., Pattabiraman, D. R., & Weinberg, R. A. (2017). Emerging Biological Principles of Metastasis. *Cell* **168**(4): 670–691, 2017. DOI: 10.1016/j.cell.2016.11.037.
- Lawler, P. R., & Lawler, J. Molecular Basis for the Regulation of Angiogenesis by Thrombospondin-1 and -2. *Cold Spring Harb. Perspect. Med.* **2**(5): a006627, 2012. DOI: 10.1101/cshperspect.a006627.

- Lebois, M., & Josefsson, E. C. Regulation of platelet lifespan by apoptosis. *Platelets* **27**(6): 497–504, 2016. DOI: 10.3109/09537104.2016.1161739.
- Lee, O. H., Bae, S. K., Bae, M. H., Lee, Y. M., Moon, E. J., Cha, H. J., Kwon, Y. G., & Kim, K. W. Identification of angiogenic properties of insulin-like growth factor II in in vitro angiogenesis models. *Br. J. Cancer* **82**(2): 385–391, 2000. DOI: 10.1054/bjoc.1999.0931.
- Lefrançois, E., Ortiz-Muñoz, G., Caudrillier, A., Mallavia, B., Liu, F., Sayah, D. M., Thornton, E. E., Headley, M. B., David, T., Coughlin, S. R., Krummel, M. F., Leavitt, A. D., Passegué, E., & Looney, M. R. The lung is a site of platelet biogenesis and a reservoir for haematopoietic progenitors. *Nature* **544**(7648): 105–109, 2017. DOI: 10.1038/nature21706.
- Li, J., Xia, Y., & Kuter, D. J. Interaction of thrombopoietin with the platelet c-mpl receptor in plasma: binding, internalization, stability and pharmacokinetics. *Br. J. Haematol.* **106**(2): 345–356, 1999. DOI: 10.1046/j.1365-2141.1999.01571.x.
- Li, N. Platelets in cancer metastasis: To help the “villain” to do evil. *Int. J. Cancer* **138**(9): 2078–2087, 2016. DOI: 10.1002/ijc.29847.
- Li, S., Huang, N. F., & Hsu, S. Mechanotransduction in endothelial cell migration. *J. Cell. Biochem.* **96**(6): 1110–1126, 2005. DOI: 10.1002/jcb.20614.
- Li, X., & Slayton, W. B. Molecular mechanisms of platelet and stem cell rebound after 5-fluorouracil treatment. *Exp. Hematol.* **41**(7): 635-645.e3, 2013. DOI: 10.1016/j.exphem.2013.03.003.
- Liu, X., Xiao, W., Zhang, Y., Wiley, S. E., Zuo, T., Zheng, Y., Chen, N., Chen, L., Wang, X., Zheng, Y., Huang, L., Lin, S., Murphy, A. N., Dixon, J. E., Xu, P., & Guo, X. Reversible phosphorylation of Rpn1 regulates 26S proteasome assembly and function. *Proc. Natl. Acad. Sci. U.S.A.* **117**(1): 328–336, 2020. DOI: 10.1073/pnas.1912531117.
- Livak, K. J., & Schmittgen, T. D. Analysis of Relative Gene Expression Data Using Real-Time Quantitative PCR and the 2 C T Method. *Methods* **25**(4): 402–408, 2001. DOI: 10.1006/meth.2001.1262.
- Lobov, I. B., Renard, R. A., Papadopoulos, N., Gale, N. W., Thurston, G., Yancopoulos, G. D., & Wiegand, S. J. Delta-like ligand 4 (Dll4) is induced by VEGF as a negative regulator of angiogenic sprouting. *Proc. Natl. Acad. Sci. U.S.A.* **104**(9): 3219-3224, 2007. DOI: 10.1073/pnas.0611206104.
- Lopes, A., Daras, V., Cross, P. A., Robertson, G., Beynon, G., & Monaghan, J. M. Thrombocytosis as a prognostic factor in women with cervical cancer. *Cancer* **74**(1): 90–92, 1994. DOI: 10.1002/1097-0142(19940701)74:1<90::aid-cnrcr2820740116>3.0.co;2-0.
- Lupher, M. L., Andoniou, C. E., Bonita, D., Miyake, S., & Band, H. The c-Cbl oncoprotein. *Int. J. Biochem. Cell Biol.* **30**(4): 439–444, 1998. DOI: 10.1016/s1357-2725(97)00075-7.
- Ma, L., Perini, R., McKnight, W., Dickey, M., Klein, A., Hollenberg, M. D., & Wallace, J. L. Proteinase-activated receptors 1 and 4 counter-regulate endostatin and VEGF release from human platelets. *Proc. Natl. Acad. Sci. U.S.A.* **102**(1): 216–220, 2005. DOI: 10.1073/pnas.0406682102.
- Ma, Y. Q., Qin, J., & Plow, E. F. Platelet integrin alpha(IIb)beta(3): activation mechanisms. *J. Thromb. Haemost.* **5**(7): 1345–1352, 2007. DOI: 10.1111/j.1538-7836.2007.02537.x.
- Machlus, K. R., & Italiano, J. E. The incredible journey: From megakaryocyte development to platelet formation. *J. Cell Biol.* **201**(6): 785-796, 2013. DOI: 10.1083/jcb.201304054.
- Maia, V., Ortiz-Rivero, S., Sanz, M., Gutierrez-Berzal, J., Álvarez-Fernández, I., Gutierrez-Herrero, S., De Pereda, J. M., Porras, A., & Guerrero, C. C3G forms complexes with Bcr-

- Abl and p38 α MAPK at the focal adhesions in chronic myeloid leukemia cells: implication in the regulation of leukemic cell adhesion. *Cell Commun. Signal.* **11**(1): 9, 2013. DOI: 10.1186/1478-811X-11-9.
- Maia, V., Sanz, M., Gutierrez-Berzal, J., de Luis, A., Gutierrez-Uzquiza, A., Porras, A., & Guerrero, C. C3G silencing enhances STI-571-induced apoptosis in CML cells through p38 MAPK activation, but it antagonizes STI-571 inhibitory effect on survival. *Cell. Signal.* **21**(7): 1229–1235, 2009. DOI: 10.1016/j.cellsig..2009.03.015.
- Manzano, S., Gutierrez-Uzquiza, A., Bragado, P., Sequera, C., Herranz, Ó., Rodrigo-Faus, M., Jauregui, P., Morgner, S., Rubio, I., Guerrero, C., & Porras, A. C3G downregulation induces the acquisition of a mesenchymal phenotype that enhances aggressiveness of glioblastoma cells. *Cell Death Dis.* **12**(4): 348. DOI:10.1038/s41419-021-03631-w.
- Märklin, M., Tandler, C., Kopp, H. G., Hoehn, K. L., Quintanilla-Martinez, L., Borst, O., Müller, M. R., & Saur, S. J. C-Cbl regulates c-MPL receptor trafficking and its internalization. *J. Cell. Mol. Med.* **24**(21): 12491–12503, 2020. DOI:10.1111/jcmm.15785.
- Marshall, R. S., McLoughlin, F., & Vierstra, R. D. (2016). Autophagic Turnover of Inactive 26S Proteasomes in Yeast Is Directed by the Ubiquitin Receptor Cue5 and the Hsp42 Chaperone. *Cell Rep.* **16**(6): 1717–1732, 2016. DOI: 10.1016/j.celrep.2016.07.015.
- Martín-Encabo, S., Santos, E., & Guerrero, C. C3G mediated suppression of malignant transformation involves activation of PP2A phosphatases at the subcortical actin cytoskeleton. *Exp. Cell Res.* **313**(18): 3881–3891, 2007. DOI: 10.1016/j.yexcr.2007.07.036.
- Martín-Granado, V., Ortiz-Rivero, S., Carmona, R., Herrero, S. G., Barrera, M., San-Segundo, L., Sequera, C., Perdiguero, P., Lozano, F., Martín-Herrero, F., González-Porras, J. R., Muñoz-Chápuli, R., Porras, A., & Guerrero, C. C3G promotes a selective release of angiogenic factors from activated mouse platelets to regulate angiogenesis and tumor metastasis. *Oncotarget* **8**(67): 110994–111011, 2017. DOI: 10.18632/oncotarget.22339.
- Massberg, S., Konrad, I., Schürzinger, K., Lorenz, M., Schneider, S., Zohlhoefer, D., Hoppe, K., Schiemann, M., Kennerknecht, E., Sauer, S., Schulz, C., Kerstan, S., Rudelius, M., Seidl, S., Sorge, F., Langer, H., Peluso, M., Goyal, P., Vestweber, D., Emambokus, N. R., Busch, D. H., Frampton, J., & Gawaz, M. Platelets secrete stromal cell-derived factor 1 α and recruit bone marrow-derived progenitor cells to arterial thrombi in vivo. *J. Exp. Med.* **203**(5): 1221–1233, 2006. DOI: 10.1084/jem.20051772.
- Matsumoto, K., & Ema, M. Roles of VEGF-A signalling in development, regeneration, and tumours. *J. Biochem.* **156**(1): 1–10, 2014. DOI: 10.1093/jb/mvu031.
- McNicol, A., & Israels, S. J. Platelet dense granules: structure, function and implications for haemostasis. *Thromb. Res.* **95**(1): 1–18, 1999. DOI: 10.1016/s0049-3848(99)00015-8.
- Meikle, C. K. S., Kelly, C. A., Garg, P., Wuescher, L. M., Ali, R. A., & Worth, R. G. Cancer and Thrombosis: The Platelet Perspective. *Front. Cell Dev. Biol.* **4**:147, 2017. DOI: 10.3389/fcell.2016.00147.
- Metcalf, D., Begley, C. G., Johnson, G. R., Nicola, N. A., Lopez, A. F., & Williamson, D. J. Effects of purified bacterially synthesized murine multi-CSF (IL-3) on hematopoiesis in normal adult mice. *Blood* **68**(1): 46–57, 1986. DOI: 10.1182/blood.v68.1.46.46.
- Miller, S. A., Dykes, D. D., & Polesky, H. F. A simple salting out procedure for extracting DNA from human nucleated cells. *Nucleic Acids Res.* **16**(3): 1215, 1988. DOI: 10.1093/nar/16.3.1215.
- Morrison, S. J., & Weissman, I. L. The long-term repopulating subset of hematopoietic stem cells is deterministic and isolatable by phenotype. *Immunity* **1**(8): 661–673, 1994. DOI: 10.1016/1074-7613(94)90037-x.

- Munch, D., Rodriguez, E., Bressendorff, S., Park, O. K., Hofius, D., & Petersen, M. Autophagy deficiency leads to accumulation of ubiquitinated proteins, ER stress, and cell death in Arabidopsis. *Autophagy* **10**(9): 1579–1587, 2014. DOI: 10.4161/auto.29406.
- Murai, K., Kowata, S., Shimoyama, T., Yashima-Abo, A., Fujishima, Y., Ito, S., & Ishida, Y. Bortezomib induces thrombocytopenia by the inhibition of proplatelet formation of megakaryocytes. *Eur. J. Haematol.* **93**(4): 290–296, 2014. DOI: 10.1111/ejh.12342.
- Murphy, A. J., Bijl, N., Yvan-Charvet, L., Welch, C. B., Bhagwat, N., Reheman, A., Wang, Y., Shaw, J. A., Levine, R. L., Ni, H., Tall, A. R., & Wang, N. Cholesterol efflux in megakaryocyte progenitors suppresses platelet production and thrombocytosis. *Nat. Med.*, **19**(5): 586–594, 2013. DOI: 10.1038/nm.3150.
- Nakano, T., Fujii, J., Tamura, S., Hada, T., & Higashino, K. Thrombocytosis in patients with malignant pleural mesothelioma. *Cancer* **58**(8): 1699–1701, 1986. DOI: 10.1002/1097-0142(19861015)58:8<1699::aid-cnrcr2820580820>3.0.co;2-b.
- Nayak, M. K., Kulkarni, P. P., & Dash, D. Regulatory role of proteasome in determination of platelet life span. *J. Biol. Chem.* **288**(10): 6826–6834, 2013. DOI: 10.1074/jbc.M112.403154.
- Nayak, S. C., & Radha, V. C3G localizes to the mother centriole in a cenexin-dependent manner and regulates centrosome duplication and primary cilium length. *J. Cell Sci.* **133**(11): jcs243113, 2020. DOI: 10.1242/jcs.243113.
- Ng, A. P., Kauppi, M., Metcalf, D., Hyland, C. D., Josefsson, E. C., Lebois, M., Zhang, J. G., Baldwin, T. M., Di Rago, L., Hilton, D. J., & Alexander, W. S. Mpl expression on megakaryocytes and platelets is dispensable for thrombopoiesis but essential to prevent myeloproliferation. *Proc. Natl. Acad. Sci. U.S.A.* **111**(16): 5884–5889, 2014. DOI: 10.1073/pnas.1404354111.
- Niiyama, H., Huang, N. F., Rollins, M. D., & Cooke, J. P. Murine model of hindlimb ischemia. *J. Vis. Exp.* **23**: 1035, 2009. DOI: 10.3791/1035.
- Noetzli, L. J., French, S. L., & Machlus, K. R. New Insights Into the Differentiation of Megakaryocytes From Hematopoietic Progenitors. *Arterioscler. Thromb. Vasc. Biol.* **39**(7): 1288–1300, 2019. DOI: 10.1161/ATVBAHA.119.312129.
- Oda, A., Miyakawa, Y., Druker, B. J., Ishida, A., Ozaki, K., Ohashi, H., Wakui, M., Handa, M., Watanabe, K., Okamoto, S., & Ikeda, Y. Crkl is constitutively tyrosine phosphorylated in platelets from chronic myelogenous leukemia patients and inducibly phosphorylated in normal platelets stimulated by thrombopoietin. *Blood* **88**(11): 4304–4313, 1996. DOI: 10.1182/blood.v88.11.4304.4304.
- Oda, A., Ozaki, K., Druker, B. J., Miyakawa, Y., Miyazaki, H., Handa, M., Morita, H., Ohashi, H., & Ikeda, Y. p120c-cbl Is Present in Human Blood Platelets and Is Differentially Involved in Signaling by Thrombopoietin and Thrombin. *Blood* **88**(4): 1330–1338, 1996. DOI: 10.1182/blood.V88.4.1330.bloodjournal8841330.
- Ohba, Y., Ikuta, K., Ogura, A., Matsuda, J., Mochizuki, N., Nagashima, K., Kurokawa, K., Mayer, B. J., Maki, K., Miyazaki, J. I., & Matsuda, M. Requirement for C3G-dependent Rap1 activation for cell adhesion and embryogenesis. *EMBO J.*, **20**(13): 3333–3341, 2001. DOI: 10.1093/emboj/20.13.3333.
- Ohba, Y., Mochizuki, N., Yamashita, S., Chan, A. M., Schrader, J. W., Hattori, S., Nagashima, K., & Matsuda, M. Regulatory proteins of R-Ras, TC21/R-Ras2, and M-Ras/R-Ras3. *J. Biol. Chem.* **275**(26): 20020–20026, 2000. DOI: 10.1074/jbc.M000981200.
- Okino, K., Nagai, H., Nakayama, H., Doi, D., Yoneyama, K., Konishi, H., & Takeshita, T. Inactivation of Crk SH3 domain-binding guanine nucleotide-releasing factor (C3G) in

- cervical squamous cell carcinoma. *Int. J. Gynecol. Cancer* **16**(2): 763–771, 2006. DOI: 10.1111/j.1525-1438.2006.00352.x.
- Ortiz-Rivero, S., Baquero, C., Hernández-Cano, L., Roldán-Etcheverry, J. J., Gutiérrez-Herrero, S., Fernández-Infante, C., Martín-Granado, V., Anguita, E., De Pereda, J. M., Porras, A., & Guerrero, C. C3G, through its GEF activity, induces megakaryocytic differentiation and proplatelet formation. *Cell Commun. Signal.* **16**(1): 101, 2018. DOI: 10.1186/S12964-018-0311-5.
- Ozel, I., Duerig, I., Domnich, M., Lang, S., Pylaeva, E., & Jablonska, J. The Good, the Bad, and the Ugly: Neutrophils, Angiogenesis, and Cancer. *Cancers (Basel)* **14**(3): 536, 2022. DOI: 10.3390/cancers14030536.
- Packham, I. M., Watson, S. P., Bicknell, R., & Egginton, S. In vivo evidence for platelet-induced physiological angiogenesis by a COX driven mechanism. *PLoS One* **9**(9): e107503, 2014. DOI: 10.1371/journal.pone.0107503.
- Patan, S. Vasculogenesis and angiogenesis. *Cancer Treat. Res.* **117**: 3–32, 2004. DOI: 10.1007/978-1-4419-8871-3_1.
- Peach, C. J., Mignone, V. W., Arruda, M. A., Alcobia, D. C., Hill, S. J., Kilpatrick, L. E., & Woolard, J. Molecular Pharmacology of VEGF-A Isoforms: Binding and Signalling at VEGFR2. *Int. J. Mol. Sci.* **19**(4): 1264, 2018. DOI: 10.3390/ijms19041264.
- Peters, C. G., Michelson, A. D., & Flaumenhaft, R. Granule exocytosis is required for platelet spreading: differential sorting of α -granules expressing VAMP-7. *Blood* **120**(1): 199–206, 2012. DOI: 10.1182/blood-2011-10-389247.
- Pipili-Synetos, E., Papadimitriou, E., & Maragoudakis, M. E. Evidence that platelets promote tube formation by endothelial cells on matrigel. *Br. J. Pharmacol.* **125**(6): 1252–1257, 1998. DOI: 10.1038/sj.bjp.0702191.
- Pluda, J. M., & Parkinson, D. R. Clinical implications of Tumor-Associated Neovascularization and Current Antiangiogenic Strategies for the Treatment of Malignancies of Pancreas. *Cancer* **78**(3 Suppl): 680–687, 1996. DOI: 10.1002/(SICI)1097-0142(19960801)78:3<680::AID-CNCR49>3.0.CO;2-S.
- Polgár, J., Clemetson, J. M., Kehrel, B. E., Wiedemann, M., Magnenat, E. M., Wells, T. N. C., & Clemetson, K. J. Platelet activation and signal transduction by convulxin, a C-type lectin from *Crotalus durissus terrificus* (tropical rattlesnake) venom via the p62/GPVI collagen receptor. *J. Biol. Chem.* **272**(21): 13576–13583, 1997. DOI: 10.1074/jbc.272.21.13576.
- Potente, M., Gerhardt, H., & Carmeliet, P. Basic and therapeutic aspects of angiogenesis. *Cell* **146**(6): 873–887, 2011. DOI: 10.1016/j.cell.2011.08.039.
- Priego, N., Arechederra, M., Sequera, C., Bragado, P., Vázquez-Carballo, A., Gutiérrez-Uzquiza, Á., Martín-Granado, V., Ventura, J. J., Kazanietz, M. G., Guerrero, C., & Porras, A. C3G knock-down enhances migration and invasion by increasing Rap1-mediated p38 α activation, while it impairs tumor growth through p38 α -independent mechanisms. *Oncotarget* **7**(29): 45060–45078, 2016. DOI: 10.18632/oncotarget.9911.
- Qian, H., Buza-Vidas, N., Hyland, C. D., Jensen, C. T., Antonchuk, J., Månsson, R., Thoren, L. A., Ekblom, M., Alexander, W. S., & Jacobsen, S. E. W. Critical role of thrombopoietin in maintaining adult quiescent hematopoietic stem cells. *Cell Stem Cell* **1**(6): 671–684, 2007. DOI: 10.1016/j.stem.2007.10.008
- Qian, S., Fu, F., Li, W., Chen, Q., & De Sauvage, F. J. Primary Role of the Liver in Thrombopoietin Production Shown by Tissue-Specific Knockout. *Blood* **92**(6): 2189–2191, 1998. DOI: 10.1182/blood.V92.6.2189.

- Radha, V., Mitra, A., Dayma, K., & Sasikumar, K. Signalling to actin: role of C3G, a multitasking guanine-nucleotide-exchange factor. *Biosci. Rep.* **31**(4): 231–244, 2011. DOI: 10.1042/BSR20100094.
- Radha, V., Rajanna, A., Mitra, A., Rangaraj, N., & Swarup, G. C3G is required for c-Abl-induced filopodia and its overexpression promotes filopodia formation. *Exp. Cell Res.* **313**(11): 2476–2492, 2007. DOI: 0.1016/j.yexcr.2007.03.019.
- Radha, V., Rajanna, A., & Swarup, G. Phosphorylated guanine nucleotide exchange factor C3G, induced by pervanadate and Src family kinases localizes to the Golgi and subcortical actin cytoskeleton. *BMC Cell Biol.* **5**: 31, (2004). DOI: 10.1186/1471-2121-5-31.
- Radley, J. M., & Haller, C. J. The demarcation membrane system of the megakaryocyte: a misnomer? *Blood* **60**(1): 213–219, 1982. DOI: 10.1182/blood.V60.1.213.213.
- Ravindranath, N., Wion, D., Brachet, P., & Djakiew, D. Epidermal Growth Factor Modulates the Expression of Vascular Endothelial Growth Factor in the Human Prostate. *J. Androl.* **22**(3): 432–443, 2001. DOI: 10.1002/j.1939-4640.2001.tb02199.x.
- Reedquist, K. A., Fukazawa, T., Panchamoorthy, G., Langdon, W. Y., Shoelson, S. E., Druker, B. J., & Band, H. Stimulation through the T cell receptor induces Cbl association with Crk proteins and the guanine nucleotide exchange protein C3G. *J. Biol. Chem.* **271**(14): 8435–8442, 1996. DOI: 10.1074/jbc.271.14.8435.
- Ren, Q., Barber, H. K., Crawford, G. L., Karim, Z. A., Zhao, C., Choi, W., Wang, C. C., Hong, W., & Whiteheart, S. W. Endobrevin/VAMP-8 is the primary v-SNARE for the platelet release reaction. *Mol. Biol. Cell* **18**(1): 24–33, 2007. DOI: 10.1091/mbc.e06-09-0785.
- Rendu, F., & Brohard-Bohn, B. The platelet release reaction: granules' constituents, secretion and functions. *Platelets* **12**(5): 261–273, 2001. DOI: 10.1080/09537100120068170.
- Rezaeeyan, H., Shirzad, R., McKee, T. D., & Saki, N. Role of chemokines in metastatic niche: new insights along with a diagnostic and prognostic approach. *APMIS* **126**(5): 359–370, 2018. DOI: 10.1111/apm.12818.
- Ribeiro, M., Ruff, P., & Falkson, G. Low serum testosterone and a younger age predict for a poor outcome in metastatic prostate cancer. *Am. J. Clin. Oncol.* **20**(6): 605–608, 1997. DOI: 10.1097/00000421-199712000-00015.
- Rodríguez-Manzanegue, J. C., Lane, T. F., Ortega, M. A., Hynes, R. O., Lawler, J., & Iruela-Arispe, M. L. Thrombospondin-1 suppresses spontaneous tumor growth and inhibits activation of matrix metalloproteinase-9 and mobilization of vascular endothelial growth factor. *Proc. Natl. Acad. Sci. U.S.A.* **98**(22): 12485–12490, 2001. DOI: 10.1073/pnas.171460498.
- Rosado, J. A., & Sage, S. O. Protein kinase C activates non-capacitative calcium entry in human platelets. *J. Physiol.*, **529 Pt 1**(Pt 1): 159–169, 2000. DOI: 10.1111/j.1469-7793.2000.00159.x.
- Rouyez, M.-C., Boucheron, C., Gisselbrecht, S., Dusanter-Fourt, I., & Porteu, O. Control of Thrombopoietin-Induced Megakaryocytic Differentiation by the Mitogen-Activated Protein Kinase Pathway. *Moll. Cell Biol.* **17**(9): 4991-5000, 1997. DOI: 10.1128/MCB.17.9.4991.
- Rowley, J. W., Oler, A. J., Tolley, N. D., Hunter, B. N., Low, E. N., Nix, D. A., Yost, C. C., Zimmerman, G. A., & Weyrich, A. S. Genome-wide RNA-seq analysis of human and mouse platelet transcriptomes. *Blood* **118**(14): e101-111, 2011. DOI: 10.1182/blood-2011-03-339705.
- Saci, A., Rendu, F., & Bachelot-Loza, C. Platelet α IIb-beta 3 integrin engagement induces the tyrosine phosphorylation of Cbl and its association with phosphoinositide 3-kinase and

- Syk. *Biochem. J.* **351 Pt 3**(Pt 3): 669-676, 2000. DOI: 10.1042/0264-6021:3510669.
- Samuelsson, J., Alonso, S., Ruiz-Larroya, T., Cheung, T. H., Wong, Y. F., & Perucho, M. Frequent somatic demethylation of RAPGEF1/C3G intronic sequences in gastrointestinal and gynecological cancer. *Int. J. Oncol.* **38**(6): 1575–1577, 2011. DOI: 10.3892/ijo.2011.972.
- Sasi Kumar, K., Ramadhas, A., Nayak, S. C., Kaniyappan, S., Dayma, K., & Radha, V. C3G (RapGEF1), a regulator of actin dynamics promotes survival and myogenic differentiation of mouse mesenchymal cells. *BBAM Cell Res.* **1853**(10): 2629–2639, 2015. 10.1016/j.bbamcr.2015.06.015.
- Saur, S. J., Sangkhae, V., Geddis, A. E., Kaushansky, K., & Hitchcock, I. S. Ubiquitination and degradation of the thrombopoietin receptor c-Mpl. *Blood* **115**(6): 1254–1263, 2010. DOI: 10.1182/blood-2009-06-227033.
- Schlesinger, M. Role of platelets and platelet receptors in cancer metastasis. *J. Hematol. Oncol.* **11**(1):125, 2018. DOI: 10.1186/S13045-018-0669-2.
- Schumacher, D., Strilic, B., Sivaraj, K. K., Wettschureck, N., & Offermanns, S. Platelet-derived nucleotides promote tumor-cell transendothelial migration and metastasis via P2Y2 receptor. *Cancer Cell* **24**(1): 130–137, 2013. DOI: 10.1016/j.ccr..2013.05.008.
- Sehgal, S., & Storrie, B. Evidence that differential packaging of the major platelet granule proteins von Willebrand factor and fibrinogen can support their differential release. *J. Thromb. Haemost.* **5**(10): 2009–2016, 2007. DOI: 10.1111/j.1538-7836.2007.02698.x.
- Seita, J., & Weissman, I. L. Hematopoietic stem cell: self-renewal versus differentiation. *Wiley Interdiscip. Rev. Syst. Biol. Med.* **2**(6): 640–653, 2010. DOI: 10.1002/wsbm.86.
- Sequera, C., Bragado, P., Manzano, S., Arechederra, M., Richelme, S., Gutiérrez-Uzquiza, A., Sánchez, A., Maina, F., Guerrero, C., & Porras, A. C3G Is Upregulated in Hepatocarcinoma, Contributing to Tumor Growth and Progression and to HGF/MET Pathway Activation. *Cancers (Basel)*. **12**(8): 1–22, 2020. DOI: 10.3390/cancers12082282.
- Shah, B., Lutter, D., Bochenek, M. L., Kato, K., Tsytsyura, Y., Glyvuk, N., Sakakibara, A., Klingauf, J., Adams, R. H., & Püschel, A. W. C3G/Rapgef1 is required in multipolar neurons for the transition to a bipolar morphology during cortical development. *PLoS One* **11**(4): e0154174, 2016. DOI: 10.1371/journal.pone.0154174.
- Shakyawar, D. K., Muralikrishna, B., & Radha, V. C3G dynamically associates with nuclear speckles and regulates mRNA splicing. *Mol. Biol. Cell* **29**(9): 1111–1124, 2018. 10.1091/mbc.E17-07-0442.
- Shintani, T., Ohara-Waki, F., Kitanaka, A., Tanaka, T., & Kubota, Y. Cbl negatively regulates erythropoietin-induced growth and survival signaling through the proteasomal degradation of Src kinase. *Blood Cells. Mol. Dis.* **53**(4): 211–218, 2014. DOI: 10.1016/J.j.bcmd.2014.06.005.
- Shivakrupa, R., Radha, V., Sudhakar, C., & Swarup, G. Physical and functional interaction between Hck tyrosine kinase and guanine nucleotide exchange factor C3G results in apoptosis, which is independent of C3G catalytic domain. *J. Biol. Chem.* **278**(52): 52188–52194, 2003. DOI: 10.1074/jbc.M310656200.
- Sierko, E., & Wojtukiewicz, M. Z. Platelets and angiogenesis in malignancy. *Semin. Thromb. Hemost.* **30**(1): 95–108, 2004. DOI: 10.1055/s-2004-822974.
- Smolenski, A. Novel roles of cAMP/cGMP-dependent signaling in platelets. *J. Thromb. Haemost.* **10**(2): 167–176, 2012. DOI: 10.1111/j.1538-7836.2011.04576.x.
- Sriram, D., Chintala, R., Parthasaradhi, B. V. V., Nayak, S. C., Mariappan, I., & Radha, V. Expression of a novel brain specific isoform of C3G is regulated during development. *Sci.*

- Rep.* **10**(1): 18838, 2020. DOI: 10.1038/s41598-020-75813-z.
- Stalker, T. J., Traxler, E. A., Wu, J., Wannemacher, K. M., Cermignano, S. L., Voronov, R., Diamond, S. L., & Brass, L. F. Hierarchical organization in the hemostatic response and its relationship to the platelet-signaling network. *Blood* **121**(10): 1875–1885, 2013. DOI: 10.1182/blood-2012-09-457739.
- Stefanich, E., Senn, T., Widmer, R., Fratino, C., Keller, G. A., & Fielder, P. J. Metabolism of thrombopoietin (TPO) in vivo: determination of the binding dynamics for TPO in mice. *Blood* **89**(11): 4063–4070, 1997. DOI: 10.1182/blood.V89.11.4063.
- Stefanini, L., & Bergmeier, W. RAP1-GTPase signaling and platelet function. *J. Mol. Med. (Berl)*. **94**(1): 13–19, 2016. DOI: 10.1007/s00109-015-1346-3.
- Stefanini, L., Lee, R. H., Paul, D. S., O’Shaughnessy, E. C., Ghalloussi, D., Jones, C. I., Boulaftali, Y., Poe, K. O., Piatt, R., Kechele, D. O., Caron, K. M., Hahn, K. M., Gibbins, J. M., & Bergmeier, W. Functional redundancy between RAP1 isoforms in murine platelet production and function. *Blood* **132**(18): 1951–1962, 2018. DOI: 10.1182/blood -2018-03-838714.
- Steinert, B. W., Tang, D. G., Grossi, I. M., Umbarger, L. A., & Honn, K. V. Studies on the role of platelet eicosanoid metabolism and integrin alpha IIb beta 3 in tumor-cell-induced platelet aggregation. *Int. J. Cancer*. **54**(1): 92–101, 1993. DOI: 10.1002/ijc.2910540116.
- Stellos, K., & Gawaz, M. Platelets and stromal cell-derived factor-1 in progenitor cell recruitment. *Semin. Thromb. Hemost.*, **33**(2): 159–164, 2007. DOI: 10.1055/s-2007-969029.
- Stork, P. J. S., & Dillon, T. J. Multiple roles of Rap1 in hematopoietic cells: complementary versus antagonistic functions. *Blood* **106**(9): 2952–2961, 2005. DOI: 10.1182/blood-2005-03-1062.
- Sufen, G., Xianghong, Y., Yongxia, C., & Qian, P. bFGF and PDGF-BB have a synergistic effect on the proliferation, migration and VEGF release of endothelial progenitor cells. *Cell Biol. Int.* **35**(5): 545–551, 2011. DOI: 10.1042/CBI20100401.
- Symbas, N. P., Townsend, M. F., El-Galley, R., Keane, T. E., Graham, S. D., & Petros, J. A. Poor prognosis associated with thrombocytosis in patients with renal cell carcinoma. *BJU Int.* **86**(3): 203–207, 2000. DOI: 10.1046/j.1464-410x.2000.00792.x.
- Tanaka, S., Morishita, T., Hashimoto, Y., Hattori, S., Nakamura, S., Shibuya, M., Matuoka, K., Takenawa, T., Kurata, T., Nagashima, K., & Matsuda, M. C3G, a guanine nucleotide-releasing protein expressed ubiquitously, binds to the Src homology 3 domains of CRK and GRB2/ASH proteins. *Proc. Natl. Acad. Sci. U.S.A.* **91**(8): 3443–3447, 1994. DOI: 10.1073/pnas.91.8.3443.
- Tanaka, S., Ouchi, T., & Hanafusa, H. Downstream of Crk adaptor signaling pathway: activation of Jun kinase by v-Crk through the guanine nucleotide exchange protein C3G. *Proc. Natl. Acad. Sci. U.S.A.* **94**(6): 2356–2361, 1997. DOI: 10.1073/pnas.94.6.2356.
- Thon, J. N., & Italiano, J. E. Platelets: Production, Morphology and Ultrastructure. *Handb. Exp. Pharmacol.*, **210**, 3–22, 2012. DOI: 10.1007/978-3-642-29423-5_1.
- Thurston, G., & Kitajewski, J. VEGF and Delta-Notch: interacting signalling pathways in tumour angiogenesis. *Br. J. Cancer* **99**(8): 1204–1209, 2008. DOI: 10.1038/sj.bjc.6604484.
- Tiedt, R., Schomber, T., Hao-Shen, H., & Skoda, R. C. Pf4-Cre transgenic mice allow the generation of lineage-restricted gene knockouts for studying megakaryocyte and platelet function in vivo. *Blood* **109**(4): 1503–1506. DOI: 10.1182/blood-2006-04-020362.
- Tomita, N., Morishita, R., Taniyama, Y., Koike, H., Aoki, M., Shimizu, H., Matsumoto, K., Nakamura, T., Kaneda, Y., & Ogihara, T. Angiogenic property of hepatocyte growth factor is dependent on upregulation of essential transcription factor for angiogenesis, ets-1.

- Circulation* **107**(10): 1411–1417, 2003. DOI: 10.1161/01.cir.0000055331.41937.aa.
- Uemura, N., & Griffin, J. D. The adapter protein Crkl links Cbl to C3G after integrin ligation and enhances cell migration. *J. Biol. Chem.* **274**(53): 37525–37532, 1999. DOI: 10.1074/jbc.274.53.37525.
- Vainchenker, W., Arkoun, B., Basso-Valentina, F., Lordier, L., Debili, N., & Raslova, H. Role of Rho-GTPases in megakaryopoiesis. *Small GTPases* **12**(5–6): 399–415, 2021. DOI: 10.1080/21541248.2021.1885134.
- Varki, A. Trousseau's syndrome: multiple definitions and multiple mechanisms. *Blood* **110**(6): 1723–1729, 2007. DOI: 10.1182/blood-2006-10-053736.
- Varner, J. A., Nakada, M. T., Jordan, R. E., & Collier, B. S. Inhibition of angiogenesis and tumor growth by murine 7E3, the parent antibody of c7E3 Fab (abciximab; ReoPro). *Angiogenesis* **3**(1): 53–60, 1999. DOI: 10.1023/a:1009019223744.
- Vishnu, V. V., Muralikrishna, B., Verma, A., Nayak, S. C., Sowpati, D. T., Radha, V., & Shekar, P. C. C3G Regulates STAT3, ERK, Adhesion Signaling, and Is Essential for Differentiation of Embryonic Stem Cells. *Stem Cell Rev. Reports* **17**(4): 1465–1477, 2021. DOI: 10.1007/S12015-021-10136-8.
- Voss, A. K., Britto, J. M., Dixon, M. P., Sheikh, B. N., Collin, C., Tan, S. S., & Thomas, T. (2008). C3G regulates cortical neuron migration, preplate splitting and radial glial cell attachment. *Development* **135**(12): 2139–2149, 2008. DOI: 10.1242/dev.016725.
- Voss, A. K., Krebs, D. L., & Thomas, T. C3G regulates the size of the cerebral cortex neural precursor population. *EMBO J.* **25**(15): 3652–3663, 2006. DOI: 10.1038/sj.emboj.7601234.
- Walsh, T. G., Metharom, P., & Berndt, M. C. The functional role of platelets in the regulation of angiogenesis. *Platelets* **26**(3): 199–211, 2015. DOI: 10.3109/09537104.2014.909022.
- Wojtukiewicz, M. Z., Sierko, E., Hempel, D., Tucker, S. C., & Honn, K. V. Platelets and cancer angiogenesis nexus. *Cancer Metastasis Rev.* **36**(2): 249–262, 2017. DOI: 10.1007/s10555-017-9673-1.
- Woolthuis, C. M., & Park, C. Y. (2016). Hematopoietic stem/progenitor cell commitment to the megakaryocyte lineage. *Blood* **127**(10): 1242–1248, 2016. DOI: 10.1182/blood-2015-07-607945.
- Wu, X., Knudsen, B., Feller, S. M., Zheng, J., Sali, A., Cowburn, D., Hanafusa, H., & Kuriyan, J. Structural basis for the specific interaction of lysine-containing proline-rich peptides with the N-terminal SH3 domain of c-Crk. *Structure* **3**(2): 215–226, 1995. DOI: 10.1016/s0969-2126(01)00151-4.
- Yan, M. J., & Jurasz, P. The role of platelets in the tumor microenvironment: From solid tumors to leukemia. *Biochim. Biophys. Acta* **1863**(3): 392–400, 2016. DOI: 10.1016/j.bbamcr.2015.07.008.
- Yang, L., Bryder, D., Adolfsson, J., Nygren, J., Månsson, R., Sigvardsson, M., & Jacobsen, S. E. W. Identification of Lin(-)Sca1(+)kit(+)CD34(+)Flt3- short-term hematopoietic stem cells capable of rapidly reconstituting and rescuing myeloablated transplant recipients. *Blood* **105**(7): 2717–2723, 2005. DOI: 10.1182/blood-2004-06-2159.
- Ye, S., Karim, Z. A., Al Hawas, R., Pessin, J. E., Filipovich, A. H., & Whiteheart, S. W. Syntaxin-11, but not syntaxin-2 or syntaxin-4, is required for platelet secretion. *Blood*, **120**(12): 2484–2492, 2012 DOI: 10.1182/blood-2012-05-430603.
- Yokouchi, M., Kondo, T., Sanjay, A., Houghton, A., Yoshimura, A., Komiya, S., Zhang, H., & Baron, R. Src-catalyzed phosphorylation of c-Cbl leads to the interdependent ubiquitination of both proteins. *J. Biol. Chem.* **276**(37): 35185–35193, 2001. DOI:

- 10.1074/jbc.M102219200.
- York, R. D., Yao, H., Dillon, T., Ellig, C. L., Eckert, S. P., McCleskey, E. W., & Stork, P. J. S. Rap1 mediates sustained MAP kinase activation induced by nerve growth factor. *Nature*, **392**(6676): 622–626, 1998. DOI: 10.1038/33451.
- Yu, M., & Cantor, A. B. Megakaryopoiesis and Thrombopoiesis: An Update on Cytokines and Lineage Surface Markers. *Methods Mol. Biol.* **788**, 291–303, 2012. DOI: 10.1007/978-1-61779-307-3_20.
- Zeiler, M., Moser, M., & Mann, M. Copy number analysis of the murine platelet proteome spanning the complete abundance range. *Mol. Cell. Proteomics* **13**(12): 3435–3445 2014. DOI: 10.1074/mcp.M114.038513.
- Zeimet, A. G., Marth, C., Müller-Holzner, E., Daxenbichler, G., & Dapunt, O. Significance of thrombocytosis in patients with epithelial ovarian cancer. *Am. J. Obstet. Gynecol.* **170**(2): 549–554, 1994. DOI: 10.1016/s0002-9378(94)70225-x.
- Zhang, X., Kazerounian, S., Duquette, M., Perruzzi, C., Nagy, J. A., Dvorak, H. F., Parangi, S., & Lawler, J. Thrombospondin-1 modulates vascular endothelial growth factor activity at the receptor level. *FASEB J.* **23**(10): 3368–3376, 2009. DOI: 10.1096/fj.09-131649.
- Zucchella, M., Dezza, L., Pacchiarini, L., Meloni, F., Tacconi, F., Bonomi, E., Grignani, G., & Notario, A. Human tumor cells cultured “in vitro” activate platelet function by producing ADP or thrombin. *Haematologica* **74**(6): 541–545, 1989.
- Zuchtriegel, G., Uhl, B., Pühr-Westerheide, D., Pörnbacher, M., Lauber, K., Krombach, F., & Reichel, C. A. Platelets Guide Leukocytes to Their Sites of Extravasation. *PLoS Biol.* **14**(5), 2016. DOI: 10.1371/journal.pbio.1002459.

